N°:_____

THÈSE DE DOCTORAT

Development and characterization of a novel flame retardant EVM-based formulation: investigation and comprehension of the flame retardant mechanisms

---

Présentée et soutenue publiquement à

L'UNIVERSITÉ LILLE 1 –SCIENCES ET TECHNOLOGIES

pour obtenir le grade de

DOCTEUR
Spécialité : Molécules et Matière condensée

Par

Oriane CÉRIN-DELAVAL

Ingénieur diplômée de l'Ecole Nationale Supérieure de Chimie de Lille

Thèse dirigée par

Prof. Serge BOURBIGOT et Prof. Sophie DUQUESNE

Soutenue le 10 décembre 2010 devant la Commission d'Examen composée de :

Prof. Jacques DEVAUX, Université Catholique de Louvain	Président du jury
Prof. Baljinder KANDOLA, University of Bolton	Rapporteur
Prof. Jean-Luc GARDETTE, Université de Clermont-Ferrand	Rapporteur
Dr. Andreas ROOS, Lanxess AG	Examinateur
Prof. Serge BOURBIGOT, ENSCL	Directeur de thèse
Prof. Sophie DUQUESNE, ENSCL	Co-directrice
Dr. Gaëlle FONTAINE, ENSCL	Co-encadrante

ACKNOWLEDGEMENTS

This project took place in the LSPES laboratory directed by Prof. Jean-Marc Lefebvre, to whom I would like to address my first thanks. He welcomed me and gave me the opportunity to start my Ph.D. in the PERF team.

I am deeply grateful to my supervisors, Prof. Serge Bourbigot and Prof. Sophie Duquesne, for their understanding, encouraging and guidance for the present thesis. I also thank Dr. Gaëlle Fontaine for her involvement in the project.

I also would like to thank Dr. Gerd Bergman and Dr. Harry Zumaqué from LANXESS for initiating the project and for their scientific impulse, and Dr. Andreas Roos with whom I created a very enjoyable and efficient collaboration.

I wish to express my sincere thanks to Prof. Baljinder Kandola and Prof. Jean-Luc Gardette for having accepted to be external examiners of my Ph.D., and also to Prof. Jacques Devaux for chairing the jury.

Solid state NMR was an essential technique for the comprehensive work of this manuscript. Particular thanks are thus addressed to Bertrand Revel for the time he spent helping me for NMR experiments and to Dr. Grégory Tricot for his help and skilful advice on the NMR correlations and simulations. Prof. Rose-Noëlle Vannier, Dr. Nicolas Renault, Nora Djelal and Laurence Burylo are also thanked for their technical assistance for XRD or TGA-GCMS analyses, such as Dirk Müller and the technical staff in Leverkusen for their help to the material compounding (and to my German speaking!).

During this work I have collaborated with many colleagues for whom I have great regard, and I wish to extend my warmest thanks to all those who have helped me with my work, or who just contributed to the warm, stimulating and friendly atmosphere of the lab. Clémence, Maryska, Antoine, Caroline Louis, Hélène, Nico, Virginie, Thomas, Aurore, Fabienne, Yohann, Christelle, Jérémy (and all the Ph.D. and internship students I may have forgotten), thanks a lot! I will also remember Pierre and Bastien as good friends but I think I will never forget their foolish humour! I am also indebt to Brigitte and Nadine for their untiring good mood, kindness and assistance for secretarial or administrative work.

I owe my most sincere gratitude to two of my colleagues, who have become real friends: Jérémie and Mathilde. I really spent good moments with you, and I greatly appreciated your help and support during the hard moments of my professional or personal life. The scientific discussions we had were really stimulating and had a positive influence on my work. I learned a lot from your experience: I became a super micro-extrusion assistant (there is nothing better than cleaning the device after a hard day at work, isn't it Jérémie?) and a glass colouration specialist. Apart from this professional aspect,

sharing my office with Jérémie and my room with Mathilde (and her cat) was a real pleasure. Our “Dîner Presque Parfait” evenings (we’re still waiting yours, Mathilde!), our week ends spent working in the lab, the song writing, the horror films night (the first and last one), the discovery of the typical “friterie” and the raclettes were source of fun! I am also grateful for your patience: supporting me during the redaction of this manuscript and during the preparation of my wedding wasn’t an easy thing but you acted as perfect friends. These good memories make the three years of my Ph.D. a personal enriching experience.

This Ph.D. was not only a way to acquire experimental, technical and scientific experience, it was also for me the mean to meet interesting, kind and fascinating people. One of them is my husband, Damien, who I met in the lab and played an essential role in this work. I owe my loving thanks to him: without his encouragement and understanding it would have been impossible for me to finish this work.

Finally, my special gratitude is due to my dear family for their loving support. This work is especially dedicated to my father, who made me love science and gave me the taste of research, my mother for all the sacrifices she’s done for us, and my brother Guillaume. I hope you are all proud of me and my work.

TABLE OF CONTENTS

ABBREVIATIONS 7
RESUME 11
INTRODUCTION 23
CHAPTER 1 – STATE OF THE ART 27
1. Ethylene vinyl acetate copolymer (EVA) 29
1.1 Polymerization mechanisms 30
1.2 Mechanical properties 32
1.3 Thermal degradation 33
1.4 Flame Retardancy of EVA 36
2. Vulcanized EVM formulations 37
2.1 Curing system and additives 37
2.2 Properties of typical cured EVM formulations 39
2.3 Industrial applications of EVM and vulcanizates 42
2.4 Conclusion 43
3. Flame retardancy of EVA 44
3.1 Halogenated compounds 45
3.2 Metal hydroxides 47
3.3 Phosphorous-based compounds 49
3.4 Melamine and derivatives 50
3.5 Flame retardant combinations 52
3.6 Nanocomposites and nano-additives 55
3.7 Conclusion 61
4. Conclusion 61
CHAPTER 2 – MATERIALS COMPOUNDING AND EXPERIMENTAL TECHNIQUES 63
1. Materials and compounding 65
1.1 Materials and formulation recipes 65
1.2 Mixing conditions 68
1.3 Vulcanization 69
2. Experimental techniques: evaluation of the materials performances 70
2.1 Mechanical testing 70
2.2 Flame retardancy 72
3. Experimental techniques: characterization of the material degradation 75
3.1 Thermal analysis 75
3.2 Gas phase analysis 77
3.3 Condensed phase analysis 78
4. Conclusion 83
CHAPTER 3 – DEVELOPMENT OF A NOVEL FLAME RETARDED FORMULATION 85
1. Flame retardant screening 87
1.1 Selected flame retardant additives 87
1.2 Mechanical and fire testing 89
2. Flame retardant combinations 97
2.1 ATH and nano-particles 97
2.2 Phosphinate and melamine derivatives 100
2.3 ATH, phosphates and phosphinates 106

3. Optimization of the complete formulation: ATH-phosphinate flame retardant combination ... 111
3.1 Selection of the ATH grade ... 112
3.2 Optimization of the ATH-OP1230 ratio ... 114
3.3 Conclusion: optimal composition ... 117
4. Conclusion ... 118
CHAPTER 4 – INVESTIGATIONS ON THE ATH MODE OF ACTION ... 121
1. Thermal degradation mechanism ... 124
1.1 Vulcanized EVM ... 124
1.2 Vulcanized EVM flame retarded with ATH ... 137
2. Kinetic analysis ... 151
2.1 Fundamentals of kinetic analysis ... 151
2.2 Thermal degradation ... 154
2.3 Friedman “model-free” analysis ... 156
2.4 Kinetic modeling ... 157
2.5 Conclusion ... 163
3. General discussion ... 165
3.1 Effect of vulcanization on the thermal degradation of EVA ... 166
3.2 Influence of ATH on the thermal degradation of vulcanized EVA ... 168
3.3 Investigation of the structure of the residues in fire conditions ... 169
4. Conclusion ... 173
CHAPTER 5 –FLAME RETARDANCY MECHANISM OF OP1230 AND ATH-OP1230 IN EVM ... 175
1. Aluminium trihydroxide - phosphinate interactions ... 178
1.1 Thermal decomposition of OP1230 ... 178
1.2 Thermal degradation of the ATH-OP1230 combination ... 182
1.3 Conclusion on the ATH-OP1230 interactions ... 192
2. Chemical interactions between the polymeric matrix, ATH and OP1230 ... 194
2.1 Thermal degradation of vulcanized EVM flame retarded with OP1230 ... 194
2.2 Thermal degradation of vulcanized EVM flame retarded with ATH and OP1230 ... 204
2.3 Conclusion on the matrix-additives interactions ... 213
3. Relationship between ATH-OP1230-EVM interactions and flame retardant properties ... 214
4. Conclusion ... 219
GENERAL CONCLUSION - OUTLOOK ... 221
REFERENCES ... 231
APPENDICES ... 241
APPENDIX 1: ... 243
APPENDIX 2: ... 246
APPENDIX 3: ... 248
APPENDIX 4: ... 249
APPENDIX 5: ... 252
APPENDIX 6: ... 255

ABBREVIATIONS

APP	Ammonium polyphosphate
ATH	Aluminium trihydroxide
CNT	Carbon nanotube
CNF	Carbon nanofibres
DSC	Differential Scanning Calorimetry
DTG	Derivative thermogravimetric (curve)
EAB	Elongation at break
EG	Expanded graphite
EPM	Electron Probe Microanalyzer
EV(A-M)	Ethylene vinyl-acetate copolymer (M:VA content varying from 40 w% to 80w%)
FR	Fire retardant (compound)
FRNC	Fire retarded non corrosive (formulation)
FTIR	Fourier-Transformed Infra-Red spectroscopy
HTT	Heat Treatment Temperature
LDH	Layered double hydroxides
(L)LDPE	(Linear) low density polyethylene
LOI	Limiting Oxygen Index
MB	Melamine borate
MDH	Magnesium dihydroxide
MDR	Moving Die Rheometry
MLR	Mass loss rate
MMT	Montmorillonite
	Na-MMT: Montmorillonite (negative charges compensated with Na^+)
	oMMT: Organo-modified montmorillonite
MP	Melamine phosphate
MWNT	Multi-walled carbon nanotubes
NMR	Nuclear Magnetic Resonance
	MAS: Magic Angle Spinning
	DD: Dipolar Decoupling
	CP: Cross-Polarization
NG	Natural graphite
ODPA	Octylated diphenylamine
OP1230	Aluminium diethyl phosphinate
	OP1311: OP1230 combined with melamine cyanurate (2:1 ratio)
PA-6,6	Polyamide 6-6
PBT	Poly(butylene terephtalate)
PE	Polyethylene
PET	Poly(ethylene terephtalate)

RHR (HRR)	Rate of heat release (or Heat Release Rate) PRHR: Peak of RHR
RP	Red phosphorus
RPW	Railway profiles and Wagons (formulation)
SBR	Styrene-butadiene-styrene rubber
SDPA	Styrenated diphenylamine
SEA	Smoke emission average
SEM	Scanning Electron Microscopy
TA(I)C	Triallyl(iso)cyanurate
(Hi-Res) TGA	(High-Resolution) Thermo-Gravimetric Analysis
THR	Total heat release
TS	Tensile strength
TTI	Time to ignition
VA(C)	Vinyl acetate (content)
XRD	X-ray diffraction
ZB	Zinc Borate

RESUME

Résumé

Ces travaux traitent du développement d'une formulation commerciale retard au feu innovante à base de copolymère éthylène-acétate de vinyle (EVA) élastomérique. La formulation, destinée aux domaines de la câblerie et des transports, comporte une combinaison d'additifs retardateurs de flamme originale : le trihydroxyde d'aluminium (ATH) et un diéthyle phosphinate d'aluminium (OP1230). L'objectif scientifique est la compréhension des mécanismes d'ignifugation mis en jeu par cette combinaison.

Les vulcanisats de copolymères éthylène-acétate de vinyle élastomériques (EVM) sont largement utilisés dans les compositions de câbles électriques ou encore de profilés dans le domaine des transports. Ces applications sont soumises à des normes feu strictes, qui requièrent pour ces matériaux une contribution minimale à l'incendie.
Des formulations retard au feu à base d'EVM sont déjà disponibles sur le marché. Les additifs retard au feu généralement utilisés dans de tels matériaux sont des hydroxydes métalliques, qui combinent les avantages d'un faible coût, d'une faible toxicité et d'une efficacité satisfaisante. Néanmoins, le seuil d'efficacité de ces composés nécessite des taux de charge élevés (50 à 60 % en masse), ce qui induit une augmentation de la dureté du matériau et une limitation de ses propriétés mécaniques.

L'objectif de ce travail est donc de développer une formulation à base d'EVM dont les propriétés feu et mécaniques seraient au moins équivalentes à celles de la formulation « usuelle » contenant un hydroxyde métallique, mais qui présenterait de plus faibles valeurs de dureté, élargissant ainsi la gamme d'application des EVM, et de comprendre les mécanismes de dégradation et les phénomènes retard au feu mis en jeu.

Le premier chapitre de ce manuscrit est consacré à l'état de l'art de l'ignifugation des EVA et des propriétés des vulcanisats. Dans un second chapitre les différentes techniques mises en œuvre pour la caractérisation mécanique (dureté Shore A, tests de traction) et les tests feu (indice limite d'oxygène (LOI), UL-94, calorimétrie à cône) des formulations ainsi que la caractérisation physique et chimique des résidus de dégradation ou de combustion (Analyses Thermogravimétriques (ATG), traitements thermiques, Résonance Magnétique Nucléaire à l'état solide (RMN), Diffraction des Rayons X (DRX), infrarouge à transformée de Fourier (IRTF), chromatographie en phase gaz).

La troisième partie de ce manuscrit répond au challenge industriel, c'est-à-dire la mise au point d'une formulation retard au feu présentant une faible dureté. L'évaluation de différents types de retardateurs de flamme incorporés à une formulation « test » en termes de propriétés mécaniques et de résistance

au feu y est présentée. Le développement et l'optimisation de combinaisons innovantes d'additifs retard au feu (en particulier la combinaison ATH-OP1230) sont également détaillés.
Les deux derniers chapitres sont dédiés à la compréhension des mécanismes d'ignifugation : celui de l'ATH et celui de la combinaison ATH-OP1230.
Le mode d'action de l'ATH, proposé dans la littérature et communément admis par la communauté scientifique n'a pourtant jamais été étudié fondamentalement dans la matrice EVM vulcanisé (et plus généralement dans les thermoplastiques). Afin de vérifier les hypothèses émises, le mécanisme d'action de l'ATH est revisité par la caractérisation de l'influence du composé sur la dégradation thermique de la matrice EVM et sur son mode de combustion.
La formulation ATH-OP1230, quant à elle, n'a jamais été étudiée. Les mécanismes retard au feu ne sont donc pas élucidés. Pour répondre à cette problématique la recherche d'interactions potentielles entre les deux composés a été mise en œuvre par la caractérisation de leur dégradation. L'influence des additifs sur la matrice EVM est également évaluée, sur le plan de la dégradation thermique comme sur celui de la combustion.

Une formulation dite commerciale à base d'EVM comporte de nombreux composants : de la silice, des plastifiants, des stabilisateurs UV…Tous ces composés sont susceptibles de réagir avec les additifs retard et feu et de modifier leur comportement. Pour déterminer si l'utilisation d'un retardateur de flamme est ou non envisageable, ce dernier doit donc être évalué dans une matrice reflétant la composition d'un matériau commercial.

Divers types d'additifs sont susceptibles d'être intégrés une matrice à base EVM, car reconnus efficaces dans l'EVA :

- les hydroxydes métalliques (trihydroxyde d'aluminium, dihydroxyde de magnésium, magnésite…)
- les dérivés phosphorés (polyphosphate d'ammonium, pyrophosphate, phosphore rouge)
- les dérivés mélaminés (mélamine, cyanurate de mélamine, borate de mélamine, phosphate/polyphosphate de mélamine)
- les graphites (graphite expansé ou expansible)
- les nano-additifs (nanotubes de carbone, silice nanométrique, montmorillonites…)

Afin de sélectionner les composés prometteurs, un screening des retardateurs de flamme précités a été mis en œuvre dans une formulation commerciale complète, dont la composition est décrite en *Table 1.* La gamme des dérivés phosphorés a été élargie aux phosphinates (diéthyle phosphinate d'aluminium OP1230, phosphinate de zinc et combinaison OP1230- polyphosphate de mélamine OP1311).

Table 1 : Composition d'une matrice « classique » à base d'EVM

Composant	Taux (phr)
Levapren 600HV (EVM)	100
Additif(s) retard au feu	X
Silice	30
Noir de carbone	2
Plastifiants	24
Stabilisant	2
Peroxyde	1
Co-agent	6
Total (phr)	*165 + X*

Les résultats de l'évaluation en termes de propriétés feu ont démontré que les hydroxydes métalliques restent les plus efficaces dans ce type de formulation, mais l'utilisation d'OP1230 en plus faibles concentrations permet d'obtenir des propriétés légèrement inférieures mais qui restent acceptables et surtout une dureté du matériau moins élevée. Ces deux familles de composés, les hydroxydes métalliques et les phosphinates, ont été retenues.

Dans l'objectif de maximiser l'efficacité de ces additifs, par l'obtention d'effets de synergie, diverses combinaisons associant les hydroxydes métalliques, les nano-additifs, les dérivés mélaminés et les phosphinates ont été investiguées. Quelques associations prometteuses en termes de propriétés retard au feu et de dureté ont été découvertes : OP1230 et phosphate de mélamine, OP1230 et borate de mélamine à l'effet suppresseur de fumées, et ATH et OP1230.
La dernière association, ATH-OP1230, a été retenue du fait de sa viabilité économique (faible coût de l'ATH). Sa concentration et le ratio hydroxyde métallique-phosphinate optimaux, respectivement 120 phr et 2 :1 (soit 80-40 phr) ont été déterminés pour fournir une formulation commerciale répondant aux critères : faible dureté et haute performance de tenue au feu.

L'ATH, l'un des composants de la combinaison, est très utilisé industriellement mais son mode d'action, considéré comme très simple, n'a jamais été fondamentalement étudié dans des matrices EVM vulcanisé. Il est communément admis que l'ATH agit en phase gaz par émission d'eau lors de sa déshydratation, ce qui dilue les gaz combustibles. L'endothermicité de la déshydratation permettrait également une action en phase condensée par absorption de chaleur, et l'alumine ainsi formée formerait une structure protectrice au sein du matériau.
Afin de vérifier ces hypothèses, le mécanisme d'action de l'ATH a été revisité. La matrice initiale, trop complexe et dont les composés sont susceptibles de réagir avec les additifs retard au feu, a été remplacée par le pur polymère vulcanisé.
La dégradation thermique d'un matériau gouverne ses propriétés retard au feu puisque celui va émettre les gaz responsables de son inflammation et de sa combustion. C'est pourquoi l'influence de l'ATH sur la dégradation thermique de l'EVM a été étudiée, tant sur le plan chimique que cinétique.

Résumé

La dégradation thermique de l'EVM a été caractérisée par l'identification des composés émis en phase gaz, suivis par le couplage des analyses thermogravimétriques à un infrarouge ATG-IRTF. Les composés formés dans la phase condensée, obtenus par traitements thermiques des matériaux (EVM vulcanisé et EVM/ATH) à des températures clefs dans des conditions similaires à celles de l'ATG ont été analysés par Résonance Magnétique Nucléaire (RMN) du solide.

La dégradation thermique oxydante de l'EVM vulcanisé se déroule en cinq étapes :

- déacétylation partielle du matériau et scission des ponts « acétate » reliant les chaînes de polymère
- déacétylation complète engendrant la formation de polyènes et d'acide acétique
- charbonisation (« charring ») du polymère i.e. condensation des polyènes en composés polyaromatiques
- dégradation de la partie aliphatique du char
- oxydation du résidu

En milieu inerte l'EVM vulcanisé se dégrade selon un schéma similaire, mais les polyènes ainsi formés ne charbonisent pas ou peu et se dégradent en composés aliphatiques et aromatiques volatils.

La présence d'ATH au sein de la matrice EVM ne modifie fondamentalement pas son mode de dégradation (thermo-oxydation et pyrolyse) : outre la formation d'alumine et la libération d'eau par la déshydratation de l'ATH, les composés formés sont les mêmes. Cependant la formation d'acétate d'aluminium est suspectée. Il est à noter que la quantité de dioxyde de carbone émise lors de l'oxydation du char est plus importante en présence d'ATH que pour le polymère seul, ce qui suggère un rôle catalytique de l'additif.

La modélisation cinétique de la dégradation thermique des deux formulations a été réalisée selon le schéma présenté en *Fig. 1*.

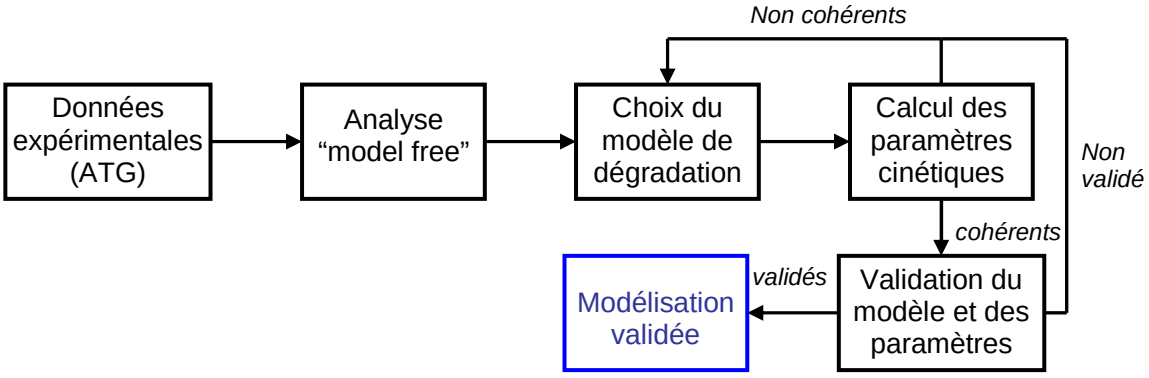


Fig. 1 : Etapes de la modélisation cinétique

La première étape consiste à obtenir les données expérimentales concernant la dégradation thermique des matériaux, ce sur la base d'ATG réalisée à différentes rampes de chauffe (de 1°C à 20°C/min). L'analyse iso-conversionnelle dite « mod el-free » de Friedman montre l'évolution de l'énergie d'activation Ea (et du facteur pré-exponentiel logA, les deux paramètres étant

interdépendants) en fonction du taux de conversion. L'allure de la courbe obtenue permet de déterminer le degré de complexité du modèle de dégradation (une seule étape ou plusieurs, présence d'autocatalyse etc) et les valeurs d'Ea et logA déterminées servent de valeurs initiales pour les algorithmes de calcul.
Les paramètres cinétiques obtenus conformément au modèle de dégradation choisi (5 étapes successives) ont permis de quantifier l'énergie d'activation relative à chaque étape de dégradation. En outre, le modèle de simulation a révélé le caractère auto-catalytique de la déacétylation dans le cas de la matrice EVM vulcanisé.

Après analyse des résultats, les conclusions sont les suivantes :

- la déshydratation endothermique de l'ATH ne modifie pas les paramètres cinétiques de la première étape de dégradation : l'effet de « refroidissement » escompté n'est donc pas démontré
- la déacétylation perd son caractère auto-catalytique lorsque l'ATH est incorporé au polymère. Ce phénomène est attribué aux interactions acide/base de Lewis entre l'alumine formée par déshydratation de l'ATH et l'acide acétique, interactions qui ont pour effet de désactiver l'acide acétique, empêchant sa participation à l'autocatalyse
- la charbonisation du polymère est ralentie et défavorisée par la présence d'alumine. L'hypothèse envisagée est que l'ATH en se déshydratant forme une structure d'alumine protectrice qui ralentit la condensation des polyènes en composés aromatiques (et donc la formation de char)
- la dégradation et l'oxydation du char sont favorisées par la présence d'alumine, qui est par ailleurs un catalyseur d'oxydation bien connu
- dans le cadre de la dégradation en conditions pyrolytiques, la dégradation de l'ATH constitue une étape supplémentaire de dégradation (qui s'opère en tout premier lieu), mais n'influence pas le déroulement des autres sur le plan cinétique

La dégradation de la matrice EVM chargée avec de l'ATH a été également étudiée dans des conditions d'incendie, simulées par calorimétrie conique à un flux radiant de 35 kW/m².
La structure du matériau a été caractérisée par DRX à des temps caractéristiques de l'essai *(Fig. 2)*: avant inflammation, au maximum de chaleur dégagée et en fin de combustion.

Avant l'inflammation le matériau est dégradé uniquement en surface, et la gibbsite (qui est la forme structurale de l'ATH utilisé) se dégrade partiellement en boehmite (AlOOH). On trouve également trace de la boehmite jusqu'au PRHR, en coexistence avec l'alumine Al_2O_3 et une forme hydratée d'alumine $Al_2O_3.H_2O$. Cette dernière peut résulter aussi bien de la déshydratation partielle de la boehmite que de la réhydratation de l'alumine lors du refroidissement de l'échantillon prélevé lors de la combustion. Cependant la présence de formes hydratées, même si elle n'est pas quantifiable, semble indiquer que l'effet endothermique de la déshydratation, peu marqué dans le cadre de

l'analyse cinétique, semble bien jouer un rôle dans le mécanisme d'action de l'ATH. Quant au résidu obtenu en fin de combustion, il est constitué d'alumine formant une structure protectrice en feuillets.

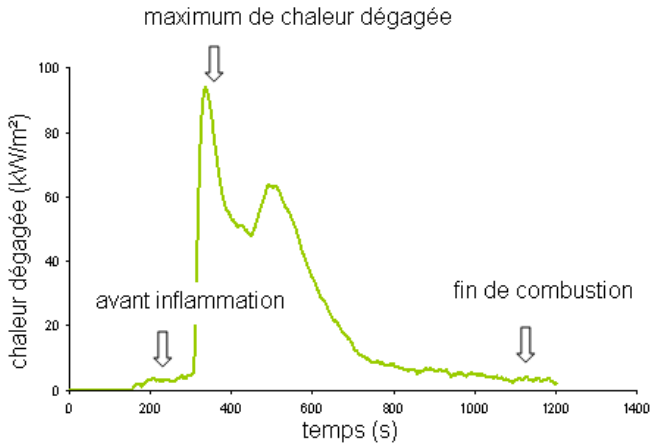


Fig. 2 : Evolution du taux de chaleur dégagée au cours de la combustion par la matrice EVM/ATH, et temps caractéristiques

Le mode d'action proposé de l'ATH est le suivant : avant l'inflammation l'ATH se déshydrate endothermiquement en boehmite, ce qui a pour effet d'absorber de la chaleur et de diluer les gaz de dégradation par dégagement de vapeur d'eau et donc d'augmenter le temps d'ignition du matériau. L'inflammation accélère ensuite la dégradation du polymère et celle de la boehmite qui se dégrade en formant une structure protectrice d'alumine. Cette structure offre, outre la limitation des transferts de chaleur, un rempart à la condensation des polyènes et ralentit la charbonisation et donc la dégradation du polymère. En fin de combustion seuls subsistent l'alumine et du 'char' résiduel.
Ceci met en lumière la complexité du mécanisme d'action de l'ATH, qui est pourtant considéré comme simplissime dans la littérature. Il apparaît que les phénomènes endothermiques ne sont prédominants qu'avant l'inflammation du matériau, et ne peuvent que la retarder. Par la suite l'effet d'écran de la structure d'alumine formée est prépondérant.

Le mode d'action de la combinaison ATH-OP1230 a été investigué selon le protocole utilisé pour le système EVM/ATH.
En premier lieu, les interactions entre les deux composés ont été identifiées. L'étude de la dégradation thermique du mélange en conditions pyrolytiques (et non oxydantes, la dégradation thermo-oxydative de l'OP1230 n'étant pas reproductible) comparée à celle du phosphinate pur, a révélé que les composés formés diffèrent. En effet, l'OP1230 forme des aluminophosphonates qui eux même se dégradent en char et aluminophosphates. La formulation ATH-OP1230 se dégrade quant à elle en aluminophosphates et acide phosphonique organique, mais ne produit pas de char.

L'ATH semble donc influer sur la dégradation thermique de l'OP1230. Le mécanisme proposé pour expliquer ce phénomène implique la chemisorption du phosphinate sur l'ATH. Tout d'abord lié par des liaisons hydrogène à la surface des particules d'ATH, le phosphinate se lie ensuite de façon covalente

par un atome d'oxygène lors de la déshydratation de l'hydroxyde métallique en boehmite. La boehmite ainsi formée se déshydrate à son tour, et le composé phosphoré perd un groupement éthyle pour former un phosphonate transitoire lié par deux liaisons oxygène au substrat. Ce composé transitoire est soit désorbé et forme alors de l'acide éthylphosphonique, soit lié au substrat déshydraté, formant alors un aluminophosphate.

Il existe donc bien une interaction entre l'hydroxyde métallique et le phosphinate d'aluminium. Mais en existe-t-il entre la matrice polymère et les additifs ? Afin de répondre à cette question la dégradation thermique des formulations vulcanisées EVM/OP1230 et EVM/ATH/OP1230 a été caractérisée.

Après analyse de la phase gaz et de la phase condensée il apparaît que la formulation EVM vulcanisé/OP1230 se dégrade en deux étapes apparentes:

- déacétylation du polymère formant des polyènes et de l'acide acétique, sublimation de l'OP1230 et décomposition en aluminophosphonates et aluminophosphate
- décomposition des polyènes en résidus carbonés volatils, formation d'aluminophosphates avec émission concomitante en phase gaz d'acide phosphonique et/ou de phosphonates

Il s'avère que les composés phosphorés issus de la dégradation de la formulation EVM/OP1230 sont identiques à ceux formés par la décomposition de l'OP1230. Cependant quelques modifications concernant la dégradation du polymère ont été observées. La déacétylation du matériau est accélérée par la présence du phosphinate, tout comme la dégradation des polyènes en composés volatils.

La matrice EVM/ATH/OP1230 se dégrade quand à elle en trois étapes apparentes :

- déshydratation de l'ATH en alumine
- déacétylation du matériau et formation de polyènes,
- formation de char, sublimation de l'OP1230 et dégradation en acides phosphonique, phosphinique et diphosphinique organiques

La décomposition thermique de la formulation ne produit donc pas les mêmes composés que ceux obtenus par la dégradation des composés traités séparément. En effet, alors que l'ATH et l'OP1230 ne forment que des aluminophosphates et de l'acide ethylphosphonique, une très large gamme de composés phosphorés est obtenue lorsque la formulation est intégrée à la matrice polymère.

L'étude des résidus de combustion obtenus aux temps caractéristiques dans le cadre de la simulation des conditions incendie, couplée aux résultats de l'étude de la dégradation thermique des matériaux, ont élucidé le mécanisme d'action retard au feu de la combinaison ATH-OP1230 dans l'EVM vulcanisé.

La matrice EVM/OP1230 dans les conditions d'un incendie se dégrade en surface pour former une fine couche de polymère dégradé et d'OP1230 *(Fig. 3)*. Parallèlement, l'OP1230 se sublime et se recondense sous forme d'agrégats dans les porosités du polymère. A l'ignition, la couche à la surface de l'échantillon poursuit sa dégradation et forme une structure de type char contenant des

aluminophosphates. Il est à noter que l'OP1230 sublimé se dépose également en surface, créant un résidu poudreux. Cet OP1230 sublimé doit également avoir une action en phase gaz en interagissant avec les radicaux formés dans la flamme, inhibant ainsi sa propagation. Quant à la couche protectrice formée, elle limite pour un temps les transferts de masse et de chaleur, mais sa faible résistance mécanique ne lui permet pas de résister aux conditions de l'incendie. Ainsi la structure se dégrade, une nouvelle pellicule se forme à la surface du matériau, est dégradée à son tour jusqu'à ce que le matériau soit dégradé en quasi-totalité, ne laissant qu'un mince résidu de char et d'aluminophosphate.

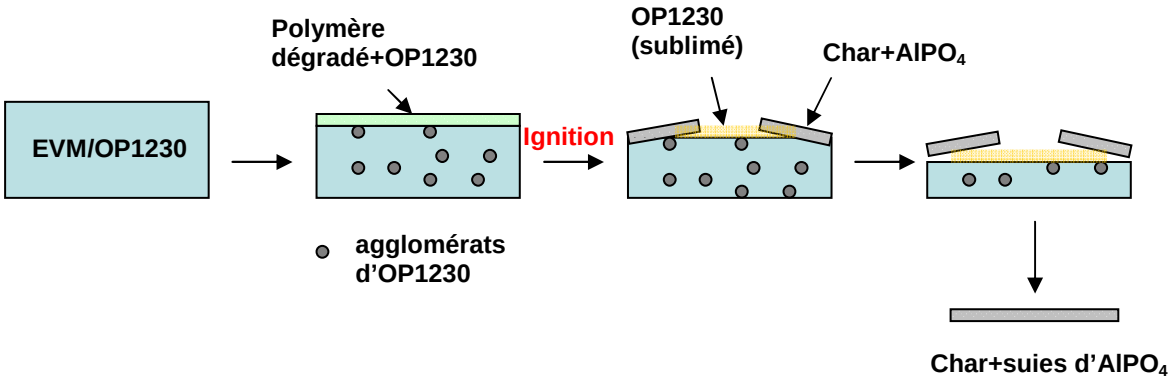


Fig. 3 : Schéma de dégradation de la matrice EVM/OP1230 en conditions incendies simulées par calorimètre mass loss

La matrice EVM/ATH/OP1230 suit un mécanisme de protection relativement similaire *(Fig. 4)*. Avant l'ignition la surface de l'échantillon est modifiée : le polymère se dégrade, et l'ATH se déshydrate. L'eau ainsi formée se retrouve en partie piégée sous la couche de polymère dégradé, des bulles se forment alors à la surface. A l'ignition la couche superficielle se dégrade totalement, libérant ainsi l'eau qui a pour effet de diluer les gaz alimentant la flamme. En outre à la surface de l'échantillon se forme une structure vitreuse issue de la dégradation de la combinaison ATH-OP1230, composée d'aluminophosphates et d'acide éthylphosphonique. Cette structure présente cependant des macroporosités qui dégradent le caractère protecteur de la surface en permettant, quoique ralenti, les transferts de masse. Dès lors, le matériau sous-jacent se dégrade au fur et à mesure de la combustion, de telle sorte que le résidu de fin de combustion est uniquement constitué de la couche d'aluminophosphates et d'acide éthylphosphonique ainsi que de char. La formulation ATH-OP1230 agit donc en ralentissant par la formation d'une structure protectrice résistante la combustion du polymère. D'autre part, les composés phosphorés émis par la dégradation de la matrice EVM/ATH/OP1230, c'est-à-dire des acides phosphoniques, phosphiniques et diphosphiniques organiques sont susceptibles d'agir en phase gaz en inhibant la flamme.

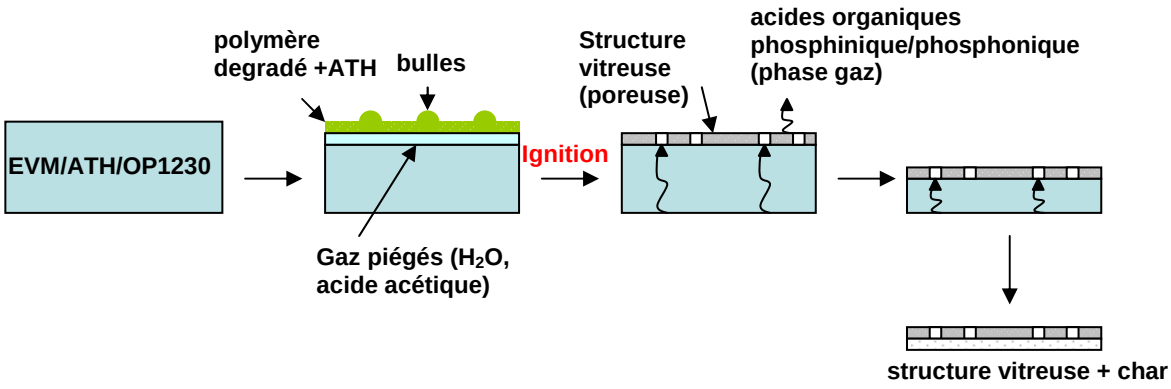


Fig. 4 : Schéma de dégradation de la matrice EVM/ATH/OP1230 en conditions incendies simulées par calorimètre mass loss

---

En conclusion, ce travail a permis de mettre au point une formulation commerciale à base EVM répondant aux attentes industrielles, c'est-à-dire des propriétés retard au feu élevées (au moins identiques à celles des formulations contenant des hydroxydes métalliques) couplées à des propriétés mécaniques satisfaisantes et à une basse valeur de dureté.

Les mécanismes de dégradation thermique de l'EVM vulcanisé ainsi que des matrices chargées en ATH, OP1230 ou la combinaison ATH-OP1230 ont été caractérisés. L'influence des retardateurs de flamme a été mise en évidence, tant sur le plan de la dégradation thermique que sur celui de la combustion, et un mécanisme d'action a pu être proposé pour chacun de ces composés.

L'étude réalisée ouvre également la voie à de nombreuses perspectives de recherche. En effet, l'un des axes à approfondir concerne l'ATH dans l'EVM vulcanisé. L'effet endothermique du à la déshydratation de l'additif, évoqué au cours de la combustion, serait à quantifier afin de quantifier sa participation dans le mécanisme de protection. En outre, la taille des particules d'ATH semble jouer un rôle sur leur efficacité : l'étude de la dispersion ainsi que de la cinétique de formation de la structure d'alumine serait un pas en avant dans la compréhension du phénomène, voire également dans l'optimisation des formulations.
Un autre axe de recherche potentiel concerne la combinaison OP1230-borate de mélamine qui a démontré un effet suppresseur de fumées inattendu. L'étude et la caractérisation du mode de formation des suies dans l'EVM chargé OP1230 ainsi que l'impact du borate de mélamine sur ce mécanisme sont donc à envisager.

INTRODUCTION

Ethylene-acetate copolymers represent the largest volume segment of ethylene copolymer market [1]. In particular elastomeric poly(ethylene vinyl acetate) EVA (called EVM as the vinyl acetate content is comprised between 40 and 80 wt-%) and their vulcanizates are used in a plethora of commercial and industrial fields, such as building (e.g. flooring) or transportation (e.g. engine hoses). These elastomeric materials present several advantages: high mechanical properties, high-filling acceptance and good resistance to aging. Nevertheless the industrial application of ethylene vinyl acetate copolymer has been limited by its inherent flammability. In order to widen the applications, the flame retardancy of this material has been extensively studied. To illustrate this *(Fig. 5)*, the number of patent dealing with EVA flame retardancy increased linearly with time and has been multiplied by six between 1997 and 2007.

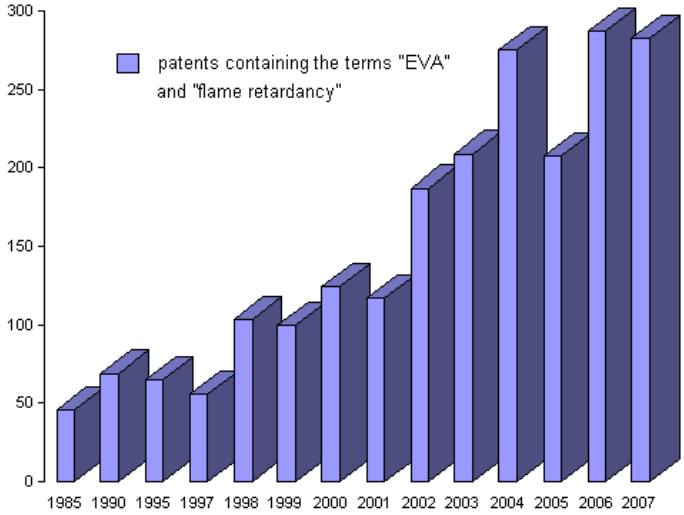


Fig. 5: A growing interest in the field of flame retardancy of EVA, Source: Scifinder, April 2009

Some flame retarded EVM-based formulations are available on the market, but their high level of flame retardant filler leads to a decrease of the mechanical properties. It is thus important to find other solutions to achieve high flame retardant performances while increasing the possibilities in terms of mechanical properties. Hardness, for example, is a major concern for elastomers and it is currently a challenge to obtain a fire resistant material with low hardness value.

The material studied in this project is a complete vulcanized formulation based on EVM (more precisely an EVA with 60 wt-% vinyl acetate), very close to that commercialized by the company Lanxess (Leverkusen, Germany). One of the objectives is to determine FR additives or combinations of additives susceptible to provide comparable or improved fire performances with regard to the mechanical aspects.

Having a good knowledge of the material is a basis to investigate potential solutions to flame retard EVA-based formulations. The first chapter of this PhD reviews the general properties of EVA and its vulcanizates. The synthesis of EVA copolymer, its mechanical, thermal and fire properties are

commented. Vulcanizates are also highlighted, through the description of the various additives they are composed of. The mechanical and fire performances of some of typical vulcanizates formulations are also detailed, such as their industrial applications.
To allow the selection of potential flame retardant additives the second section of the chapter reports the basics of flame retardancy and the various mechanisms of action which can be involved. The fire retardants existing in the market or described in the literature and used in EVA are then reviewed.

The second chapter describes the evaluated materials, that is to say EVM-based formulations. Their composition and compounding will be detailed, such as the flame retardant additives used in the formulations. It also deals with the experimental techniques used in this work. The methods allowing the evaluation of the thermal, flame retardant and mechanical behaviour of the materials are presented. The analysis techniques necessary to carry out the comprehensive investigations on the flame retarded matrices are also described.

The main goal of the industrial project was to provide a flame retardant EVM-based formulation with satisfactory mechanical behaviour. The third chapter is thus devoted to the screening of fire retarding additives in the complete vulcanizates in order to propose a selection of promising additives. The selected additives are then tested in innovative combinations to develop synergies. The optimization of the commercial formulation with the best flame retardant combinations, that is to say aluminium trihydroxide (ATH) and aluminium diethyl phosphinate (OP1230) will be detailed.

The fourth chapter has the aim to revisit the mode of action of ATH, as it has never been fundamentally studied in a vulcanized EVM matrix. Indeed, previous chapter demonstrates that aluminium trihydroxide is the major component of the flame retardant combination with phosphinate. Moreover, thanks to its low price and high efficiency (even if it needs to be incorporated at very high loadings), it remains the most used additive for elastomers. The influence of ATH on the degradation mechanism of the polymeric matrix is first presented. Then, the kinetic modelling of the thermal degradation of the matrices is reported. In the last section of this chapter the mechanism of action of ATH will be discussed.

The last chapter of this manuscript is dedicated to the synergistic effect produced by the ATH-OP1230 combination in vulcanized EVM. The potential chemical interactions between the additives will be studied, such as the interactions between the polymeric matrix and the flame retardant compounds. To complete these investigations the physical aspect of residue created during combustion will be the subject of the last part of the chapter.

CHAPTER 1 – STATE OF THE ART

The first patent dealing with the production of ethylene-vinyl acetate copolymer (EVA) was filed in 1938 [2]. Nevertheless, it took over twenty years until the polymerization process allowed an industrial production of the material. Today, a large panel of EVA is commercially available, for a wide range of industrial applications.

This chapter aims to give an overview of the mode of production, of the raw material properties and of the applications of poly(ethylene vinyl acetate) as well as to understand the various strategies to make it flame retardant. This chapter aims to familiarize the reader with the used material, with describing briefly processes and properties.

1. Ethylene vinyl acetate copolymer (EVA)

Poly(ethylene vinyl acetate), noted EVA, results from the copolymerization of ethylene and vinyl acetate monomers *(Fig. 6)*.

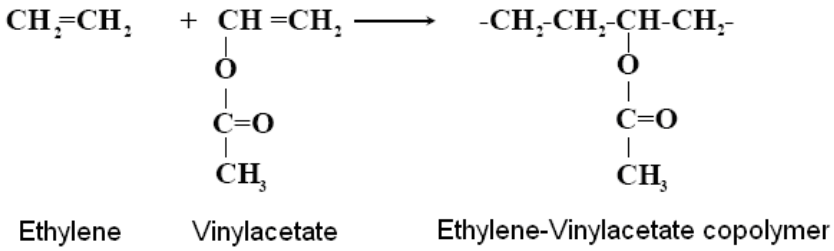


Fig. 6: Schematic representation of the polymerization reaction

This reaction can be carried out for every ratio of the co-monomers, and the vinyl acetate content determines the behaviour of the resulting material *(Fig. 7).* If vinyl acetate (VA) is added up to 33 wt-% the copolymers are still thermoplastic, and above 80 wt-% the properties of the poly (vinyl acetate) become predominant: these thermoplastic materials are denoted by “EVA”.
Between 40 and 80 wt-% of VA, the material exhibits an elastomeric behaviour and is generally noted “EVM”.

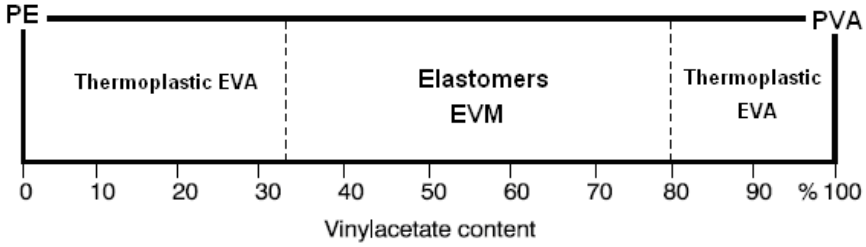


Fig. 7: Schematic classification of ethylene-vinyl acetate copolymers according to their VA content

1.1 Polymerization mechanisms

The radical copolymerization of ethylene and vinyl acetate is known since 1938 [3]. It is carried out under high pressure and at relatively low temperature. As an example, at 1000 bar and 90℃ the copolymerization parameters are quite close for both monomers [4]. Consequently, the distribution of the co-monomers along the chain is random. Higher percentages of ethylene can be obtained with increasing the temperature. Higher rates of ethylene incorporation with increasing pressure have also been found [5]; this was attributed to heterogeneous reaction conditions, that is to say a phase separation diminishing the contact between VA and ethylene [6, 7]. Nuclear Magnetic Resonance (NMR) investigations confirmed the random distribution of monomers in EVM-type copolymers [8].

Polymerization is initiated with peroxides, hydroperoxides or azo compounds [9]. The choice of initiators depends on the polymerization temperature and the desired polymerization time. Important crude polymer properties, such as short-chain branching, depend strongly on these parameters [10]. An ethylene-vinyl acetate copolymerisation process has been described on a laboratory scale that uses organo-metallic catalysts. The catalysts are based on rhodium(III) chloride-triethyl aluminium complexes [11].

EVM solid rubber is produced in industry by three processes, depending on the expected vinyl acetate content (VAC) of the polymer *(Fig. 8)*. The covered vinyl acetate range is 0-45 wt-% for high-pressure process, 55- 100 wt-% for the low-pressure emulsion process and 30-100 wt-% for the medium pressure process in solution.

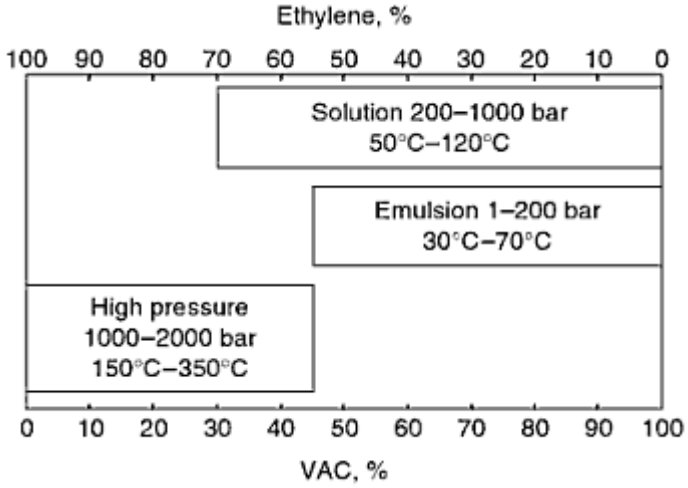


Fig. 8: EVA production methods and products thereof

1.1.1 High-Pressure Process

The high-pressure or bulk process is similar to the production process for low-density polyethylene (LDPE). It is carried out at 1000- 2000 bar and 150- 350 ℃ without the addition of solvents. Stabilis ed

vinyl acetate is first mixed with pre-cooled ethylene, which has been compressed to 100- 500 bar. The monomer stream is compressed further and charged continuously to a stirred autoclave or tube reactor [9]. The initiator solution and, if required, a chain-transfer agent (as an alkane, a ketone, or an aldehyde) are injected. The conversion is 10- 20 %, based on the monomers. The reaction mixture is then depressurised in stages; the residual monomers are separated and recycled. The polymer melt is chilled and palletised.

Monomer vinyl acetate has chain-transfer properties that limit the molecular mass of the polymer chain. As a result for the high VA concentration in EVA obtained from the high pressure process, only relatively low average molar masses can be obtained [12]. High- pressure EVM products are therefore produced only up to a vinyl acetate content of 45 wt% and with Mooney[i] viscosities of 15- 20 Mooney units.

1.1.2 Solution Process

The solution process [13] is operated in the medium-pressure region (200 - 1000 bar) at 50- 120 °C using solvents with low transfer constants. Suitable solvents are *tert*- butanol [14-16] benzene, toluene, methyl acetate [12], methanol [17, 18], and dialkyl sulfoxides [19]. The process enables the production of gel-free copolymers that are characterised by a high Mooney viscosity (20- 35 Mooney units) and a high vinyl acetate content (from 40 to 80 wt%).

Polymerisation occurs in a cascade of stirred-tank reactors at conversions of 50 to 70 %. During workup the product solution is freed from solvent and residual monomers. Pellets from 2 to 4 mm in size are finally produced for formulation, which give a free-flowing material when treated with a suitable coating to lower the self-adhesion of polymer particles.

1.1.3 Emulsion Process

The emulsion process operates between 30 and 70 °C at a pressure lying between 1 and 200 bar [20]. The polymers have vinyl acetate contents between 30 and 100 wt% and are produced as lattices. The products are not suitable for vulcanisation because of their high proportion of gel. Dispersions of EVM copolymers are used as binders for exterior paints and plasters, as components of wood adhesives, and as thickeners in varnishes.

[i] Mooney viscosity is defined as the shearing torque resisting rotation of a cylindrical metal disk (or rotor) embedded in rubber within a cylindrical cavity. ASTM D1646

1.2 Mechanical properties

The different copolymerization processes allow obtaining a large variety of EVA polymers covering a wide range of mechanical properties. The chemical composition of these materials (the vinyl acetate content) is directly linked to these mechanical properties.

In order to give an overview and a range of the most used polymer characteristics, the mechanical properties of a 33 wt-% VAC EVA are gathered in *Table 2*.

Table 2: Characteristic properties of EVA (33%VA)

Property	Value
Density (g/cm^3)	0.95
Surface Hardness (ShA)	65
Tensile Strength (MPa)	10
Elongation at Break (%)	900
Melting Temperature Range (°C)	130 - 190

The hardness Shore A[i] value is about 65 ShA, and the tensile tests reveal an elongation at break (EAB) of 900% and a tensile strength (TS) of 10 MPa. These properties can be influenced by the composition of the copolymer (that is to say the vinyl acetate percentage) or by its molecular weight [21].

The evolution of some of the properties of EVA, that is to say the glass transition temperature T_g, the crystallinity, the melt temperature (T_m) and the heat of fusion ΔH_g, depending on the VA content is reported in *Table 3*. Both crystallinity and T_g are very important for the low-temperature properties of an elastomer as they condition the mobility of the polymer chains.

Polyethylene exhibits very high crystallinity, because of the regular structure of the polymeric chain. Vinyl acetate groups, because of their voluminous acetate side-chain disturb the regularity and consequently reduce the crystallinity (from 30 % for a polyethylene to 6 % for an EVA with 50 wt-% VA) [22]. The glass transition temperature T_g steadily increases. The melting temperature decreases with increasing vinyl acetate content. This is due to a deterioration of the crystallite perfection. The ethylene sequences, which are able to crystallize, become smaller and, thus, the resulting crystallites are smaller and less perfect.

[i] The shore A Hardness is the relative hardness of elastic materials such as rubber or soft plastics The hardness value is determined by the penetration of an indenter foot into the sample. ASTM D2240 or ISO 868

Table 3: Influence of the VA content on thermodynamic properties of EVA and PE [22]

VA content (wt-%)	T_m (°C)	T_g (°C)	Crystallinity (%)	ΔH_g (J/g)
0 (PE)	133	-120	30	293
21	86	-35	26	75
28	77	-34	22	65
40	36	-33	9	12
50	12	-31	6	6
60	-	-26	-	-
70	-	-17	-	-
90	-	17	-	-

The increase of the VA content thus leads to some changes in the material behaviour (*Table 4)*: the introduction of the vinyl acetate monomer leads to crystallization decrease, and thus to the diminution of material rigidity. This allows more flexibility and then a better impact resistance [23]. Up to 80 wt-% VAC, the elastic properties and the impact strength of the material is improved, such as the polarity and the filler acceptance of the polymeric matrix. Nevertheless, low temperature properties are damaged. The molecular weight is also an important factor, as its diminution decreases the hardness and mechanical properties (EAB, TS) of the resulting material.

Table 4 : Influence of the VA content and of the molecular weight on EVA properties [23]

Vinyl acetate content ↗	Cristallinity - Melting point ↘ Flexibility - Impact strength ↗ (0-80% VA, then ↘) Low temperatures properties ↘ Polarity- Adhesion - Filler acceptance ↗
Molecular weight ↘	Fluidity - MFI - Wettability ↗ Mechanical properties ↘ Hardness ↘

So, the structure and composition of the copolymer is a major factor influencing the mechanical properties of the polymeric matrix, such as its thermal degradation.

1.3 Thermal degradation

The thermal stability of EVA also depends on the VA content of the copolymer. The thermo-oxidative degradation of EVA (or EVM) occurs in three main steps *(Fig. 9)*.

It starts with the elimination of acetic acid (chain stripping) in the temperature range of 300 to 380°C, leaving a double-bond in the chain backbone, hence EVA is converted into poly(ethylene-*co*-acetylene), producing acetic acid and polyethylene which undergoes further degradation [24]. It is

noticeable that the higher the vinyl acetate content, the more pronounced is the first step since it is linked to the vinyl-acetate group degradation.

The second step (400 to 500℃) corresponds to the degradation of the poly(ethylene-co-acetylene) chains. The third step (500 to 520℃) may be assigned to the thermo-oxidative degradation of the carbonaceous residue formed during the degradation of the partially unsaturated polyene chains [25].

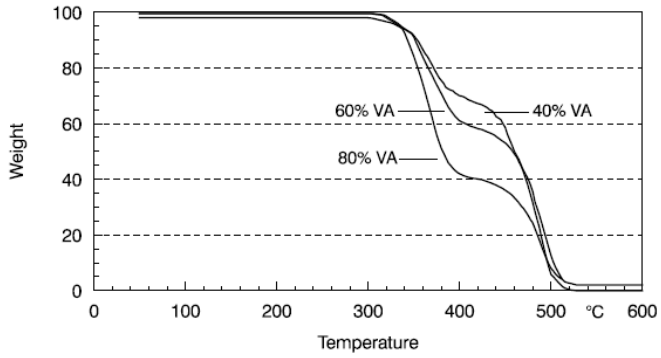


Fig. 9: Thermogravimetric analyses of Levapren elastomers: 40, 60, and 80 wt-% vinyl acetate copolymers (heating-rate: 20℃/min, under air)

The degradation mechanism and kinetics of EVA was investigated by Rimez *et al.* [26, 27]. The author has shown that between 300 and 400 ℃, acetic acid is eliminated (deacetylation), leaving a highly unsaturated residue or polyene *(Fig. 10)*.

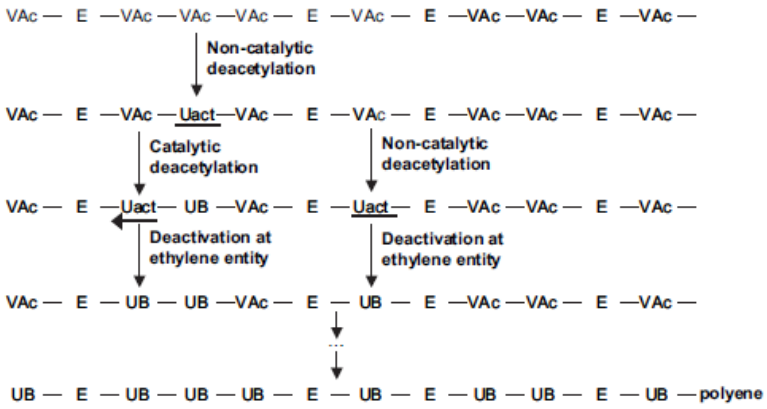


Fig. 10: Schematic representation of the deacetylation of EVA. The term UB corresponds to unsaturated bonds in the polymer chain Uact to active double bond [27]

The deacetylation of poly (vinyl acetate) (PVA) is autocatalytic *(Fig. 11)*. The catalysing double bond is denoted as an active unsaturation in the polymer main chain (Uact). After the elimination of acetic acid in a catalytic deacetylation reaction, a new active double bond Uact is formed and the former catalysing double bond is simultaneously deactivated and therefore denoted as UB [28]. Upon incorporation of ethylene entities (denoted E) into the polymer backbone, autocatalysis decreases.

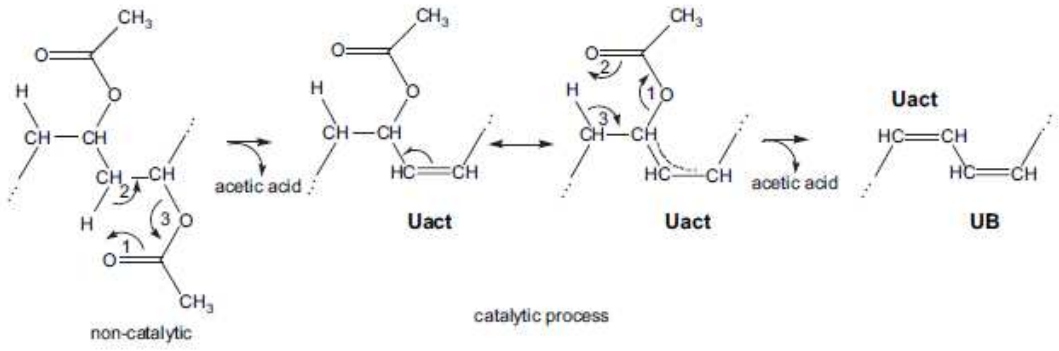


Fig. 11: Deacetylation process occurring during the thermal degradation of EVA [27]

Between 400 and 500 °C, the polyene degrades furthe r by chain scission reactions in inert conditions or aromatises in an oxidative environment.

The inert degradation of the polyene of all EVA copolymers is characterised by the balance between the formation of aromatic and aliphatic volatiles. The aromatic volatiles originate from deacetylated vinyl acetate entities and the aliphatic volatiles are formed by chain scission reactions of ethylene entities. When the amount of VA increases in the (co)polymers, the aromatic traces become higher than the aliphatic ones.

In an oxidative environment, the polyene degrades into a carbonaceous layer, called char, and oxidized eventually into CO_2 beyond 500 °C. It is noteworthy that charring only occurs for EVA with high vinyl acetate content. Large exothermal effects are found for each degradation step. This indicates the occurrence of additional oxidation reactions during deacetylation; of an important re-organisation of the polyene during char formation and of oxidation of the latter into CO_2.

The mechanistic model is proposed in *Fig. 12*. The term AB corresponds to aromatized char and Ac to acetic acid.

A Deacetylation and formation of polyene

VAc (s) → Uact (s) + Ac (g)	Non-catalytic deacetylation
VAc (s) + Uact (s) → Uact (s) + UB (s) + Ac (g)	Catalytic deacetylation
Uact (s) → UB (s)	Deactivation

B Inert degradation of polyene

Chain scission reactions:

UB (s) → aromatic volatiles

E (s) → aliphatic volatiles

C Oxidative degradation of polyene

Charring	Oxidation of the char
UB (s) → AB (s) + H_2O (g), aromatic volatiles	AB (s) → CO_2 (g)
E (s) → aliphatic volatiles	

Fig. 12: Mechanistic model for deacetylation (A), inert (B) and oxidative (C) polyene degradation of EVA [27]

Kinetic parameters (pre-exponential factor *A* and activation energy E_a) of the degradation reactions of EVA60 were determined by the authors [26]. The values are reported in *Table 2*.

Table 5: Kinetic parameters of the degradation processes of EVA (optimized for EVA 60 wt-% VA) [26]

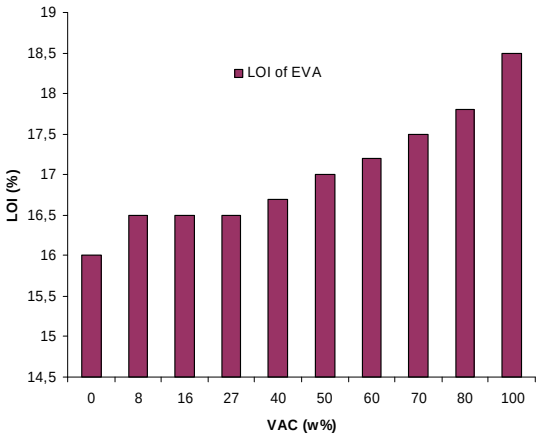
Reaction processes		logA (s, kg, mol)	E_a (kJ.mol^{-1})
Deacetylation	Non-catalytic	12.7	177.5
	Catalytic	11.6	163.8
	Deactivation	14.3	178.5
Inert chain scission	UB → aromatic volatiles	10.4	176.9
	E → aliphatic volatiles	16.3	260.7
Oxidative processes	E → aliphatic volatiles	20.3	302.6
	Charring	10.5	173.2
	Decomposition of the char	11.9	211.6

This complete set of parameters, both in inert and oxidative conditions, can be used for the simulation of the full degradation of the polymer.

1.4 Flame Retardancy of EVA

Flame retardants are used to increase the fire properties of materials. But the composition of the material itself can play a role in terms of flame retardancy; and its intrinsic properties (polarity, acidity…) have to be considered in the choice of compatible additives.

Such as the mechanical properties, the reaction to fire of EVA copolymer depends on its VA content [25]. Indeed, the higher the EVA contains vinyl-acetate groups the higher is its Limiting Oxygen Index[iii] (LOI) and the lower is its heat of combustion, but this improvement is not really significant since values remain poor (*Fig. 13* and *Fig. 14*).



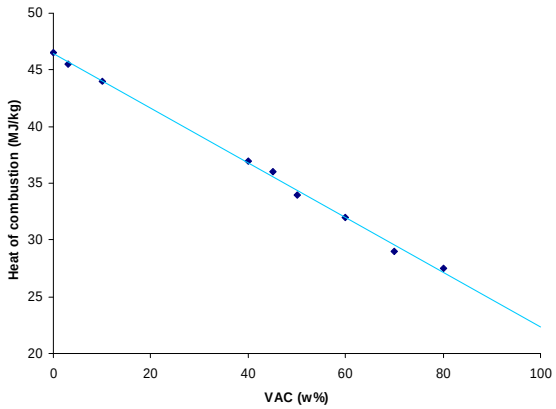


Fig. 13: Influence of the VAC on the LOI of EVA [25] ***Fig. 14: Influence of the VAC on the heat of combustion [25]***

[iii] The limiting oxygen index (LOI) is the minimum concentration of oxygen expressed as a percentage that will support the combustion of a polymer. ISO 4589 or ASTM D2863

For all VA content, the UL-94 rating of the copolymer is HB. So, the virgin polymer is considered highly flammable and needs to be flame retarded to achieve legal fire requirements.

2. Vulcanized EVM formulations

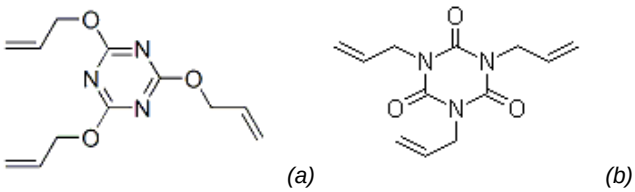
EVA is generally used as a flexible thermoplastic. To obtain sufficient elastomeric properties it is necessary to reinforce the EVM structure by cross-linking: EVA can be vulcanized. Depending on the final required properties (mechanical behaviour, UV-resistance, flame retardancy…) complex formulations containing specific additives, can be built. In this part these compounds are detailed the curing agents, the special additives, and the fillers commonly used in EVM vulcanizates. Some typical EVM-based formulations are also presented: their mechanical and flame retardant properties are evoked.

2.1 Curing system and additives

2.1.1 Curing system

EVM elastomers belong to the group of rubbers with fully saturated backbone. As there are no sulfur-curable sites in the side-chain, they have to be cured via radical reaction trough the use of peroxides [29] or high-energy radiation [30].

The mechanism of the reaction is first an abstraction of an hydrogen atom from the polymer chain leading to the formation of a reactive radical site. Then two polymer radicals can combine which results in a polymer network. The network formed by those reactions is very irregular. In order to improve the network, the addition of compounds named co-agents, with multiple double-bonds, e.g. triallylcyanurate (TAC) or triallylisocyanurate (TAIC) *(Fig. 15)* is necessary.



(a) *(b)*

Fig. 15: Structure of triallylcyanurate (a) and triallylisocyanurate(b)

They are often referred to act as activators. The effect is described as an addition to the peroxide radical site at the polymer chain and transfer of the radical to the activator. The network is formed by reaction of the transferred radical with another chain.

The selection of the appropriate peroxide is determined by the mixing temperature, and the possible need for odorless materials. Among the peroxides available on the market bis(tert-butylperoxy isopropyl) benzene *(Fig. 16)* is widely used [12].

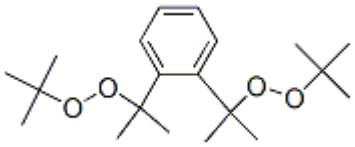


Fig. 16: Structure of bis(tert-butylperoxy isopropyl) benzene

The resulting network of a peroxide-coagent cured system is pictured in *Fig. 17*. Cross-links can be derived from (A) polymer radicals, (B) coagent forming effective cross-links, and (C) thermoset domains of coagent grafted to polymer chains.

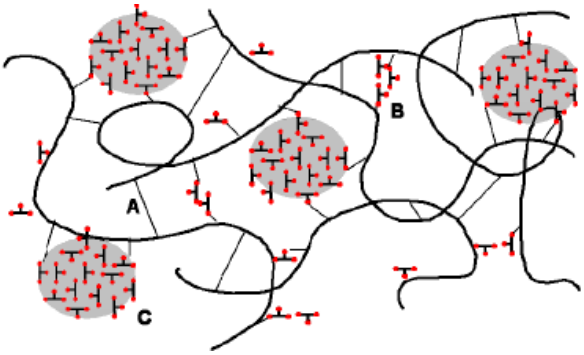
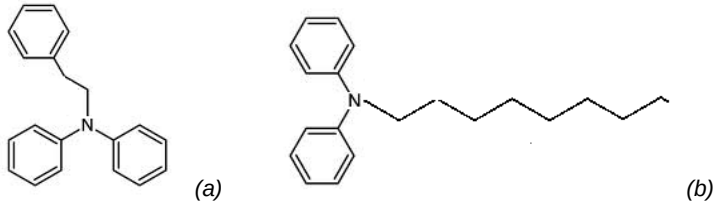


Fig. 17: Idealized network derived from a peroxide-coagent cure system [31].

2.1.2 Antioxidants

Since they have no reactive double bonds, EVA elastomers have an inherently excellent oxidation resistance. But for an optimum stability it is necessary to add approximately 1 phr of an antioxidant. Here it is necessary to select the right substance, because many well-known antioxidants cannot be used in peroxide cure. For an optimum resistance, the addition of a small quantity of Vulkanox OCD or Vulkanox DDA (styrenated or octylated diphenylamine (SDPA or ODPA) respectively, described in *Fig. 18* is recommended [32]. Aralkylated phenols can be used as non-staining antioxidants [33].



(a) *(b)*

Fig. 18: Structure of SDPA (a) and OPDA (b)

To protect the vulcanizates from hydrolysis at elevated temperatures and higher humidity the addition of a polycarbodiimide may be necessary.

2.1.3 Plasticizers

The use of plasticizers is not mandatory in EVM grades with low Mooney viscosity. Plasticizers can be used especially in compounds based on high viscosity grades, or in highly-filled mixtures. The most appropriate plasticizers for EVM compositions are paraffinic mineral oils. Oils containing double bonds (aromatic or naphthenic) should be avoided as they can affect the peroxide curing.
Synthetic plasticizers should be added to improve the cold flexibility of high vinyl acetate containing grades. Good results have been obtained by using adipate- and sebacate-type plasticizers.

2.1.4 Fillers

Carbon black is used in EVM compounds up to 60 phr to enhance the electrical conductivity of the materials [34].
White fillers denote reinforcing inorganic fillers. The term “white” is employed to indicate that these fillers do not include coloured additives such as carbon black. They have to be selected carefully since they can decrease the degree of vulcanization. Good results have been achieved by using talcum (or micro-talcum), silica and neutral clay. Active silica provides higher tensile strengths but the degree of curing is reduced. A vinyl silane compatibilizer is recommended with these white fillers [35].
Other fillers can be added, such as colouring agents or flame retardant additives. The colouring agents should be selected carefully as many organic pigments disturb the peroxide cure.
It is noteworthy that the use of a small amount of stearic acid (or zinc stannate as a substitute) reduces the sticking of compounds based on low-viscosity EVM, and improves the fillers dispersion in the same time.

2.2 Properties of typical cured EVM formulations

To achieve acceptable fire and mechanical properties (especially for EVM), the use of fillers and/or additives acting as flame retardants is necessary. According to the important number of components of a formulation and to the variety of additives potentially used for each function, a quasi-infinite number of combinations can be envisaged. In this part, two typical examples of cured EVM-based formulations are presented: a common injection molding material and a Flame Retarded Non Corrosive formulation (FRNC), close to the one further studied in this manuscript.

Table 6 reports the recipe of a common injection molding compound [36]. It is based on an EVM with 60 wt-% VA, and the main filler is carbon black (25 wt-%).

Table 6: Formulation of a compound for injection moulding

Compound	Content (phr)
EVM (60% VA)	100
Carbon black	40
Stearic acid	1
Polycarbodiimide stabilizer	3
Antioxidant SDPA	2
Polyethylene wax	2
Zinc stannate	2
TAIC (triallylcyanurate)	1.5
Peroxide	5
Total	**156.5**

The mechanical testing of the formulation reveals the physical properties of the vulcanizates *(Table 7)*. The hardness value of 62 Shore A meets the requirements of a majority of application fields, such as the elongation at break (390 %) and the tensile (16 MPa). Nevertheless the fire properties of such a compound are too poor to be used for applications following strict fire regulations.

Table 7: Vulcanizates physical properties

Physical properties	Value
Shore A at 23℃	62
Shore A at 70℃	50
Tensile strength (MPa)	16
Elongation at break (%)	390
Modulus at 100% (MPa)	3.2

A typical recipe for Flame Retarded Non Corrosive (FNRC) formulations [36] is described in *Table 8*.

Table 8: Typical FRNC formulation

Compound	Content (phr)
EVM	100
ATH (aluminium trihydrate)	190
Silane	2
Zinc borate	10
Dioctylsebacate	6
Co-agent	6
Peroxide	0.5
Antioxidant	1
Total	**315.5**

The elongation at break, tensile strength and hardness Shore A of the FRNC compound with various VA content after compounding and after aging for 14 days at 150℃ are gathered in *Fig. 19.* It appears that the hardness value (around 65 ShA) and the tensile strength are comparable to that of the injection molding compound, but the elongation at break are damaged (less than 250% for EAB). However the mechanical properties of the materials are enhanced by an increase of the vinyl acetate content (increasing the matrix polarity and thus the compatibility with the fillers). Concerning the aging there is a satisfying conservation of the mechanical properties, especially for EVA with medium VA content.

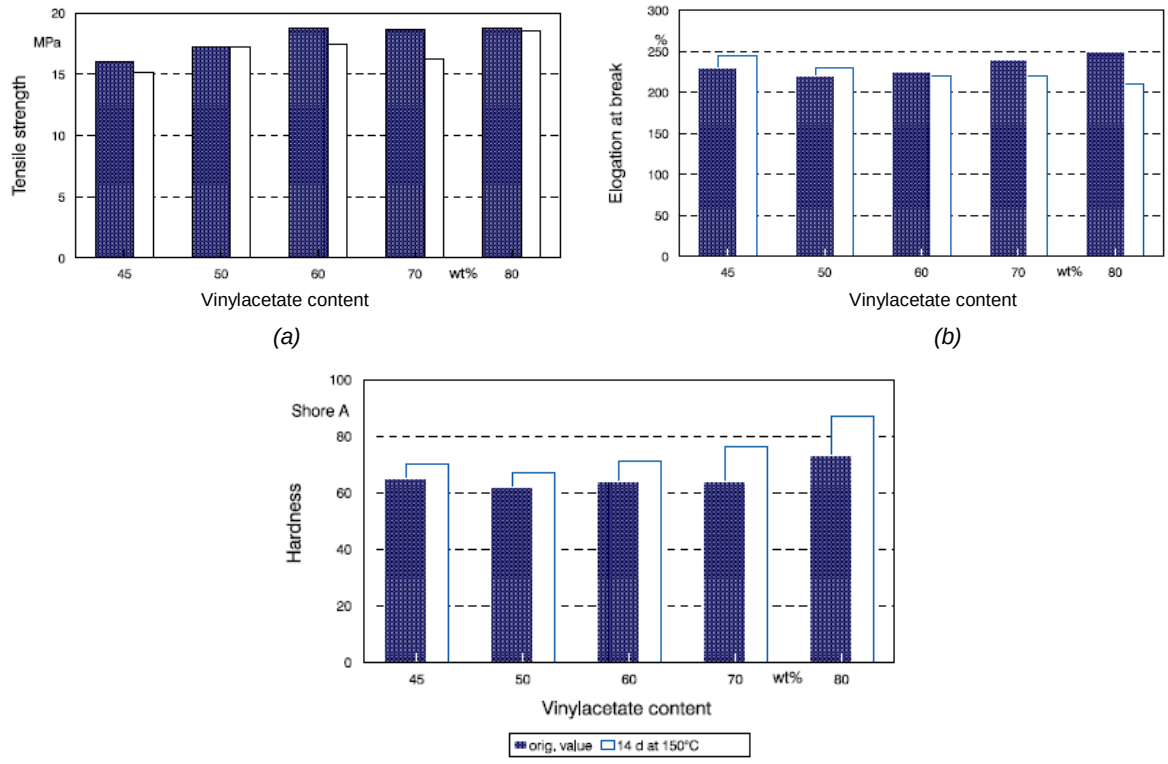


Fig. 19: Tensile strength (a), elongation at break (b) and hardness (c) of FRNC compounds with different vinyl acetate contents, aged 14 days at 150℃, compared t o the original values[22]

LOI confirms the great flame retardant behaviour of the formulation. The VA content also plays an important role as between the compound with 40 wt-% VA and the material with 80 wt-% VA, the LOI is increased of 14 vol-%. The main advantage of the FRNC compound is the fact that no halogenated compound is used, so that they did not produce any corrosive combustion gases in case of fire [37].

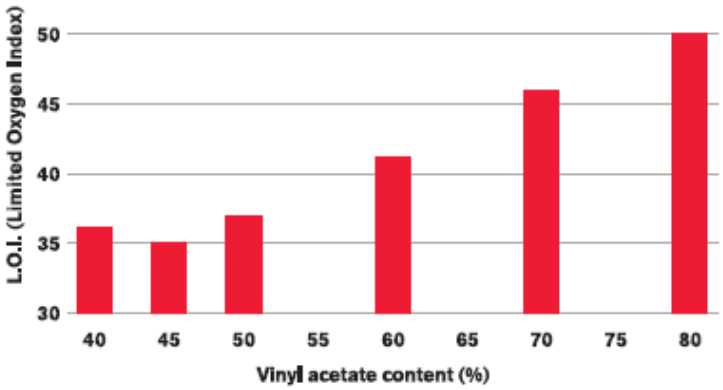


Fig. 20: LOI results of the FRNC compound [38]

Furthermore, depending on the additives incorporated into the EVM-based vulcanized formulation a large range of mechanical and fire properties can be achieved, allowing the use of EVM in a wide panel of application fields.

2.3 Industrial applications of EVM and vulcanizates

The main areas of application of EVM rubbers are in the cable sector, adhesives, and the modification of thermoplastics. As a result of the increasing high temperature requirements in the automotive industry, EVM is being introduced for use in fuel hoses and seals or floor covering *(Fig. 21* and *Fig.18).* EVM also has excellent dynamic properties which make it a suitable material for roll covers. In the cable sector, EVM is used in heat-resistant electrical insulation (in floor heating, ignition wires, night storage heaters, rear window heating, electric motors, toasters and grills) [39].



Fig. 21: Fuel hoses made of EVM (Levapren®)



Fig. 22: Floor covering made of EVA (Levapren®)

Wires and cables, as well as floors and noise absorption mats based on EVM, offer increased safety for people and materials in the event of fire. They are used, for example, in subways, shops, offices, hospitals, ships, control stations, computer centers, and radio or television stations. Underground conveyor belts based on EVM also satisfy strict flame resistance regulations [38].

EVM copolymers with up to 45 wt% vinyl acetate are used as solvent-free, hot-melt adhesives [40]. Formulation with waxes permits control of the melt index and the viscosity of the molten adhesive. Adhesion is strengthened by the addition of adhesive resins. EVM copolymers with 50-80 wt% vinyl acetate can also be used as pressure sensitive adhesive.

In contrast to most common thermoplastic EVA copolymers with low vinyl acetate content, EVM copolymers can be processed easily for thin layer applications. The specific molecular weight distribution allows the preparation of high quality, transparent and homogeneous composites, either as cast film or as blown film.

EVM copolymers are also suitable for modifying thermoplastics, such as poly (vinyl chloride) (PVC), styrene-acrylonitrile copolymers (SAN), and cellulose esters. For example, EVM-PVC graft polymers with 5-10% EVM (45 wt% vinyl acetate) give impact-resistant products, which are used in plastic windows. EVM copolymers with 60- 70 wt% vinyl acetate are completely compatible with PVC and could thus be used as polymeric plasticizers. These types of mixtures are processed to give sheets for car fittings.

Ethylene-vinyl acetate copolymers can be completely or partially saponified. Here the ester groups are formally converted into vinyl alcohol units, with loss of acetic acid. EVM grades modified in this way are suitable for woven fabric coatings and as hot-melt adhesives. Other applications are in pigment dye printing, paints for paper, and varnishes, where they are used as thickeners.

The so-called flame-retardant, noncorrosive (FRNC) application is especially important. EVM vulcanizates containing flame-retardant fillers, such as aluminium hydroxide, magnesium hydroxide, or zinc borate, meet most of the safety requirements in case of fire. They are characterized by a low flammability, a low smoke density release and the emission of corrosion-free combustion gases. They are mainly used in the field of electrical cables or transportation.

2.4 Conclusion

This part has given a brief description of the polymerization mechanisms and processes of EVA, and of its thermal, mechanical and fire properties (LOI). The different components of EVM vulcanizates were evoked, and two typical examples of EVM formulations were presented. The subject of the project is the reaction to fire of EVM and vulcanizates. Indeed, the various industrial and commercial applications of the polymer and of the vulcanizates imply that it is necessary to cover a large range of mechanical properties, as well as drastic flame retardant properties to comply with the strict fire requirements of the fields of building or transportation. Some FRNC based on metal hydroxides already exist, with satisfactory mechanical and fire properties. But it is now important to widen the

flame retardant panel to be used in EVM and vulcanizates to obtain larger ranges of mechanical and thermal properties. That is why the next part will review the flame retardancy of EVA.

3. Flame retardancy of EVA

To have a good understanding of the strategic routes to obtain flame retarded EVA it is necessary to first answer some basic questions about flammability of polymers and flame retardancy.

At first, **why is a polymer flammable?** When it is exposed to heat or flame, during a fire scenario for example, the temperature of a polymer increases, leading to its thermal degradation. Thus, chemical bonds of the polymeric chains are broken to generate highly flammable volatiles. These volatile compounds spontaneously form combustible mixtures with air which ignite easily and burn with a high velocity through the formation of radicals (implying H• and OH•). So, a low thermal stability associated to the release of highly flammable volatile molecules is responsible for the flammability of the material.

Second, **how is it possible to decrease flammability**? Two major ways can be followed: influencing physically the combustion process, or leading a chemical action in the condensed and/or in the gas phase. Among the processes dedicated to the condensed phase can be cited:

- the artificial cooling of the matrix, by the addition of fillers which decomposes endothermically during combustion (metal hydroxides, carbonates…), thus delaying the polymer degradation [41]. This effect is generally associated to a ceramization effect, that is to say the creation during the degradation of a ceramic protective structure [42, 43].
- the creation of a protective layer. The additives can form during combustion a shield with a low thermal conductivity which can reduce heat transfer. It then reduces the degradation rate of the polymer and decreases the pyrolysis gases rate. This is the basic principle of the intumescence process. Intumescence is defined by the creation during combustion of an expanded foamed cellular charred layer on the surface which protects the underlying material slowing down heat and mass transfer [44].

The gas phase modifications concern:

- the dilution of the flame-feeding gases by non-flammable ones. For example the use of metal hydroxides releasing water, or nitrogenated-based compounds generating ammonia [45]
- the flame inhibition. The radical mechanism of the combustion process occurring in the gas phase is interrupted by the radicals generated by the flame retardants. Halogenated and some phosphorus-based compounds are involved in such reactions [46].

The various ways presented above give an overview of the flame retardant principles. Nevertheless the described processes generally not occur singly but are part of a complex process in which many modifications occur simultaneously with one dominating.

Various methods can be used to impart flame retardant properties to polymers, such as the graft-polymerization with flame retarding monomers or the use of surface treatments. The first attempts concerning EVA and flame retardancy indeed consisted in using halogenated fire retardants, grafted into the EVA chain [47]. Our approach will not consider these techniques, so we will only focus in this state of the art on the addition of FR additives in the polymer matrix. Thus, the main question is **what are the common flame retardant additives and what is their influence on the flame retardancy of the elastomeric composites?** We propose to answer those questions it in the following part. The different flame retardant additive classes will be presented, such as their use alone and then in combination in EVA. The flame retardant effect of nano-additives will be determined.

3.1 Halogenated compounds

Halogen, particularly brominated compounds [48, 49], occupied an important position among the fire-extinguishing and fire retardant agents. Halogenated compounds are historically the first additives used in EVA as flame retardants.

3.1.1 Mode of action

To interrupt the combustion process in the gaseous phase, the flame retardant or its decomposition products need to react with the radicals implied in the oxygen-hydrogen combustion mechanism, that is to say $OH^{\bullet}$ and $H^{\bullet}$.

The role of the halogenated FR additives is to interact with the hydrogen radicals formed in the combustion chain reaction. The hydro-halogen acids that are the active retarding elements scavenge the hydrogen radicals and stop the exothermal chain reactions taking place in the combustion process, resulting in a cooling down and decrease of the mass fluxes in the system [50, 51]. The mechanism of the inhibitory action of halogen compounds is described in *Fig. 23* [52] . The active $H^{\bullet}$ and $OH^{\bullet}$ radicals are thus replaced by less active halogens atoms ($X^{\bullet}$).

Decomposition reactions:

$R\text{-}X \rightarrow R\bullet + X\bullet$

$X\bullet + P\text{-}H \rightarrow H\text{-}X + P\bullet$

with R-X the halogenated flame retardant and P-H the polymer

Flame retardation mechanism

$H\text{-}X + HO\bullet \rightarrow H_2O + X\bullet$

$H\text{-}X + H\bullet \rightarrow H_2 + X\bullet$

Fig. 23: Decomposition reactions and flame retardant mechanism of halogen-containing flame retardants

The two critical factors concerning the use of halogenated flame retardants is their thermal stability versus the used polymer [50] and the trapping activity of the halogen atom. According to Rahman *et*

al.[50], the recommended decomposition temperature of the flame retardant halogenated compound should be 50°C lower than that of the host polymer : brominated compounds [49] particularly assess this condition. On the other hand, the trapping activity essentially depends on the size of the halogen atom; therefore the flame retardant efficiency exhibits the following order: I> Br > Cl > F.

To increase the efficiency of halogenated flame retardants, antimony oxide (or trioxide) can be incorporated as a synergist. Two mechanisms take place in the synergistic system [53].
First, the "free radical capture" process takes place in the vapour phase. On combustion at a temperature of over 316°C, the halogen forms hydrochloric or hydrobromic acid that reacts with the antimony oxide to form antimony trichloride, antimony oxychloride, antimony tribromide, or antimony oxybromide acting as "free radical traps" and take up free radicals. They inhibit ignition and pyrolysis in the solid, liquid, and vapour phases. A second process occurs in a solid phase; a charring phenomenon. The antimony oxide promotes the formation of a char through the formation of $SbCl_3$ and SbOCl (dehydrating agents) on the substrate which reduces volatile gas formation.

Halogenated systems offer the advantage of low additive contents to achieve the desired levels of flame retardancy. Moreover, antimony oxide and halogenated organic compounds combine to produce a synergistic action that flame retards plastics at lower loading levels. Many combinations of antimony oxide and halogenated additive systems are available. However, their use is contested because of their potential toxicity, as explained further.

3.1.2 Halogenated compound used in EVA

Halogenated compounds, in particular brominated compounds were used as flame retardants in EVA. The only reference in the scientific literature is that of Yang *et al.* [54]. They investigated the influence of tetrabromo-*p*-cresol and pentabromophenol *(Fig. 24)* on the flame retardancy of EVA and styrene-butadiene rubber (SBR). Their efficiency was demonstrated, and the study was widening to their allyl ether derivatives added as additive in the polymeric matrix.

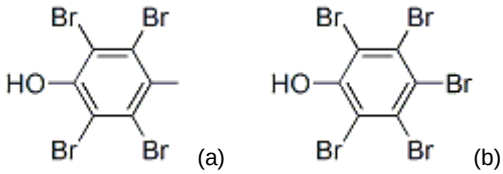


Fig. 24: Chemical structure of tetrabromo-p-cresol (a) and pentabromophenol (b)

3.1.3 Environmental impact

The use of halogenated flame retardants is however contested. Most of them, in particular polybrominated biphenyls and polybrominated diphenyl ethers, are withdrawn as allowed additives since 2006 in accordance to the Risk of Hazardous Substances Directive from the European Union.

Apart from the positive characteristic of being fire protective, halogenated compounds have negative attributes to health and environment. Especially some of them show hazardous impacts to health and environment as they are persistent and bio-accumulative [50]. Furthermore, in the case a fire, some flame retardants are suspected to form corrosive or toxic decomposition products.
That is why the use of such compounds is avoided when possible [55, 56].

3.2 Metal hydroxides

As they are environment friendly additives, metal hydroxides have been extensively used in the halogen-free flame-retarded polymeric materials. These additives are the most used fire retardants in EVA copolymers, because of their low cost and high level of flame retardancy according to numerous normalized tests. Three types of metal hydroxides are currently used in EVA copolymers: magnesium dihydroxide (MDH), aluminium trihydroxide (ATH) and less commonly hydromagnesite ($Mg_5(CO_3)_4(OH)_2.4H_2O$) [57-59].

3.2.1 Mode of action

Magnesium dihydroxide $Mg(OH)_2$ acts as FR decomposing endothermically at relative low temperature (353℃) and releasing non combustible g as (water steam) (*Eq. 1*).

$$Mg(OH)_2 \rightarrow MgO + H_2O \qquad \textbf{\textit{Eq. 1}}$$

This process dilutes the concentration of any other gaseous products and also decreases the concentration of fuel available for combustion. The decomposition also generates an oxide residue (MgO) that has relatively high heat capacity, reducing the amount of thermal energy available to further degrade the substrate [60].
Acting in a similar way as MDH, ATH absorbs energy from the flames by decomposing into aluminium oxide and water according to *Eq. 2*.

$$2\ Al(OH)_3 \rightarrow Al_2O_3 + 3H_2O \qquad \textbf{\textit{Eq. 2}}$$

As its decomposition occurs 50 ℃ earlier than MDH *(Fig. 25)*, ATH plays its role more rapidly in a fire scenario, but the energy this phenomenon requires (1127J/g) is lower than for MDH (1344J/g). In addition to the cooling effect, a ceramization occurs during the degradation of ATH, thus producing an insulating alumina ceramic-like structure [61].

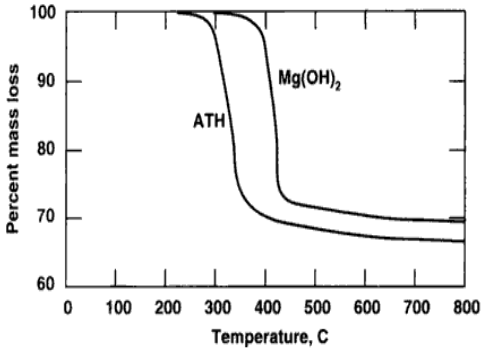


Fig. 25: TG curves of ATH and MDH (in air, 10℃/min) [62]

3.2.2 Metal hydroxides in EVA

Aluminium trihydroxide (ATH) is the most widely used halogen-free fire retardant in EVM because of its low cost [25]. It has been found that increasing levels of ATH in EVM steeply raise the LOI and COI[iv] (Critical Oxygen Index) *(Fig. 26).*

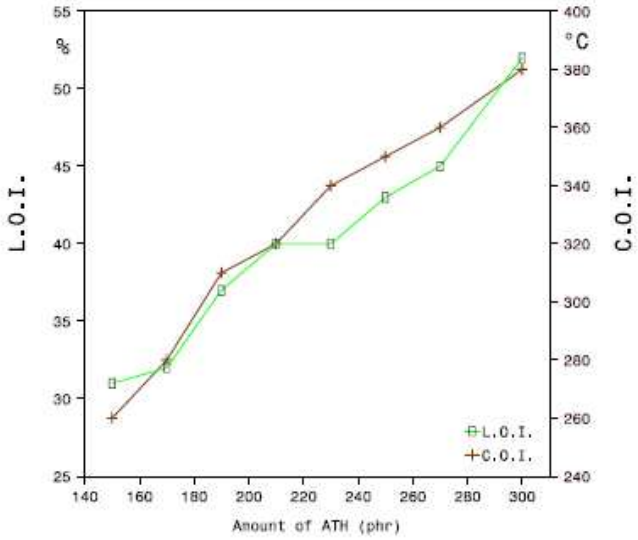


Fig. 26: Influence of the amount of ATH in EVM50 on the Critical Oxygen Index acc. to NES 715 and on the Limiting Oxygen Index acc to ISO 4589 [25]

To enhance fire retardant properties, the particle size and size distribution of the metal hydroxides as well as the effect of synergistic agents were widely studied. A good distributive dispersion and a small particle size tend to results in a better flame retardancy, as well as mechanical behaviour of the formulation [63]. Inorganic tin compounds [64, 65], zinc stannate or zinc hydroxystannate, possess excellent smoke suppressant properties and are added to metal hydroxides formulations to increase their activity. Similar synergistic effects with metal hydroxides in EVA are reported for silicon-based

[iv] The critical oxygen index (COI) is the minimum concentration of oxygen that will support the combustion of a polymer. ASTM D2863 or NES 715

additives [66], talc, zinc borate [60], fumed silica [67] and nanocomposites (described further in this chapter).

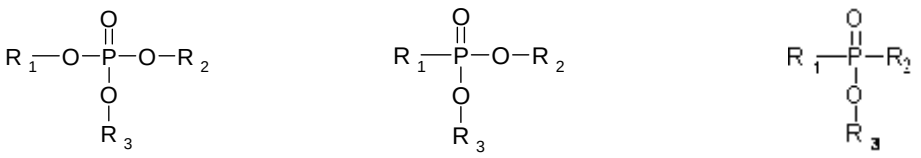
The smoke emission of the flame retarded formulations is an important parameter to be taken into account, as it participates to the fire hazards. ATH is often considered as smoke suppressant as it reduces smoke emission by “diluting” flammable degradation products from EVA. When CO and CO_2 release is expressed as grams per gram of copolymer, rather than as grams per gram of material, it appears that EVA/ATH gave higher CO yields than pure EVA.
Metal hydroxides are environmentally friendly and do not present any toxicity in EVA. EVA and EVA filled with ATH produces smokes and its toxicity was investigated [68]. Under well ventilated conditions, CO and CO_2 emission are greater for ATH-filled EVA compare with pure EVA. Under less ventilated conditions, the CO and CO_2 yields drops for both samples. This implies that a significant quantity of polymer is only partially decomposed and lost as volatile organic carbon. In the case of the ATH-filled material this can indicate that some non-degraded polymer is trapped during combustion in the solid matrix.

Thus, metal hydroxides are environmentally friendly, cheap and very efficient in EVA when incorporated at sufficient concentration. Nevertheless they have some disadvantages, e.g. the use of high additives content leads to deteriorate the mechanical properties of the polymer composites [66, 69, 70]. This is the reason why some research was carried out on other flame retardants, such as phosphorous compounds, melamine derivatives or nano-additives.

3.3 Phosphorous-based compounds

The use of phosphorous-based compounds as flame retardants in polymers is currently increasing as they represent an alternative to the use of halogenated compounds and metal hydroxides.

Phosphorus-based additives can be classified according to the phosphorus oxidation state. Red phosphorus (elementary phosphorus), phosphates and polyphosphates, phosphinates and phosphonates *(Fig. 27)* are widely used FR additives.



Phosphate **Phosphonate** **Phosphinate**

Fig. 27: Structure of the phosphorous compounds

3.3.1 Mode of action

These flame retardant additives mainly act in the condensed phase. They favour the polymer charring, thus creating a protective carbonaceous shield inhibiting the fire by the reduction o heat and mass transfer. Nevertheless, a gas phase action is also assumed, similar to that of halogenated compounds [71]. The phosphorous radicals implied in this mechanism are, by decreasing importance, $HPO_2^{\bullet}$, $PO^{\bullet}$, $PO_2^{\bullet}$ and $HPO^{\bullet}$.

3.3.2 Ammonium polyphosphate in EVA

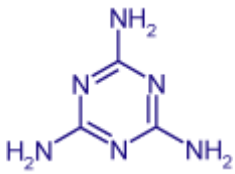
In EVA, the use of ammonium polyphosphate (APP) is reported. Unfortunately, APP and EVA exhibit low compatibility, so that they may not be used for industrial applications [72].

APP seems to be an efficient FR compound in EVA matrices, with a char former PA6 or other synergists such as zinc borate (ZB) [73], as it increases both LOI and UL 94 values and decreases the contribution to fire and the smoke production. However, this additive is water-sensitive, which could lead to some aging problems.

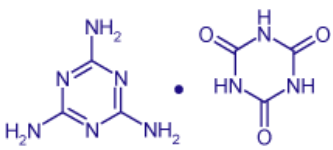
Except from phosphates, phosphorous compounds have not been evaluated in EVA or EVA blends. Nevertheless, some of them are used in combination with other flame retardant additives. These combinations will be detailed further in the chapter.

3.4 Melamine and derivatives

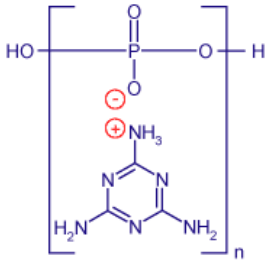
Various melamine-based additives are used in thermoplastics and elastomers such as pure melamine, organic or inorganic melamine salts (melamine cyanurate, melamine phosphates) or the melamine degradation products (melam, melem and melon). The chemical structures of some of these additives are gathered in *Fig. 28*.



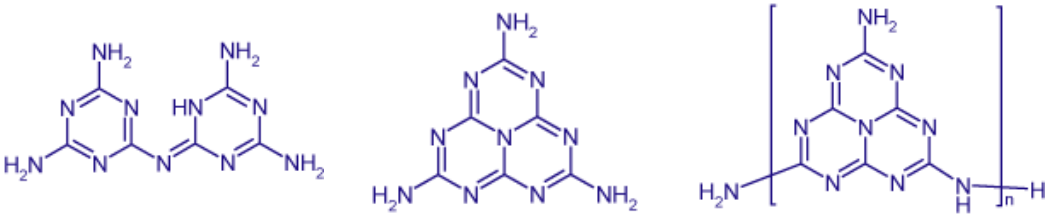
Melamine
(1,3,5-triaminotriazine)



Melamine cyanurate
Melamine and cyanuric acid salt



Melamine phosphates
n=1 melamine phosphate,
n=2 melamine pyrophosphate
n>2 melamine polyphosphate



Melam
(1,3,5- triazine-2,4,6-triamine-n - (4,6-diamino-1,3,5- triazine-2-yl)

Melem
(2,5,8-triamino 1,3,4,6,7,9,9b - Heptaazaphenalene)

Melon
(poly [8-amino- 1,3,4,6,7,9,9b-Heptaazaphenalene-2,5-diyl)imino]

Fig. 28: Various melamine based FR additives

These flame retardants have the advantage to present a smoke suppression effect and the smokes released, in case of fire, exhibit low toxicity and corrosiveness.

3.4.1 Mode of action

The flame retardant mode of action varies depending on the type of additive. Pure melamine combines the gas phase and condensed phase action since its degradation implies two processes: its endothermal sublimation and its condensation and decomposition in the condensed phase into melam, melem and finally melon, which are thermally stable compounds [74].

The melamine salts exhibit a more important condensed phase action. Indeed, while degrading the salts evolve melamine, which can sublimate or condensate, but the condensation phenomenon is more pronounced than for the pure component. Some oxynitride-type structures are formed at temperatures higher than 600°C, and the high thermal stability of these compounds explains the retention of melamine in the condensed phase [75].

3.4.2 Melamine in EVA

The influence of melamine on fire retardancy of EVA26 (26 wt-% VA) was investigated by Zilbermann *et al.* [76]. They compare two formulations in the same matrix. The first one (Formulation 1) corresponds to an EVA filled with 60 wt-% ATH and the second one (Formulation 2) corresponds to an EVA filled with the same amount of melamine. The cone calorimeter tests results are gathered in *Table 9*.

Incorporating melamine in EVA led to an apparent decrease of the flame retardant properties under cone calorimeter conditions, as the peak of rate of heat release (PRHR) increases drastically. This may be attributed to the fact that in the case of the non-flame retarded EVA abundant dripping of molten polymer out of the burning zone by boiling (up to 25% of initial weight) was observed. However, the noticeable increase in time to ignition and reduction in the CO production indicate that the addition of melamine in EVA does impart flame retardant properties to the polymer.

Table 9: Cone calorimeter results of EVA, EVA-ATH and EVA-melamine formulations (heat flux 35kW/m^2, 100x100x2,5mm^3)

Parameters	EVA	Formulation 1	Formulation 2
Time to ignition (s)	88	131	116
PRHR (kW/m²)	398	111	435
Time to PRHR (s)	235	270	405
Total smoke release	236	3.35	4.98
Average CO (kg/kg.10^{-3})	3.5	16	2

Formulation 1: EVA/ATH 40/60; Formulation 2: EVA/melamine 40/60

In addition, the combustion of melamine-containing EVA under the cone calorimeter conditions resulted in a considerable char residue, whereas no char residue remained after the combustion of EVA. Therefore, it becomes evident that this favourable effect of melamine in EVA in retaining the material from volatilization originates from a positive interaction between melamine and the polymer matrix.

However, the cone calorimeter results of EVA-melamine mixture does not reach those of EVA-ATH at the same loading level. The probable reason for this is that, unlike ATH, melamine is a flammable product contributing to the evolution of heat.

In spite of slight smoke suppression and significant CO reducing properties, melamine alone cannot be considered as suitable flame retardant candidate for EVA because of the very high RHR values. Nevertheless, no other melamine-based compound was evaluated in the EVA matrix. As a consequence, these additives can be envisaged for further studies about EVA and flame retardancy.

3.5 Flame retardant combinations

Combination of two or more of the flame retardant compounds presented in the previous parts of this chapter can be imagined to develop synergistic effect in EVA. Nevertheless, the literature only reports very few systems in EVA matrices: intumescent systems and ATH, APP and melamine.

3.5.1 Intumescent systems

Intumescence consists in developing on the outer surface of a material an expanded shield which may, at least partially, limit the fuel transfer to the gas phase, the heat transfer from the flame to the material (condensed phase) and eventually the diffusion of oxygen in the condensed phase. In particular, fire retardant intumescent compounds are halogen-free system and form when heated a foamed cellular charred layer on the surface, which protects the underlying material *(Fig. 29)*.

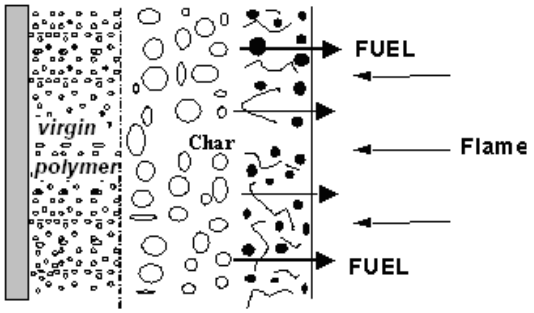


Fig. 29: Description of the intumescence process

Intumescent formulations generally consist of three ingredients: an acid source (phosphate, borates…), a char former (it can be the polymer itself) and a blowing agent. Upon heating, the acid source yields a mineral acid, which takes part in the dehydration of the char former that forms a cellular structure when the blowing agent decomposes into non flammable gases. Some examples of common intumescent systems are reported in *Table 9*.

Some intumescent additives are specifically used in EVA: the phosphorous compounds and in particular the phosphate-based molecules.
Intumescent mixtures of APP and polyamide-6 (PA-6) have been developed for use in polypropylene, ethylene propylene rubber, ethylene-vinyl acetate copolymers and other polyolefins. The APP-PA-6 mixture has been selected, as it increases the "compatibility" of APP in an ethylene vinyl acetate copolymer matrix, and in addition PA-6 acts as a synergistic carbonizing agent [77]. Bourbigot *et al.* [78] used APP (AP422, Clariant) as the acid source and polyamide-6 as the carbonisation agent as fire retardant intumescent additive in EVA 8 (8 wt-% VA). It leads to a significant improvement of the fire performances of the material

The same author [79] used Exolit AP750 (from Clariant) to flame retard EVA24 (24 wt-% VA) at 30w% loading). This additive consists in an ammonium polyphosphate (APP) used as acid source coated by an ester of tris(2-hydroxyethyl) isocyanurate used as carbonization and blowing agent and bounded by an epoxy resin, The reported values of the rate of heat release (RHR) for the flame retarded polymer are strongly lowered in comparison with those of the virgin polymer. A delay in the appearance of the last peak of smoke production was also observed. It was assigned to the delayed degradation of a protective structure which is thermally stable.

A mechanism of action of the APP-based intumescent system in the conditions of the cone calorimeter was proposed [78]. In a first step, the polymer melts; APP degrades and can catalyse the carbonisation of the material. Intumescence develops after ignition with the formation of a phospho-carbonaceous structure which can trap the polymer chains. In the second step, this structure degrades and the polymer chains are evolved so the flame is fed in "fuel". Finally, a carbonaceous residue is formed, there are no longer polymer chains maintained in the intumescent structure and so no longer fuel; the combustion stops.

Table 10: Common components of intumescent systems

Acid source	Char former	Blowing agent
Acids : phosphoric, sulphuric, boric **Ammonium salts :** Phosphates, polyphosphates, Borates, Sulphates, Halogens **Amines or phosphate amides :** Reaction products of urea and phosphoric acid, Melamine phosphate **Organophosphorous compounds :** Tricresyl phosphate, alkyl phosphate	**Polyhydric compounds :** Starch, Dextrin, Sorbitol, pentaerythritol Formaldehyde resins – phenol **Others:** Charring polymers (PA6, PA6-clay nanocomposite, polyurethane, polycarbonate,…)	**Amines /amides :** Urea, urea – formaldehyde resins, Dicyandiamide, Melamine, Polyamides

A Patent from Clariant related the use of a synergistic flame retardant combination for thermoplastic polymers (and thus for EVA) [80]. It is composed of a phosphinic or diphosphinic salt *(Fig. 30)* (or polymers thereof) and a nitrogen-containing compound. This last component can be melamine, its salts (melamine cyanurate, phosphate or borate) or pyrrolidine, pyridine, imidazole…

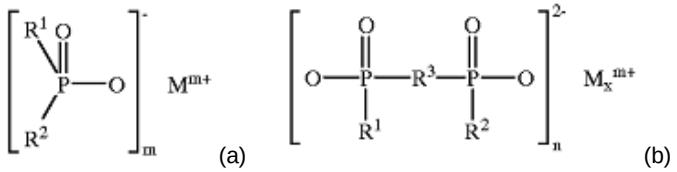


Fig. 30: Chemical structure of phosphinic(a) and diphosphinic (b) salts

This mixture was found intumescent and efficient in poly(butylene terephthalate). However, there is no fire properties results reported in EVA, so that we can only extrapolate the potential efficiency of such compounds in EVA matrices.

3.5.2 ATH, APP and melamine

The interactions between ATH, APP and melamine (and melamine-pentaerythritol) in EVA26 (26 wt-% VA) were studied by Zilberman *et al.* [76].

It was found that the melamine-APP combination was effective in lowering the average rate of heat release, but the ignition occurs earlier. The melamine-APP formulation showed a decrease in the smoke emission compared with ATH. Using APP-melamine in combination with pentaerythritol as a carbonising additive in EVA did not impart to the polymer any noticeable advantages in its flame retardant characteristics, on the contrary the resistance to ignition seriously deteriorated.

The ATH-APP combination was also tested. APP-containing formulations burned with the formation of intumescent chars. The decrease of Rate of Heat Release for the char forming formulations (40%ATH, 20%APP), in comparison with that with pure ATH (60%ATH), was attributed to the insulating properties of the intumescent chars. Moreover, it has been reported, that some inorganic fillers react at high temperatures with APP resulting in crystalline phosphates [76]. These improved the quality of the

char and, as a result, its flame retardant characteristics. Therefore, one can assume that in this case, alumina originated from ATH reacted with APP (or its decomposition products) to give alumino-phosphates which increased the protective properties of the intumescent char.
The study of the interactions between ATH and APP by Riva *et al.* [81] shows the evolution of water from ATH takes place at about 400℃, with a fair ov erlap with ammonia and water evolution from APP degradation. Ammonia evolution from APP is facilitated by the presence of ATH, in their mixture heated alone or in the polymer matrix. UL-94 test shows that the interaction between ATH and APP modifies the combustion behaviour of the mixture.

As a conclusion, the materials based on the combinations of APP with a sufficient amount of ATH or melamine may be considered of interest for wire and cable insulation based on EVA. These formulations burned with the formation of protective intumescent chars and better properties in terms of the heat release rate, mass loss rate and smoke production can be achieved as observed by other researchers. The CO production for the APP-melamine containing EVA was also significantly reduced in comparison with the ATH-EVA system. In the case of the APP-ATH-EVA formulation, the total CO yield increased to some extent by comparison with the ATH-EVA mixture. EVA was a source of carbon for the formation of the intumescent chars. Using pentaerythritol (in combination with APP-melamine) as a carbonific additive in EVA, did not impart to the polymer system any noticeable advantages in any of the flame retardant characteristics when compared with the APP-ATH- EVA and APP-melamine-EVA systems. Moreover, the resistance to ignition is strongly deteriorated in the presence of pentaerythritol.

3.6 Nanocomposites and nano-additives

The use of flame retardants is not the only way to obtain thermally stable and flame retarded elastomers. Indeed, the classical flame retardants have to be used in relatively large amounts (minimum 10 wt-% and usually at 30 wt.-%) in the matrix. An attractive way to replace the flame retardants or to reduce their loadings is thus the use of nano-additives, alone or in combination with conventional additives. This approach was initiated in the 90's by Gilman et al. has received a particular attention of the scientific community in the last decades.

3.6.1 Nanocomposites

Some categories of nano-additives are widely used to enhance the polymers properties, among them the thermal stability and/or the flame retardancy. The most common ones are layered silicates (clays), silica, metal hydrates, oxides (Fe_2O_3, $TiO_{2)}$, calcium carbonates or even graphene-based nanofillers. Less commonly can be used polyhedral silsesquioxane (POSS) or layered double hydroxides (LDH). The mechanisms of action of the nanoparticles in elastomeric composites are commented in the following.

Clay minerals are part of the larger class of silicate minerals. Included in this layered silicates family are the natural montmorillonites (MMT). Undoubtedly, montmorillonite clay is the most commonly used silicate for producing thermal resistant and flame retardant nanocomposites. By compounding clay into a polymer matrix, three categories of composites can be obtained: (i) microcomposite, (ii) intercalated and (iii) exfoliated (where the clay is dispersed as a single sheet) nanocomposites (Fig. 31). The following part will only evoke the last two cases, where a real nano-dispersion is achieved.

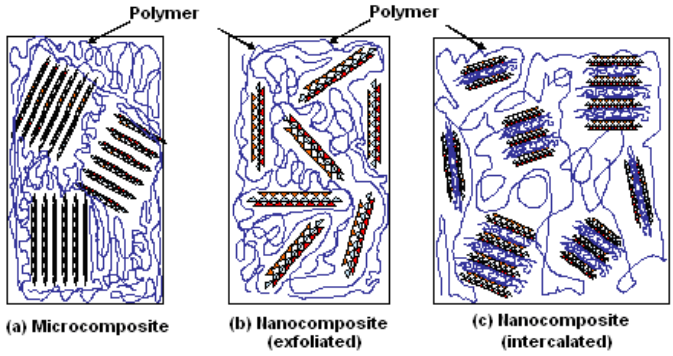


Fig. 31: Illustration of a microcomposite, exfoliated and intercalated nanocomposite morphologies

According to Gilman *et al.* [82], the flame retardant mechanism of clay based nanocomposites is a build-up of a high performance carbonaceous silicate char on the surface during burning. Two hypotheses can explain how MMT-rich char surface is produced [83]. There is an assumption that the MMT is precipitated during pyrolysis as a result of progressive gasification of the polymer, but another approach suggested a migration of MMT during and after decomposition of the nanocomposite structure due to the lower surface energy of MMT [84]. This layer insulates the underlying material and slows the mass loss rate of decomposition products.

Recently Leszczynska *et al.* [85] studied the mechanism that controls thermal stability of polymer/MMT nanocomposites. According to these authors, there are several factors that influence thermal stability, among which:

- a labyrinth effect induced by intercalated or exfoliated structure of MMT, which limits oxygen diffusion inside the nanocomposite sample,
- a steric effect, due to the interactions between the polar MMT layers and the polymer matrix thus limiting the polymer chain motion,
- a barrier effect, which protects the bulk of sample from heat, decreases the rate of mass loss during thermal degradation of polymer nanocomposite and generates more intensive char formation on the surface,
- a catalytic effect of the clay effectively promoting char-forming reactions.

The main parameter responsible for the dispersion quality in the composites is the compatibility of the nanofillers with the polymer matrix. So, to improve the dispersion of the nano-additives it is important to increase this compatibility by modifying the filler or the matrix. According to Duquesne *et al.* [86] the

modification of the surfactant of the clay layers is an efficient way to increase MMT dispersion and thus thermal and flame retardant properties of EVA.

Apart from the layered silicates, another class of nanofillers is able to impart thermal stability or flame resistance through the creation of a physical protective barrier: the graphene-based nanoparticles such as graphite and carbon nanotubes. Carbon nanotubes can be seen as elongated fullerenes: they are graphene sheets rolled up into a hollow cylinder, with each end capped with half of a fullerene molecule. There are two major types of carbon nanotubes (*Fig. 32)*: single-walled carbon nanotubes (SWNTs) and multi-walled carbon nanotubes (MWNTs).

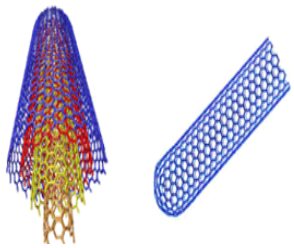


Fig. 32:Schematic representation of a multi-wall and single-wall carbon nanotube

These particles act principally in forming a charred residue, playing a protective role during combustion of EVA [87]. Indeed, fire property measurements by cone calorimeter revealed that the incorporation of multi-walled carbon nanotubes into EVA significantly reduced the peak heat release rates compared with the virgin polymer. Concerning graphite nano-platelets, two types can be mentioned: natural graphite (NG), and expanded graphite (EG). The effective method of preparing the expanded graphite is by rapidly heating pre-treated natural graphite to a high temperature, which separates the platelets and also to some extent destroys the crystalline structure. This treatment generally allows a better dispersion of the platelets. The efficiency of such additives was only tested in terms of thermal stability in the case of EVA [88]. They lead to an increase of the thermal stability of the polymeric matrix, and also favour the creation of a carbonaceous residue.

Another particle exhibits behaviour comparable to that of metal hydroxides: the nano-layered double hydroxides (LDH). Its structure is based on brucite ($Mg(OH)_2$)-like layers *(Fig. 33)*.

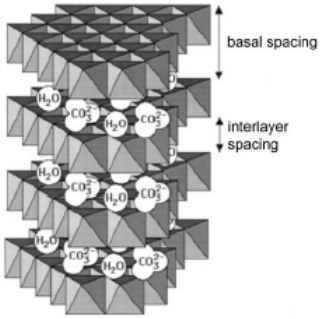


Fig. 33: Idealized structure of LDH

The flame retardation mechanism of LDH has been studied. According to Jiao *et al* [63] they act in EVA as a combination of aluminium trihydroxide and magnesium dihydroxide. LDH decomposes and

absorbs the heat in different temperature range. However this interpretation of the mode of action of LDH is probably not complete: According to Zhang *et al.* [89] nano-LDH have a capacity to catalytically oxidize a char-rich compound in the presence of oxygen; they can thus accelerate the carbonization of the char-rich compound to obtain a more sustainable char, improve the graphitization degree of the formed char, and further encourage the formation of an intumescent and heat-insulating carbonaceous layer to some extent.

Some nano-additives are incorporated in polymeric matrices at relatively high loadings (typically 60wt-% for nano-MDH). However there is an interrogation concerning the relevance of incorporating nanoparticles at such loadings: making a calculation of an ideal dispersion (nanoparticles evenly dispersed individually) will reveal that the distance between two molecules is too low to avoid the agglomeration of particles. So the term “nano” is not suitable in that case, except for the elementary size of the particle.
However, we propose to enlarge the notion of “nanocomposite” to composites filled with nanoparticles but where nano-dispersion is not always achieved. That is why this part of the chapter is dedicated to the EVA elastomeric matrices, flame retarded with nano-additives but not necessarily nano-dispersed.

3.6.2 Nanoadditives

The flame retardancy and mechanical properties of EVA containing 18% vinyl acetate (EVA18) and containing magnesium dihydroxide $Mg(OH)_2$ have been investigated by Huang *et al*. with reference to the particle size of MDH [90]. At a filling level of 55 wt %, there is little difference in mechanical properties and LOI values among four composites varying the particle size of MDH. The fire retarded formulations, whatever the nano or micro-size MDH, exhibit equivalent fire retardant properties. According to these results, the expected effect of particle size does not exist. But it could be explained by the poor dispersion of nano-MDH observed in EVA compared with micro sized MDH since nano-size particles aggregate easier than micro-size one.
At the opposite Lu *et al.* [91] with lamellar-like nano MDH noticed interesting properties. If UL-94 is not modified with nanoparticles compared to the same microparticles, the LOI is sharply increased (46 vol-% for nano-MDH versus 39 vol-% for micro-MDH at the same loading of 150phr). This might be explained by the better dispersion of the nanoparticles compared with microparticles, even if the presence of aggregates is detected by TEM analyses.
It thus appears that dispersion is an essential parameter determining the efficiency of the flame retardant effect of MDH. Considering the need of mechanical properties and flame retardancy of composites, it is suggested that the smaller size MDH should be selected as flame retardant, but appropriate methods must be conducted to improve the dispersion of smaller particles.

Concerning LDH, they have been tested in EVA with 14% vinylacetate (EVA14) [63] and proved to be efficient, as a LOI value of 42vol-% and a V-0 UL-94 rating are reached with a filler content of 150phr *(Table 11)*.

Table 11: Effect of nano-LDH concentration LOI and UL-94 rating of the EVA14-LDH blends (specimens 117x12.7x3mm) [63]

EVA-LDH (phr)	UL-94 rating	Dripping	LOI (vol-%)
100-50	Fail	Yes	27
100-80	Fail	Yes	32
100-100	Fail	No	37
100-120	V1	No	40
100-150	V-0	No	42

3.6.3 Combinations of nano-additives

The use of the above commented nano-additives in EVA nanocomposites proved to have a positive effect in terms of thermal stability and flame retardancy. Nevertheless, it seems to be possible to combine the properties of the nanoparticles to obtain higher performance. That is why many researches are dedicated to potential synergistic effects between nanoparticles.

A promising combination in terms of flame retardancy is the clay-graphene nano-filler mixture. Thermoplastic polyurethane elastomer was modified with different loadings of montmorillonite nano-clays and carbon nano-fibres (CNFs) [92]. It was found that thermoplastic polyurethane elastomer with 10wt% CNFs and with 5wt% nano-clays gave the best thermal performance with respect to protecting a substrate. Indeed, the combination of the two nanoparticles resulted in the formation of a char layer, thus increasing the thermal insulative properties of the material.

The combination of clay with carbon nanotubes was also reported in the literature in EVA [87, 93]. It appeared that the PRHR reduction is slightly increased when the two particles are nano-dispersed in the matrix, but the aspect of the remaining char is radically different. The char produced by the clay-composite showed cracks on its surface, while the combination provides a smooth-surfaced carbonaceous shield. Gao *et al*. found that nanotubes may act as nucleation agents for graphitisation, leading to the formation of turbostratic and graphitic carbons. The formation of graphitic carbon in char may contribute directly to the reduction of the peak of heat release rate of the composites. This effect has been enhanced when both nanotubes and clay are used. It was attributed to a better resistance to char oxidation in presence of clay. The nanotubes also have the function to reduce the formation of cracks of chars at the surface of the material, leading to the increase of barrier resistance to the evolution of flammable volatiles and to the oxygen transfer to the condensed phase.

The use of carbon nanotubes with MMT in nanocomposites seems of interest as MWNT can provide mechanical properties to the char produced by the composite during combustion leading to an increase of the heat and mass barrier properties of the char and thus to improved fire retardant properties of the material.

3.6.4 Combinations of flame retardants and nano-additives

The incorporation of nanofillers to improve the flame retardancy of elastomers, flame retarded with conventional additives, is also reported in the scientific literature [94]. In the case of elastomers, the main combinations involve metal hydroxide and nano-additives, such as clays, inorganic whiskers, carbon nanotubes and fumed silica.

The decrease of the overall filler content is illustrated by the work of Beyer [95] about ATH, clays and carbon nanotube combinations. The RHR is maintained at 200kW/m² by the incorporation of only 5wt-% nano-filler while the ATH content is decreased from 65wt-% to 45wt-%.
Szep *et al.* [94] added modified montmorillonite (IMM = polybutene/polysiloxane intercalated motmorillonite) and unmodified montmorillonite (MMT) to EVA/MDH formulations. It appeared that the addition of MMT and IMM was detrimental to the UL-94 rating and slightly beneficial for LOI. The simultaneous use of modified and non-modified montmorillonite in EVA with magnesium hydroxide increases the effectiveness of flame retardants *(Table 12)*. The synergistic effect between MDH and MMT+IMM was explained by the increased and sustained viscosity, by the early pre-carbonisation before the beginning of intense degradation and by the formation of a tough, stable ceramic-like residue from the montmorillonites and metal hydroxide interaction in the combustion process.

Table 12: LOI and UL-94 data of EVA28 compounds containing MMT and MMT-MDH [94]

Material	Weight ratio	LOI (vol-%)	UL-94
EVA+MDH	1:1	33	V-1
EVA+MDH+MMT	8:8:1	34	V-2
EVA+MDH+IMM	8:8:1	36	V-2
EVA+MDH+IMM+MMT	16:16:1: 2	43	V-0

Silica particles can also be used as synergists in combination with metal hydroxides. The influence of fumed silica of different particle size on the fire retardant properties of EVA-ATH-MMT-silica blends was investigated by Laoutid *et al.* [96]. The partial substitution of ATH by 5 wt% of silica in an EVA/ATH/MMT system did not improve significantly the overall fire behaviour. The presence of silica reduces the PRHR, especially for silica particles of small size and large specific surface area, but reduces the appearance time of the second PRHR, due to the poor cohesion of the char formed with silica. The addition of silica in EVA-ATH-MMT blends seems not beneficial regarding to fire retardant properties as it decreases char cohesion during combustion

3.7 Conclusion

The main strategies and additives used to obtain flame retarded EVA were reviewed. It was found that a gas phase or a condensed phase action can be implied in the flame retardation process. The two modes of action can also be combined.

To improve the fire properties of EVA different “families” of FR can be used, with more or less success: halogenated compounds, metal hydroxides, phosphorous compounds, melamine and its derivatives. Melamine has a smoke suppressant effect but does not increase the fire retardant properties of the polymeric matrix. Phosphorus compounds and melamine derivatives could provide some interesting fire retardancy. They could achieve similar effects as metal hydroxides but their price does not make them competitive flame retardants at the current loadings.

If the efficiency of such additives was demonstrated, their high loadings (typically 30 wt-%) can lead to some decrease of the mechanical properties of the polymer or of polymer-based formulations. To decrease the flame retardant loading or to replace it, another approach was described: the use of nano-additives. The addition of nano-additives (nanotubes, clay) confers the EVA matrix good fire properties, also in combination with metal hydroxides. The use of such compounds allows the decrease of the loading of metal hydroxide while keeping the same flame retardant behaviour. However, their high price is a huge limitation to their industrial implementation.

4. Conclusion

EVM and vulcanizates are used in a very wide range of application fields, from flooring to electrical cables or wagon profiles. These applications require a high level of flame retardancy combined with specific mechanical properties.
Non-corrosive flame retardant EVM-based formulations are already available. They are essentially based on ATH as this additive has the advantage to be cheap and commercially available in high quantities. Nevertheless a very high loading is necessary to achieve satisfying flame retardant behaviour, and thus limits the range of the mechanical properties of the formulations that can be achieved.
The main objective of this work is to find a suitable flame retardant additive for EVM which could surpass the mechanical and fire properties of metal hydroxides at reasonable loading and at acceptable cost. The given overview of the potential flame retardants for EVA and EVM vulcanizates allows defining the different approaches to obtain a flame retarded material. Despite their high efficiency, halogenated compounds are suspected to induce environmental hazards, so their use should be avoided when possible. The use of nano-additives, because of their expensiveness, does

not appear valuable. Metal hydroxides are economically the most interesting additives, but the phosphorous and melamine-based additives are also promising flame retardants. A screening is thus necessary to determine in a commercial EVM-based formulation which of them (or their combination) are the most valuable components. It will be discussed in the following (Chapter 3).

The next chapter, chapter 2, will describe the materials used in this work and the various techniques and protocols implemented for the flame retardant screening and the comprehensive studies.

CHAPTER 2 – MATERIALS COMPOUNDING AND EXPERIMENTAL TECHNIQUES

This chapter is dedicated to the description of the materials of this work and to the presentation of the various techniques used to evaluate these materials, to characterize them and then to understand the flame retardant mechanisms of the developed formulations.

To perform the screening of potential flame retardants, it is necessary to define the basic material in which they will be tested. The first part of the chapter then explains the motivations leading to the choice of the materials and describes the selected recipe for the EVM-based formulations. Since it is important to have a good knowledge of the different parameters involved during compounding, the mixing and vulcanization conditions are also detailed.

The project aims to design an innovative flame retarded EVM-based formulation. It is thus of primary importance to precise the experimental techniques used to characterize and to evaluate the developed materials. The methods allowing the evaluation of the mechanical and flame retardant behaviour of the materials will then be presented.

The comprehension of the flame retardant mechanisms is the key to produce well-designed materials. The analysis techniques necessary to carry out comprehensive investigations about the mechanisms of flame retardancy are lastly described. The thermal analysis, as the analyses performed on the gas phase and the condensed phase of the materials are detailed in the last part of the chapter.

1. Materials and compounding

This part is dedicated to the description of the approach that has been followed to select the basic materials and recipes used in this work in *Chapter 3*. Moreover, to define the compounding parameters the mixing and vulcanization methods and conditions are described.

1.1 Materials and formulation recipes

At first it is important to define which type of EVM will be used in the project. The chosen EVM grade in this PhD work is an EVA containing 60 wt-% of vinyl acetate: the Levapren® 600 HV from Lanxess (Leverkusen, Germany). The general properties of the pure material are reported in *Table 13*.

This grade of EVM was selected because it exhibits an intermediate vinyl acetate content of 60 wt-% (in EVM, the VA content is comprised between 40 and 80 wt-%). Thus the mechanical properties and the thermal stability of the material can be considered as medium values which could be extrapolated for the other EVM matrices.

Table 13: Properties of Levapren 600HV

Property	Nominal value	Unit
Mooney viscosity ML (1+4) 100℃	24 ± 4	MU
Vinyl acetate content	60 ± 1.5	wt-%
Volatile matter 6h at 105℃	max. 0.6	wt-%
Total ash	max. 0.8	wt-%
Specific density	Approx. 1.04	
Solubility	Soluble in chlorinated and aromatic hydrocarbons	

Since the objective of the project is to develop a commercial formulation, a Levapren-based formulation was chosen as a reference to evaluate the industrial validity of the flame retardants: the Railway Profiles & Wagon (RPW) formulation presented in *Table 14*.

Table 14 : Railway Profiles & Wagon formulations

Commercial reference	Compound	Loading (phr)
Levapren 600 HV	EVM	100
Apyral 40CD	ATH	120
Vulkasil N	Silica	30
Carbon black N550	Carbon black	2
Zinc borate	ZB	10
Disflamoll TOF	Disflamoll TOF	20
Vulkanox HS	Anti-aging	2
Stearic acid	Stearic acid	2
Aflux 18	Plasticizer	2
Rhenofit TAC/S	Co-agent	1
Perkadox 14-40	Peroxide	6
	Total phr	**295**

This commercialized formulation is composed of several additives, each of them playing a specific role.

Apyral 40 CD is aluminium trihydroxide, used as mineral filler and also as flame retardant. In the same way, the fumed silica, Vulkasil N, is added to the mixture to reach the desired hardness value of 65 Shore A. Carbon black plays the role of hardener and gives the black colour to the resulting material. Disflamoll TOF (tris-(2-ethylhexyl)-phosphate), described in *Fig. 34*, and stearic acid are plasticizers; they make the compounding easier.

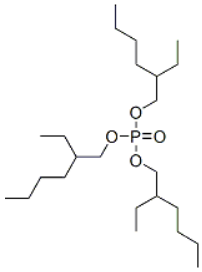


Fig. 34: Structure of Disflamoll TOF

Vulkanox HS (polymerized 2,2,4-trimethyl- 1,2-dihydroquinoline) is an anti-aging (anti-oxidant and UV preservative) compound. Aflux 18, an octadecylamine, plays the role of plasticizer and optimizes the vulcanization of Levapren. Rhenofit TAC/S (triallyl cyanurate) and Perkadox 14-40 (di-(tert-butylperoxyisopropyl)benzene) are cross-linking agents and co-agents for EVA.
The combination of all the ingredients is a commercialized Levapren-formulation with good fire retardant and mechanical properties, and is representative for a wide range of applications.

An "adapted" recipe for this PhD work *(Table 15)* was defined based on the Railway Profiles & Wagon (RPW) model. Disflamoll, used as plasticizer in the RPW formulation, is a phosphate and so could present a potential flame retardant [97]. This additive was then replaced by another plasticizer DOS (di-n-octyl sebacate) in order to avoid uncontrolled interactions between the plasticizer and the tested fire retardants. Zinc borate, which can be a synergistic agent for flame retardants [42, 60, 98], has also been removed.

Table 15 : Reference Levapren-based formulation

Compound	Loading (phr)
Levapren 600 HV	100
Fire Retardant (and combinations)	**X**
Vulkasil N	30
Carbon black N550	2
DOS	10
Vulkanox HS	2
Stearic acid	2
Aflux 18	2
Rhenofit TAC/S	1
Perkadox 14-40	6
Total phr	**165 + X**

In this reference recipe will be tested various potential flame retardant additives during the screening phase reported in *Chapter 3*.

Lastly, to have a better understanding of the flame retardant mechanisms occurring when the selected flame retardants are incorporated, it is necessary to reduce to a minimum the parameters that potentially influence the processes. That is why it was decided to test the flame retardant additives in a simplified formulation of vulcanized Levapren. The base recipe is detailed in *Table 16*.

Table 16: Base recipe of flame retarded vulcanized Levapren

	Loading (phr))
Levapren 600HV®	100
Rhenofit TAC/S	1
Perkadox 14-40	6
FR	X
Total phr	**107+ X**

The testing of the flame retardant compounds in this basic recipe will confirm if they are effectively responsible for the flame retardant properties observed in the complete reference formulation, since all potential interactions with the other additives are avoided. Moreover, the basic vulcanized Levapren-based formulations are used to investigate the flame retardant mechanisms of the additives in the polymeric matrix, as reported in *Chapter 4* and *Chapter 5*.

The composition of the recipes implemented in the study was defined. The next step consists in the mixing of the materials.

1.2 Mixing conditions

To keep constant all parameters (except the flame retardant content) between the different tested formulations the compounding was almost carried out in a same way. Two types of polymeric matrices were compounded: complete formulations and vulcanized EVM. In this work, “complete formulation” means the RPW recipe (*Table 14*) or the reference Levapren-based formulation (*Table 15*).

1.2.1 Complete formulation

The devices were an internal mixer GK 1.5 L (Werner & Pfleiderer, Stuttgart, Germany) type for black mixtures and the corresponding two-roll mill. The mixing conditions were EVM-standard: an initial temperature of the mixer of 20℃, a rotation speed of 40 rpm and a temperature of the two-roll mill of 20℃.

The incorporation of each ingredient followed an “upside-down” process: this technique is widely used in the rubber industry as it allows achieving good dispersion within short mixing times when high filler

loadings are used [99]. First the fillers and the plasticizers are added to the mixer, then the polymer. The total mixing time is 4 minutes.
As the temperature of the Levapren-based material during mixing reaches 100℃ (effect of the shear rate), the peroxides and co-agents (Perkadox TAC/s and Rhenofit) were added on the two-roll mill. This prevents the vulcanization agents and co-agents to react with the polymer before the hot pressing.

1.2.4 Vulcanized Levapren

The devices were an internal mixer GK 1.5L type for white mixtures and the corresponding two-roll mill. The term “white mixtures” corresponds to EVM-based mixtures which do not contain carbon black.

The first route which was followed for the mixing was the “classical” upside-down route with the standards conditions: a total mixing time of 4 minutes, an initial temperature of the mixer of 20℃, a rotation speed of 40 rpm. However, the pellets of Levapren did not agglomerate and so did not produce a consistent polymeric matrix (probably because of the low shear rate).
To solve this problem a step was added in the mixing process: the Levapren® pellets were submitted to the two-roll mill until they agglomerate. Then upside-down mixing was carried out with the standard conditions.
Similarly, the peroxides and co-agents (Perkadox TAC/s and Rhenofit) were added on the two-roll mill.

1.3 Vulcanization

The hot-pressing time and temperature chosen to achieve a complete vulcanization were EVM standard: 180℃ for 15 minutes. The Moving Die Rheo metry (MDR) curves validated these conditions, indicating that a total vulcanization was achieved. The duration of the hot-pressing can vary when basic flame retarded vulcanized Levapren is vulcanized: 10 minutes are generally enough to obtain an optimal cross-linking, according to the MDR curves.

After the compounding of the materials, the complete formulations or the flame retarded vulcanized EVM, it is necessary to describe the experimental techniques allowing their characterization and their evaluation.

2. Experimental techniques: evaluation of the materials performances

This part of the chapter is devoted to the description of the techniques used in this work. In the next section the evaluation of the materials will be detailed. This evaluation aims to determine the mechanical behaviour and the flame retardant properties of the formulations.

2.1 Mechanical testing

During the screening of the flame retardants in the complete commercial formulation *(Chapter 3)*, two aspects were considered to select the suitable compounds: the flame retardant properties of the mixtures, and their mechanical properties. Indeed, it is necessary to achieve a sufficient level of mechanical performances to envisage commercial applications of the flame retarded material. Three particular properties are investigated: the hardness shore A, the elongation at break and the tensile strength.

2.1.1 Hardness Shore A

The hardness Shore A is measured according to the standard test ASTM D2240 [100] (DIN 53505). This test method is based on the penetration of a specific type of indenter forced into the material. The indentation hardness is inversely related to the penetration and is dependent on the elastic modulus and viscoelastic behaviour of the material.

The Shore A test uses a hardened indenter (described in *Fig. 35*), an accurately calibrated spring, a depth indicator, and a flat presser foot. The device used for the tests, a Digitest durometer from Bareiss, is pictured in *Fig. 36*.

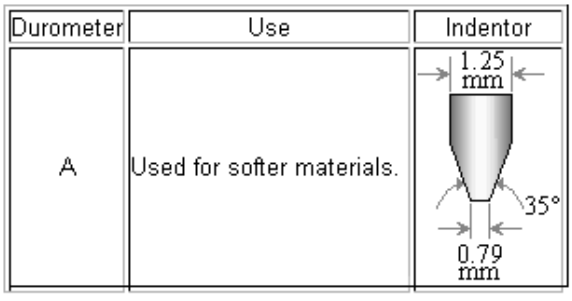


Fig. 35: Description of the indenter used for Shore A hardness measurements

The indenter is mounted in the middle of the presser foot and extends 2.5mm from the surface of the foot. In the fully extended position the indicator displays zero. When the indenter is depressed flat

even with the presser foot's surface, the indicator displays 100 ShA. Therefore, every Shore point is equal to 0.0025 mm penetration.

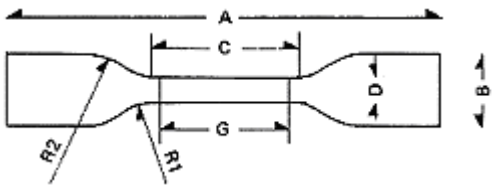


Fig. 36: Shore A durometer (DIgitest, Bareiss)

The evaluated specimens are 6.3 mm thick, with a diameter of 36 mm. For each formulation the measurements were repeated three times and the final value corresponds to the average of the values obtained by the three tests.

2.1.2 Stress-strain tests

The elongation at break (EAB) and the tensile strength are measured according to the ASTM D412 standard [101] (DIN 53504) stress-strain tests.
The tested specimens have particular shape and dimensions as depicted in *Fig. 37*.



	Length (mm)
A	75
B	12.5
C	25
D	4
G	20
thickness	2
R1	12.5°
R2	8°

Fig. 37 : DIN 53504 test specimen

Specimens were carefully loaded into a Zwick ZO10 tensile tester *(Fig. 38)*, which was equipped with a robot to enable automated testing. Testing was then carried out at room temperature (23 ℃) and at a tensile strain rate of 200 mm/min.



Fig. 38: Zwick Z010 stress-strain device

The elongation at break is measured optically: the sample is marked in its middle and a camera follows the deformation of the sample by the evolution of this mark.

2.2 Flame retardancy

Fire behaviour can be described through three major parameters: the ignitability, the contribution to flame spread and the heat release. Depending on the material application fields some specific tests can be implemented to simulate the desired conditions, but more generally, three tests are usually used since each of them quantifies the ignitability, the contribution to flame spread and/or the heat release. These tests are the Limiting Oxygen Index (LOI), the UL-94 and the mass loss cone calorimeter test.

2.2.1 Limiting Oxygen Index (LOI)

The Limiting Oxygen Index (LOI) is determined according to ISO 4589 [102]. This flammability test consists in the introduction of a mixture of oxygen and nitrogen in a chamber where the testing specimen is fixed from the bottom. The relative concentrations of both gases gradually vary depending on the behaviour of the samples when a flame is applied on the top of the sample. A butane/propane flame is applied less than 10 seconds to the top of the sample until it ignites, and then is withdrawn. If the flame extinguishes, the concentration of oxygen is increased and the sample is re-ignited until it finally continues to burn.
The concentration of oxygen just before this point is defined as the LOI, the concentration of oxygen which will just support combustion for a time higher than 3 minutes or on a length higher than 5cm.



Fig. 39: Limiting Oxygen Index apparatus

Measurements were carried out with a Fire Testing Technology apparatus on barrels of (100x10x3 mm^3). The margin of error of the obtained results is estimated at ± 1 vol-%.

2.2.2 UL-94 test

This small-scale test described in UL-94 [103] determines tendency of a material either to extinguish or to spread the flame once the specimen has been ignited. Specimens are clamped vertically and exposed to a defined flame ignition source from the bottom for a specified period of time of 10 seconds. The test flame is applied twice if the sample self-extinguished after the ignition source was removed. A cotton indicator is also placed below the sample *(Fig. 40)*.

There are three main classifications specified in UL-94 that are assigned to materials based on their behaviour regarding burning, flame propagation and dripping: V-2, V-1 and V-0, V-0 considered the best. If the material does not meet the criteria, it is non-classified at the UL-94 test (NC). The criteria required for the ratings are presented in *Table 17*. Five samples are tested for each formulation. The thickness of the barrels can be 0.8, 1.6 or 3.2 mm. The thinner the barrel, the more drastic is the test.

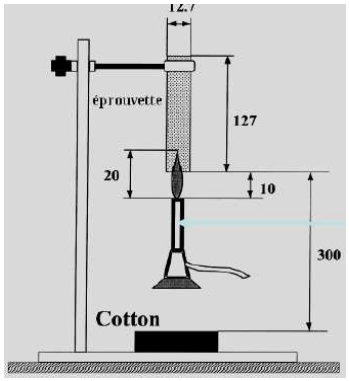


Fig. 40: Description of the vertical burning tests UL-94

Table 17: UL-94 Vertical rating classifications

Criteria	V-0	V-1	V-2
Afterflame time for each individual flaming	≤10s	≤30s	≤30s
Afterflame+ afterglow time for each individual specimen, after second flaming	≤30s	≤60s	≤60s
Total afterflame time for any condition set (5 flamings)	≤50s	≤250s	≤250s
Cotton indicator ignited by flaming drops	No	No	Yes
Afterflame or afterglow of any specimen up to the holding clamp	No	No	No

The UL-94 tests were realized on a Fire Testing and Technology UL-94 apparatus. The samples were 12.7x1.3x0.15 cm^3, which is close to the recommendations of the standard. They are ignited by a blue propane flame (without cone) of 2 cm as defined in the standard.

2.2.3 Mass loss cone calorimeter

The mass loss calorimeter allows the simulation of the conditions of fire in a small bench scale according to ASTM E2102 [104]. A schematic representation of the mass loss calorimeter is given in

Fig. 41. The core of the instrument is a radiant electrical heater in the shape of a truncated cone, irradiating a flat horizontal sample (100x100x3 mm^3) placed beneath it, at a preset heating flux (35 kW/m^2 to simulate a mild fire or 50 kW/m^2 for a developed fire). Ignition is provided by an intermittent spark igniter located 13 mm above the sample.

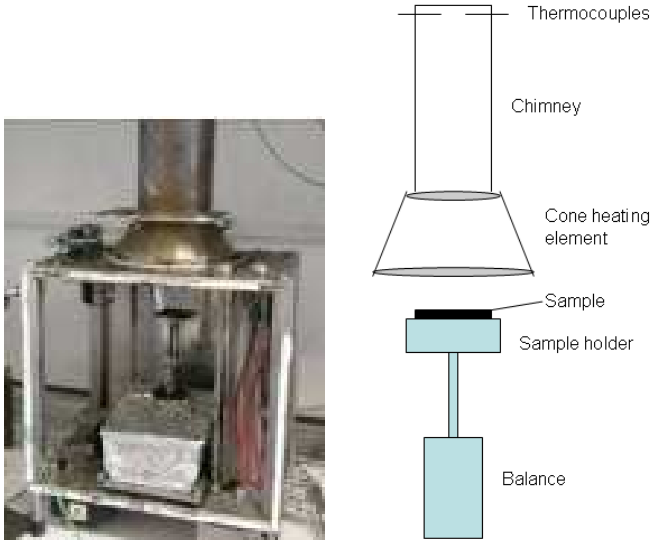


Fig. 41: Schematic representation of a mass loss calorimeter

The mass loss cone calorimeter measures the temperature at the top of the chimney. The calibration of the heat release rate (RHR) is performed with methane. A methane flow of 0 to 6.7 ml/min is burnt above the sample holder to obtain a calibration curve of the heat release as a function of temperature.

The measured parameters are among others in particular the Rate of Heat Release (RHR), the Total Heat Release (THR) and the Time to Ignition (TTI). These parameters permit to evaluate the contribution to a fire of the material.

The cone calorimetry measurements were performed on a Fire Testing Technology (FTT) mass loss calorimeter device at 35 kW/m^2 according to the ASTM E906 on specimens of 100x100x3mm^3. All measurements were repeated two times, the presented curves are calculated as the average of two experiments. The acceptable margin of error is estimated 10% for the RHR and 15% for the time to ignition.

3. Experimental techniques: characterization of the material degradation

After the determination of an interesting flame retarded formulation, the project aims to understand the flame retardant mode of action of the selected additives.
Flame retardant behaviour can be due to a condensed phase mechanism (degradation reactions occurring in the condensed phase) or a gas phase mechanism (due to gaseous degradation products). To elucidate flame retardant mechanisms we propose to investigate the thermal degradation of the materials, polymers and additives: the modifications in the condensed phase such as the gaseous products emitted.
To characterize these chemical modifications the thermal degradation characteristic temperatures are first determined through thermogravimetric analyses. Then thermal treatments can be carried out at the selected temperatures to obtain intermediate degradation residues. These residues, analyzed through condensed phase analysis techniques allow to determine a degradation mechanism and to point out potential interactions between the additives and/or the polymer.
To complete the analysis of the condensed phase, the gaseous emissions are also characterized through TGA-FTIR.

In the next section the thermal analysis methods, the gas phase and the condensed phase analyses performed during the project are consequently presented. They will allow determining the flame retardant mode of action of ATH in *Chapter 4* and of an innovative flame retardant combination in *Chapter 5.*

3.1 Thermal analysis

The flame retardant behaviour depends on the degradation reaction occurring in the gas and condensed phases. Thus, thermogravimetric analyses (TGA) investigating the thermal stability and degradation of the materials, is widely used to carry out a comprehensive study of flame retarded materials.

3.1.1 Thermogravimetric analysis (TGA) and high-resolution TGA (Hi-Res TGA)

Thermogravimetry is a technique in which the weight change of a sample is monitored versus time or temperature while the sample is heated at a defined temperature ramp. The measurements can be carried out in oxidative or inert atmosphere (in this case to avoid oxidation phenomena).

TGA measurements were conducted on a TA Instruments TGA Q5000IR with alumina crucibles. Balance and purge flow rates were set to 10 and 25 ml/min respectively. The purge was either nitrogen for inert conditions or dried air for oxidative degradation. The samples of 15 mg ± 0.2 mg were submitted to an isotherm at 50℃ for 5 minutes then followed by a heating ramp (from 1 to 500℃/min) up to 800℃. Every TG analysis is repeat ed 2 times to ensure the reproducibility of the measurements.

Besides linear heating and isothermal temperature programs, High-Resolution (Hi-Res) experiments can be conducted to enhance the resolution of a TGA experiment. Resolving successive weight losses is important to obtain accurate, reproducible weight change values and components identification (if coupled with a Fourier transformed infrared spectrometer). Three different Hi-Res modes can be implemented: dynamic rate, constant reaction rate and stepwise isothermal. In this work only the dynamic rate will be used: the heating rate is dynamically and continuously varied in response to the rate of weight loss of the sample in order to optimize the resolution. The applied instantaneous heating rate β depends on mass loss rate $d\alpha/dt$, on the initial heating rate β_{init} and on the chosen resolution and sensitivity (Eq.3).

$$\beta = f\left(\beta init, \frac{d\alpha}{dt}, resolution, sensitivity\right) \qquad \textbf{Eq. 3}$$

As the resolution is increased, the instrument reacts to smaller changes in the weight loss rate. Sensitivity controls the magnitude of the response relative to weight loss. Resolution and sensitivity are therefore connected to each other.

The chosen conditions for the Hi-Res TGA are a heating rated of 10℃/min, a resolution of 2 and a sensitivity of 2.

3.1.2 Difference weight loss curve

In order to determine potential interactions between a polymer and flame retardant additives during the thermal degradation, difference weight loss curves (∆M) are calculated. They represent the difference between experimental and theoretical TG curves of mixtures, and are calculated as described in Eq.4:

$$\Delta M = M_{exp} - M_{calc} \text{ with } M_{calc} = \sum x_i M_i, \qquad \textbf{Eq. 4}$$

with M_i the mass of the component I and x_i the fraction of *i* in the mixture.

The ∆M curves allow pointing out a potential increase or decrease in thermal stability of the polymeric matrix related to the presence of one or more additives. When the experimental curve is higher than the theoretical one (or when the difference weight loss curve is positive), the weight loss is higher than expected, showing that the reactivity of the polymer with the additives leads to a thermal stabilization of the resulting material. On the contrary, if the ∆M curve is negative, a thermal destabilization occurs.

After evaluating the thermal stability of the materials, it is of great importance to determine the nature of the potential interactions between the additives and/or the polymer. This can be done through a complete analysis of the gas phase and of the condensed phase using adapted techniques.

3.2 Gas phase analysis

The gas phase analysis is a way to get information about the nature of the degradation products of the materials and could be carried out through TGA coupled with gas infrared analysis. The smoke production can also be evaluated by the NBS smoke chamber test.

3.2.1 Thermogravimetric analysis (TGA) coupled with FTIR

Evolved gas analysis (EGA) is defined as a technique to determine the nature of volatile products formed during an analysis. Common examples of EGA are thermogravimetry combined with mass spectrometry (TGA-MS) [105, 106] or Fourier Transformed Infrared Spectrometry (TGA-FTIR) [107, 108].

Infrared spectroscopy exploits the fact that bonds have specific frequencies at which they rotate or vibrate corresponding to discrete energy levels. So, infrared absorptions at characteristic frequencies are related to chemical groups. The TGA-FTIR coupling has the advantage to analyze the evolved gases continuously during the degradation [108].

The TGA Interface is connected to the TGA via a heated transfer line. As gases evolve during the TGA experiment, they pass into the flow cell of the TGA-IR interface where the infrared spectra are collected. The TGA-IR Interface is beneficial in determining sample characteristics such as decomposition pathways or thermal stability. The TGA flow cell is compatible will all types of evolved gases and materials. Additionally, the large flow cell diameter provides high throughput and prevents spectral interference caused by deposits on the walls.

The experiments are performed on a TA Instruments TGA Q5000IR with alumina crucibles. Balance and purge flow rates were set to 10 and 50 ml/min respectively to ensure a good evacuation of the evolved species. The gas flow was either nitrogen for inert conditions or dried air for oxidative degradation. The samples of 15 mg ± 0.2 mg were submitted to a High-resolution TGA at 10℃/min up to 800℃. The heat transfer line temperature is set at 225℃ to avoid condensation of the evolved gases. The used FTIR device is a Nicolet is10 from Thermo Fischer. The IR spectra were recorded in the 400-4000 cm^{-1} spectral range through the OMNIC® software. The obtained spectra correspond to the accumulation of 8 scans with a resolution of 4 cm^{-1}.

3.2.2 NBS Smoke chamber test

Fire side effects can be observed, the most important one being the emission of smoke during combustion. This aspect is characterized through NBS smoke chamber tests.

The Smoke Density Chamber (ASTM E662 [109]) illustrated in *Fig. 42* measures smoke generation from small, solid specimens exposed to a radiant flux level of 25 kW/m^2, in a flaming (piloted ignition) or non-flaming mode. The smoke produced by the burning specimen in the chamber is measured by a light source – photometer combination. The quantity of smoke that a material will generate under the given conditions leads to some attenuation of the light beam received by the sensor. The measure of the optical density allows the calculation of the emitted smoke quantity.

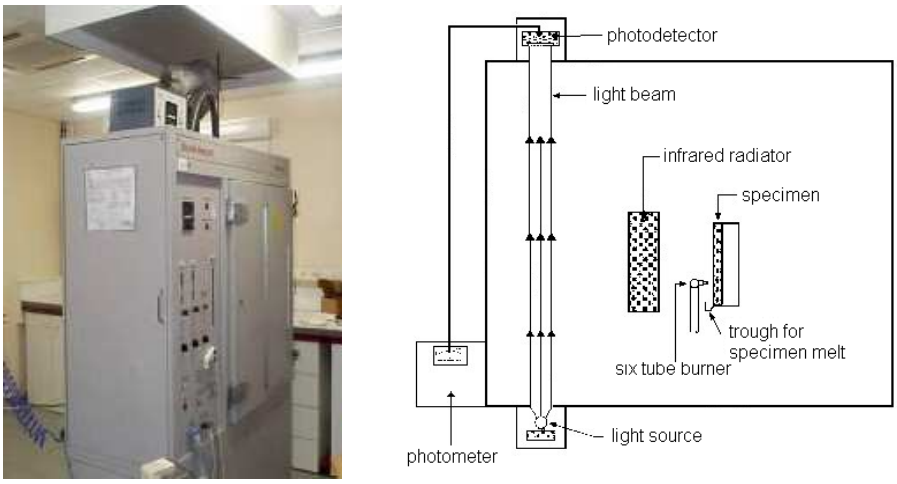


Fig. 42: Smoke density chamber apparatus

The smoke emission index is a combination of the maximum optical density (Dm) and the summation of optical density up to 4 min (VOF4). These two parameters Dm and VOF4 are assessed during the smoke chamber test.

3.3 Condensed phase analysis

The flame retardant behaviour also depends on the degradation reactions occurring in the condensed phase. Thus, it is necessary to characterize and to identify the condensed phase modifications occurring during degradation. The presented methods gather the thermal treatment, the characterization with solid state nuclear magnetic resonance and electron probe micro analysis and the characterization through x-ray diffraction and microscopy.

3.3.1 Thermal treatments

The thermal treatments consist to submit a sample in a furnace at a determined temperature (Heat Treatment Temperature HTT) under controlled gas flow, either dried air to simulate thermo-oxidative degradation or nitrogen to simulate the pyrolysis conditions *(Fig. 43)*. The treatment temperatures are determined according to thermogravimetric analyses as they correspond to the characteristic degradation steps of the systems.

The chosen experimental conditions were a heating rate of 10°C/min, from the ambient to the treatment temperature followed by an isotherm for one hour. The sample is then cooled to ambient temperature.

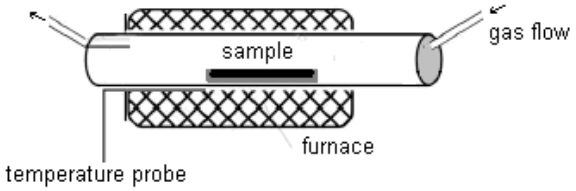


Fig. 43 : Description of the furnace used for thermal treatments

The residues obtained after thermal treatments were stored in a desiccator to avoid hydrolysis of the residues and then analyzed by various techniques.

3.3.2 Solid state nuclear magnetic resonance NMR

The nuclear magnetic resonance (NMR) in the solid state turns out to be a particularly effective tool to evidence the changes of chemical environment in a given material.

In the solid state, i.e. a semi-crystalline or glassy polymer, the Chemical Shift Anisotropy (CSA, anisotropy of the magnetic moment) has a severe effect on the spectra in broadening the absorption peaks; this effect becomes worse when the mobility of the chains or molecules decreases [110]. Through a tensoral analysis of the magnetic moments in a molecule it is possible to demonstrate that there exists a “Magic Angle” with respect to the applied magnetic field at which rapid spinning of the solid sample leads to minimization of absorption line broadening due to CSA. This method is called “magic angle spinning” or MAS.

The low abundance of some atoms compared to the protons leads to poor absorption of the radiofrequency pulse in a FT-NMR experiment. This limitation can be overcome by exciting the protons in a sample, followed by a sequence of two series of long-time pulses which make the protons and the other nuclei resonate at the same frequency. This latter is called the “Hartman-Hahn” condition, and the process is called “cross-polarization” (CP). The time of cross polarization is called the “contact time” or “spin-lock time” [111].

Cross-polarization leads to a large enhancement of the excitation of the nuclei. The large number of protons in the sample however interferes with the decay of the isolated nuclei due to weak interactions of the spins. This dampening of the signal can be removed by a strong radiofrequency signal which essentially holds the protons in a highly resonating state so they are not capable to absorb resonance from the nuclei. This is called "^{1}H decoupling" or "^{1}H dipolar decoupling" (DD) [112].

^{27}Al NMR Measurements were carried out on a Bruker Avance II 400 with a probe head of 4 mm using magic angle spinning (13 kHz). The repetition time was fixed at 1 s for all samples, a minimum of 1024 scans was necessary to obtain a satisfactory signal to noise ratio. Al in aqueous solution was used as a reference.

To increase the resolution of some spectra and to reduce induced quadrupolar effects some measurements were realized on a Bruker Avance II 800 with a probe head of 3.2 mm using MAS. The same conditions (rotation frequency, spin lock and references) were used.

^{31}P NMR Measurements were performed on a Bruker 400 spectrometer at a spinning rate of 13 kHz. Brucker probe heads equipped with 4 mm MAS assembly were used. Experiments have been carried out with ^{1}H dipolar decoupling because of the high relaxation time of the phosphorus nuclei (from 10 to 500 seconds). A repetition time of 120s [79] was applied for all samples. H_3PO_4 in aqueous solution (85%) was used as a reference.

^{13}C NMR Measurements were performed on the same apparatus with MAS (10 kHz), high-power ^{1}H decoupling and ^{1}H-^{13}C cross-polarization (CP). The reference used to determine the chemical shifts is glycine.

^{27}Al-^{31}P D-HMQC:

The spatial proximity between the phosphorous and aluminium sites was investigated with the 2D MAS-NMR D-HMQC (Dipolar Heteronuclear Multiple Quantum Coherence) sequence [113]. This NMR experiment uses the standard HMQC pulse sequence to produce heteronuclear coherences but an additional pulse scheme allows for the creation of through-space coherences in place of the standard through bonds signals obtained with the basic HMQC sequence. As a consequence, the 2D spectrum displays correlation signals between spatially close atoms. The ^{27}Al{^{31}P} D-HMQC spectrum has been obtained at 9.4 T ($\nu_L(^{27}Al)$= 104.2 MHz and $\nu_L(^{31}P)$= 161.9 MHz) on a Bruker spectrometer equipped with a 4mm triple channels probe operating at a spinning frequency of 12.5 kHz. The through space correlations were created by a scheme pulse based on the SFAM (Simultaneous Frequency and Amplitude Modulation) technique [114] applied during 1 ms. The 2D spectrum was recorded with the following acquisition parameters: number of scans = 640, recycle delay = 0.5 s, number of points = 2474 x 120.

3.3.3 X-ray diffraction spectroscopy (XRD)

X-ray diffraction spectroscopy (XRD) is the principal technique used to investigate long-range order of atoms and molecules in the solid state [115]. X-ray is the portion of the electromagnetic spectrum covering the range of 1 to 200 Å. Only a small part of the total X-ray spectrum (0.2- 20 Å) is used by conventional X-ray spectrometer. The X-rays reflected from a lattice plane follow the Bragg's equation *(Eq.3)*

$$n\lambda = 2d_{hkl}\sin\theta \qquad \textbf{Eq.3}$$

where n is an integer (order of reflection)

λ is the wavelength of the X-rays

d_{hkl} the interplanar spacing between planes having miller indices *h*, *k*, *l*

and θ the angle at which the X-ray beams are incident on the plane.

In a poly crystalline material or the powder of a crystalline material, the crystals are randomly oriented. If such a sample is struck by an X-ray beam, there may be many planes which are oriented in such a way that the Bragg's law is satisfied and we obtain a resultant diffraction pattern with peaks corresponding to all such planes.

From a study of the XRD spectra, a flood of information on the structural aspects of the sample can be obtained. The XRD pattern is unique for every sample, so the position of the peaks helps in the determination of the crystallographic parameters, the d values and the shape of the unit cell. The orientation of the crystallites can also be determined from the relative intensities of the peaks [116].

X-ray diffraction spectroscopy (XRD) analyses were carried out with a Philips X'Pert diffractometer by the use of the Cu K_α (λ = 1,540562 Å) radiation source. 2θ angles between 7 and 70° were applied.

Some measurements carried out at high temperature were performed on a Brüker D8 equipped with a high temperature chamber XRK 900 and a Lynxeye detector using Cu K_α radiation source.
The experiments were performed under air and nitrogen flow, the powder samples were placed on a gold foil to avoid interactions with the alumina sample holder. From the room temperature to 800 °C the sample were heated at a heating ramp of 0.05 °C /min. For each 25 °C increase, the temperature is stabilized and a DRX scanning is realized in the 2θ range between 7° to 70° (with steps of 0.0195°).

3.3.4 Scanning Electron Microscopy (SEM)

Scanning Electron Microscopy (SEM) is a technique based on the principle of electron-matter interactions. The surface of the sample is scanned by a thin electron beam, leading to various phenomena such as secondary electrons or back-scattered electrons (BSE) emission by the sample.
Each of these phenomena allows, by the use of a specific detector, to produce a high resolution surface image: the secondary electrons provide topographic information while BSE evidence the sample chemical contrasts.

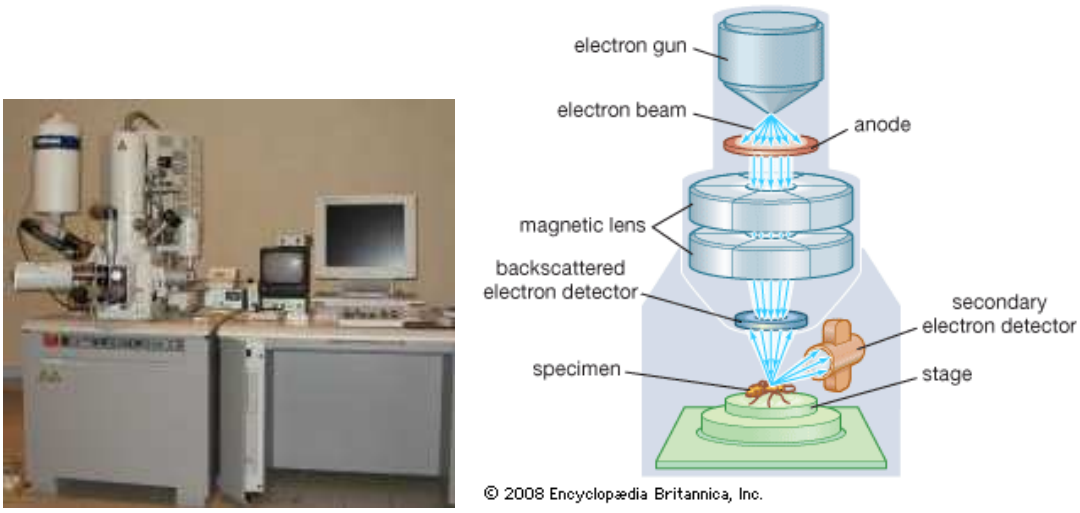


Fig. 44: SEM apparatus

The resolution of the image is linked to the beam diameter at the surface of the analyzed sample, to the chemical composition of the material and the electron type chosen to obtain the image. Electrons of low energy come from regions located near the surface while SBE come from deeper layers of the material.

The device used to obtain SEM images was a Hitachi S4700 equipped with a Field Emitting Gun (FEG). Before analysis the sample is covered by a conducting layer of carbon (metalized) in a Bal-Tec SCD005 carbon-evapourator to avoid electron overload. The images were realized at 6 kV and 15 mA at different magnifications.

3.3.5 Electron probe micro-analyser

The electron probe micro-analyser (EPMA) *(Fig. 45)* is an elemental analysis method. It consists in bombarding a solid sample by an accelerated and focused electron beam, and in analysing the X-ray and the back-scattered electrons thus emitted [117]. The X-ray generation is produced by the collisions of the incident electrons with the electrons of the inner shell of atoms; when an inner-shell electron is ejected from its orbit, leaving a vacancy, a higher-shell electron falls into this vacancy and must shed some energy (as an X-ray) to do so. These quantized x-rays are characteristic of the element, so that the analysis of the X-ray spectrum of the sample submitted to this solicitation allows knowing its exact chemical composition. The back-scattered electrons are useful for imaging the surface or obtaining an average composition of the material [118].

The electrons are focused on the sample on a surface of almost $1\mu m^3$, producing an impact energy varying from 100 eV to 30 keV. The X-ray photons are analyzed by wavelength dispersion scanning (WDS) X-ray spectrometers.

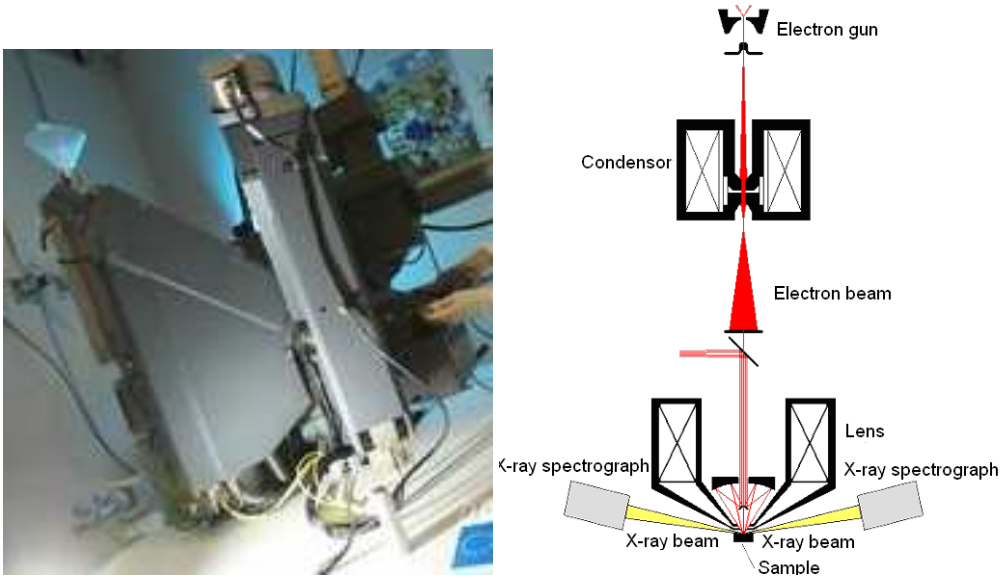


Fig. 45 : Description of the EPMA apparatus principle

The samples were prepared by cryofracture in liquid nitrogen, and then metalized with carbon in a Bal-Tec SCD005 carbon-evapourator.

The experiments were carried out on a Cameca SX100 device. SEM images and phosphorus (P) and aluminium (Al) cartography were realized through BSE at 6 kV and 20 nA. The crystal used for the detection of the K_α radiation of Al was a Thallium Acid Phthalate (TAP) crystal, the phosphorus K_α radiation was determined through a pentaerythritol crystal.

4. Conclusion

This chapter defined the main strategies and techniques used during the project to achieve the major challenge of this work: determining an innovative formulation with high flame retardant performances and acceptable mechanical behaviour.
The recipes and the compounding of the complete commercial formulations for the screening phase of *Chapter 3* and the simplified formulations were described. The testing methods used to determine the mechanical (Hardness Shore A, Traction tests) and the flame retardant properties (LOI, UL-94, mass loss calorimeter) of the materials have been also presented.

The strategy implemented in *Chapter 4* and *Chapter 5* to elucidate the flame retardant mechanisms of the innovative flame retardant combination determined in *Chapter 3* was detailed. The various techniques used in to characterize the gas phase (TGA-FTIR) and the condensed phase (solid state NMR, FTIR, XRD, EPM) of the flame retarded formulations have been presented. The next step, *Chapter 3*, now consists in evaluating the efficiency of potential flame retardant additives and to optimize the most promising ones.

CHAPTER 3 – DEVELOPMENT OF A NOVEL FLAME RETARDED FORMULATION

The collaboration with LANXESS aims to find potential flame retardants providing an optimized new fire retarded EVM-based formulation. The goal of this preliminary study is to determine the most efficient commercial flame retardant (FR) additives and to develop further an innovative optimized flame retarded formulation.

The first part of this chapter is dedicated to the screening of flame retardant compounds in a complete commercial Levapren-based formulation from Lanxess. Only one parameter varies in this first section, i.e. the type of flame retardant. Mechanical and fire testing are evaluated to determine their performances and to allow focusing on the promising types of fire retardants.

As a second step the efficiency of some combinations made of the selected additives is evaluated. To determine if the measured flame retardant properties are effectively due to synergisms between the FR compounds and not due to interactions with the other fillers or additives of the complete formulation, the combinations will also be tested in pure vulcanized Levapren.

In the last part our attention will be focused on an innovative combination: the metal hydroxide (ATH)-phosphinate mixture which has never been investigated before (patent and open literature). The complete EVM-based formulation will be optimized in terms of mechanical and fire properties through the choice of the suitable ATH particle size, flame retardant loading and ratio of the two additives.

1. Flame retardant screening

1.1 Selected flame retardant additives

A screening is necessary to determine what sorts of flame retardant additives are the most valuable components in a commercial EVM-based formulation. The recipe of the chosen reference complete formulation was already detailed in *Chapter 2*. According to the previous bibliographical study *(see Chapter 1)* five flame retardants “families” were selected to be tested in the EVM-based complete formulation: metal hydroxides, phosphates, phosphinates, melamine and its derivatives and graphite-based compounds.

Metal hydroxides are the most commonly used flame retardants in EVA copolymers because of their low cost and high level of flame retardancy. Two types of metal hydroxides are currently used: magnesium dihydroxide (MDH) with formula $Mg(OH)_2$ and aluminium trihydroxide (ATH) with formula $Al(OH)_3$. These additives were highly studied and are known to provide both acceptable mechanical properties and fire retardant performance at 50- 60 wt-% loadings in EVA [42]. That is why Magnifin

H5 (from Albermarle) and Apyral 40CD (from Nabaltec), which are commercially available MDH and ATH respectively, are chosen as **references**. The influence of coating on metal hydroxides on the properties of the material will be determined through Charmax FS-ZHSA (from PAG), which is a zinc hydroxystannate-coated ATH. The loading of these additives is 200 phr because it is that incorporated into commercially available ATH-based FRNC.

The phosphate-based additives constitute the second flame retardant family selected for the screening. Are tested in this study ammonium polyphosphate (APP) and intumescent mixtures based on APP. Are tested in the formulation pure APP (Exolit AP423 of Clariant, Germany) and intumescent coated APP (Exolit AP from Clariant and Budit products from Budenheim). According to the scientific literature the loading for a maximum efficiency is about 30 w% [54]. That is the reason why to determine an optimal concentration in the EVM formulation two loadings are tested: 60 and 80 phr (respectively 28 and 33 wt-% in the complete formulation).

The use of phosphinates in EVA has never been reported in literature, but they are suitable flame retardants for polyamides at about 30 wt-% [119]. As no work was done about this type of additives in EVM or vulcanizates, it is interesting to evaluate their performances: some organic phosphinates (Exolit OP series of Clariant, Germany) were added to the formulation at 60 and 80 phr. Exolit OP1230 is an aluminium diethyl phosphinate, Exolit OP1311 corresponds to a mixture of OP1230 and melamine phosphate at a 2:1 ratio. A calcium inorganic phosphinate salt, Phoslite B55CM (Italmatch, Italy), was chosen to compare the efficiency of organic and inorganic phosphinates.

Melamine in EVA is known to be a smoke suppressant, but it does not provide any flame retardant properties [76]. In order to keep the smoke suppressing properties of melamine and to confer resistance to fire to the compounded material some melamine derivatives were selected for this screening: melamine phosphate (MP), melamine borate (MB), melamine cyanurate (MC), melamine polyphosphate and melamine pyrophosphate (from Ciba).

Expandable graphite (EG) was also selected as a potential flame retardant. It contains sulphuric and/or nitric acid between the carbon layers, at high temperature the acids decompose into gases which allow blowing and separate the platelets. This induces a physical reinforcement as the graphite platelets create a network into the char [120]. According to the literature, the loadings of 20 and 30 phr (respectively 11 and 15 wt.-%) correspond to an optimum efficiency in EVA. So, EG was incorporated in the reference formulation at these levels. Expanded graphite, which is graphite submitted to a thermal treatment allowing a good exfoliation of the platelets, was also tested in the same concentration for comparison.

The tested additives are listed in *Table 18*. The main characteristics (chemical structure, particle shape and size…) of the flame retardants are further detailed in *Appendix 1*.

Table 18: Selected flame retardants: type, commercial name, supplier and loading in the reference formulation

FR type	FR type	FR name and supplier	Loading (phr)
Metal hydroxides	$Mg(OH)_2$ $Al(OH)_3$ $Al(OH)_3$ coated with zinc hydroxystannate	Magnifin H5, Albermarle Apyral 40CD, Nabaltec Charmax FS-ZHSA-10, Polymer Additives Group / USA	200
Phosphates	APP Coated-APP (intumescent) Coated-APP (intumescent) Coated-APP (intumescent)	AP423, Clariant AP765 and 766, Clariant Budit 3167, Budenheim Budit 3178, Budenheim	60 & 80
Phosphinates	Aluminium phosphinate Zinc phosphinate Aluminium phosphinate + melamine phosphate Inorganic phosphinate salt	OP 1230, Clariant OP 950, Clariant OP 1311, Clariant Phoslite B 55 CM, Italmatch	60 & 80
Melamine derivatives	Pure melamine Melamine polyphosphate Melamine pyrophosphate Melamine borate Melamine cyanurate Melamine orthophosphate	DSM MP 200, Ciba Budit 311, Budenheim Melagard MB, Italmatch Melagard MC, Italmatch Melagard MP, Italmatch	60 & 80
Graphite	Expandable graphite Expanded graphite	Inca	20 & 30

1.2 Mechanical and fire testing

The results of the mechanical and fire testing for each flame retardant are gathered in the figures presented below (from *Fig. 46* to *Fig. 52*). On each axis of the radar plots is reported a specific property (hardness, LOI …) at a specific scale. The reference material (containing MDH as FR) is red lined on each diagram for comparison.

It is noteworthy that the fire testing only focuses on LOI and UL-94 test: it was not performed any mass loss calorimeter experiment. This choice is explain by the rapidity of the two flammability tests compared with the mass loss calorimeter one. Moreover the LOI and UL-94 specifications are commonly required in the industry.

1.2.1 Metal hydroxides

The reference materials containing MDH (Magnifin H5) and ATH (Apyral 40CD) exhibit very good mechanical and fire retardant properties *(Fig. 46)*. Indeed a V0 rating is achieved and the LOI value reaches 49 vol-% and 44 vol-% respectively. The EVM-based mixture without any flame retardant was also tested for comparison: it was non-classified at UL-94 test and its LOI was 22 vol-%. Concerning the mechanical properties a hardness of 68 and 60 ShA for the mixtures with MDH and ATH is measured, such as an elongation at break (EAB) of 600 % and a tensile strength (TS) of 6.1 and 5.3 MPa respectively.

The formulation with the zinc hydroxystannate coated-ATH (Charmax) presents poorer LOI value than the non-coated ATH: only 35 vol-%, that is to say a loss of 9 vol-%. The mechanical behaviour is very close to that of the recipe with raw ATH.

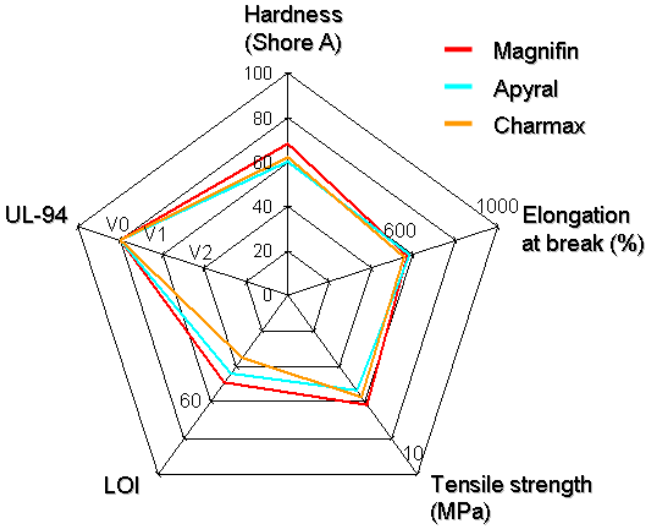


Fig. 46: Influence of metal hydroxides on the mechanical and flame retardant properties of the complete formulation

The zinc hydroxystannate coating does not provide any improvement in terms of mechanical behaviour or flammability of the material. This result is in total contradiction with the literature, since it claims an increase of the flame retardant properties [121, 122] when ATH is coated with zinc hydroxystannate in EVA, reflecting improved dispersion and possible synergism in this system. Nevertheless such effect is not perceptible in our formulation. The proposed explanation is an antagonism effect between the zinc hydroxystannate and a component of the complete formulation (the phosphate of Disflamoll TOF for example).
In our case the use of the coated additive should thus be further avoided.

1.2.2 Phosphate-based additives

The APP-based formulations were also compounded and evaluated. The obtained results for APP (AP423) and intumescent coated-APP (AP765, AP766, Budit 3167 and 3178) are gathered in *Fig. 47* and *Fig. 48*.
The most impressive modification induced by the use of such additives, compared to the reference formulation containing MDH, concerns the mechanical behaviour of the material. Indeed, the overall filler content is decreased from 55 wt-% for the metal hydroxide to 27 and 33 wt-% for the phosphorus-based compounds, thus leading to an increase of the mechanical properties.
The elongation at break of the formulations is maintained around 570 %, and even increased up to 630 % by the use of AP766.

The tensile strength is also improved. The reference material exhibits 6.1 MPa, versus 7.5 MPa for the materials containing 60 phr additives and 6.5 MPa on average with 80 phr filler. AP423 in particular imparts high TS.

The hardness values are sharply decreased by the replacement of MDH by the APP-based additives. It goes down from 68 ShA for the reference formulation to 59 ShA for the material with 60 phr AP423, 53 ShA for the formulations with 60 phr AP765 and Budit, and 42 ShA for the samples with 60 phr AP766. With higher flame retardant content (80 phr) the hardness value of the formulations is around 60 ShA. It is noteworthy that after compounding the Budit 3178 presented some dispersion problems in the matrix. Indeed, some white flame retardant agglomerates were visually noticeable in the black cured polymeric matrix

The addition of APP-based additives in the matrix is responsible for a global decrease of the flame retardant properties compared to MDH. It is noticeable that the LOI of phosphate-containing formulations are very low: around 27 vol-%. However the UL-94 rating gets higher when the FR content increases: with 80 phr AP423, AP766 and Budit 3167 the formulations reach a V0 classification at the UL-94 test.

During the flammability testing, no intumescence phenomenon was observed. It was however expected such a phenomenon, since the use of phosphate-based additives in EVA leads to the rapid formation of an expanded intumescent shield [79]. Nevertheless in the cross-linked EVM of our formulation does not melt on the contrary to the uncured EVA, thus preventing the formation of this charred layer.

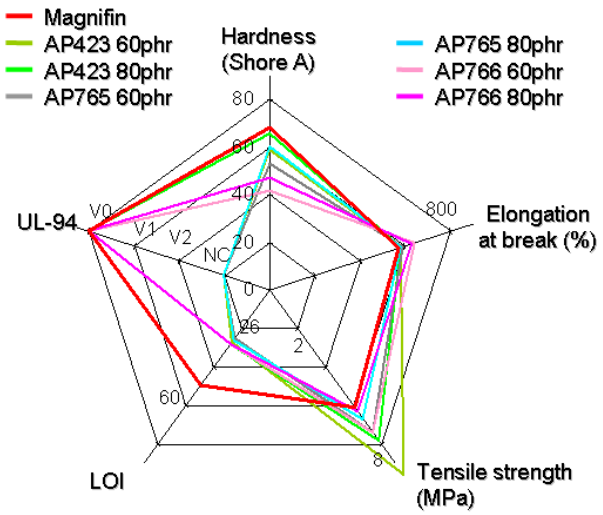


Fig. 47: Influence of phosphates on the mechanical and flame retardant properties of the complete formulation

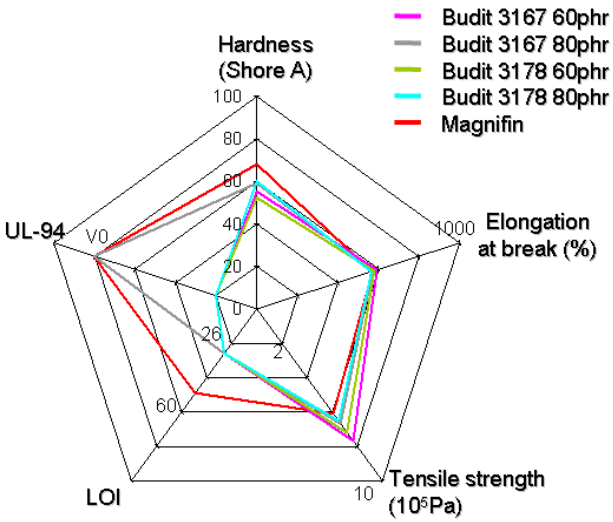


Fig. 48: Influence of intumescent compounds on the mechanical and flame retardant properties of the complete formulation

The screening reveals that the flame retardant additives based on APP do not allow reaching sufficient LOI values, but can lead to a V0 classification at UL-94 test. Since their poor LOI performances, APP based additives do not seem suitable flame retardants for the complete recipe. Nevertheless, thanks to the high UL-94 rating they provide, it can be envisaged to combine phosphates to other additives in flame retardant combinations to enhance their properties.

1.2.3 Phosphinate-based additives

Since the phosphinate-based additives have never been evaluated in elastomeric matrices, and since they proved their efficiency in some thermoplastic polymers, they were selected to be screened in the EVM-based complete formulation. Aluminium diethyl phosphinate OP1230, zinc phosphinate OP950, calcium inorganic phosphinate salt (Phoslite) and a combination of OP1230 and melamine polyphosphate MP200 (OP1311) were evaluated and compared *(Fig. 49)*.

The mechanical behaviour of the compounded materials is globally maintained in comparison to the reference formulation. The elongation at break is higher than 600 %, and the tensile strength reaches 9.5 MPa with the inorganic phosphinate salt Phoslite, and a minimum of 6.8 MPa for OP1230. Nevertheless the mechanical properties of the samples flame-retarded with OP950 are sharply damaged: the EAB is decreased down to 530 % and the TS to 4.1 MPa. This is explained by the poor dispersion of this additive in the polymeric matrix, since some agglomerates were visually observable. The dispersion quality of OP1311 is also low, but it has obviously a smaller impact.

The hardness of the phosphinate-based materials is also lower than that of the reference formulation. Indeed, organic phosphinates lead to a hardness of 45 and 50 ShA for at 60 and 80 phr respectively. The inorganic phosphinate exhibits higher values: 52 and 57 ShA.

Organic phosphinates in the complete formulation give promising fire retardant results. Their LOI, around 35 vol-%, are quite high compared to APP-based samples which only reaches 27 vol-%. The zinc phosphinate, due to its poor dispersion, also induces low LOI values (25 vol-%). The inorganic Phoslite is also less efficient as the measured LOI is only 30 vol-% at the highest concentration. However, the best phosphinate additives do not reach the same level of flame retardancy as the reference MDH.
The V0 rating at UL-94 test is achieved with OP1311 and Phoslite at 80 phr, while all other formulations are non-classified.

OP1311 additive from Clariant is known to exhibit an intumescent behaviour during the combustion of polyamide or polyester [123, 124], but this phenomenon is not observed for OP950 in PET [125]. In our EVM-based formulation, it was not observed any intumescence during fire testing.

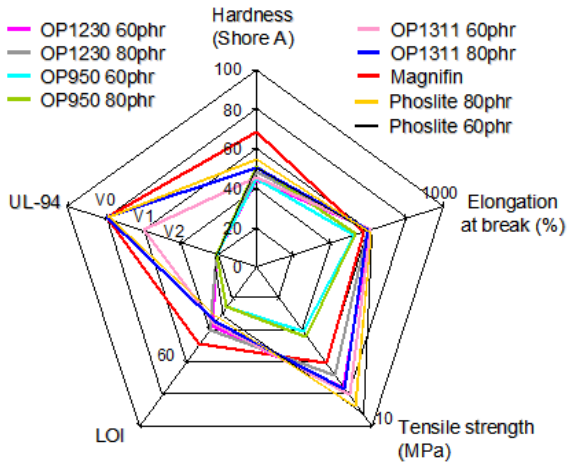


Fig. 49: Influence of phosphinate and combinations on the mechanical and flame retardant properties of the complete formulation

Organic phosphinate OP1230 was found efficient with high LOI values, such as OP1311, but only the latter allowed the reaching of a V0 rating. However OP1311 is a mixture based on OP1230: this

indicates that the aluminium diethyl phosphinate can be a promising compound for flame retardant combinations for further work.

It is known that OP1311 is a mixture of OP1230 and MP200, at a 2:1 ratio, and it presents better fire properties than OP1230 alone. MP200 and Melagard MP are quite similar products, melamine polyphosphate and melamine orthophosphate respectively, and moreover Melagard MP has a lower particle size and so no dispersion problems in EVM. So it could be interesting to investigate the efficiency of an OP1230-Melagard MP mixture in the same ratio as in OP1311.

1.2.4 Melamine and derivatives

The use of melamine was reported in the literature as a flame retardant in EVA. However, the described improvement in terms of flame retardancy is not really significant. This is the reason why it was decided to evaluate melamine salts, with the hope to improve the fire properties of the material.
The compounding revealed the poor dispersion of two compounds: MP200 and pure melamine. For MP200 some small agglomerates were visually noticeable at the surface of the cured samples, and melamine exhibited a low compatibility with the matrix since big clusters of melamine particles were detected.
In *Fig. 50* and *Fig. 51* picture the results obtained for the melamine-based formulations.

The mechanical properties for the material with pure melamine are very low: low hardness (40 ShA) and low tensile strength (6.3 and 4.8 MPa). This is due to the poor dispersion of the additive, tensile strength being reduced dramatically by the local aggregation of particles [126].
The other flame retardants allow the conservation of good mechanical behaviour. The elongation at break is around 580 % (only 553 % for the sample with melamine), the tensile strength minimum is 7.1 MPa (for Melagard MP at 80 phr) and the maximum is 10.4 MPa (for melamine cyanurate MC at 60 phr).

The hardness value is globally decreased compared to the reference formulation (68 ShA), but it remains relatively high. Indeed the melamine salts impart a hardness value close to 55 or 60 ShA depending on the flame retardant loading.

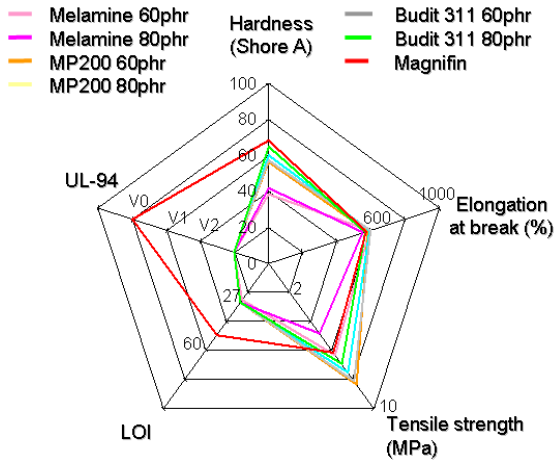


Fig. 50: Influence of melamine and MP200 on the mechanical and flame retardant properties of the complete formulation

Concerning the flame retarding properties, melamine and derivatives are quite disappointing: for all loadings the LOI values are low (25 to 27 vol-%) and the formulations did not pass the UL-94 vertical test.

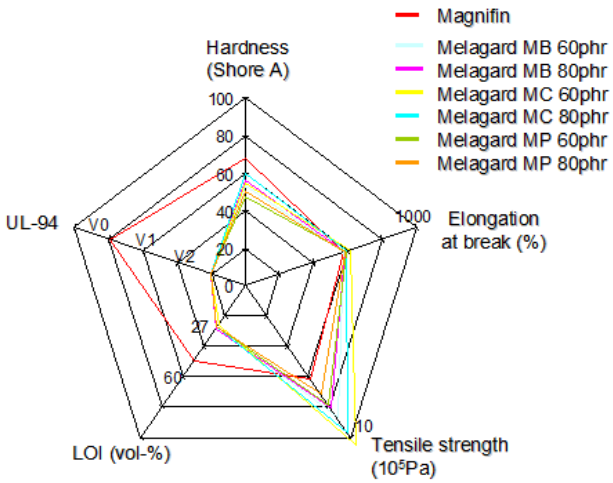


Fig. 51: Influence of melamine derivatives on the mechanical and flame retardant properties of the complete formulation

The use of these additives as single flame retardant in a complete formulation should be avoided since they provide poor flame retardant properties, but some of them could be efficient when combined with other flame retardants, such as MP200 or Melagard MP with phosphinates, as reported in the literature [127].

1.2.5 Graphite

The last flame retardant type which was tested in the complete EVM formulation is a carbon-based additive: graphite. Two graphite types were evaluated: expandable graphite and expanded graphite. The results of the mechanical and fire testing of the formulations compounded with this filler are gathered in *Fig. 52*.

The behaviour of the material with graphite is quite different from the other tested flame retardants. Indeed, the elongation at break is maintained at 600 % and the tensile reaches 11 MPa. This is explained by the plasticizer and lubricant role of the carbon platelets [128].

The flame retardant properties of the graphite compounds are very poor. The formulations did not pass the UL-94 test, they are all non classified. Concerning the LOI, the values are also very low: 25 vol-%.

It is noteworthy that the supposed blowing effect produced by expandable graphite was not observed during the combustion of the flame retarded material. As for the previously tested intumescent compounds the cross-linking of the material prevents the polymer melting and thus the blowing of the graphite platelets.

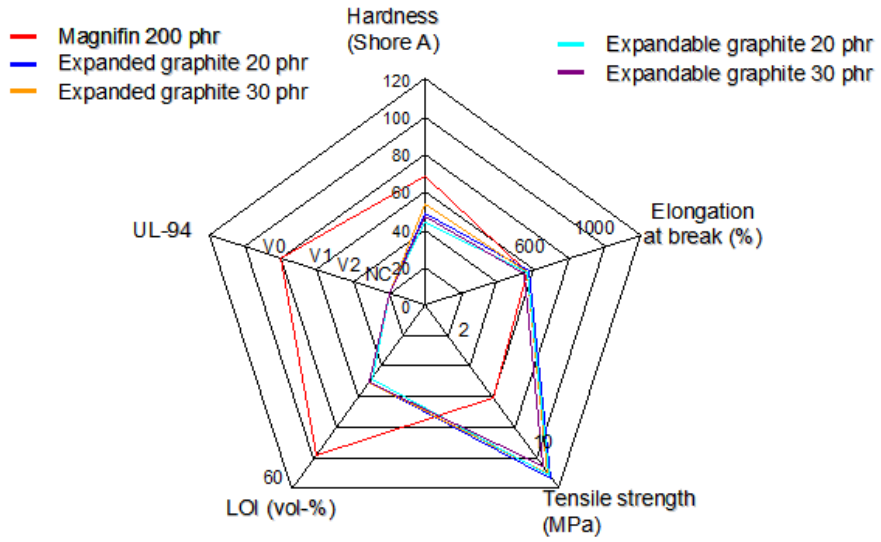


Fig. 52: Influence of melamine derivatives on the mechanical and flame retardant properties of the complete formulation

Graphite compounds reveal an interesting plasticizing effect in the complete formulation. Nevertheless, these additives do not impart any significant flame retardant effect. So, their use will be avoided for further investigations.

1.2.6 Conclusion

The screening of the flame retardants allowed the selection of some interesting additives: metal hydroxides, phosphinate-based compounds OP1311 and OP1230, intumescent APP. Concerning the metal hydroxides, magnesium dihydroxide imparts the best fire retardant properties, but its price is much higher than that of aluminium trihydroxide ATH. The latter is thus chosen for further work.

Moreover, even if no tested FR surpassed metal hydroxides for fire retardancy, it was noticeable that the lower loadings required by the phosphorous-based compounds induced better mechanical properties (higher elongation at break and tensile strength), even if the hardness values are too low.

Phosphinates in particular showed promising fire properties: high LOI and V0 rating at UL-94 test. So, phosphinates are selected as potential flame retardants to be used further in the project in combination with other additives.

2. Flame retardant combinations

Some additives were selected through the previous screening: metal hydroxides, since they are particularly cheap and phosphinates which showed promising fire properties.

To increase the flame retardant efficiency of these compounds it could be interesting to create synergies by the use of combinations. We propose in this part of the chapter to evaluate the combination of ATH and nanoparticles in order to decrease the ATH content, the combination of phosphinates and melamine derivatives and the combination of the two most promising flame retardants ATH and phosphorus compounds.

To determine if the measured flame retardant properties are effectively due to synergisms between the FR compounds and not due to interactions with the other fillers or additives of the complete formulation, the combinations will also be tested in pure vulcanized Levapren.

2.1 ATH and nano-particles

ATH is widely use in EVA both as filler and as flame retardant because of its low cost, but the required loadings are very high. However, diminishing the ATH content in a formulation or increasing the fire retardant properties of this FR with the use of very little amount of synergistic agents could be beneficial in terms of mechanical properties, processing (nanoparticles could be processing aids) and filler loading.
This is the reason why this section focuses on the interactions between ATH and some nano-synergists: organomodified nanoclay Cloisite 30B, octamethyl polyhedral silsesquioxane (OMPOSS) and multi-walled carbon nanotubes.

The expected role of these nanoparticles is to create physical and/or chemical interactions with the flame retardant, in order to increase its efficiency [87, 129].

The loadings and the compositions of the nano-synergists combined with ATH are given in *Table 19* and *Table 20*.

Table 19 : Loadings in the complete formulation and references of the nano-synergists

	ATH	Cloisite clay	OMPOSS	Carbon nanotubes
Loading (phr)	200	-	-	-
	190	10	-	-
	196	-	4	-
	199	-	-	1

Table 20 : Description of the nano-synergists

Designation	ATH	C30B	OMPOSS	MWNT
Commercial name and supplier	Apyral 40CD, Nabaltec	Cloisite 30B, Southern Clay	OMPOSS, Hybrid Plastics	Nanocyl 7000, Nanocyl
Composition	Aluminium trihydroxide $Al(OH)_3$	bentonite clay organically modified by bis(hydroxyethyl)methyl tallow alkyl ammonium	Octamethyl polyedral oligomeric silsesquioxane	Multi wall nanotubes

Note: A more detailed description of the nano-synergists is presented in Appendix 1.

The results of the mechanical, LOI and UL-94 testing of the ATH-nanoparticles containing formulations are gathered in *Fig. 53*. It is remarkable on the diagram that the presence of nano-synergists in the complete formulation influences neither the LOI value (46 to 48 vol-%) nor the UL-94 rating which remains V0.

If there is no noticeable influence of the nanoparticles on fire properties, this is not the case for mechanical ones. The hardness value of the material increases when nano-synergists are added in the polymeric matrix, up to 72 ShA (when Cloisite 30B is used). Moreover, tensile strength and elongation at break decrease to low values (about 5 MPa and 500%), apart from Cloisite 30B which allows an increase of tensile strength.

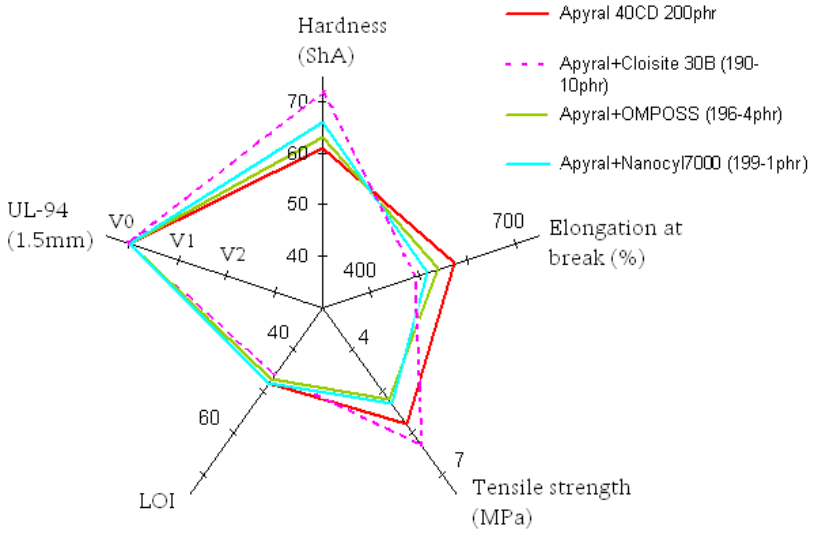


Fig. 53 : Influence of the nanoparticles on the properties of the ATH – EVM based formulations

To conclude with, the use of nanoparticles seems to damage the mechanical properties of the ATH containing formulations, and presents no noticeable influence on fire properties regarding LOI and UL-94. However, these nano-synergists may have an impact on the behaviour of the material during cone calorimeter tests, as reported in the literature [96, 130, 131] (see the previous chapter) .

The following part investigates the behaviour of the formulation when exposed to cone calorimeter. As shown in *Fig. 54* the partial substitution of ATH by nanoparticles does affect neither the shape of the RHR curves nor the peak of RHR or even the time to ignition *(Table 21)*. It is noticeable that the flame retardant efficiency of the fillers is very high as proven by the mass loss calorimeter data of pure vulcanized EVM (55 s and 340 kW/m²).

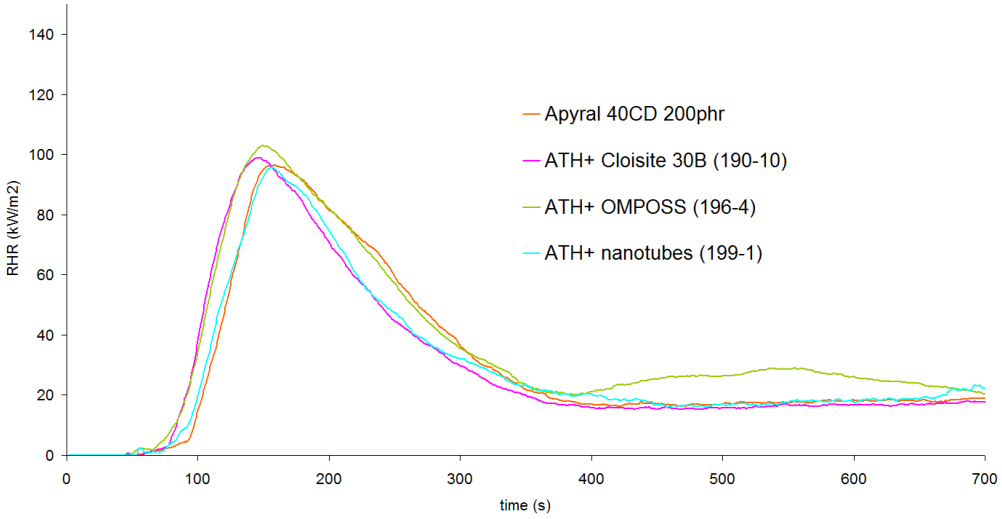


Fig. 54: RHR curves of the complete formulations flame retarded with ATH and nanoparticles

Nevertheless a second peak of RHR is noticeable on the curve of the ATH/OMPOSS combination. As for the others formulations, the first peak of RHR corresponds to the formation of a glassy protective layer, in this case mainly composed of alumina Al_2O_3 with little carbonaceous residue. The second peak is attributed to a decohesion of the alumina structure, which allows the combustible materials trapped in this structure to escape and to feed the flame. The preferred hypothesis explaining this phenomenon is that OMPOSS degrades the cohesion of the mineral residue since it sublimates [132].

Table 21: Mass loss calorimeter data of the formulations flame retarded with ATH and nanoparticles

Complete formulation+	Time to ignition (s)	PRHR (kW/m^2)
ATH Apyral 40CD (200 phr)	48 ± 7	97 ± 10
ATH+ Cloisite 30B (190-10 phr)	48 ± 7	99 ± 10
ATH+ OMPOSS (196-4 phr)	49 ± 7	103 ± 10
ATH+ carbon nanotubes (199-1 phr)	55 ± 8	96 ± 10
Vulcanized EVM	50 ± 7	340 ± 34

So, the combination of ATH with nanoparticles does not lead to any improvement in terms of flame retardancy as the LOI, the UL-94 rating and the mass loss calorimeter data remains unchanged compared to ATH alone. This result was not expected since the use of nanoparticles with ATH (clays in particular) is reported to decrease the PRHR of EVA [130]. In this case the char of the EVA/ATH/organoclay compound created by the cone calorimeter is very rigid and showed only very few small cracks whereas the char of the EVA/ATH compound exhibits a reduced mechanical strength and had many large cracks. This is also the explanation why the peak heat release rate in the case of the nanocomposite is reduced. Using such combinations in the vulcanized matrix, where charring is limited by the crosslinking of the polymeric chains, may not provide the same protective behaviour as in raw EVA.

To conclude with, the use of nanoparticles for the partial substitution of ATH is beneficial neither in terms of mechanical behaviour nor for the reaction to fire of the material. These combinations are thus abandoned for the rest of the project.

2.2 Phosphinate and melamine derivatives

Phosphinate-based compounds were selected as promising flame retardant additives through the previous screening. Indeed, aluminium diethyl phosphinate (OP1230) and the mixture of the latter with melamine polyphosphate (MP200) proved to be efficient in terms of fire retardancy.

A patent from Clariant [127], applied to thermoplastic matrices, also evokes the use of phosphinic acid salts in combination with nitrogen-containing additives, such as melamine salts. Our objective is now to evaluate the performances of such combinations in the complete elastomeric formulation.

2.2.1 Complete formulation

Zinc borate (ZB) and Disflamol TOF were avoided in the complete reference formulation as they are potential flame retardant additives. Since the combinations will be tested in pure vulcanized EVM to determine if the flame retardant properties are due to synergisms between the FR compounds and not due to interactions with the other fillers or additives of the complete formulation, the complete formulation recipe reintegrates these two products.

The compounded recipe thus corresponds to the RPW formulation *(see Chapter 2)*, where ATH is replaced by the flame retardant combinations reported in *Table 22*. ATH is selected as a flame retardant reference at 200 phr. The choice of this filler was motivated by economical considerations in accordance with the common commercially available formulations. Indeed, it has been demonstrated in the previous part of the chapter that MDH exhibits higher flame retardant properties than ATH, but

the higher price of MDH compared to ATH makes its use in commercial formulations quite rare. OP1230 was incorporated at three different loadings: 30, 90 and 150 phr.

The OP1230-Melamine orthophosphate (OP1230-MP) mixture was also tested at the same loadings, with a ratio of 2:1. Since melamine borate is considered less efficient than melamine phosphate, it was decided to increase the phosphinate content: the formulations were compounded with a OP1230-MB mixture at a 3:1 ratio.

Table 22: Loadings of the flame retardant combinations in the complete formulation (phr)

ATH (Apyral 40CD)	OP1230	OP1230-MP	OP1230-MB
200	30	20-10	27-3
-	90	60-30	68-22
-	150	100-50	113-37

The mechanical properties of the compounded materials are gathered in *Table 23*. The hardness of the formulations with OP1230 and combinations is lower or equivalent to that of the reference formulation, except the samples filled with 150 phr flame retardant additives which exhibit higher hardness, around 75 ShA.

The elongation at break is also affected by the use of phosphinate-based combinations. Compared to the sample with ATH the measured values are quite low: around 440 % for the formulations filled with 150 phr and 510 % with 30 phr.

The tensile strength is modified as well. It decreases with the FR loading, but up to 90 phr the TS remains higher than that of the reference sample.

It appears that up to 90 phr the mechanical properties (hardness, EAB and TS) are maintained. The use of OP1230 and combinations as flame retardants is not detrimental to the mechanical behaviour, they can thus be considered as valuable compounds.

Table 23: Mechanical properties of the phosphinate-melamine derivatives combinations in the complete formulation

Formulation with		Hardness (ShA)	EAB (%)	TS (MPa)
ATH 200 phr		65	582	5.3
OP1230	30 phr	58	507	9
	90 phr	68	478	6.3
	150 phr	78	439	4.6
OP1230-MP	20-10 phr	55	510	9
	60-30 phr	65	492	6.2
	100-50 phr	71	458	5
OP1230-MB	27-3 phr	53	514	9.5
	68-22 phr	69	475	6.3
	113-37 phr	77	435	4.6

The flame retardant properties of the materials were evaluated through LOI and UL-94 *(Fig. 55)*. They reveal the interest of using the combinations of OP1230 and melamine derivatives. Indeed, OP1230 alone in the complete formulation leads to LOI increasing from 27 vol-% to 37 vol-% and no classification at the UL-94 test, while the combinations allow to reach a V-0 ranking at a sufficient loading.

Moreover the use of melamine orthophosphate MP induces higher LOI values, up to 41 vol-%, which is close to that of the formulation flame retarded with ATH (44 vol-%).

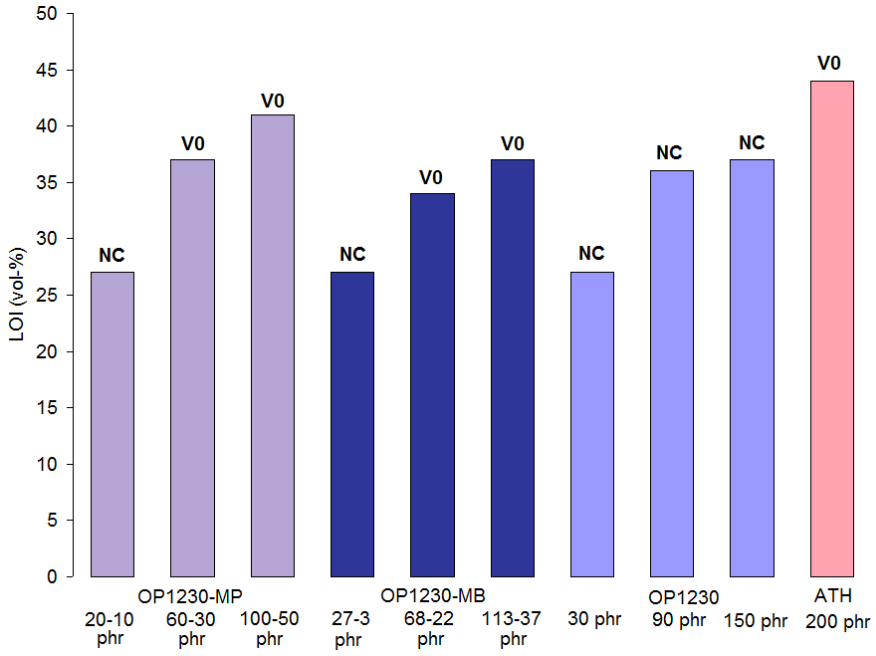


Fig. 55: LOI and UL-94 rating of the phosphinate-melamine derivatives combinations in the complete formulation

The reaction to fire of the materials was tested through mass loss calorimeter tests to simulate a fire scenario. The obtained RHR curves and data are reported in *Fig. 56* and *Table 24*.

It appears that the use of phosphinate or of phosphinate-melamine derivatives leads to a decrease of the time to ignition, from 65 to 50 s.

The combination with melamine borate MB is detrimental in terms of peak of RHR. Indeed, the PRHR values of the formulations flame retarded with this mixture are always higher (167 kW/m²) than that of pure phosphinate. Concerning the use of melamine orthophosphate MP it seems beneficial to the reaction to fire of the compounded material as it induces the lowest PRHR values (around 110 kW/m²), close to that of the reference sample containing ATH (100 kW/m²).

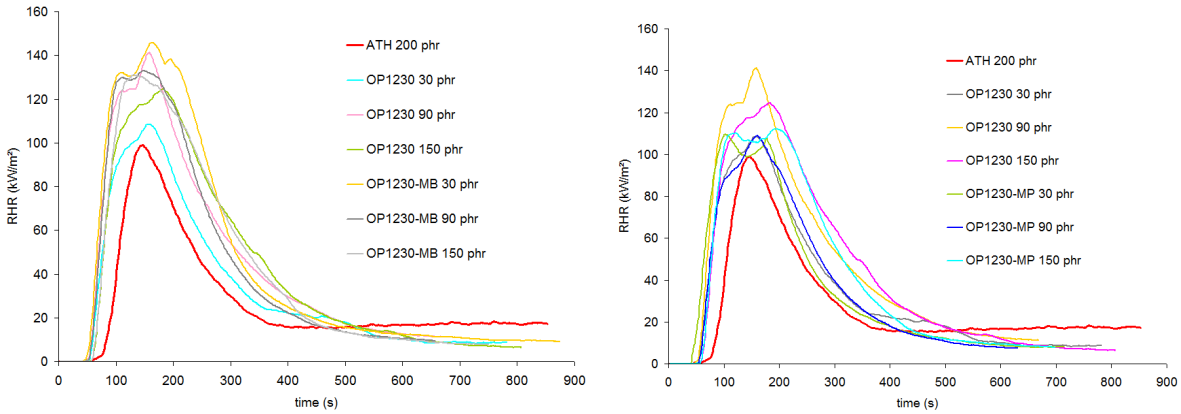


Fig. 56: RHR curves of the complete formulation flame retarded with OP1230 and OP1230-melamine derivatives combinations

Table 24: Mass loss calorimeter data of the complete formulation flame retarded with OP1230 and OP1230-melamine derivatives combinations

Complete formulation with		PRHR (kW/m²)	TTI (s)
ATH (40CD) 200phr		100 ± 10	65 ± 10
OP1230	30 phr	109 ± 11	50 ± 8
	90 phr	141 ± 14	50 ± 8
	150 phr	125 ± 13	54 ± 9
OP1230-MB	27-3 phr	167 ± 17	50 ± 8
	68-22 phr	133 ± 13	48 ± 7
	113-37 phr	131 ± 13	56 ± 8
OP1230-MP	20-10 pht	110 ± 11	42 ± 6
	60-30 phr	109 ± 11	52 ± 8
	100-50 phr	112 ± 11	50 ± 8

The flame retardant properties achieved by the use of phosphinate-melamine derivatives combinations in the complete formulation are equivalent to that of the reference material, flame retarded with ATH. In particular, a synergistic effect is observed between OP1230 and MP. To determine if the phenomenon is effectively due to interactions between the additives, the FR combinations were tested in pure vulcanized EVM, in order to avoid the presence of other additives potentially interfering.

2.2.2 Vulcanized EVM

To confirm the previous results obtained in the complete formulation, ATH, OP1230 and OP1230-melamine derivatives combinations were incorporated into vulcanized EVM. The loadings are presented in *Table 25*.

As this section investigates the potential synergisms between the additives some additional combinations of additives were tested: OP1311, which is a mixture of OP1230 and MP200 (melamine

polyphosphate) at a 2:1 ratio. To verify that the 2:1 and 3:1 ratios are optimal for the OP1230-MP and OP1230-MB combinations respectively the two ratios were evaluated for each combination.

The interactions between phosphates and melamine were also checked, but no synergistic effect was revealed *(see Appendix 3)*.

Table 25: Loadings of the flame retardant combinations in vulcanized EVM (phr)

Combination	Loading (phr)	
ATH (40CD) 130 phr	130	
OP1230	55	
OP1311	55	
OP1230-MP	37-18	41-14
OP1230-MB	37-18	41-14

The LOI and UL-94 tests reveal that there is a great influence of the phosphinate-melamine derivative ratio. Indeed, the 2:1 ratio for the OP1230-MP mixture allows the reaching of a V0 rating and a LOI of 57 vol-% whereas a 3:1 ratio only leads to a V1 rating and a LOI of 55 vol-%. This effect is even more perceptible with OP1230-MB, as the LOI increases from 32 to 47 vol-% when the ratio of 2:1 is changed for a 3:1 ratio. However the formulations remain non classified.

The LOI value for OP1311 is around 44 vol-%, but the sample does not pass the UL-94 test. This can be explained by the poor dispersion of the product, diminishing the flame retardant efficiency of the filler.

It is noteworthy that the LOI of the samples exhibit higher or equivalent LOI to the reference formulation with ATH. Indeed, the reference formulation has a LOI of 32 vol-%, such as the sample with the OP1230-MB (2:1 ratio) mixture, whereas the other formulations present LOI higher than 40 vol-%.

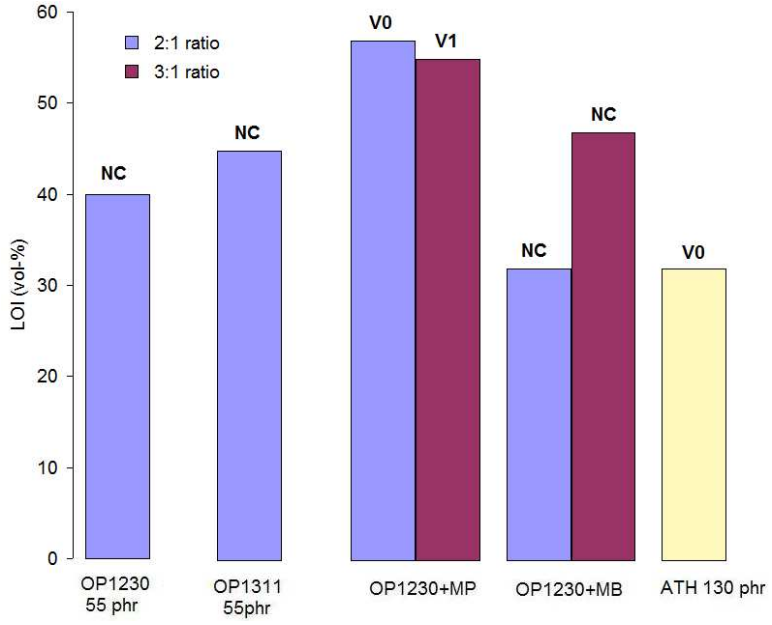


Fig. 57: LOI and UL-94 rating of the phosphinate-melamine derivatives combinations in vulcanized EVM

It was demonstrated that the chosen ratio in the complete formulation were adapted to the flame retardant combinations. Moreover the synergistic effect observed between the aluminium phosphinate and melamine orthophosphate and melamine borate is confirmed. The best level of flame retardancy is achieved with the use of the OP1230-MP mixture at the 2:1 ratio.

It is assumed in the literature that melamine possesses smoke suppressant properties. Melamine derivative can potentially have such suppressing effect. It is thus interesting to investigate the smoke emission of vulcanized EVM flame retarded with phosphinate and melamine derivatives. NBS smoke chamber tests were carried out, the obtained results are gathered in *Table 26*.

Vulcanized EVM containing ATH as a reference, 55 phr OP1230 and the same level of OP123-MP and OP1230-MB combinations was tested. The smoke density (Dm) of the samples containing phosphinates is very high (1007 and 1288 for OP1230 and OP1230-MP respectively) compared to that of the reference polymer with ATH (140). The smoke release is also increased with the use of phosphinate (from 19 to 1000).

Table 26: NBS smoke chamber test results for vulcanized EVM flame retarded with ATH, OP1230 and OP1230-melamine derivatives combinations

Vulcanized EVM with	Dm	VOF4
ATH 130 phr	140	19
OP1230 55 phr	1007	843
OP1230-MP 55 phr (2:1)	1288	1033
OP1230-MB 55 phr (3:1)	619	497

Dm = maximum smoke density VOF4 = total smoke release

It is however noticeable that melamine borate MB induces a sharp decrease of the smoke emission, such as of the smoke density: compared to OP1230 used alone in the polymer the maximum smoke density and total smoke release are divided by two.

So, the incorporation of melamine borate in the phosphinate-melamine derivatives combinations seems very valuable in terms of smoke suppression.

2.2.3 Conclusion

The use of phosphinate-melamine derivatives combinations in the complete formulation does not appear detrimental to the mechanical properties. Moreover they appeared very valuable in terms of flame retardancy, especially the OP1230-MP mixture. The flame retardant synergistic effect between the compounds was clearly demonstrated in vulcanized EVM, and the choice of the ratios (2:1 for OP1230-MP and 3:1 for OP1230-MB) was confirmed.

So, aluminium diethyl phosphinate and melamine orthophosphate mixture is worth for its high flame retardant properties. OP1230 and melamine borate exhibit lower flame retardancy than the other

combinations but provide an interesting smoke suppressant effect. Nevertheless, despite of their high efficiency these additives remain expensive, which would limit their use in commercial formulations. That is why it was decided not to carry out further experiments on these combinations.

2.3 ATH, phosphates and phosphinates

ATH is widely used in EVA both as filler and as flame retardant because of its low cost and its efficiency. However, decreasing the ATH content in a formulation while keeping the same level of flame retardant properties is a current challenge as it could allow for lower hardness. It is proposed in this part of the chapter to combine ATH (with low price and high efficiency) with phosphorous compounds which are, according to the previous study, valuable flame retardants in EVA.

This part of the chapter aims to determine if the combinations between ATH and phosphorous compounds are valuable and if they deserve further study or not. ATH-phosphate and ATH-phosphinate combinations will be tested in the complete "reference" formulation, the influence of the phosphorous additives on fire and mechanical properties will be evaluated.

2.3.1 ATH grade selection

Different Apyral grades can be used in the EVM-based formulations, mostly differing by their particle size and by their specific surface area *(Table 27)*.

Table 27: Particle size, specific surface area and oil absorption of the different Apyral grades

	[1]D_{50} (µm)	[2]BET (m^2/g)	Oil absorption (ml/100g)
Apyral 40CD	1.3	3.5	21
Apyral 60CD	1.0	6.0	28
Apyral 120E	0.9	11	37
Apyral 200SM	0.3	22	48

The different grades of ATH have a similar morphology *(Fig. 58)*. They are platy-like, and their shape does not change whatever the particle size.

[1] D_{50} means that at least 50 wt-% of the particles have a diameter $<D_{50}$
[2] Estimation of the surface area by the so-called BET method (Brunauer, Emmett and Teller, 1938).

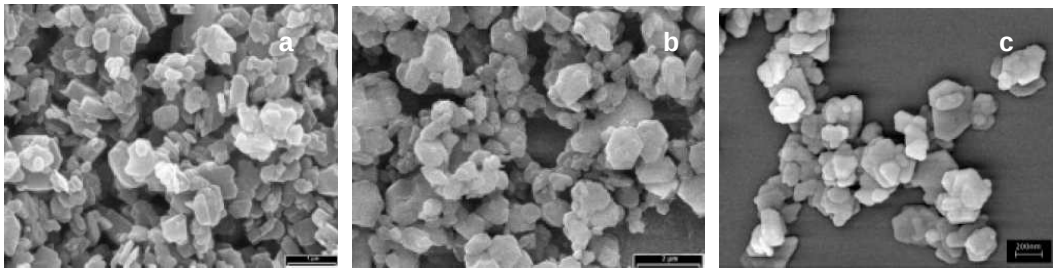


Fig. 58: SEM images of Apyral 40CD (a) Apyral 60CD/120E (b) Apyral 200SM (c) particles

The different ATH grades were compounded at 130 phr in vulcanized EVM. By this way it is expected to highlight the potential effect of the ATH particle size on the flame retardant properties.

The flammability of the samples was investigated through LOI and UL-94 tests *(Fig.2)*. The results of these tests revealed a trend: the flame retardancy is improved when the ATH particle size decreases. In particular the UL-94 rating increases from V1 for vulcanized EVM containing 130 phr Apyral 40CD to V0 for the others formulations. The LOI is slightly increased from 32 to 35 vol-%.

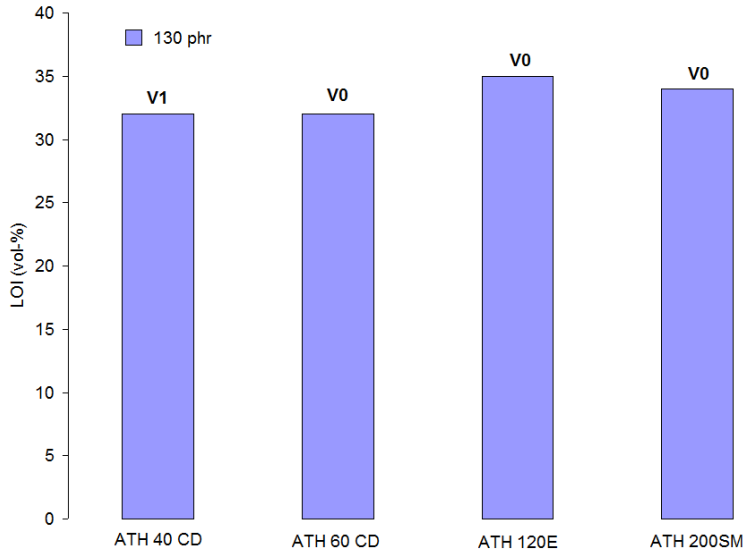


Fig. 59: LOI and UL-94 rating of vulcanized EVM flame retarded with different ATH grades

Cone calorimeter tests revealed the influence of the ATH particle size on the reaction to fire. At iso-phr (130 phr ATH in vulcanized EVM) the use of lower particle sizes i.e. Apyral 120E and 200SM induces an increase of the time to ignition of the formulations (from 72 to 109 s) *(Fig.3 and Table 2)*.

Concerning the peaks of RHR an influence of the particle size on the shape of the curves is noted. Indeed, the first peak is the less intense for the formulations containing 40CD and 60CD while the second one is the less intense for lower ATH particle size.

Another phenomenon is noticeable: the total heat release (THR) of the formulations decreases with decreasing particle size (from 30 to 22 MJ/m²).

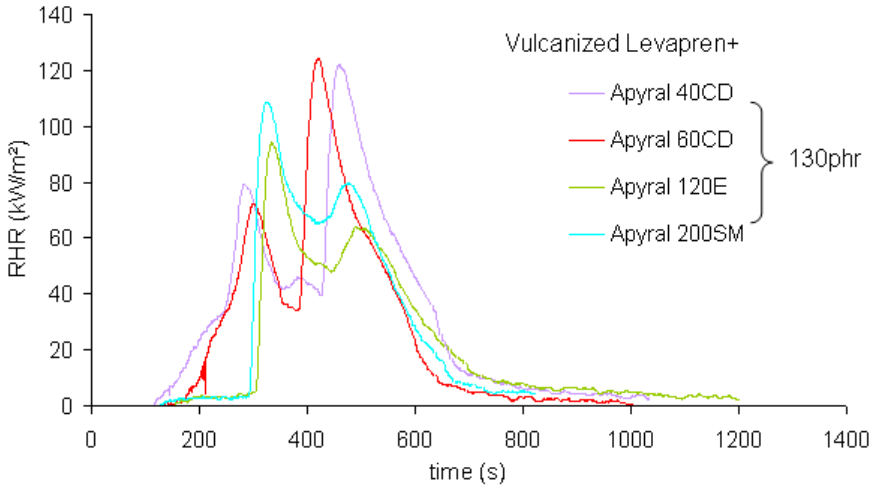


Fig. 60: RHR curves of the formulations composed of vulcanized EVM and ATH for different ATH particle size

Table 28: Cone calorimeter data of vulcanized EVM containing different Apyral grades

	Apyral 40CD	**Apyral 60CD**	**Apyral 120E**	**Apyral 200SM**
Ti (s)	78	72	94	109
PRHR1 (kW/m²)	78	72	94	109
PRHR2 (kW/m²)	122	124	64	78
THR (MJ/m²)	30	25	22	23

As a conclusion it can be said that the smaller the particle size, the higher the flame retardant properties. However beyond a certain limit (0.9 µm) there is no more improvement of the flame retardancy of the material. So, **ATH 120E** can be considered the optimum ATH grade.

2.3.2 Complete formulation

As for the previous study the complete formulation recipe corresponds to the RPW recipe *(see Appendix 2)*.

Table 29 reports the investigated loadings of the ATH-phosphate (AP423), ATH-phosphinate (OP1230) and ATH-phosphinate-melamine polyphosphate (OP1311). The ATH grade used in the study is Apyral 120E.

Table 29 : ATH and phosphorous compounds contents in the complete formulation (phr)

Apyral 120E	190	160	160	160	100	100	100
AP423	-	30	-	-	90	-	-
OP1230	-	-	30	-	-	90	-
OP1311	-	-	-	30	-	-	90

The effects generated by the partial substitution of ATH by phosphate or phosphinate in the complete formulation on the mechanical behaviour are shown in *Table 30*.

The use of phosphinates in combination with ATH is beneficial for the mechanical properties. The formulations containing ATH and OP1230 or OP1311 exhibit lower hardness values (around 70 ShA) than the reference formulation with pure ATH (81 ShA), and also higher elongation at break and equivalent tensile strength (around 5.2 MPa).

On the other hand the ATH-AP423 combination leads to a material presenting a higher hardness, around 90 ShA, than that of the reference. Moreover the tensile strength is decreased, such as the elongation at break which goes down from 433 % for the reference material to 418 % and 406 % for the samples with the ATH-phosphate combination at 160-30 and 100-90 phr respectively.

Table 30 : Hardness, Elongation at break and tensile strength of the ATH-phosphorous compounds combinations in the complete formulation

	ATH 120E (190 phr)	**160-30 phr**			**100-90 phr**		
		ATH-AP423	**ATH-OP1230**	**ATH-OP1311**	**ATH-AP423**	**ATH-OP1230**	**ATH-OP1311**
Hardness (Shore A)	81	89	71	72	93	71	72
Elongation at break (%)	433	418	520	509	406	481	475
Tensile strength (MPa)	5.6	5.6	5.3	5.2	4.2	5	5

So, the mechanical properties are improved for the formulations containing the combinations of FR additives compared to ATH alone, except for the ATH/AP423 mixture.

The flame retardancy of the compounded formulations was investigated through LOI and UL-94 test. The results *(Fig. 61)* show that the substitution of ATH by phosphate or phosphinates is not detrimental to the UL-94 rating as all formulation remains V0 classified.

The ATH/phosphinate combinations have a positive impact on the LOI compared with the formulation containing pure ATH. The LOI increases, with a maximum of + 6 vol-% and + 8 vol-% respectively for ATH/OP1230 and ATH/OP1311 at 100-90 ratio. On the contrary, the presence of AP423 is detrimental to the LOI.

The ATH-phosphinate combinations are valuable in the complete formulation since they allow an increase of the mechanical and flame retardant properties compared to ATH used alone. Concerning the ATH-phosphate combination, it does not appear beneficial nor for the mechanical neither for the flame retardant behaviour. As OP1311 is a combination of phosphinate OP1230 and melamine polyphosphate MP200, it is reasonable to suppose that there can exist some synergisitic effect between ATH, phosphinates and melamine derivatives. This possibility was investigated *(see Appendix 4)* but no improvement was observed with the use of the ternary combinations.

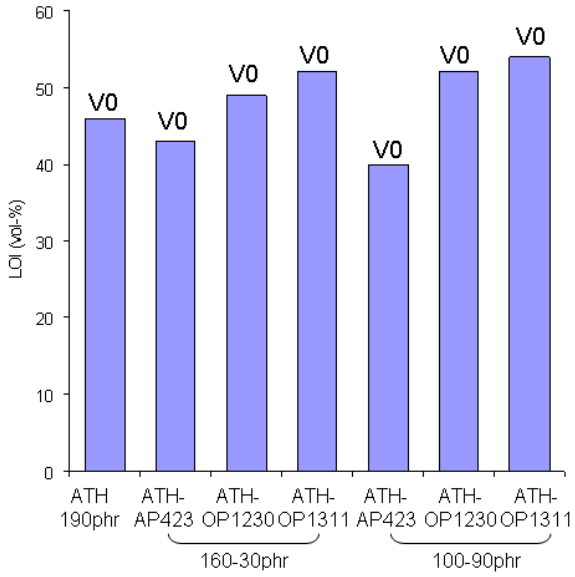


Fig. 61: LOI and UL-94 rating of the ATH-phosphorous compounds combinations in the complete formulation

To ensure that the synergistic effect between observed ATH and OP1230 is effectively due to an interaction between the additives and is not polluted by parallel interactions with other components of the complete formulation, the same combinations were have been compounded into vulcanized EVM.

2.3.3 Vulcanized EVM

The same combinations were tested in vulcanized EVM. The additive loadings are reported in *Table 31*.

Table 31 : ATH and phosphorous compounds contents in vulcanized EVM (phr)

Apyral 120E	190	160	160	160	100	100	100
AP423	-	30	-	-	90	-	-
OP1230	-	-	30	-	-	90	-
OP1311	-	-	-	30	-	-	90

The flame retardant properties were evaluated through LOI and UL-94 test *(Fig. 62)*. As observed in the complete formulation the positive effect between ATH and phosphinate OP1230 is also noticeable in vulcanized EVM. Indeed, the LOI is increased from 54 vol-% for ATH alone to 65 vol-% for the sample with ATH and OP1230 at a 10:9 ratio. Concerning the UL-94 ranking it remains unchanged at V0.

It is noteworthy that there is no synergism anymore between ATH and OP1311: the use of MP200 with the phosphinate and ATH does not impart any supplementary flame retardant efficiency.

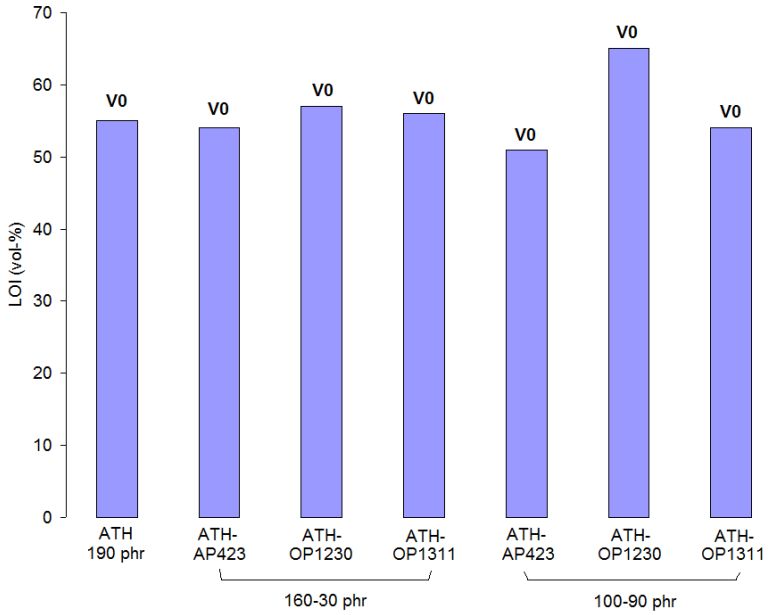


Fig. 62 : LOI and UL-94 rating of the ATH-phosphorous compounds combinations in vulcanized EVM

2.3.4 Conclusion

The combination of ATH and phosphate is valuable neither in the complete formulation nor in vulcanized EVM since it is detrimental to the mechanical behaviour and to the flame retardant properties compared to ATH used alone.

On the contrary adding phosphinate to ATH imparts interesting flame retardant properties. Moreover the combination allows maintaining the mechanical properties while decreasing the hardness of the complete formulation. The observed synergistic effect is confirmed in vulcanized EVM.

It appears that the ATH-phosphinate mixture is of great interest in EVM vulcanizates, since it combines good mechanical behaviour and exceptional flame retardant properties. The next step will thus consist in designing an optimized complete formulation flame retarded with ATH and phosphinate OP1230.

3. Optimization of the complete formulation: ATH-phosphinate flame retardant combination

The aim of this part of the chapter is to design a complete formulation flame retarded with the ATH-OP1230 combination. Thus, it is important to determine the optimum ATH grade in combination with phosphinate, and to evaluate the optimal ratio of the flame retardant mixture.

3.1 Selection of the ATH grade

The influence of the ATH particle size on the flame retardant properties of vulcanized EVM was demonstrated in *Appendix 4*. It is now important to ensure that the previously chosen grade is adapted to the ATH-OP1230 combinations.

For that, the four ATH grades (40CD, 60CD, 120E and 200SM) were tested at 69 phr in combination with OP1230 (61 phr) in vulcanized EVM.
The results of LOI and UL-94 rating tests are presented in *Fig. 63*. LOI values remain stable at 54 vol-% whatever the ATH Apyral grade used in the formulation, while the UL-94 rating is improved when the ATH particle size decreases. Indeed, the V1 ranking of the sample containing the 40CD grade is improved to a V0 classification with 60CD, 120E and 200SM.

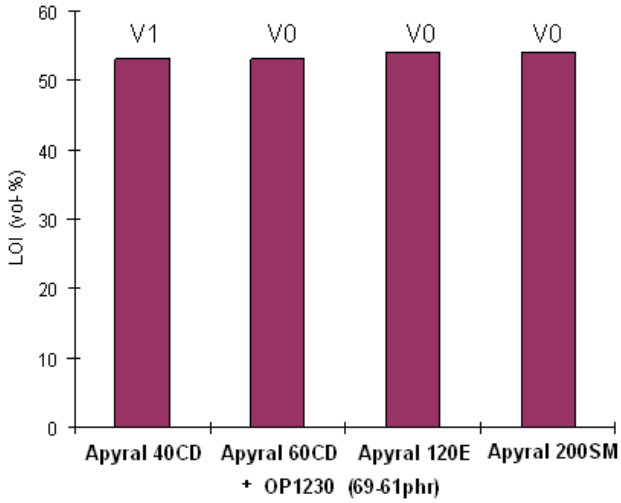


Fig. 63 : Evolution of LOI values of vulcanized EVM containing ATH and OP1230 depending on the ATH particle size

RHR curves *(Fig. 64 and Table 32)* reveal an effect of the variation of the ATH particle size. The peak of RHR decreases with the particle size (from 108 to 80 kW/m²) and the time to ignition increases. Moreover, the Total Heat Release (THR) corresponding to the area of the RHR curve is lower for the formulation containing the smallest ATH particle size.

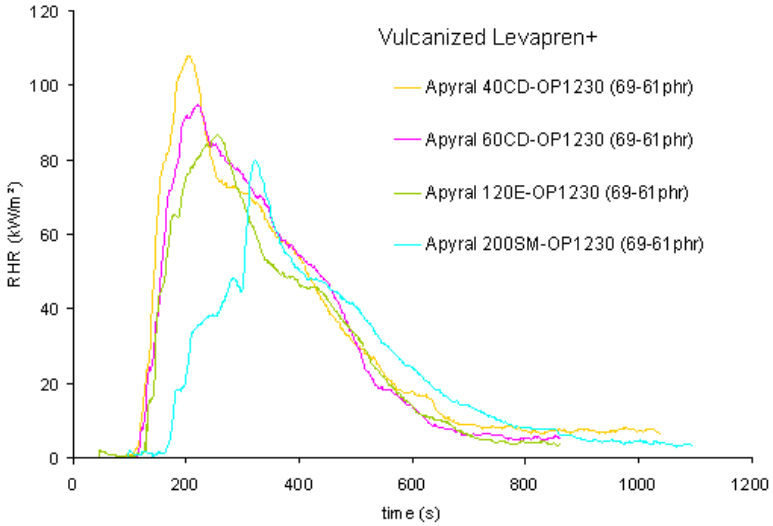


Fig. 64 : RHR curves of vulcanized EVM containing ATH and OP1230 depending on the ATH particle size (irradiance 35kW/m²)

Table 32 : Cone calorimeter data (35kW/m²) of vulcanized EVM containing ATH and OP1230 depending on the ATH particle size

OP1230 61phr+	**Apyral 40CD**	**Apyral 60CD**	**Apyral 120E**	**Apyral 200SM**
Loading (phr)	69	69	69	69
Ti (s)	110 ± 17	116 ± 17	129 ± 19	165 ± 25
PRHR (kW/m²)	108 ± 11	95 ± 10	87 ± 9	80 ± 8
THR (MJ/m²)	31 ± 3	27 ± 3	26 ± 3	21 ± 2

The fire testing of the formulations containing the ATH-OP1230 combination revealed that the UL-94 rating and cone calorimeter data are improved by the use of small-sized ATH particles, in particular the 200SM grade.

Mechanical testing showed that the modification of the ATH particle size does not change the mechanical behaviour of vulcanized EVM containing the OP1230-ATH combinations. So, the best ATH grade was chosen regarding its flame retardant efficiency.

The fire testing of the formulations containing the ATH-OP1230 combination revealed that the UL-94 rating and cone calorimeter data are improved by the use of small-sized ATH particles, in particular the Apyral 200SM grade. Nevertheless the flame retardant properties of 120E are equivalent to that of 200SM, and 120E is moreover less expensive. So, ATH 120E is recommended for the ATH-phosphinates combinations.

3.2 Optimization of the ATH-OP1230 ratio

The ATH/OP1230 loading is chosen to be 120 phr, that is to say 41wt-%, which is the same flame retardant content as the RPW reference formulation. The selected ATH grade is 120E, as recommended by the previous study.

The flame retardant ratios for the complete recipe are presented in *Table 33*. The recipe of the complete commercial formulation corresponds to the RPW recipe *(see Chapter 2)*.

Table 33 : ATH/OP1230 loadings (phr) of the complete formulations

ATH (Apyral 120E)	OP1230	Loading (wt-%)
120	-	41
110	10	41
100	20	41
90	30	41
80	40	41
70	50	41

The elongation at break and the tensile strength of the complete formulations are presented in *Fig. 65*.

The EAB of the complete formulations show a beneficial effect of the substitution of ATH by OP1230 whatever the ratio. Nevertheless this effect becomes less when the OP1230 content increases: the EAB goes from 466 % for the formulation without OP1230 to 525 % with ATH-OP1230 at 100:20 ratio, and decreases to 494 % for the 70:50 ratio.

The TS is also modified by the OP1230 substitution. It remains stable at 7.2 MPa for low substituted formulation and then goes down to 6.1 MPa for the sample containing 50 phr OP1230.

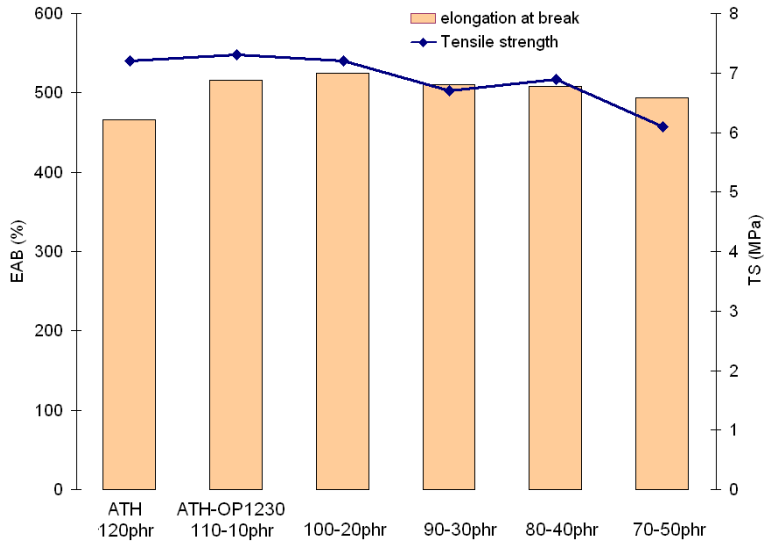


Fig. 65 : TS and EAB of the complete formulations flame retarded with various ATH-OP1230 ratios

The variation of the ATH-OP1230 ratio incorporated into a complete formulation leads to some variation of the mechanical properties. The elongation at break is improved by higher OP1230 quantities in the formulations while the tensile strength is decreased beyond certain OP1230 content (20phr).

It appears that the optimal ratio in terms of mechanical behaviour is the 100:20 ratio as it presents in a complete formulation the highest EAB and TS values. Nevertheless, up to 40 phr OP1230 the mechanical properties are maintained compared to ATH used alone, so that it is not really detrimental to substitute ATH by OP1230 below this point.

The LOI values and the UL-94 ratings of the complete formulations depending on the level of substitution of OP1230 are presented in *Fig. 66*. It appears that the LOI remains quite constant up to the substitution of ATH by 30 phr OP1230. Beyond this point (40 and 50 phr OP1230) the LOI increases from 37 to 42 vol-%.

Concerning the UL-94 rating the formulations are all V0 classified except from the sample with the lowest OP1230 loading (10 phr) which is V1. This could be explained by the fact that at this concentration OP1230 is not efficient enough to compensate the loss of 10 phr ATH, thus leading to a diminution of the UL-94 rating.

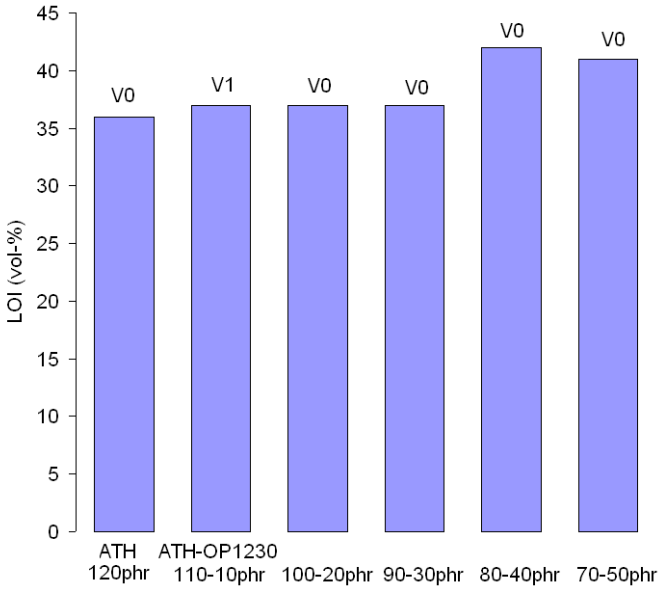


Fig. 66 : LOI and UL-94 rating of the complete formulations flame retarded with various ATH-OP1230 ratios

To complete the study about the reaction to fire of these materials, some mass loss calorimeter tests were carried out. The results for the complete formulations flame retarded with ATH-OP1230 combinations are reported in *Fig. 67* and *Table 34*.

The shape of the RHR curves is modified by the ATH-OP1230 ratio. Indeed, the RHR curves widen when the OP1230 concentration increases. This effect is attributed to the substitution of the non flammable inorganic part (ATH) by a flammable organic compound (the diethyl groups of the phosphinate). The peak of rate of heat release (PRHR) slightly varies depending on the OP1230

content. The formulations with ATH and OP1230 at low OP1230 content (10 to 30 phr) present PRHR values close to that of the sample containing only ATH (around 100 kW/m²). The other samples exhibit slightly higher PRHR values, up to 140 kW/m².

Concerning the time to ignition it is quite not influenced by the substitution of ATH by OP1230 as it remains stable around 85 s.

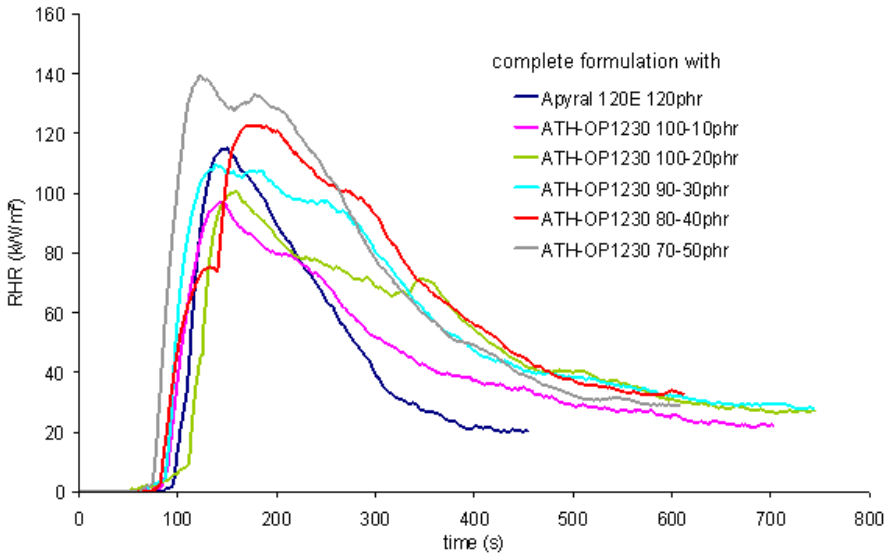


Fig. 67 : RHR curves of complete formulations flame-retarded with various ATH-OP1230 ratios

Table 34 : Mass loss calorimeter data of the complete formulations (margin of error TTI: 20%, PRHR: 10%)

Complete formulation with:	TTI (s)	PRHR (kW/m²)
ATH 120phr	95 ± 14	109 ± 11
ATH-OP1230 110-10phr	82 ± 12	97 ± 10
ATH-OP1230 100-20phr	111 ± 17	101 ± 10
ATH-OP1230 90-30phr	83 ± 12	110 ± 11
ATH-OP1230 80-40phr	81 ± 12	123 ± 12
ATH-OP1230 70-50phr	74 ± 11	139 ± 14

The variation of the ATH-OP1230 ratio incorporated into the complete formulation leads to some variation of the mechanical properties. The elongation at break is improved by higher OP1230 quantities in the formulations while the tensile strength is decreased beyond certain OP1230 content (20phr).

The optimal ratio in terms of mechanical behaviour is the 100:20 ratio as it presents in a complete formulation the highest EAB and TS values. Nevertheless, up to 40 phr OP1230 the mechanical properties are maintained compared to ATH used alone.

Concerning the flame retardant properties the LOI of the complete formulations is increased when the 80:40 ratio is used, while maintaining the UL-94 ranking at a V0 rating. The mass loss calorimeter tests revealed no particular detrimental effect of this combination compared to ATH used alone.

So, the optimum ratio of the ATH-OP1230 combination is considered 2:1 (80:40) as it allows the conservation of good mechanical properties while increasing the flame retardant properties in comparison to ATH used alone.

3.3 Conclusion: optimal composition

This part of the study allowed the determination of the best flame retardant compounds for the EVM-based complete formulation. It was found that ATH Apyral 120E was the optimal grade for the ATH-phosphinate combination. Then this additive was selected to investigate the optimum ATH-OP1230 in the complete formulation. It appeared that the 2:1 ratio is the best compromise between a preserved mechanical behaviour and increased flame retardant properties.
It was thus designed an optimal complete formulation recipe, detailed in *Table 14*. The flame retardant properties thereof are presented in *Table 36*, and confirm the interest of partially substituting ATH by OP1230.

Table 35 : Optimized flame retardant complete formulation

Commercial reference	Compound	Loading (phr)
Levapren 600 HV	EVM	100
Apyral 120E	ATH	80
Exolit OP1230	phosphinate	40
Vulkasil N	Silica	30
Carbon black N550	Carbon black	2
Zinc borate	ZB	10
Disflamoll TOF	Disflamoll TOF	20
Vulkanox HS	Anti-aging	2
Stearic acid	Stearic acid	2
Aflux 18	plasticizer	2
Rhenofit TAC/S	Co-agent	1
Perkadox 14-40	peroxide	6
	Total phr	**295**

Table 36: Flame retardant properties of the optimal complete formulation

Property	Value
LOI (vol-%)	42
UL-94 rating	V0
Time to ignition (s)	81
PRHR (kW/m²)	123

4. Conclusion

The screening of the flame retardant additives selected through the previous bibliographical study tested metal hydroxides, phosphorous-based compounds, melamine derivatives and graphite. It allowed the selection of some interesting additives: ATH thanks to its low price and high efficiency, phosphinate-based compounds OP1311 and OP1230 and intumescent APP.
The tested FR did not reach the same level of flame retardancy as metal hydroxides. However it was noticeable that the lower loadings required by the phosphorous-based compounds induced better mechanical properties. Phosphinates in particular showed promising fire properties: high LOI and V0 rating at UL-94 test. So, phosphinates are selected as potential flame retardants to be used further in the project in combination with other additives in order to create synergies.

Different combinations based on ATH or on phosphinates were evaluated: ATH and nanoparticles, phosphinate and melamine derivatives, ATH and phosphorus compounds.

The combinations of ATH with nanoparticles are not beneficial either in terms of mechanical behaviour or for the reaction to fire of the material since the LOI, the UL-94 rating and the mass loss calorimeter data remain unchanged compared to ATH alone. These combinations are thus abandoned for the rest of the project.

The use of phosphinate-melamine derivatives (melamine polyphosphate, orthophosphate and melamine borate) combinations were also evaluated in the complete formulation. They appeared very valuable in terms of flame retardancy, especially the phosphinate-melamine orthophosphate mixture. The flame retardant synergistic effect between the compounds was clearly demonstrated in vulcanized EVM.
So, aluminium diethyl phosphinate and melamine orthophosphate mixture is worth for its high flame retardant properties. OP1230 and melamine borate combination exhibits lower flame retardancy but an interesting smoke suppressant effect. Nevertheless, despite of their high efficiency these additives remain expensive, which would limit their use in commercial formulations. That is why it was decided not to carry out further experiments on these combinations.

The ATH-phosphate and ATH-phosphinate combinations were tested in the complete formulation. The combination of ATH and phosphate was not found valuable since it is detrimental to the mechanical behaviour and the flame retardant properties compared to ATH used alone.
On the contrary adding phosphinate to ATH imparts interesting flame retardant properties. Moreover the combination allows maintaining the mechanical properties while decreasing the hardness of the complete formulation. The observed synergistic effect is confirmed in vulcanized EVM.
So, the ATH-OP1230 combination seems to be an adapted answer to our challenge: finding a flame retardant composition with comparable flame retardant properties to ATH, but inducing improved mechanical behaviour.

The last part of the chapter consisted in designing an optimized complete formulation flame retarded with ATH and phosphinate OP1230. This study allowed us to determine the best flame retardant compounds for the EVM-based complete formulation. It was found that ATH Apyral 120E was the optimal grade for the ATH-phosphinate combination. Then this additive was selected to investigate the optimum ATH-OP1230 in the complete formulation. It appeared that the 2:1 ratio is the best compromise between a preserved mechanical behaviour and increased flame retardant properties.
It was finally designed an optimal complete formulation recipe with high flame retardant efficiency.

The industrial challenge was achieved: developing a flame retardant formulation with lower hardness but high mechanical properties. The synergism between ATH and the phosphinate OP1230 is responsible for the high level of flame retardancy of the formulation. The next step now consists in having a better understanding of the flame retardant mechanisms. It is thus necessary to investigate the mechanisms of action of the additives, and the type of interactions occurring between aluminium trihydrate and phosphinate.
The flame retardant role and mechanism of ATH has never been determined in vulcanized EVM matrices by now. This will be the core of the next chapter, dedicated to the comprehension of the ATH mode of action in vulcanized EVM.

CHAPTER 4 – INVESTIGATIONS ON THE ATH MODE OF ACTION

The investigations previously reported provided an optimized novel fire retarded EVM-based formulation combining aluminium trihydrate and phosphinate, exhibiting lower hardness value but high mechanical properties. This combination has never been investigated in the literature and it is thus necessary to have a better understanding of the flame retardant mechanisms of such a material. Since the flame retardant behaviour of a formulation depends on the degradation reactions occurring in the condensed phase, and thus in the evolved gas phase, it is important to determine how the FR additives influence the thermal degradation of the polymeric matrix. However, before going into details in the investigation of the tri-components formulation (EVA/ATH/phosphinate), the mode of action of ATH in vulcanized EVM will be primarily studied since it has never been reported (even if it is widely reported for EVA). Moreover, to decrease the number of influencing parameters, the investigations will be carried out in pure vulcanized EVM (and not in commercial formulation) to avoid the potential interactions of the other components included in the complete formulation.
Based on the results of this chapter, the interactions between ATH and the phosphinate compound will then be studied in vulcanized EVM in *Chapter 5*.

The goal of this chapter is thus to investigate the influence of ATH in EVM vulcanizate. To have a complete understanding of the mode of action of ATH, three questions have to be answered:

- How does pure vulcanized EVM degrade? Is there an influence of the cross-linking?
- Is there an influence of ATH on its degradation?
- If yes, what sort of influence? And could it be linked to the flame retardant performances?

So, the first part of this chapter is dedicated to the mechanistic study of the thermal degradation of pure vulcanized EVM, and of the same matrix flame retarded with ATH. The chemical pathway of the thermal degradation will be discussed, such as the influence of ATH on the degradation chemistry.

As a second step, the kinetic modelling of the thermal degradation of the materials will be performed. The influence of ATH on each degradation step of vulcanized EVM will thus be explained. The use of the kinetic analysis will allow revisiting the mode of action of ATH in the matrix and thus will be fully characterized.

The last part of this chapter is devoted to a general discussion about the influence of vulcanization and of the flame retardant additive (ATH) on the degradation mechanism of the cross-linked polymer. Finally, as an applicative part the evolution of the structure of the residue in fire conditions (simulated by a mass loss calorimeter) will be investigated and discussed to validate the proposed flame retardant mechanism.

1. Thermal degradation mechanism

The flame retardant behaviour of a material depends on the degradation reactions occurring in the condensed and gas phases. It is then necessary, to determine the ATH flame retardant mode of action, to investigate the reactions occurring during the thermal degradation of the pure vulcanized EVM and of the matrix flame retarded with ATH.

1.1 Vulcanized EVM

On the contrary to raw EVA, widely studied in the literature [26, 27, 52, 133, 134], the thermal degradation mechanism of vulcanized EVM has never been determined. So, it is of scientific interest to determine its degradation pathway and thus the influence of the vulcanization on the thermal degradation of EVM. Moreover, it will allow be used as a reference when the influence of ATH on the thermal degradation of EVM will be examined. The chemical modifications, occurring in the condensed such as in the gas phase, are thus investigated.

1.1.1 Thermal degradation

The thermal degradation was studied by thermogravimetric analyses (TGA). Two atmospheres were investigated: nitrogen to simulate the pyrolysis of the material, and air to study the thermo-oxidative degradation. It is generally admitted that during the combustion of a material the atmosphere is mainly oxidative at the beginning, then inert and once again oxidative at the end. Nevertheless, since there is no predominance of oxidation or inert degradation, both are studied to bring a reliable mechanism.

The oxidative degradation of vulcanized EVM was investigated by high-resolution TGA in air. TGA and the corresponding derivative TG curve (DTG) are pictured in *Fig. 68*.
Five apparent degradation steps can be distinguished. The first one *(1)* occurs between 200 and 220 °C and leads to a mass loss of 6 wt-%. Then, up to 305 °C *(2),* the material loses 40 wt-%. At 405 °C *(3)*, the total loss reaches 58 wt-%. The fourth step *(4)* from 405 to 445 °C corresponds to a mass loss of 15 wt-%. The DTG curve may suggest that this step could be the superimposition of two steps. In the last part of the degradation curve *(5),* vulcanized EVM loses 20 wt-%, up to 525 °C. The final degradation residue of 1.5 wt-% is attributed to the presence of silica. Indeed, the used Levapren EVM pellets are slightly coated with silica (about 0.9 wt-%) to avoid agglomeration as reported in *Chapter 1*: this mineral part is thermally stable and thus still present at high temperature. The difference of 0.7 wt-% is in the margin of error.

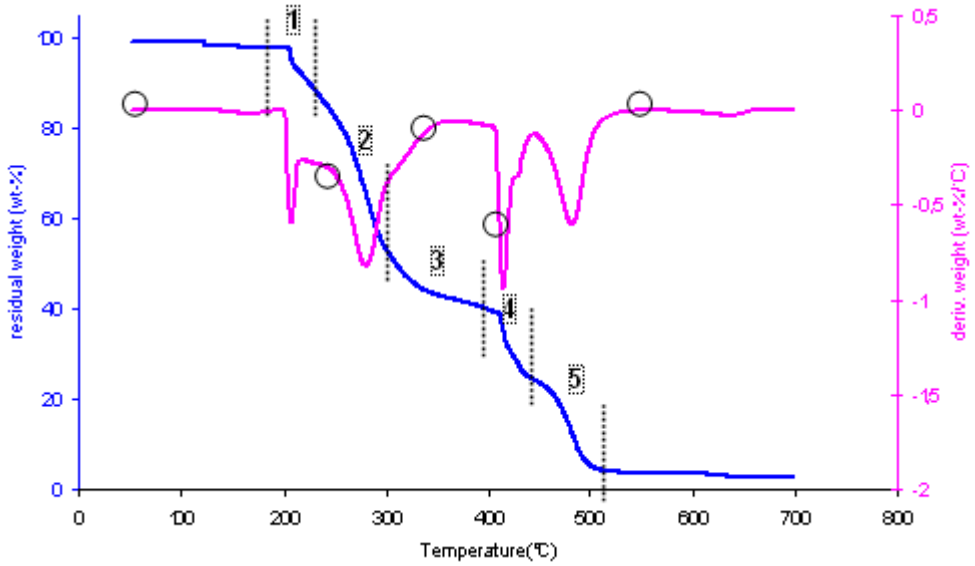


Fig. 68: Hi-Res TG curve and the corresponding DTG curve of vulcanized EVM in air (10°C/min)

The degradation mechanism of EVM investigated by Rimez *et al.* [26, 27], detailed in *Chapter 1*, is composed of three apparent steps: between 300 and 400 °C acetic acid is eliminated (deacetylation), leaving a highly unsaturated residue or polyene. The polyene thus forms a char, also releasing aromatic and aliphatic volatiles. Then, the char is oxidized in the last part of the degradation. Compared to raw EVM, the vulcanized polymer exhibits more degradation steps in air. It appears that the oxidative degradation of the vulcanized polymer follows a more complex degradation scheme.

To investigate the influence of cross-linking in EVA on the thermal degradation of EVM, the described methodology was followed. The key temperatures of the thermal degradation of the materials are determined through TGA analyses. Then, thermal treatments can be carried out at the key temperatures to obtain degradation residues. The mass lost during thermal treatment is also compared to that of the TGA. Slight differences can be observed, attributed to heat and mass transfer phenomena occurring in the heat-treated barrel and not in the powder used for TGA (where these phenomena can be neglected). However, if the mass lost at the heat treatment temperatures (HTT) is in the range of the one observed in TGA for the same degradation step, the heat treatment is validated. The mass losses will thus be presented as comparison elements but not commented.
The analysis and chemical characterization of the obtained residues will then allow the determination of a degradation mechanism.

The chosen HTT (symbolized by the black circles on *Fig. 68*) for the oxidative degradation are 250 °C at the junction between the first and the second degradation step, 340 °C between the third and the second one, 400 °C since it corresponds to the end of the third step and the beginning of the fourth. The temperature of 550 °C was chosen to achieve a f ull degradation of the material.

The obtained residues for the oxidative degradation are pictured in *Fig. 69*. Vulcanized EVM before thermal treatment *(a)* consists in a pale yellowish elastomeric polymer barrel. After the treatment at

250 °C *(b)* the yellow colour becomes more pronounced, and some "bubbles" are noticeable in the polymer. At 340 °C, the degraded barrel is black, contains bubbles and still remains flexible *(c)*. A strong odour of acetic acid was also noticed. At 400 °C, the dark residue is more fragile and crunchy *(d)*. Finally at 550 °C, it only remains in the alumina pan a thin carbonaceous residue *(e)*.

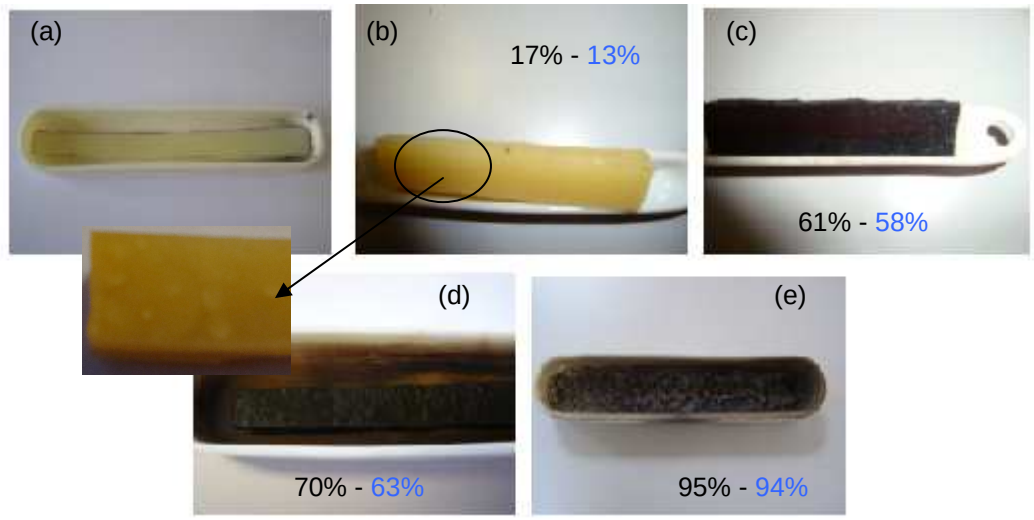


Fig. 69: Pictures of the thermal treatment residues of vulcanized EVM in air at 20 °C (a), 250 °C (b), 340 °C (c), 400 °C (d) and 550 °C (e)- in black: expected mass loss (according to the TGA), in blue: experimental mass loss

In the same way, the Hi-Res TG analysis of vulcanized EVM was performed in nitrogen to simulate pyrolysis conditions *(Fig. 70)*. Three degradation steps are detected on the TG and DTG curves. The first one begins at 280 °C and ends at 375°C leading to a mass loss of 41 wt-% *(1)*. This corresponds to the theoretical mass loss of the deacetylation (evolution of acetic acid). Indeed, the release of acetic acid leads to a mass loss of the polymerized vinyl acetate monomer of 69.8 % ($CHCH_2COOCH_3$ = 86 g/mol, $HOOCCH_3$ = 60 g/mol). Since the vinyl acetate monomer content is of 60 wt-%, the deacetylation should lead to a mass to a loss of 69.8 x 0.60 = 41.8 wt-%; corresponding to that obtained for the first step pyrolysis in TGA.

The second step *(2)* from 375 to 457 °C corresponds to a weight loss of 25 wt-%. The last step *(3)* ends at 500 °C with a final residue of 6 wt-%. This degradation residue is attributed to the silica contained in the EVM pellets and to some remaining degradation organic products according to visual observations (the black colour is given by the degraded organic compounds, whereas silica residues are white). Moreover, the mass of the residue obtained in air, where all organic products are degraded, is lower (1.5 wt-%) confirming the presence of condensed carbonaceous material in the high temperature residue.

The inert degradation of vulcanized EVM is quite identical to that of raw EVA, investigated by Rimez *et al.* as mentioned at the beginning of this section, which exhibits three degradation steps [27]. The first one (300- 400 °C) was attributed to the deacetylation of the polymer leading to the formation of polyene. This polyene completely degrades, into aliphatic and into aromatic volatiles, up to 500 °C.

TG curves of EVM and vulcanized EVM are quite similar, the main difference concerning the final residue. The cross-linking bonds seem to favour the condensation of carbonaceous species, so that a small amount of char is yield. It is indispensable to verify this hypothesis by determining the chemical degradation mechanism.

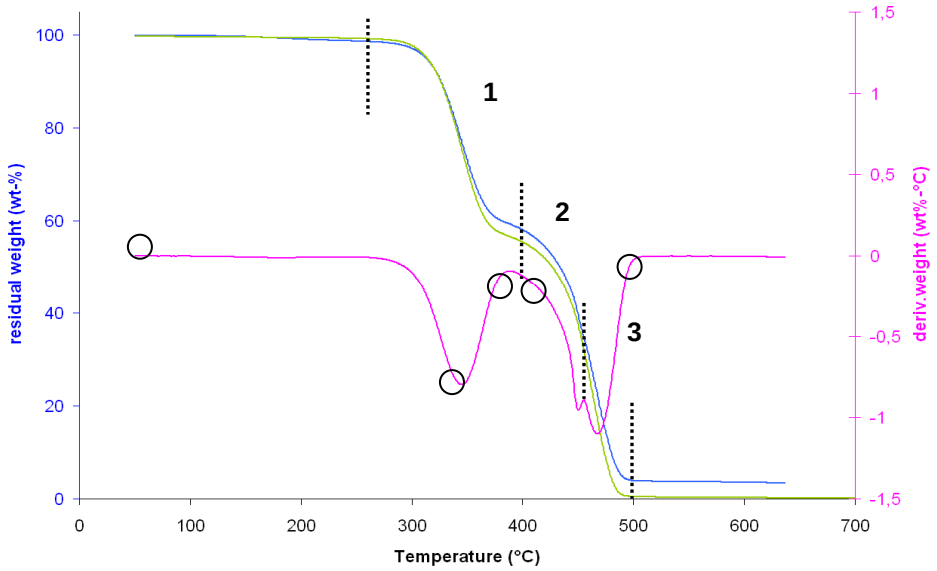


Fig. 70: Hi-Res TG curve of vulcanized EVM (in blue) and raw EVM (in green) and the corresponding DTG curve of vulcanized EVM, in nitrogen

The heat treatment characteristic temperatures (pictured by the circles in *Fig. 70*) are determined according to the TG curve of cured EVM. 350 °C is chosen since it corresponds to maximum degradation rate of the first degradation step, 375 °C as the junction between the first and the second step, 450 °C between the second and the third step. 500 °C is the temperature where a high temperature residue is formed.

The residues of the thermal treatments in inert atmosphere (nitrogen) are pictured in *Fig. 71*. When heated at 350 °C the sample becomes yellowish and emits a strong odour of acetic acid. At 375 °C, some large pale yellow “bubbles” are noticeable in the barrel. The residue obtained at 400 °C is brownish but, on the contrary to the residue heat treated in air, is still flexible. The last thermal treatment led to a black carbonaceous powder.

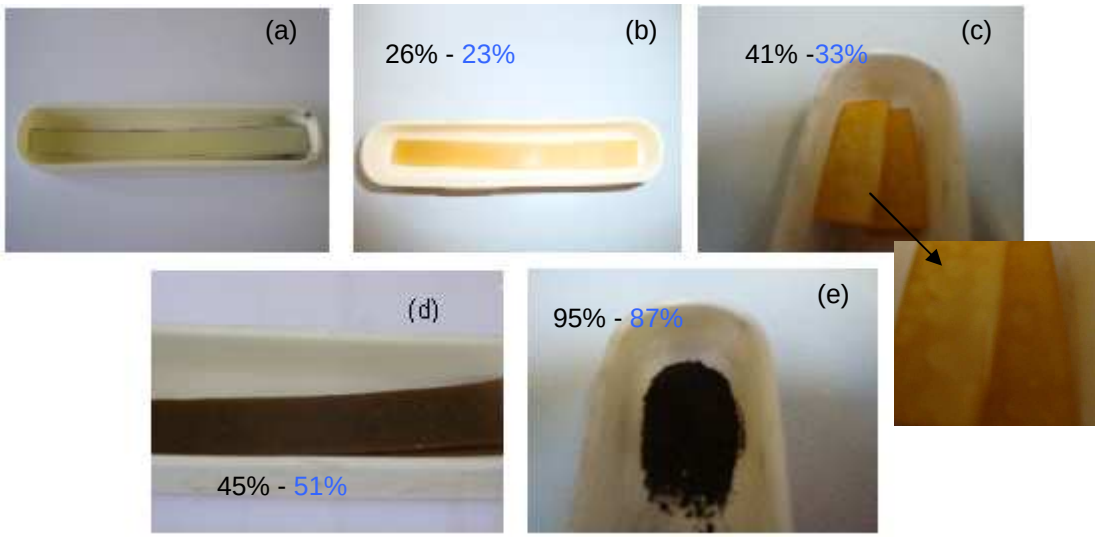


Fig. 71: Pictures of the thermal treatment residues of vulcanized EVM in nitrogen at 20 °C (a), 350 °C (b), 375 °C (c), 400 °C (d) and 500 °C (e) - in bla ck: expected mass loss (according to the TGA), in blue: experimental mass loss after treatment

The thermogravimetric analyses allowed determining the temperatures at which the degradation steps occur. To sort out the chemical degradation pathway, it is now necessary to characterize the intermediate degradation residues (condensed phase) and the products evolved during the degradation (gas phase) by the use of adapted tools.

1.1.3 Gas phase analysis

In addition to the characterization of the condensed phase (presented later in the chapter), gas phase analysis was performed using TGA-FTIR.

It is noteworthy that the design of the FTIR leads to some perturbation of the carbon dioxide and water signals, since before going through the sealed gas cell the light beam interferes with ambient air (which contains atmospheric carbon dioxide and humidity). This signal may be eliminated by the substraction of the background spectrum, but experimentally we observed that is was not sufficient. It is thus considered that the intensity of the cited peaks before the start of the polymer degradation corresponds to that of atmospheric gases. The increase of the peaks intensity thus implies a release of these gaseous species by the material during its degradation.

The spectra versus time of the gases evolved during the TG measurement in air are presented in *Fig. 72*. The degradation begins at 45 min (corresponding to 250 °C) and ends at 140 min (corresponding to 610 °C). A slight delay between the evolved gase s and the mass loss can be observed, because of the design of the TGA-FTIR coupling, involving a transfer line heated at 250 °C in which the gases can eventually condense. At the beginning of the thermo-oxidation, some peaks appear around 3500, 1600 and 1000- 1200 cm^{-1}. No additional peak appears up to 80 minutes (corresponding to 300 °C) where the previously cited signals disappear, replaced by intense peaks at 2300 and 600 cm^{-1}.

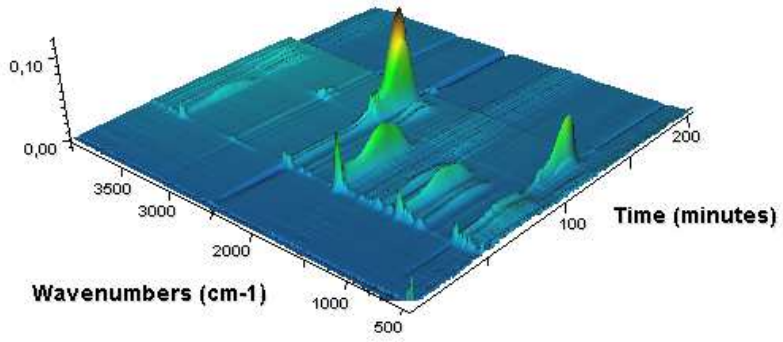


Fig. 72: FTIR spectra of the gases evolved during the thermo-oxidative degradation of vulcanized EVM versus time

The spectra obtained at defined characteristic temperatures are pictured in *Fig. 73*. The attributions of the observed bands are gathered in *Table 37*. On the first spectrum collected at 200 °C, several peaks are noticeable. The bands at 3735, 2310, 2357, 1507 and 670 are linked to the presence of atmospheric carbon dioxide (as an impurity) while the bands at 3580, 1796, between 1397 and 1084 and at 998 cm^{-1} characterises the acetic acid released during the first degradation step. This confirms the fact that we have some deacetylation during this first step.

At 250 °C, the spectrum shows an increase of the intensity of the bands linked to acetic acid produced during the second degradation step by deacetylation. Concerning the spectrum at 300 °C, it only reveals the presence of carbon dioxide: it is not evolved any other organic specie. Since the mass loss is very low at this temperature, this is coherent with the TGA. Then, some bands around 3050 and 2960 cm^{-1} appear, revealing the emission of products containing aromatic and/or ethylenic (3050 cm^{-1}) and aliphatic carbons (2960 cm^{-1}). Finally the spectrum at 400 °C shows very intense carbon dioxide and carbon monoxide bands (explained by the partial oxidation of the gaseous products during the thermal degradation) that can be linked to the char oxidation. The last spectrum at 500 °C, when the degradation is complete, only exhibits the presence of atmospheric carbon dioxide and water.

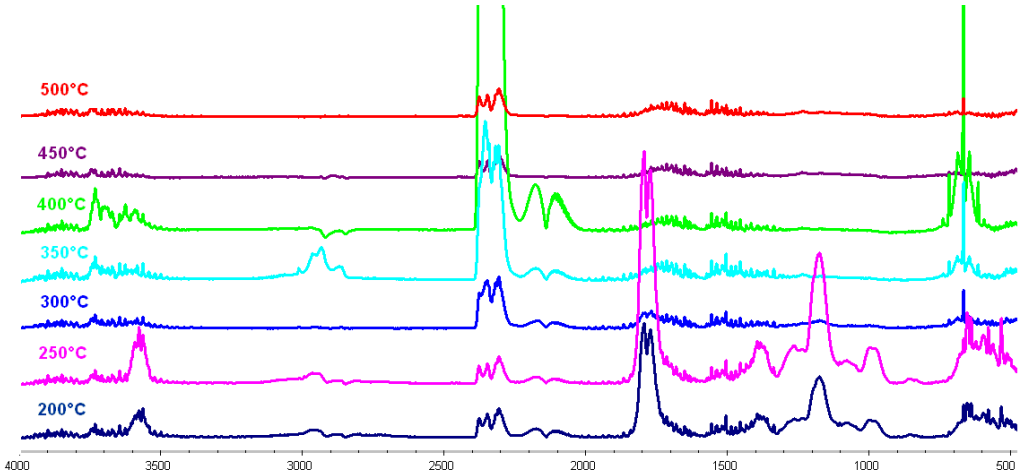


Fig. 73: FTIR spectra of the gases evolved during the thermo-oxidative degradation of vulcanized EVM collected at characteristic temperatures

Table 37: Attribution of the IR bands of the gases evolved during the degradation in air of vulcanized EVM

Wave Number (cm^{-1})	Attribution	Wave number (cm^{-1})	Attribution
3735	Fermi combination resonance (CO_2)	1397	-O-H in plane bending (acetic acid)
3580	O-H stretching (acetic acid)	1270	C-OH asymmetrical stretching (acetic acid)
3050	=C-H stretching (aromatic compounds)	1176	Skeletal stretching (acetic acid)
2900-2950	C–H asymmetrical stretching (aliphatic compounds)	1122	$-CH_3$ stretching (acetic acid)
2357, 2310	CO_2	1084	-C-OH stretching (acetic acid)
2181, 2115	CO	998	-O-H bending (acetic acid)
1796	C=O stretching (acetic acid)	670	CO_2 bending
1507	CO_2		

The same analyses were performed during the pyrolytic degradation of vulcanized EVM. The resulting FTIR spectra are gathered in *Fig. 74* and *Fig. 75*.

The evolution of the IR bands versus time reveals that from 25 to 35 minutes (corresponding to a temperature range between 250 and 350℃), some gase s are evolved in the gas cell, with a maximum of absorbance at 35 minutes (i.e. 350 ℃). The band s are located in the regions of 3500- 3600 cm^{-1}, 1800 and 1000- 1500 cm^{-1}. From 35 to 40 minutes (that is to say from 350℃ to 400℃), the previous bands disappear, and additional bands around 2900 cm^{-1} appear.

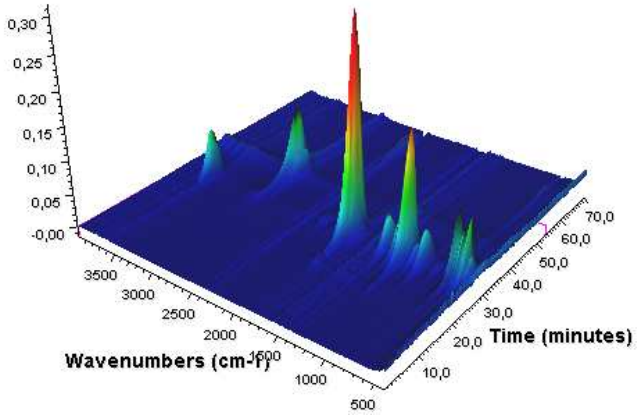


Fig. 74: FTIR spectra of the gases evolved during the pyrolysis of vulcanized EVM versus time

The spectra at characteristic temperatures (*Fig. 75*) reveal what sorts of gases are evolved during the pyrolysis of vulcanised EVM. At 350 ℃, the bands a t 3580, 1790, 1397, 1270, 1176, 1122, 1105, 1084 and 998 cm^{-1} attributed to acetic acid *(see Table 37)* confirm that the first degradation step consists in a deacetylation of the material. At 400 ℃, the spe ctrum exhibits only two bands around 2850 and 2900 cm^{-1}, corresponding to aliphatic compounds. The proposed mechanism assuming the production of aliphatic volatiles during the second and third degradation steps is then confirmed. At 500 ℃, som e bands can still be distinguished: very weak ones around 2300 cm^{-1}, corresponding to some

atmospheric CO_2 traces and some between 2800 and 3050 cm^{-1}, assigned to aliphatic (2800 cm-1) and to ethylenic and/or aromatic products (3050 cm-1).

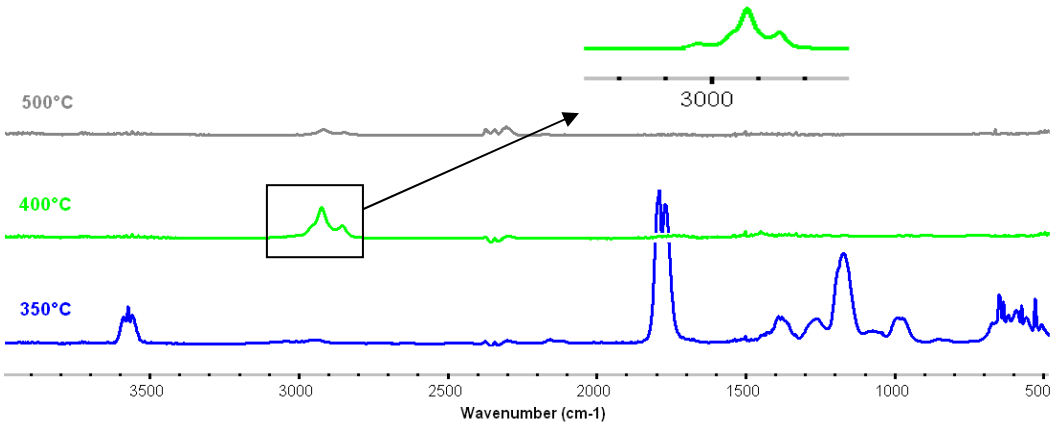


Fig. 75: FTIR spectra of the gases evolved during the inert degradation of vulcanized EVM collected at characteristic temperatures

1.1.2 Analysis of the thermal treatments residues

Vulcanized EVM was submitted to thermal treatments under the two atmospheres at characteristic temperatures to obtain the "intermediate" residues corresponding to each degradation step. They are then analyzed using ^{13}C solid state NMR to determine their chemical structure.

The spectra corresponding to the thermo-oxidation are gathered in *Fig. 76*. It is noteworthy that the signal intensity on the spectra at 400 and 550 °C w as increased to facilitate the peaks observation.

Analysing the spectrum of the untreated polymer reveals several peaks regions. A signal at 170 ppm is distinguished which is attributed to the ester carbonyl of the acetate function [135]. The peaks from 25 to 36 ppm (25.6, 30.7 and 36.5 ppm) are assigned to CH_2 in the polymer chain. The multiplicity of the peaks is due to the fact that when VA monomer copolymerises with ethylene, a random copolymer is obtained leading to several different monomer sequences in the chain. According to Delfini *et al.* [136], the chemical shift depends on the position of the carbon in a monomer triad, as defined by the peaks attributions presented in *Table 38*. This work was carried out in liquid state NMR, and thus does not take into account structural effects, but since all the reported bands are present on our solid state NMR spectrum we can reasonably assume that the assignments are transposable to our case.

Examination of the CH bond of the VA monomer on the spectrum (around 70 ppm) reveals that the peak is actually not a single band. This multiplicity is also explained by the sequence distribution of pentads in the polymers [136]. The single peak at 21 ppm is assigned to the methyl group of the acetate function ($OCOCH_3$) [135]. Peaks exhibiting a very low intensity can be also distinguished around 125 ppm: they are assigned to the aromatic carbon double bonds of the cross-linking agents (dicumyl peroxide and triallyl cyanurate) [137].

Table 38: ^{13}C chemical shifts according to Grant and Paul[138], corresponding triad and experimental shifts

Triad sequences **A=VA ; B=E**	**^{13}C shifts** **(ppm-calculated)**	**^{13}C shifts** **(ppm-observed)**
-CH(OCOCH$_3$)***CH$_2$***CH(OCOCH$_3$) ***CH$_2$***CH(OCOCH$_3$)CH$_2$- (AAA)	37.9	Not observed
-CH(OCOCH$_3$)CH$_2$CH(OCOCH$_3$)***CH$_2$***CH$_2$CH$_2$- (AAB) - CH$_2$CH$_2$CH(OCOCH$_3$)***CH$_2$***CH(OCOCH$_3$)CH$_2$- (BAA) -CH$_2$CH$_2$CH(OCOCH$_3$)***CH$_2$***CH$_2$CH$_2$- (BAB) -CH(OCOCH$_3$)CH$_2$CH$_2$***CH$_2$***CH(OCOCH$_3$)CH$_2$- (ABA)	35	36.5
-CH$_2$CH$_2$***CH$_2$CH$_2$***CH$_2$CH$_2$- (BBB)	30.6	30.7
-CH(OCOCH$_3$)CH$_2$***CH$_2$***CH$_2$CH$_2$CH$_2$- (ABB) -CH$_2$CH$_2$***CH$_2$***CH$_2$CH(OCOCH$_3$)CH$_2$- (BBA)	26	25.6

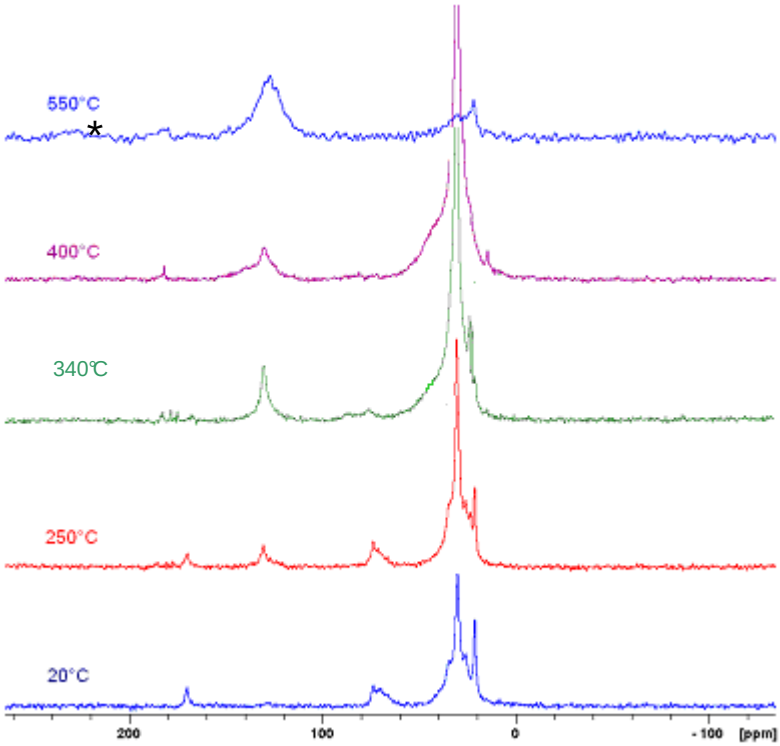


Fig. 76: ^{13}C CP-DD-MAS NMR spectra of the thermal degradation residues of vulcanized EVM in air; * = spinning sideband

When heated at 250°C the material presents some mod ifications. The peaks are similar compared to the spectrum at ambient temperature in the aliphatic region (20-40 ppm), but the intensity of the peaks located at 125 ppm increases. This suggests chain scission reactions, leading to the formation of carbon double bonds in the material. According to the gas phase analysis these chain scissions are due to deacetylation (maybe at the surface of the sample, where the diffusion of the evolved gaseous products is not a limiting parameter). Since deacetylation induces the formation of carbon double bonds in the polymeric chains [27] it is consistent with condensed phase analysis.

It is noticeable that some peaks are appearing around 180 ppm: they are assigned to carboxylic acid functions [139]. Their multiplicity implies that several acidic species are formed during the first degradation step, and not only acetic acid. Since the methyl group of the acetate function is a probable site for the formation of a radical during the vulcanization, some acetate functions could be implied in cross-linking bridges. The explanation we propose is that these cross-linking bonds form by the deacetylation mechanism a carboxylic acid, which is still linked to a polymeric chain, as schemed in *Fig. 77*. Depending on the triad sequence of this chain the resonance of the carboxylic carbon, and thus its chemical shift, will be modified.

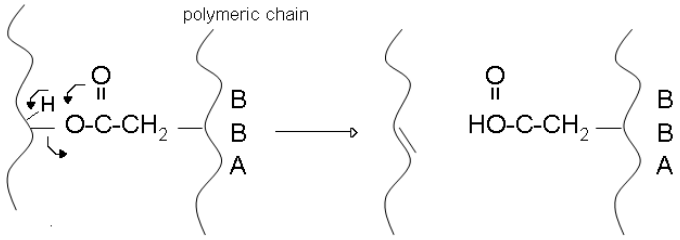


Fig. 77: Schematic description of the cross-linking bond cleavage, example for a specific triad BBA (A=VA, B=E)

At 340 °C, the sharp decrease of the resonances at 170, 70 and 21 ppm, linked to the presence of the acetate function, is attributed to the deacetylation of the EVM. The fact that the peak at 21 and 170 ppm do not completely disappear could be explained by the trapping of the released acetic acid, forming the "bubbles" observed in the thermal treatment residues.

At 400 °C no significant modifications are observed on the NMR spectrum, except the quasi-disappearance of the peaks attributed to the acetate group or acetic acid. The small quantity of gaseous acetic acid gas trapped into the polymer is released. The broadening of the signal at 130 ppm suggests the aromatisation of the residue [140], that is to say the formation of a char. This assumed charring process occurring in the condensed phase is coherent with the gas phase analysis which did not reveal any evolution of organic compounds.

Finally, the spectrum of the residue obtained at 550 °C presents two major peak regions: between 20 and 30 ppm, indicating the presence of aliphatic compounds, and the region centred on 130 ppm characterizing aromatic species. Some other low intense peaks are noticeable around 185 ppm, and reveal some oxidation of the degradation residue. Indeed, at this temperature the presence of carboxylic acid is less probable than that of conjugated ketones resulting from the char oxidation, and the production of carbon monoxide and dioxide in the gas phase seems to confirm this hypothesis. It is noteworthy that the gas phase analysis shows, before the char oxidation, the char degradation by the release of volatile organic compounds (ethylenic and/or aromatic and aliphatic products). This observation correlates the proposed mechanism for the fourth degradation step, that is to say the char degradation by volatilization.

The thermo-oxidative degradation pathway of vulcanized EVA does not appear very different from that of non-cross-linked EVA, except from the first degradation step (breaking of the cross-linking bonds). This question will be fully discussed in the third part of this chapter.
The same techniques were used to obtain and to characterize the pyrolysis residues of vulcanized EVM. The resulting spectra (^{13}C solid state NMR) are gathered in *Fig. 78*. It is noteworthy that the signal intensity on the spectrum at 400 and 500 °C was increased to facilitate the peaks observation.

The peaks attributions for the untreated vulcanized EVM spectrum have already been detailed in the previous section. The spectrum of the polymer at ambient temperature is thus not further commented.
When heated at 350 °C, the material presents modifications. Indeed the peak located at 70 and 170 ppm nearly disappears, but not totally, such as the peak at 21 ppm linked to the presence of the acetate group in the polymer. This is consistent with the degradation scheme, described in *Fig. 77*. This is due to the deacetylation process (as confirmed previously by the gas phase analysis), thus producing carbon/carbon double bonds, characterized by the additional resonance at 130 ppm. As for the thermo-oxidative degradation several signals appear around 175- 180 ppm, indicating that some cross-linking bonds are broken, forming carbonyls by the same mechanism as described in *Fig. 77*.
Between 350 and 375 °C, only few modifications occur. The -CH- resonance disappears, indicating that the deacetylation is complete. Moreover, the intensity of the peak attributed to unsaturated material increases. The resonance at 180 ppm indicates that some acetic acid remains in the material.
At 400 °C the peaks are broadened, especially the collection of bands in the 20- 30 ppm region. This is attributed to cleavage of the polymer chains and/or to the cross-linking bonds forming wide range of aliphatic products. Aromatic species can be detected in the range of 130- 140 ppm. The superimposition of the two peaks could be explained by the presence of highly unsaturated polyenes (around 135- 140 ppm) and some polycyclic aromatic compounds (130 ppm) [141]. Acetic acid or acidic functions still remain in the residue since peaks are observed at 180 ppm and 21 ppm.

It is noticeable that the intensity of the peaks related to aliphatic compounds is very high whatever the HTT. This does not necessary imply that the quantity of aliphatic compounds is higher than that of ethylenic or aromatic species, since the cross-polarization increases the intensity of the signals of carbon surrounded by hydrogen atoms. The signal of aromatic species (containing less hydrogen) can thus appear less intense.

The last spectrum corresponding to vulcanized EVM heated up to 500 °C is similar to the previous one. Nevertheless in the aliphatic zone (10- 40 ppm) several intense peaks are noticeable which are related to a wide range of aliphatic parts, linked or not to unsaturated compounds.

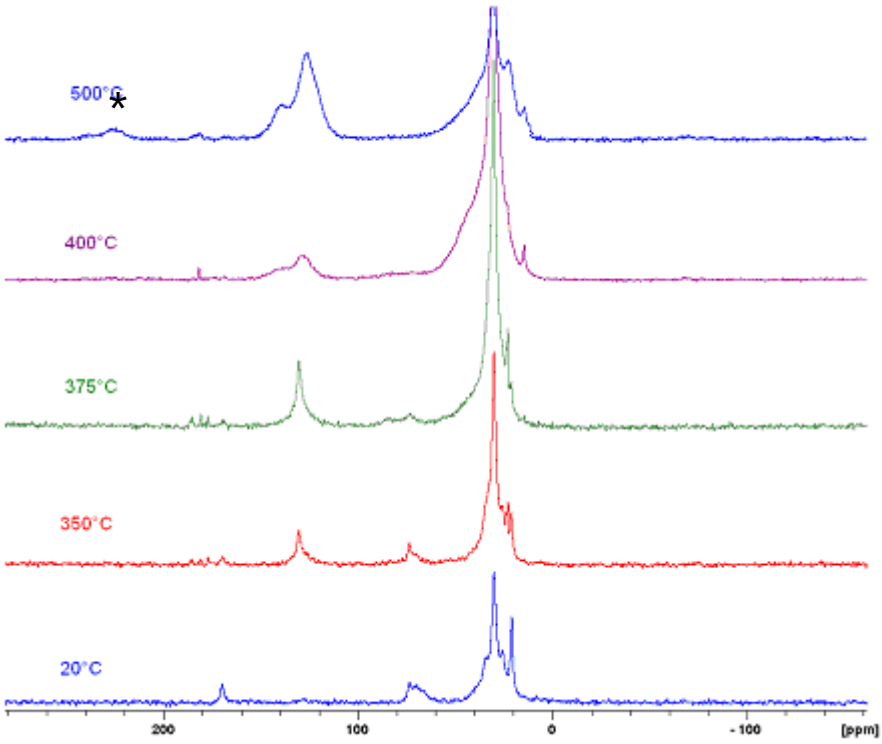


Fig. 78: ^{13}C CP-DD-MAS NMR spectra of the thermal degradation residues of vulcanized EVM in nitrogen; *=spinning sideband

Based on the characterization of both condensed and gas phase during the thermal degradation of vulcanized EVM (in oxidative or inert conditions), it is now possible to propose a degradation scheme for the polymeric matrix which will be commented in the next section.

1.1.4 Degradation mechanism

The thermo-oxidative degradation of vulcanized EVM, according to the previous TGA, TGA-FTIR and NMR analyses, is assumed to be divided into five chemical steps *(Fig. 79)*. The degradation starts at 200 °C with some chain scission reactions, most probably corresponding to the cleavage of the weakest cross-linking bonds (the bridged acetate groups) and some deacetylation, up to 250 °C.
Then, all acetate groups are deacetylated (before 300 °C), leading to the formation of unsaturated polyene residues. Up to 350 °C, the formation of aromatic char occurs. It results from the polyenes degradation by chain scission reactions (without oxidization), producing carbonaceous compound condensing to form a char. The resulting char is rapidly degraded into aliphatic and aromatic volatiles, and lastly oxidized up to 550 °C.

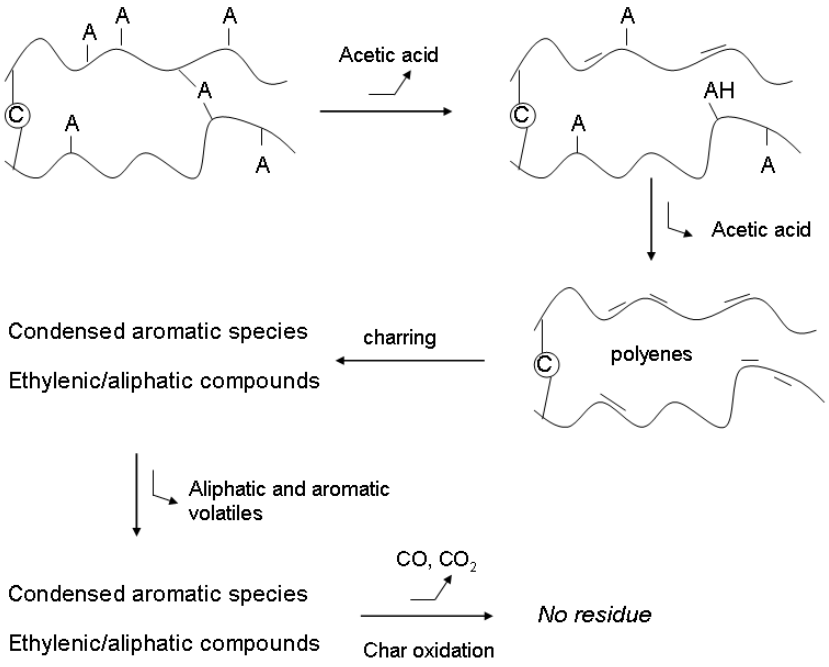


Fig. 79: Thermo-oxidative degradation scheme of vulcanized EVM (A= acetate, C=peroxide/coagent cross-linking)

According to our investigations, it is supposed that the inert degradation of vulcanized EVM occurs into three steps *(Fig. 80)*. The first one, from 300 to 375 °C consists in the deacetylation of the material, producing acetic acid and polyenes (also resulting from the cleavage of certain cross-linking bonds). Then, unsaturated compounds are produced up to 450 °C and aliphatic carbonaceous material is evolved. In the last part of the degradation (450- 500 °C), some aromatisation of the residue occurs, leading to a residue made of unsaturated and aromatic compounds.

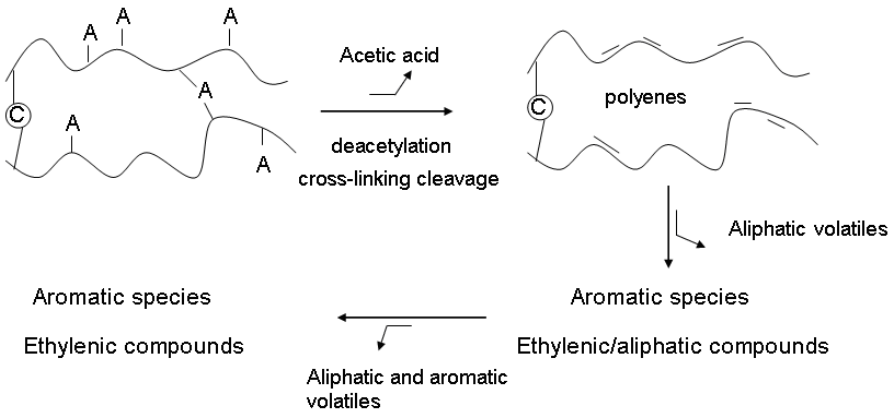


Fig. 80: Pyrolysis degradation scheme of vulcanized EVM (A= acetate, C=peroxide/coagent cross-linking)

It is noteworthy that the presence of oxygen during the degradation plays an important role on the degradation pathway of EVM vulcanizate. Indeed, the deacetylation (and the cleavage of some specific cross-linking bonds) of vulcanized EVM occurs at lower temperature in oxidative conditions. It

can thus be supposed that oxygen plays a role on the deacetylation. It can be assumed, according to the literature on EVA or on polyethylene, that the presence of oxygen catalyses the formation of intermediate unstable hydroperoxides [142]. As noted by Flynn [143], all thermal oxidations of vinyl polymers at moderate temperatures are postulated to involve the hydroperoxide radical in the propagation step of the degradation. Degradation in oxygen begins via an initiation step which produces the radical precursors.

$$\text{Initiation: } RH \rightarrow R^{\circ} + H^{\circ} \quad (6)$$

When oxygen is allowed to react with the newly formed chain radical (R*), an intermediate peroxy radical is produced during the propagation step.

$$\text{Propagation: } R^{\circ} + O_2 \rightarrow ROO^{\circ} \quad (7)$$

Highly reactive ROO° then abstracts a labile hydrogen from another polymer molecule giving rise to the hydroperoxide species, as well as another polymer radical, through which the process can continue.

$$ROO^{\circ} + RH \rightarrow ROOH + R^{\circ} \quad (8)$$

These hydroperoxides lead to the formation of ketones thus activating the chain degradation. Since these species are unstable, they are not apparent on NMR spectra. The carbonaceous organic species formed during these first steps of degradation, according to the ^{13}C NMR spectra, are the same whatever the degradation atmosphere.

The difference between the inert and oxidative conditions also concerns the last degradation steps. During the charring in oxidative conditions (that is to say between 290 and 410 °C) there is only a tiny amount of mass loss, and a very little release of gaseous compounds: the degradation of the carbonaceous residue occurs in an additional step at higher temperature. In nitrogen, the formation of the carbonaceous residue and its degradation into volatiles run in the meantime.

It can thus be concluded that the same reactions are involved (except the char oxidation, which constitutes the last step of the degradation of the cured polymer in air and which only appears in oxidative conditions), but their occurrence (in several successive steps or at the same moment) depends on the conditions (oxidative or not).

1.2 Vulcanized EVM flame retarded with ATH

To determine the influence of ATH on the chemical degradation pathway of the polymeric matrix, it is necessary to compare the thermal degradation mechanism of the pure and of the flame retarded material.

Since the ATH Apyral 120E was found to be the most efficient compared to the other grades *(see Chapter 3)*, it was decided to study the degradation of vulcanized EVM, filled with 130 phr ATH 120E. This loading corresponds to 55 wt.-%.

The same methodology as for vulcanized EVM was followed to determine the degradation pathway of the flame retarded material. But at first, the thermal degradation of the pure additive was investigated.

1.2.1 Thermal degradation of ATH

As shown in *Fig. 81,* the thermal degradation of aluminium trihydroxide (ATH 120E) occurs in a single step between 200 and 320 °C. The final alumina residue of 65 wt-% results from the dehydration of ATH. Indeed, ATH degrades following the reaction reported in *Eq.1* leading to a mass of residue of 65.13 wt-% ($Al(OH)_3$ = 78 g/mol and Al_2O_3 = 101.6 g/mol, 0.5 x 101.6 / 78 = 65.13).

$$Al(OH)_3 \rightarrow 0.5\ Al_2O_3 + 1.5\ H_2O \qquad \textbf{Eq.1}$$

The difference of 0.13 wt-% between the calculated value and the mass remaining after the TGA, is comprised within the margin of error of the experiment.

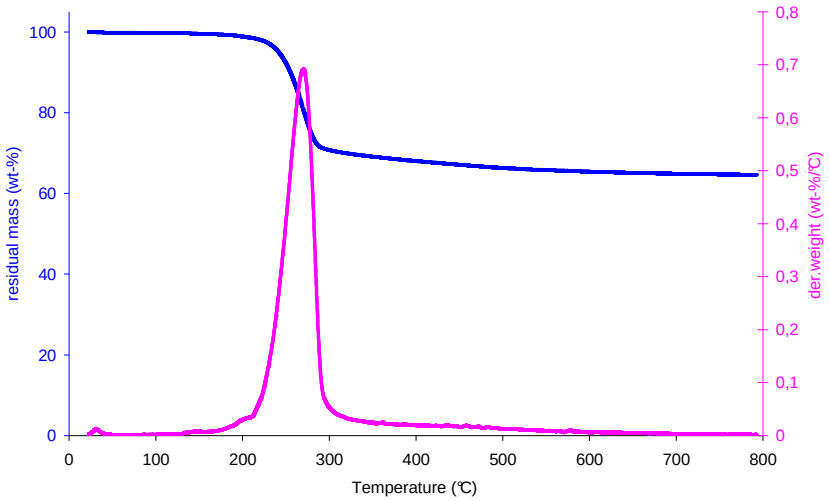


Fig. 81 : TG and DTG curves of ATH Apyral 120E (10°C/min in nitrogen)

With the hope to characterize the different phases formed during the degradation of ATH (exhibiting different crystalline morphologies), the evolution of the crystallographic structure of ATH during its thermal degradation was recorded versus temperature using high-temperature XRD *(Fig. 82)*. The analyses were carried out in-situ.

The first diffractogram at 50 °C was identified through the Powder Diffraction File (PDF) (International Centre for Diffraction Data (ICDD), Philadelphia) XRD database of 2008. The crystalline structure of $Al(OH)_3$ corresponds to the gibbsite form, characterized by the bands at 18°, 20.5°, several ones between 26.5 and 28.5°, 36.5°, between 39 and 41.5° , between 44 and 47.5°, 50.5°, 52°, 54° and between 63.5 and 68°. It does not appear any modification in the gibbsite structure up to 225 °C. At this temperature the signal corresponding to the gibbsite decreases, and the observed bands (of very low intensity) can be as attributed to boehmite Al(OOH) (14.5, 28, 32, 38.5, 49, 52 and 64°) and/or to some remaining gibbsite. Indeed, the majority of the rays obtained for boehmite can be superimposed to that of gibbsite. It is thus impossible to conclude definitely on the composition of the material at this

temperature but the formation of boehmite can be reasonably assumed.. Beyond 250 °C, the material becomes mainly amorphous.

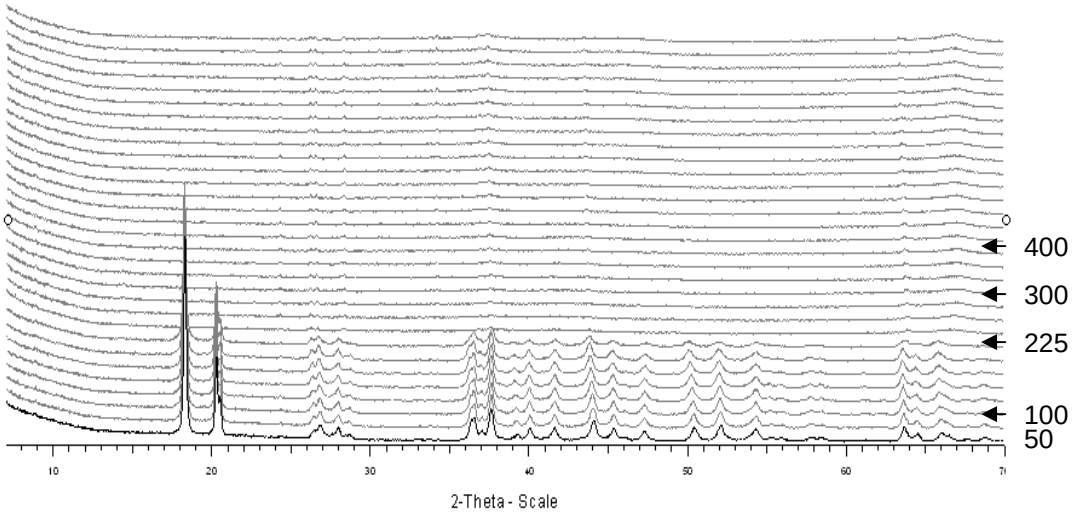


Fig. 82: High-temperature XRD diffractograms of ATH (from 50 to 800 °C, a diffractogram is collected e very 25°C)

The degradation of ATH can be schemed by:

$$Al(OH)_3 \text{ (gibbsite)} \rightarrow AlOOH \text{ (boehmite, suspected)} + \text{gibbsite} \rightarrow \text{amorphous } Al_2O_3$$

20-200°C 200-225 °C 225-800 °C

It appears that XRD does not provide much information about the additive degradation because of the amorphization of the compound. Since vulcanized EVM is also an amorphous material, this technique was not retained for the further characterization of the flame retarded formulations.

1.2.2 Thermal degradation of vulcanized EVM/ATH

As for vulcanized EVM, the thermal degradation of the matrix flame retarded with ATH (120E grade) was investigated in air and nitrogen using high-resolution TGA.

The TG and DTG curves of vulcanized EVM filled with ATH in air are presented in *Fig. 83*. Five degradation steps can be distinguished. The degradation starts at 200 °C with a mass loss of 13 wt-% from 200 to 290 °C *(1)*. Then, the second step *(2)* leads to a loss of 21 wt-% between 290 and 330 °C, immediately followed by a weight loss of 12.5 wt-% in the temperature range 330-420 °C *(3)*. The fourth step *(4)* is characterized by a weight loss of 13 wt-% up to 470 °C. The last step *(5)* occurs between 470 and 575 °C, leading to a residue of 36 wt-%.

The residual mass is similar to the alumina mass contained in the formulation. Indeed, ATH degrades leading to a mass of residue of 65.38 wt-%, since the material contains 54.85 wt-% of ATH (130 phr ATH for a total of 237 phr in the formulation) the expected residue remaining if the entire polymer is degraded corresponds to 54.85 x 0.6538 = 35.86 wt-%. This confirms that the final residue is only constituted of alumina obtained from the dehydration of ATH (and some silica used as coating agent, but at less than 1 wt-%).

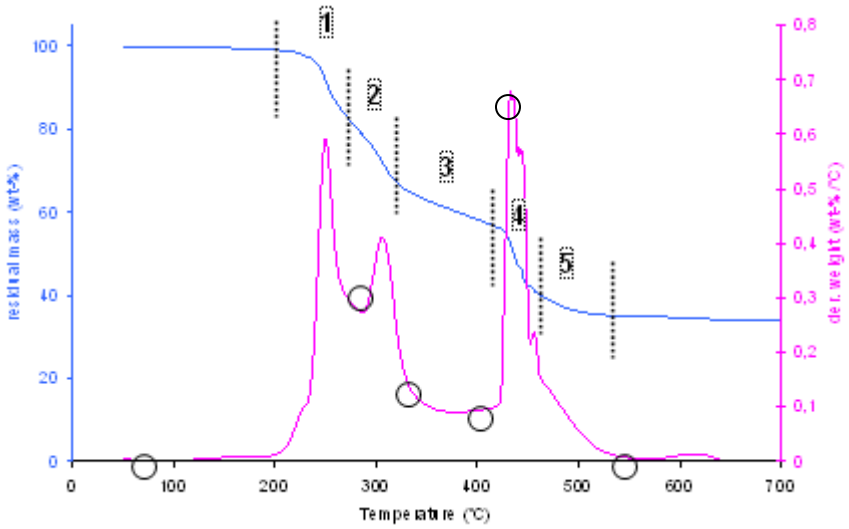


Fig. 83: Hi-Res TG curve and the corresponding DTG curve of vulcanized EVM flame retarded with ATH 120E in air (10°C/min)

It is noteworthy that the number of degradation steps is unchanged compared to the neat vulcanized EVM in oxidative conditions. Nevertheless, the reactions involved during this degradation can be different. For example, it can be expected that the dehydration of ATH [62] occurs in parallel to the first step, and the presence of alumina in the residue can induce some chemical reactions modifications.

The characteristic temperatures for thermal treatments under air are thus determined as 32, 350, 400, 450 and 550 °C (pictured by circles in *Fig. 83*). The first HTT (320 °C) corresponds to the end of the second degradation steps, 350 °C to an intermediate residue of the third one. 400 °C is the temperature at the beginning of the fourth degradation step and 450 °C of the fifth one. The final residue is formed at 550 °C.

The images of the residues obtained during the oxidative degradation of the material are gathered in *Fig. 84*. The untreated material is a white and solid barrel. After a thermal treatment at 320 °C, it becomes yellowish, and then brownish at 350 °C. At 400 and 450 °C, the barrel exhibits quite similar aspect: a brownish skin and a white powder-like core. The last thermal treatment at 550 °C, leads to a white powder (as discussed above it is constituted of alumina mainly).
It is noteworthy that that the heat and mass transfer affects the degradation of the barrel, since a clear core/skin effect is observed. This phenomenon, neglected in TGA, explains the differences obtained in terms of mass loss (lower for the heat treatment that in TGA).

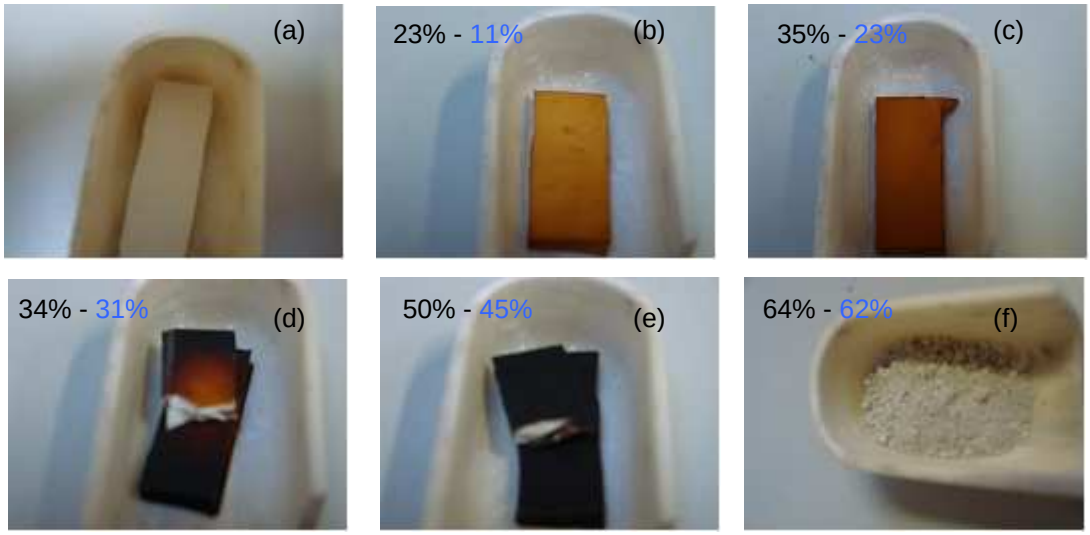


Fig. 84: Pictures of the thermal treatment residues of vulcanized EVM flame retarded with ATH 120E in air at 20 ℃ (a), 320 ℃ (b), 350 ℃ (c), 400 ℃ (d) , 450 ℃ (e) and 550 ℃ (f) - in black: expected mass loss (according to the TGA), in blue: experimental mass loss after treatment

The curves obtained in nitrogen atmosphere indicate that the pyrolysis occurs into four steps *(Fig. 85)*. The material starts degrading at 210 ℃. From this temperature to 310 ℃ *(1)*, the mass loss reaches 11 wt-%. Then, up to 390 ℃ *(2)*, the flame retarded matrix loses 13 wt-% and a total mass loss of 48 wt-% is achieved at 470 ℃ *(3)*. The last degradation step *(4)* ends at 650 ℃, leading to a residue of 38 wt-%. As for the thermal degradation under air, this residue is attributed to alumina resulting from the degradation of ATH, silica plus some organic matter trapped into alumina (as suggested by the greyish colour of the final residue). This organic matter is supposed to be due to some carbonization of the polymer. This hypothesis will be investigated further.

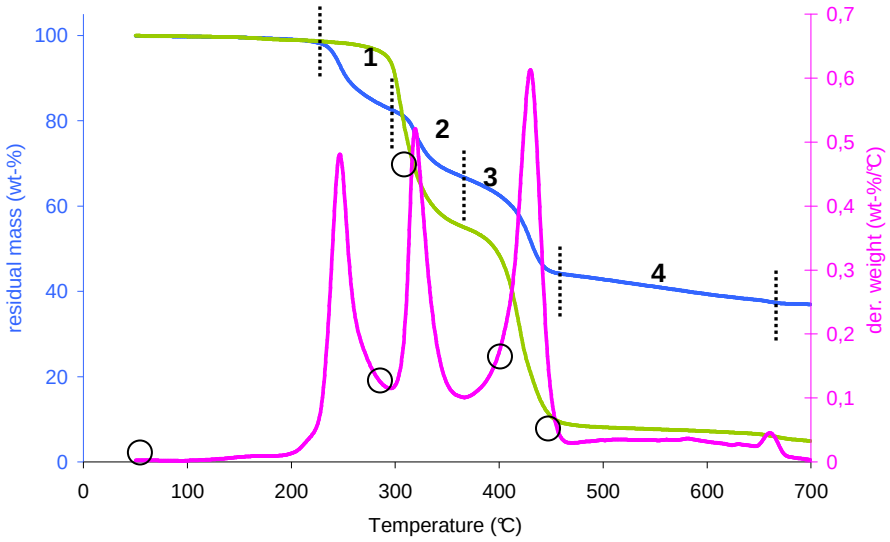


Fig. 85: Hi-Res TG curve of vulcanized EVM (in green) and Hi-Res TG (in blue) and DTG curves of vulcanized EVM /ATH 120E in nitrogen (10℃/min)

Compared to the TG curves of pure cross-linked EVM, the flame retarded polymer begins its degradation earlier (200 °C instead of 300 °C). The temperature range of this first degradation step corresponds to that of the ATH dehydration [62]. It is noteworthy that the last degradation step ends 100 °C later than without ATH.

The characteristic degradation temperatures for the flame retarded polymeric matrix in inert atmosphere are thus determined. The temperature of 330 °C is chosen since it corresponds to the end of the first degradation step, 350 °C corresponds to the maximum mass loss rate of the second step and 400 °C to the beginning of the third one. The heat treatment temperature (450 °C) leads to the high temperature stable residue.

The pictures of the thermal degradation residues of EVM/ATH in inert atmosphere are gathered in *Fig. 86*. It appears that at 330 and 350 °C the materials is visually unchanged, except from a slight yellowing whereas a weight loss of respectively 8 and 28% are observed. At 400 °C, the skin of the material becomes brownish while the core exhibits a white colour and a powder-like structure. At 450 °C, a greyish powder, essentially composed of alumina and remaining carbonaceous residue, is obtained. As for the thermo-oxidation of the material, a core/skin effect is clearly noticeable.

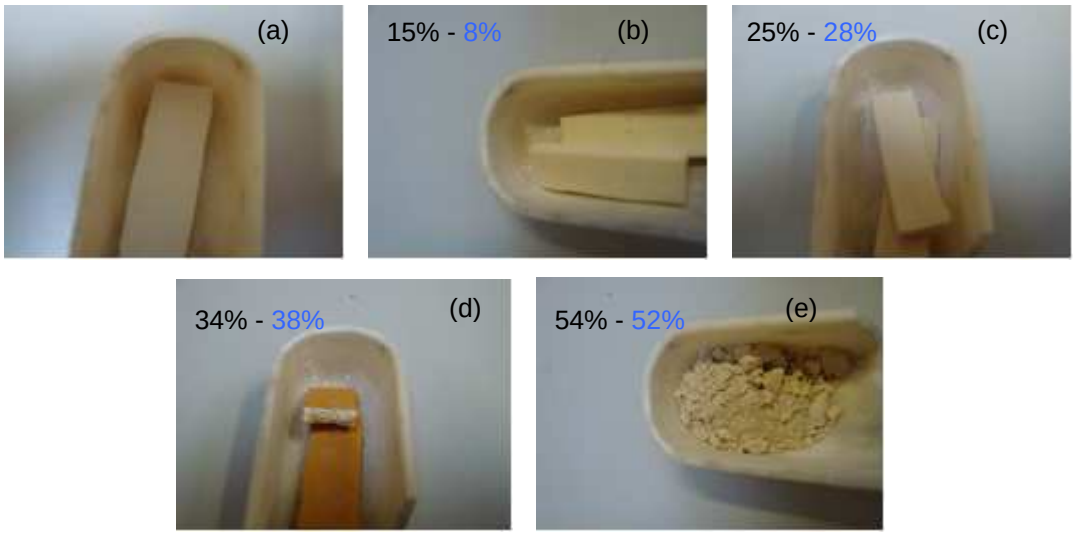


Fig. 86: Pictures of the pyrolysis residues of vulcanized EVM flame retarded with ATH 120E at 20 °C (a), 330 °C (b), 350 °C (c), 400 °C (d) and 450 °C (e) - in black: expected mass loss (according to the TGA), in blue: experimental mass loss after treatment

The degradation steps have thus been determined. In the next section, the chemical structure of the intermediate degradation compounds will be investigated.

1.2.3 Analysis of the residues

The residues collected after heat treatments of the flame retarded vulcanized EVM have been analyzed by ^{13}C and ^{27}Al solid state NMR.

The resulting ^{13}C NMR spectra of the thermo-oxidative degradation residues are presented in *Fig. 87*. It is noteworthy that the signal intensity on the spectrum at 500 and 550 °C was increased to facilita te the peaks observation.

The spectrum of the material at room temperature is the same as that obtained for untreated pure vulcanized EVM. It exhibits a signal at 170 ppm (ester carbonyl function), peaks from 30 to 36 ppm (CH_2 sequences), some peaks around 70 ppm (CH groups) and a single resonance located at 21 ppm (methyl group of the acetate function).

When heated at 320 °C, the material presents some s ignificant chemical modifications since peaks appear at 125 ppm (carbon/carbon double bonds) and at 175- 185 ppm (characteristic of carboxylic acid). It suggests that, as for pure vulcanized EVM, deacetylation and cleavage of the acetate cross-linking bridges occur. Acetic acid is released and some is supposed to be trapped into the polymeric matrix, part of it forming with ATH aluminium acetate (peak at 183 ppm [144]). Some hydrolysis of the polymer can also occur. The deacetylation is not complete up to 350°C, since the spectrum exhibits a peak at 70 ppm (-CH- carbon) revealing that some acetate group still remain in the polymeric chains. At 400 °C, the peak located at 170 ppm and 21 ppm d isappear. As a consequence, deacetylation is total only for a HTT around 400°C. Moreover, it may be assumed that some acid or acetate functions (trapped in the matrix or linked to the polymer chain) are present in the matrix since peaks at 175- 185 ppm for such a HTT. It can also be proposed that some oxidation of the material occurs at this temperature, producing conjugated ketones or acid.

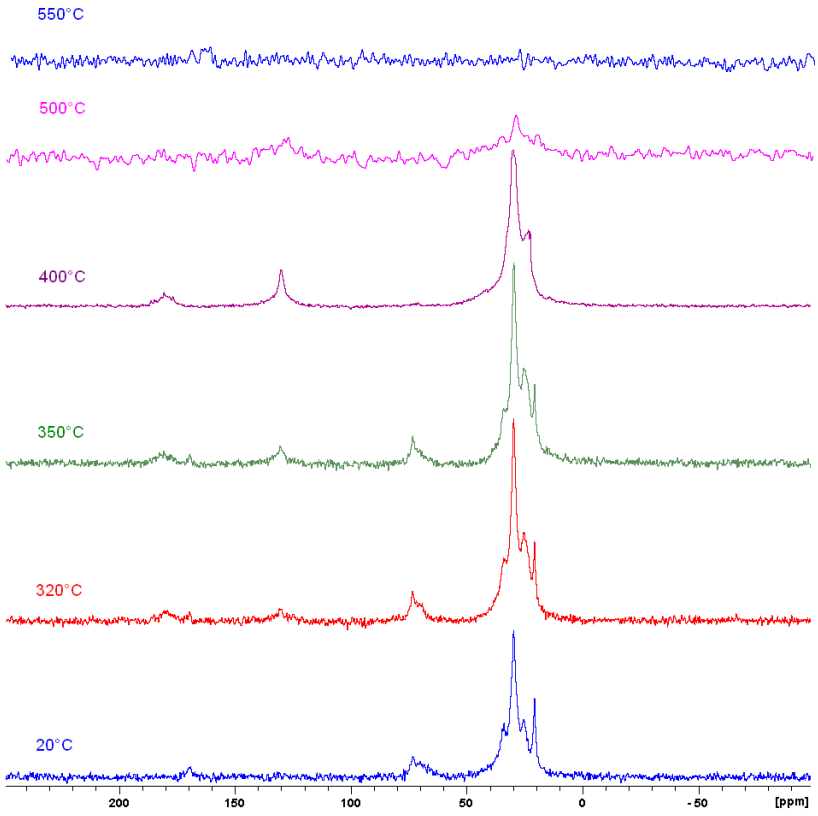


Fig. 87: ^{13}C CP-DD-MAS NMR spectra of the thermal degradation residues of EVM/ATH (degradation under air)

The spectrum of the residue obtained after heat treatment at 500 ℃ exhibits two large bands, respectively centred at 30 and 130 ppm. It indicates the formation of aromatic compounds while aliphatic groups are still present in the material. The broadness and the weakness of the observed signals can be due to a paramagnetic effect of the char, thus reducing the intensity and the resolution on the spectrum.

The last spectrum, corresponding to the completely degraded material, does not exhibit any signal indicating that only alumina remains in the sample. This result is in good agreement with the results deduced from TGA

Compared to vulcanized EVM, it is noticeable that the aliphatic compounds are preserved at higher temperatures, and the formation of unsaturated bonds is less pronounced. Indeed, for the filled polymer, the spectra exhibit a narrow band at around 130 ppm, whereas for the pure matrix, a wide signal (indicating the presence of several species) in the same region is visible. The same observation can be made for the signals at 170- 180 ppm.

To complete the chemical characterization of EVM/ATH degradation residues, ^{27}Al NMR spectra have been performed *(Fig. 88)*. The signal intensity on the spectrum at 450 and 550 ℃ was increased to facilitate the peaks observation.

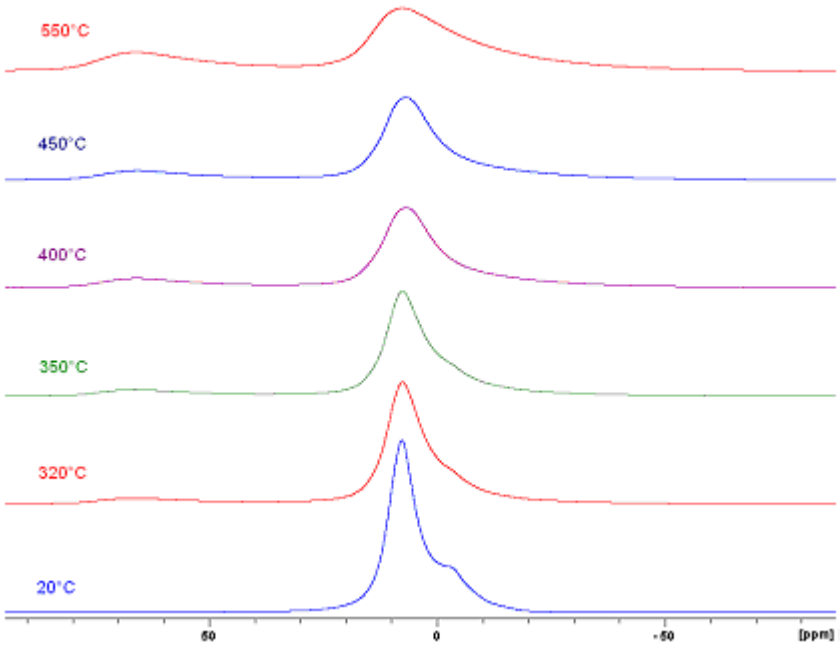


Fig. 88: ^{27}Al MAS NMR spectra of the thermo-oxidative degradation residues of EVM/ATH

The ATH used in the material is known to be a gibbsite form. The untreated material shows the single octahedral resonance at 7.7 ppm expected from the known structure of gibbsite and as reported elsewhere [145]. Another site is observed at –4.7 ppm, attributed to extra-framework aluminium in octahedral coordination impurities [146].

Heating the material above the temperature of the endothermic dehydration of ATH produces an additional signal located at 68 ppm attributed to aluminium in tetrahedral coordination. The appearance of this tetrahedral aluminium is a consequence of the elimination of structural water leading to the formation of a close-packed oxygen lattice in which some of the tetrahedral interstices are occupied by Al.

The peak at –4.7 ppm disappears beyond 400℃. This disappearance is hidden by the octahedral resonance at 7.7 ppm exhibiting a quadrupolar broadening, as confirmed by the peak simulation (performed with the Dmfit software) presented in *Fig. 89*. At this temperature, the octahedral form is partially replaced by a tetrahedral one, with a signal at 67 ppm.

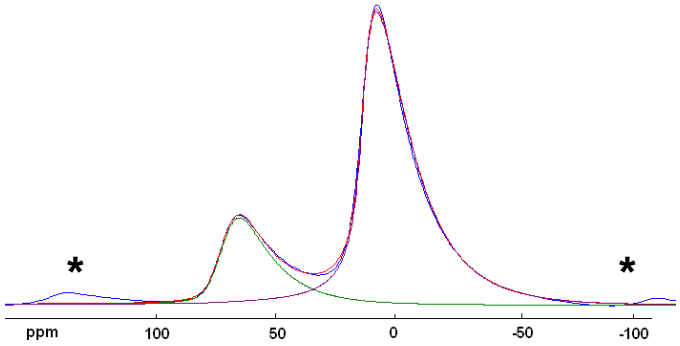


Fig. 89: Experimental spectrum at 550℃ (in blue) a nd simulated one (in red); * = spinning sideband

During the thermal degradation of the material, it is assumed that aluminium trihydroxide degrades into boehmite (γ-AlOOH) and then into alumina. Since boehmite contains only octahedrally coordinated aluminium, it produces a signal at a chemical shift between 5 and 9 ppm [147]. The signals of gibbsite and boehmite thus overlap.

The degradation of ATH in the polymer can however be schemed by:

$$Al(OH)_3 \text{ (gibbsite)} \rightarrow AlOOH \text{ (boehmite)} + \text{gibbsite} \rightarrow \text{ boehmite} + Al_2O_3 \rightarrow Al_2O_3$$

It appears that the peaks linked to octahedral aluminum sites widen with the increasing treatment temperature, suggesting that the crystallinity of the material decreases with increasing temperature. Concerning the hypothesis assuming the formation of aluminium acetate during the degradation, it is difficult to conclude. Indeed, the aluminium acetate should exhibit two peaks located at 12 and 68 ppm, as reported by Tuttle et *al.* [144]. Since these signals are located in the same chemical shift range as boehmite and alumina, it is not possible to conclude about the presence (or the absence) of aluminium acetate.

The pyrolysis products of the flame retarded material were also investigated. ^{13}C solid state NMR spectra of the materials collected after heat treatment of EVM/ATH are presented in *Fig. 90*. The intensity of the two last spectra was increased to facilitate the peaks observation.

The untreated polymer spectrum is the same as for untreated pure vulcanized EVM and thus peaks assignments will not be detailed again.

The spectrum of the material heated up to 330 °C reveals that the deacetylation process has occurred. Indeed, the spectrum exhibits a resonance at 125 ppm, related to carbon/carbon double bonds, while the peaks at 170, 70 and 21 ppm related to the acetate are significantly reduced. Moreover a broad signal is noticeable around 45 ppm, attributed to cyclic aliphatic compounds [139]. Some hydrolysis can also be suspected.. At 350 °C, the spectrum is quite the same, but the collection of aliphatic peaks around 30 ppm is narrowed and an additional resonance at 180 ppm assigned to the presence of acetic acid (or aluminium acetate) trapped in the polymeric matrix is observed.

On the spectrum of the material treated at 400 °C, the same peak at 180 ppm is noticeable, and an additional band at 17 ppm, corresponding to methyl groups linked to carboxylic acid, is visible. It is reasonable to assume that these signals correspond to aluminium acetate.

The last degradation step (450°C) leads to a spectrum exhibiting several signals. Two large but not intense bands are noticeable at 130 and 140 ppm. As previously described for the unfilled polymer, the double peak is explained by the presence of highly unsaturated polyenes (around 135- 140 ppm) and some polycyclic aromatic compounds (130 ppm). The aliphatic region also presents intense peaks, linked to the remaining aliphatic compounds. As for the sample heat treated at 400 °C, aluminium acetate is suspected.

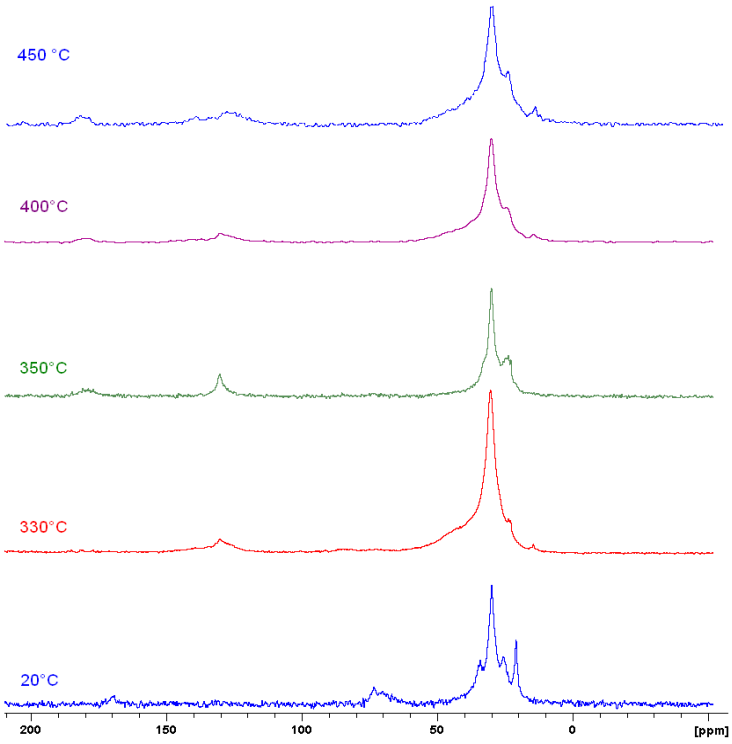


Fig. 90: ^{13}C CP-DD-MAS NMR spectra of the pyrolysis residues of EVM/ATH

The ^{27}Al NMR spectra are gathered in *Fig. 91*. The signal intensity on the spectrum at 450 °C was increased in order to facilitate the peaks observation.

It is noteworthy that the spectra are similar to that obtained for the thermo-oxidative degradation of the flame retarded EVM. As previously discussed, it was demonstrated that aluminium trihydroxide degrades into boehmite (γ-AlOOH) and then into alumina. This is in accordance with the known degradation pathway of $Al(OH)_3$ [148]. It can thus be reasonably assumed that there is not any chemical modification in the filler degradation mechanism when incorporated into the polymeric matrix and heat treated in pyrolytic conditions.

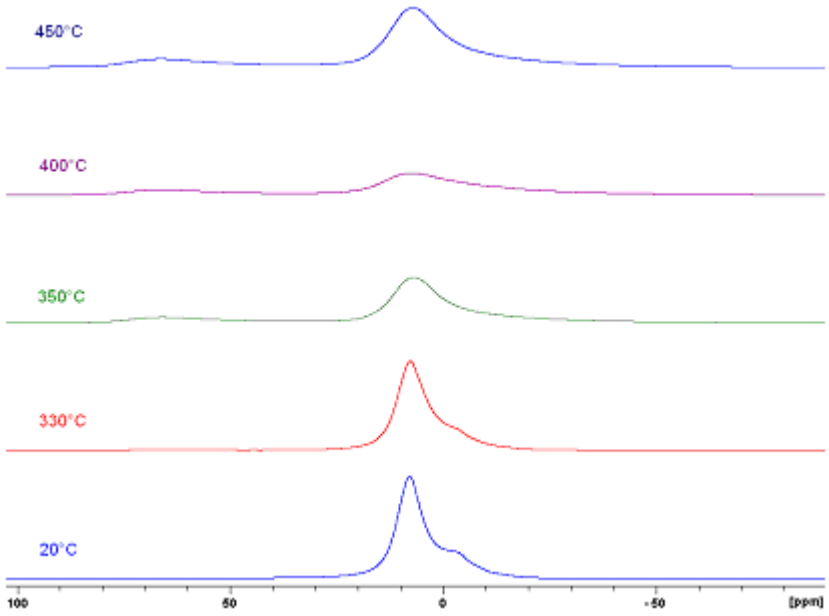


Fig. 91: ^{27}Al MAS NMR spectra of the pyrolysis residues of EVM/ATH

So, it appears that the degradation of the flame retarded cured EVM is effectively influenced by the presence of ATH. The determined mechanisms for the thermo-oxidative and the inert degradation are apparently similar to that of unfilled material, but some differences are noticeable.

Indeed, the deacetylation is complete at a lower temperature compared to pure cured EVM, and the formation of aluminium acetate (resulting from a reaction between alumina and acetic acid) is suspected. The signal on the carbon spectra around 130 ppm, linked to the carbon/carbon double bonds, is narrowed. This suggests that the variety of formed carbonaceous species is different, the condensation of the aromatic products is thus supposed to be less important in the presence of alumina. This effect is particularly noticeable in oxidative conditions.

1.2.4 Gas phase analysis

To complete the investigation of the degradation pathway the gas phase evolved during the degradation of EVM/ATH was also analyzed.

The spectra versus time of the gases evolved during the TG measurement in air are presented in *Fig. 92*. The degradation begins at 22 min (corresponding to 220 °C) and ends at 60 min (600 °C). At the beginning of the thermo-oxidation, some peaks appear around 3500, 1600 and 1000- 1200 cm^{-1}. No additional peak appears up to 40 minutes (corresponding to 400 °C) where the previously cited signals

disappear, replaced by intense peaks at 2300 and 600 cm^{-1}, and signals of low intensity around 3000 cm^{-1}.

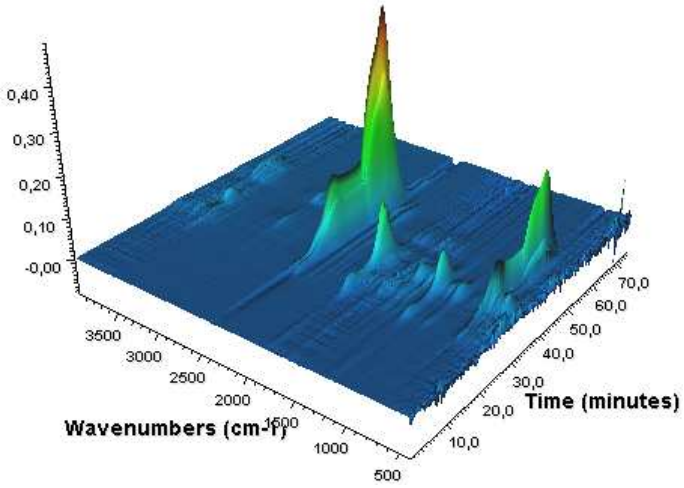


Fig. 92: FTIR spectra of the gases evolved during the thermo-oxidation of vulcanized EVM/ATH versus time

The FTIR spectra of the gas phase at some characteristic temperatures are gathered in *Fig. 93*, and the peak attributions in *Table 39*. It appears that the degradation starts at 220 ℃ with the emission of acetic acid (peaks at 3580, 1796, 1397, 1270, 1176, 1122, 1084 and 998 cm^{-1}) and water resulting from the ATH dehydration. Acetic acid is produced up to 300 ℃, and a non-negligible quantity of water and carbon dioxide is also released. The latter is the major component of the gases evolved from 400 ℃ to 550 ℃ (where the CO_2 peaks reach their maximum). Some traces of aliphatic compounds are also detected (around 2900 cm^{-1}) and some carbon monoxide impurities are also detected.

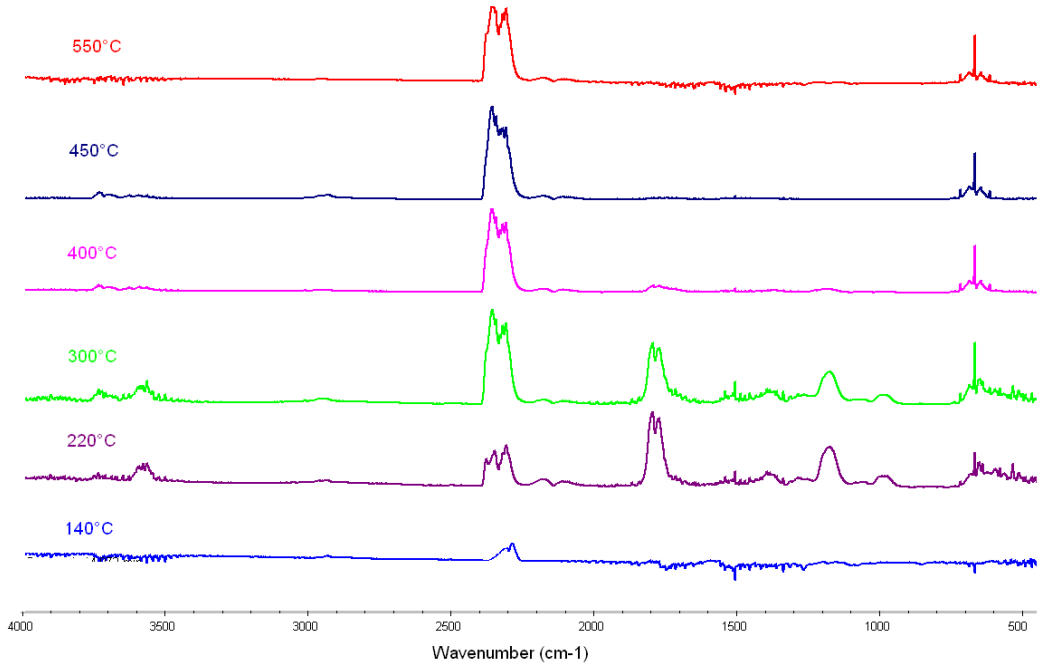


Fig. 93: FTIR spectra of the gases evolved during the thermo-oxidation of vulcanized EVM/ATH collected at characteristic temperatures

Table 39: Attribution of the IR bands of the gases evolved during the degradation in air of vulcanized EVM/ATH

Wave Number (cm^{-1})	Attribution	Wave number (cm^{-1})	Attribution
3735	Fermi combination resonance (CO_2)	1397	-O-H in plane bending (acetic acid)
3580	O-H stretching (acetic acid)	1270	C-OH asymmetrical stretching (acetic acid)
2900-2950	C–H asymmetrical stretching (aliphatic compounds)	1176	Skeletal stretching (acetic acid)
2357, 2310	CO_2	1122	$-CH_3$ stretching (acetic acid)
2181, 2115	CO	1084	-C-OH stretching (acetic acid)
1796	C=O stretching (acetic acid)	998	-O-H bending (acetic acid)
1507	CO_2	670	CO_2 bending

The production of acetic acid and that of carbon dioxide at low temperatures (from 300℃) differ from the thermo-oxidative decomposition of cured EVM. Concerning the release of carbon dioxide, it suggests that ATH or the produced alumina promote the oxidation of the residue during the thermal degradation.

The pyrolysis of the material flame retarded with ATH was also investigated. The evolution of the IR bands versus time *(Fig. 96)* reveals that from 25 to 35 minutes (corresponding to a temperature range between 250 and 350℃), some gases are evolved in the gas cell, with a maximum of absorbance at 35 minutes (i.e. 350 ℃). The bands are located in the regions of 3500- 3600 cm^{-1}, 1800 and 1000-1500 cm^{-1}. From 35 to 40 minutes (that is to say from 350℃ to 400℃), the previous bands disappear, and additional bands around 2900 cm^{-1} appear.

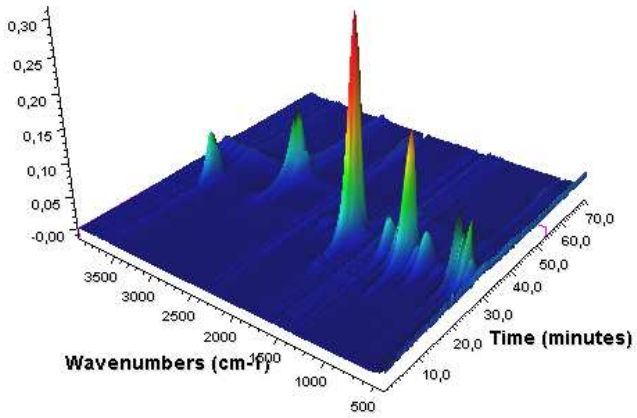


Fig. 94: FTIR spectra of the gases evolved during pyrolysis of vulcanized EVM/ATH versus time

The spectra at characteristic temperatures *(Fig. 97)* reveal what sorts of gases are evolved during the pyrolysis of vulcanised EVM. The spectrum at 250 ℃ only shows the presence of water, released by the ATH dehydration as discussed in the previous section. At 300 ℃, the bands at 3580, 1790, 1397, 1270, 1176, 1122, 1105, 1084 and 998 cm^{-1} attributed to acetic acid *(see*

Table 39) confirm that the second degradation step is a deacetylation of the material. At 400 °C, the spectrum exhibits only three bands around 2850, 2900 and 3100 cm^{-1} (plus the peaks of atmospheric CO_2 and water), corresponding to aliphatic (bands at 2800 and 2900 cm-1) and aromatic compounds (band at 3100 cm-1). The proposed mechanism assuming the production of aliphatic volatiles during the second and third degradation steps is then confirmed. At 500 °C some specific bands remain: around 2300 cm^{-1}, corresponding to some CO_2 traces and some between 2800 and 3050 cm^{-1}, assigned to aliphatic, ethylenic and aromatic products.

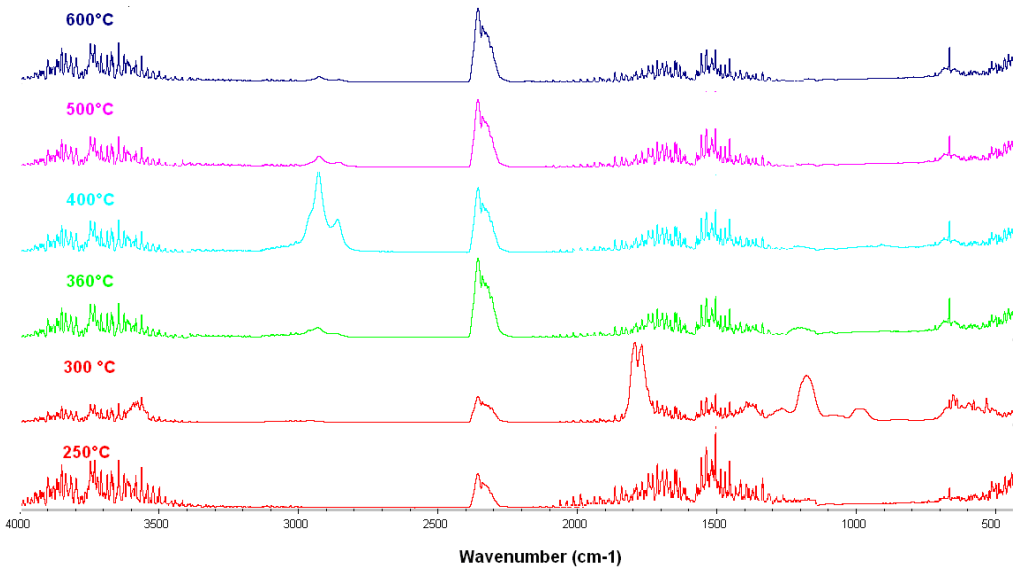


Fig. 95: FTIR spectra of the gases evolved during the pyrolysis of vulcanized EVM/ATH collected at characteristic temperatures

It is noteworthy that, compared to pure cured EVM, no changes appear in the gas phase, except the emission of water resulting from the ATH dehydration. The presence of the aluminium trihydroxide does not seem to modify the pyrolytic degradation pathway of the material.

1.2.4 Degradation mechanism

The previous results allow the drawing of a global description of the degradation mechanisms of the flame retarded EVM.

Vulcanized EVM flame retarded with ATH (120E grade) degrades in oxidative conditions into acetic acid and polyene. In the meantime, ATH dehydrates into boehmite and alumina, and the combination of these compounds with acetic acid to form aluminium acetate can be envisaged. The degradation of the alumina/polyene material leads to the formation of aromatic compounds (charring) then degraded and oxidized in the last part of the degradation. It is noteworthy that the degradation of polyenes (by chain scissions and emanation of volatile compounds) is concurrenced by the oxidation of the material.

This thermo-oxidative degradation is quite similar to that of the neat cross-linked polymer. The major difference is that the oxidation of the condensed phase seems favoured in the presence of ATH.
Concerning the inert degradation of the material, four degradation steps are determined. The first one corresponds to the dehydration of ATH, leading to the formation of alumina. Then deacetylation forms polyene-containing residues. These polyenes are further degraded into aliphatic and/or aromatic compounds, evolved as volatiles. Some char remains in the condensed phase.

It appears that the incorporation of ATH does not modify the nature of the species that are formed during the thermal degradation mechanism of vulcanized EVM (except the suspected formation of aluminium acetate). Nevertheless, if their nature remains unchanged, they are not formed at the same temperatures in the presence of ATH (for example the oxidation of the carbonaceous compounds starts at lower temperature). It is suspected that these differences result from kinetic modifications. That is why, it is now of interest to study the kinetics of degradation of EVM and EVM/ATH materials.

2. Kinetic analysis

Kinetic analysis of the pure vulcanized EVM and of the flame retarded matrix should provide information about how ATH influences the thermal decomposition of the polymeric matrix.

To perform a kinetic analysis of the thermal degradation of a material, it is necessary to go through several steps [149]. The first one consists in obtaining the TGA experimental data of the studied materials. Then, a preliminary model-free analysis (e.g. Ozawa or Friedman analysis [150]) is performed on these data in order to get estimation of kinetic parameters such as the activation energy and the frequency factor. Finally, degradation models are evaluated, and the calculations of the kinetic parameters for the different degradation steps can be done.

2.1 Fundamentals of kinetic analysis

It is proposed in this part of the chapter to follow the methodology described above to model the kinetics of the pyrolytic and oxidative thermal degradation of pure vulcanized EVM and of vulcanized EVM containing ATH.

The kinetic parameters of thermal decomposition can be calculated using methods developed by Kissinger [151], Ozawa [152], and Friedman [150]. These classical methods are iso-convertional methods and provide only apparent results depending on the experimental conditions.

Friedman iso-convertional method is based on the intercomparison of the rates of weight loss ($d\alpha/dt$) for a given fractional weight loss (α) determined using different linear heating rates (β).
The method is based on the equation *Eq.2.*

$$d\alpha/dt = A\, f(\alpha) \exp(-Ea/RT) \qquad \textbf{Eq.2}$$

with Ea the activation energy, $f(\alpha)$ the degradation function, R the gas constant, T the temperature and A the rate constant.
The Friedman analysis uses the resulting logarithmic differential equation *(Eq.3)*.

$$\ln(d\alpha/dt) = \ln[\beta(d\alpha/dT)] = \ln A + \ln f(\alpha) - Ea/RT \qquad \textbf{Eq.3}$$

Through this equation, it is possible to obtain values for Ea over a wide range of conversions.

Our kinetic approach is based on that proposed by Opfermann [149, 153] where the reaction is expressed by the equation *(Eq.4)*.

$$A_{solid} \rightarrow B_{solid} + C_{gas} \qquad \textbf{Eq.4}$$

A thermal decomposition can occur in several steps, for example with the breaking of chemical bonds, heat transfer reactions or desorption of gaseous products. Because of the complexity of the process, it is quite impossible to find an accurate equation to describe all types of thermal decomposition, especially in the case of kinetics varying during the process [154]. Indeed, the thermal degradation of a solid is followed by the emission of gaseous products by a heterogeneous process. It is characterized by a nucleation or diffusion (from one to three dimensions) mechanism, and thus by various degradation functions $f(\alpha)$.

The degradation of a polymer follows a complex scheme, so that it cannot be described by a single degradation function $f(\alpha)$. A model including many degradation functions is necessary. The different possible types of degradation functions are reported in *Table 40*.

Table 40: Common kinetic degradation functions

Degradation function f(α)	Reaction type
$(1-\alpha)$	reaction of first order
$(1-\alpha)^2$	reaction of second order
$(1-\alpha)^n$	reaction of *n*th order
$2(1-\alpha)^{1/2}$	two-dimensional phase boundary
$3(1-\alpha)^{1/3}$	three dimensional phase boundary
0.5/p	one-dimensional diffusion
$-1/\ln(1-\alpha)$	two-dimensional diffusion
$1.5\,(1-\alpha)^{2/3} / (1-(1-\alpha)^{1/3})$	three-dimensional diffusion Jander's type
1.5/((1- α)^(-1/3) -1)	three-dimensional diffusion Ginstling-Brounstein type

Degradation function f(α)	Reaction type
$(1-\alpha)\alpha$	Prout-Tompkins equation
$(1-\alpha)^n.\alpha^a$	expanded Prout-Tompkins equation (autocatalysis)
$2(1-\alpha)(-\ln(1-\alpha))^{1/2}$	two-dimensional nucleation
$3(1-\alpha)(-\ln(1-\alpha))^{1/3}$	three-dimensional nucleation
$n(1-\alpha)(-\ln(1-\alpha))^{(n-1)/n}$	*n* - dimensional nucleation according to Avrami-Erofeev

In the framework of this study, this approach will be considered: the modelling of the thermal degradation will be done by the use of several degradation functions, and not by the use of a single kinetic law. Such an approach avoids making an hypothesis on the degradation type of the system. The only hypothesis is that the rate of reaction dα/dt, as in isothermal conditions, only depends on two functions k(T) and f(α), according to *Eq. 5*.

$$d\alpha/dt = k(T).f(\alpha) \qquad \textbf{Eq.5}$$

where α is the degree of conversion or the fractional weight loss in the case of TGA and f(α) is the so-called ‘‘reaction equation’’ or in the case of TGA, the “degradation function”. Moreover, in the conditions of thermogravimetric analyses, k is not a constant and depends on the temperature T. In order to integrate *Eq.6*, it is supposed that it verifies the Arrhenius law *(Eq.6).*

$$k(T) = Ae^{-Ea/RT} \qquad \textbf{Eq.6}$$

where A is the frequency factor, Ea is the activation energy.

In the TGA conditions, the heating rate β is linear *(Eq.7)*.

$$\beta = dT/dt = \text{constant} \qquad \textbf{Eq.7}$$

The combination of the equations 4 to 7 gives the differential equation *(Eq.8)*.

$$\frac{d\alpha}{f(\alpha)} = \frac{A}{\beta}\exp(\frac{-E_a}{RT})dT \qquad \textbf{Eq.8}$$

All reactions are assumed to be irreversible. In the case of degradation and as the evolved gases are continuously removed by the fluid flow in the TGA chamber, this is a reasonable assumption. It is also assumed that the overall reaction is the sum of individual reaction steps with constant activation energy. The model can then include competitive, independent and successive reactions. The equations are solved with multivariate kinetic analysis (determination of the parameter via a hybrid regularized Gauss-Newton method or Marquardt method) [155].

2.2 Thermal degradation

To implement the kinetic study of the degradation of vulcanized EVM, thermogravimetric analyses were performed at various heating rates: 1, 2, 5, 10 and 20 °C/min. A wide range of heating ramps is covered, favouring low-energy reactions at low-speed heating and high-energy reactions at higher speed.

2.2.1 Vulcanized EVM

TG curves of the thermo-oxidative degradation of vulcanized EVM are reported in *Fig. 96*. It appears that the shape of the curve is identical for all heating rates. Five apparent degradation steps are noticeable as previously observed using high resolution TGA. Concerning the intermediate (and the final) residues, their amount are not modified varying the heating ramps. This indicates that there are no competitive (or parallel) reactions occurring during the degradation process.

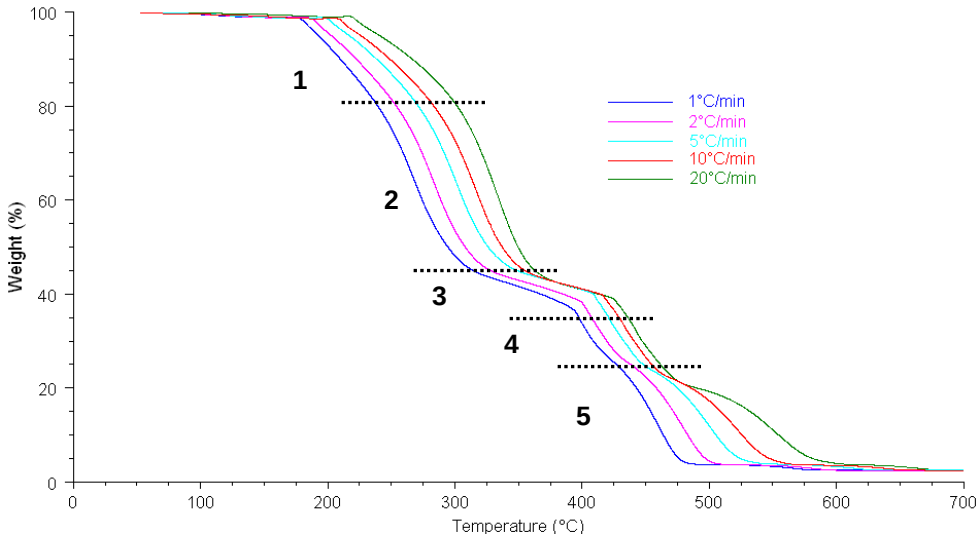


Fig. 96: TG traces of vulcanized EVM depending on the heating rate (in air)

The thermal degradation of vulcanized EVM in nitrogen occurs into three steps *(Fig. 97)*: the first one between 300 and 400 °C, the second and third one overlapping between 400 and 500 °C (as demonstrated by the Hi-Res TGA in the first section of the chapter). It is remarkable that whatever the heating ramp the residual mass remains stable at 2.7 %. Moreover, the intermediate residue observed after the first degradation step has the same residual mass for all heating rates, suggesting unbranched reaction steps.

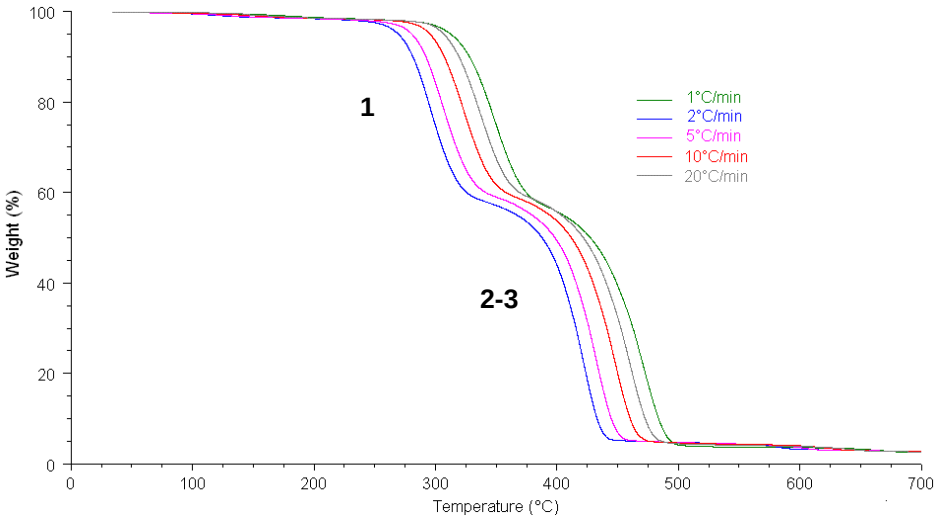


Fig. 97: TG curves of vulcanized EVM depending on the heating rate (in nitrogen)

2.2.2 Vulcanized EVM flame retarded with ATH

To carry out the kinetic modelling of the thermal degradation of the flame retarded EVM, TG analyses were similarly performed on the vulcanized EVM/ATH material.

TG curves in air are gathered in *Fig. 98*. Five degradation steps are visually noticeable whatever the heating ramp, and the global shape of each curve remains identical. However, the final residue varies with the heating ramp. This could suggest branched reactions (e.g. competitive reactions) in the degradation pathway.

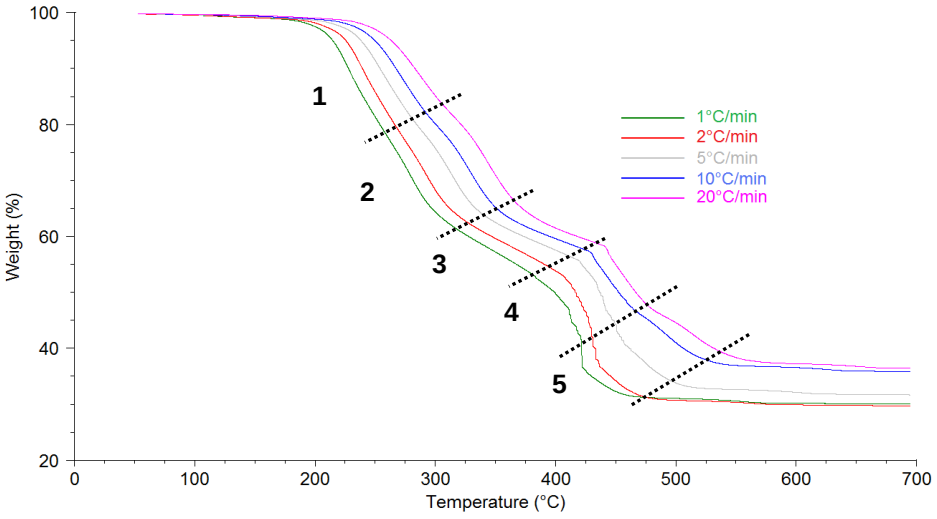


Fig. 98: TG curves of vulcanized EVM flame retarded with ATH 120E depending on the heating rate (in air)

The same analyses in an inert atmosphere are presented in *Fig. 99*. It appears that the shape of the curve is identical for all heating rates. Four degradation steps are noticeable, as previously observed using high-resolution TGA. The final degradation residue remains stable at 38 wt-%. Concerning the

intermediate residues, they are not modified by the heating ramps. This indicates an unbranched degradation pathway.

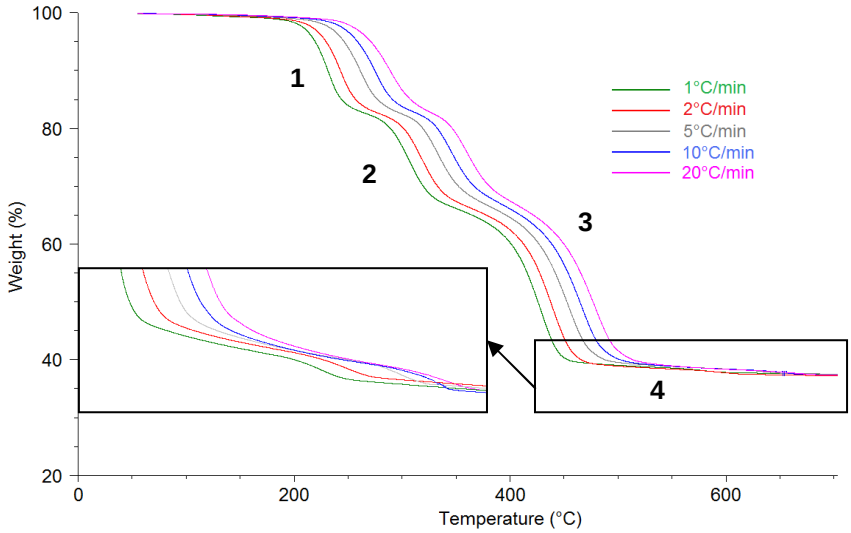


Fig. 99: TG curves of vulcanized EVM flame retarded with ATH 120E depending on the heating rate (in nitrogen)

TG analyses have thus been performed. The next step consists in making a preliminary analysis of these data to get information about the kinetic parameters.

2.3 Friedman "model-free" analysis

A classical approach consists in using a model-free analysis as a preliminary step to the kinetic simulation [153, 156]. The chosen one is the Friedman analysis [150] which is probably one of the most general of the derivative techniques.

The apparent activation energy Ea (red curve) and logA (blue curve) obtained through the Friedman analysis are plotted versus the fractional mass loss. The Ea and logA values provided by the Friedman analysis will then be used as starting data to model the degradation in order to facilitate the convergence of the resolution algorithm. On the other hand, the literature [157] claims that more information can be read from the Friedman analysis than just the activation energy and the pre-exponential factor. If the activation energy shows a clear dependence on the conversion degree, this is an indication of the presence of a complex reaction path. If, in the plot of the Friedman analysis the experimental points exhibit several maxima, this is the indication that several steps occur.

The results obtained for the vulcanized EVM thermo-oxidative degradation are presented in *Fig. 100* as an example. The Friedman energy plots of the degradation of vulcanized EVM in nitrogen and for the flame retarded EVM in air and nitrogen are gathered in *Appendix 5*.

It appears that for the thermo-oxidative degradation of vulcanized EVM, the energy is not constant during the whole degradation. Five areas can be defined. Between 0.2 and 0.4 fractional mass loss the energy is stable at around 130 kJ/mol and from 0.4 to 0.6 at around 150 kJ/mol. Then, it increases up to 300 and 350 kJ/mol. The last part (from 0.85 to 1) presents an activation energy of 130 kJ/mol. This indicates that the thermal decomposition occurs in a complex way including several degradation reactions.

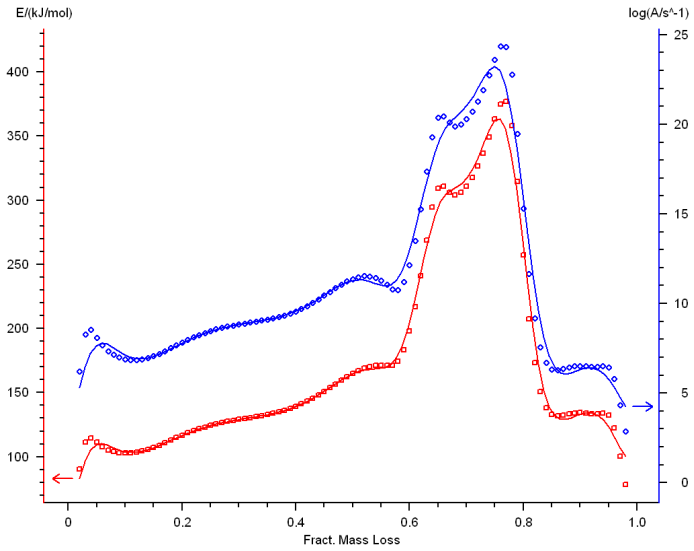


Fig. 100: Friedman energy plot of vulcanized EVM (in air)

The Friedman analysis results provide some approximate Ea and logA values (as cited above). These data will be used as starting values to initiate the calculations. Then, the results of the kinetic simulation will allow the determination of the best degradation models.

2.4 Kinetic modeling

The kinetic modelling of the thermal degradation of the materials was then performed according to the tested model and degradation functions. For the simulation of the thermal degradation of polymers, the most used functions are the n-th order model and the n-th dimension Avrami-Erofeev function modelling an assumed random nucleation [158, 159]. These expressions generally provide satisfying and accurate results for polymers. But for certain type of reactions, these models are not adapted, for example in the case of autocatalytic degradation. Thus, some specific functions can be selected, such as the Prout-Tompkins autocatalysis corresponding to the auto-catalyzed formation of branching nuclei. For each degradation step of the model, a kinetic function is assigned. The selection of the degradation functions is based on physical considerations (what we know about the chemistry and physics of the reaction) and on the fit quality of the simulation.

The results of the kinetic modelling are presented in the following figures (from *Fig. 101* to *Fig. 104*). The experimental TG curves are plotted in coloured lines, and the simulated curves are black-lined.

2.4.1 Vulcanized EVM

The best tested model for the thermo-oxidative decomposition of vulcanized EVM is composed of five unbranched steps:

$$A \xrightarrow{1} B \xrightarrow{2} C \xrightarrow{3} D \xrightarrow{4} E \xrightarrow{5} F$$

This model was chosen in accordance with the Hi-Res TGA results, indicating five degradation steps. These steps were considered successive as there was no evidence for branched reactions as previously discussed. The kinetic functions assigned to the each degradation steps of the model are presented in *Table 41*. The chosen degradation functions and model were the best one to obtain a good fit between the computed curves and the experimental TGA curves of the thermo-oxidative degradation of vulcanized EVM *(Fig. 101)* (correlation coefficient of 0.99987). Moreover, the model provided the best F-test fit quality.

Table 41: Degradation functions modelling the thermo-oxidative degradation steps of vulcanized EVM

	Vulcanized EVM
1	n^{th} order
2	Prout-Tompkins, autocatalysis
3	n^{th} order
4	n^{th} dimension Avrami-Erofeev
5	n^{th} order

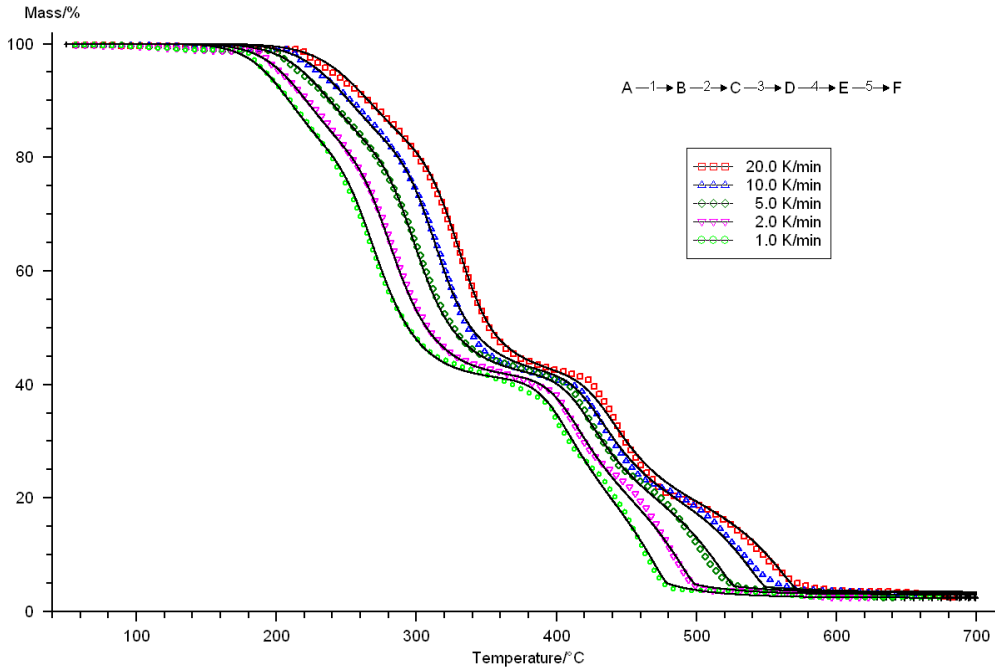


Fig. 101: Simulation of the degradation of vulcanized EVM in air

The kinetic parameters obtained through this simulation are gathered in *Table 42*. It is recalled that logA and Ea are correlated by a compensation effect: the value of Ea determines the pre-exponential factor value and reciprocally. Thus, we will only discuss the activation energy values.

Table 42: Kinetic parameters of thermo-oxidative degradation of vulcanized EVM

	Log A (A: s^{-1})	Ea (kJ/mol)	n	a^2
Step 1	8.4 ± 0.4	106 ± 2	1.91 ± 0.1	-
Step 2	7.5 ± 0.3	102 ± 2	1.00 ± 0.05	0.51 ± 0.02
Step 3	3.71 ± 0.07	56.2 ± 0.8	1.01 ± 0.05	-
Step 4	18.1 ± 0.1	274 ± 2	0.88 ± 0.02	-
Step 5	9.53 ± 0.06	179.4 ± 0.9	0.92 ± 0.02	-

According to the degradation mechanism determined in the previous part of the chapter, it is possible to attribute a chemical mechanism for each kinetic degradation step.

The first step exhibits a pre-exponential factor of 8.4 and activation energy of 106 kJ/mol. It corresponds to the cross-linking cleavage (of acetate bridges) and to the beginning of deacetylation. This activation energy value is also consistent with the thermal oxidation (postulated to involve the hydroperoxide radical in the propagation step of the degradation), since most oxygen initiated depolymerizations have activation energies in the 80–110 $kJ.mol^{-1}$ range [143].

Then, with roughly the same kinetic parameters (7.5 and 102 kJ/mol), the deacetylation of the polymeric chains proceeds. It is noticeable that the reaction is autocatalytic with a reaction coefficient of 0.51. It was demonstrated by Rimez *et al.* [26] that the deacetylation of EVM (60%VA) is not catalytic, because the catalytic double bonds, formed by deacetylation, only activate the release of a neighbour acetate group in a certain triad sequence configuration. But this result is not surprising since the acetic acid trapped into the matrix in the cured polymer can activate deacetylation by acidic catalysis (and thus the formation of polyene). The next step consists in the “charring” of the residue with the formation of aromatic compounds (56.2 kJ/mol), followed by the degradation of the remaining polyenes with an activation energy of 274 kJ/mol and a pre-exponential factor of 18.1. The charring activation energy is quite low compared to that of uncured EVM (214 kJ/mol) and confirms that the cross-linking impacts the charring of the material. The last degradation step corresponds to the oxidation of the remaining residue (logA = 9.53 and Ea = 179.4 kJ/mol). These values are consistent with that of the literature [26, 160].

According to the Hi-Res TGA and to the Friedman analysis, the model for the pyrolysis of pure vulcanized EVM was determined as three non-competitive degradation steps as described below:

$$A \xrightarrow{1} B \xrightarrow{2} C \xrightarrow{3} D$$

The material A decomposes into the intermediate product B, then degrading into C, the latter leading to the formation of the residual product D. The chosen degradation function for each step is an Avrami-Erofeev ($f(\alpha) = (n\,[-\ln(1-\alpha)^{n}](1-\alpha))$) function. These model and degradation function provided

the best fits (best correlation coefficient and F-test fit quality) during the kinetic modelling computations. As shown in *Fig. 102*, the computed curves perfectly fit the experimental ones, with a correlation coefficient of 0.99982

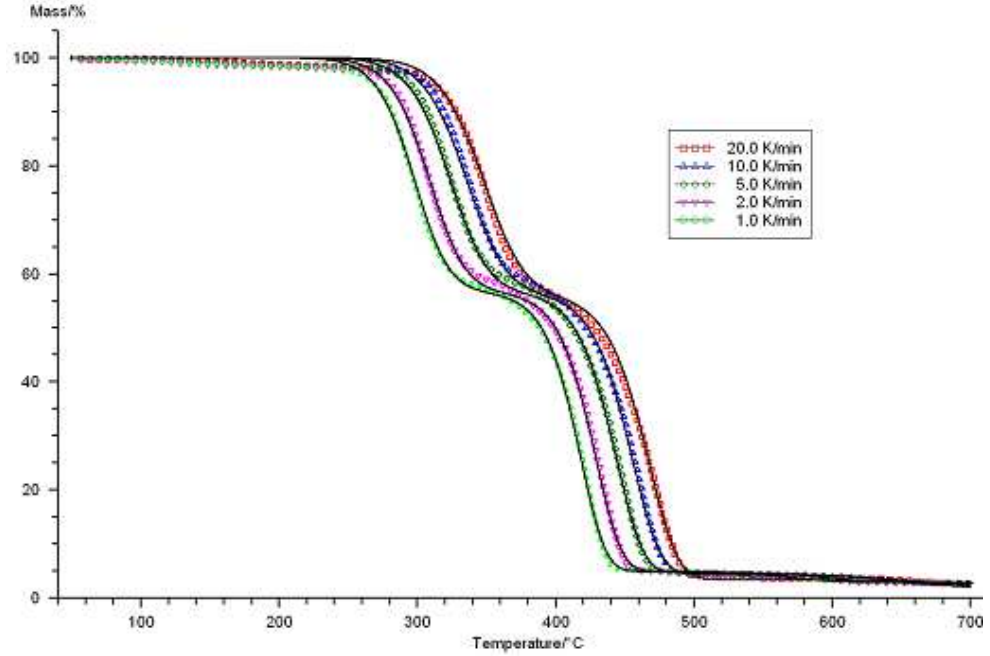


Fig. 102: Simulation of the degradation of vulcanized EVM under nitrogen

The kinetic parameters obtained through this simulation are gathered in *Table 43*. The calculated kinetic parameters correspond to those described in the literature [26, 27] for non-cross-linked EVM. Indeed, no significant difference between the degradation pathway of EVM and the vulcanized polymer were observed. The first step of the pyrolysis of the cross-linked polymer exhibits activation energy around 170 kJ/mol and a pre-exponential factor of 12.12. This corresponds to parameters determined for the deacetylation with loss of acetic acid of EVM. Moreover, this is consistent with the mechanism described in the first part of this chapter.

The two other degradation steps respectively between 400 and 450°C; and between 450 and 500°C are attributed to the degradation of polyenes into ethylenic, aliphatic and/or aromatic volatiles.

Table 43: Kinetic parameters of inert degradation of vulcanized EVM

	Log A (A: s^{-1})	**Ea (kJ/mol)**	**n**
Step 1	12.12 ± 0.05	165.7 ± 0.5	1.48 ± 0.01
Step 2	15. 6 ± 0.2	246 ± 2	1.09 ± 0.02
Step 3	6.6 ± 0.1	163.5 ± 0.6	0.61 ± 0.08

The kinetic analysis allowed the modelling of the pyrolysis and the thermo-oxidative degradation of vulcanized EVM. Now to determine the influence of ATH on this degradation and further on the flame retardant mechanism, it is necessary to determine the kinetic parameters in the case of the degradation of the flame retarded matrix.

2.4.2 Vulcanized EVM flame retarded with ATH

The kinetic model for the thermo-oxidative degradation of the matrix flame retarded with ATH is identical to that of the unfilled matrix (five successive steps). Nevertheless, one difference was noticed: the best value in the F-test fit quality was obtained for a n-th order degradation function instead of Prout-Tompkins for the second step *(Table 44)*. This result is physically coherent with the observations resulting from the NMR spectra analysis, showing that acetic acid may react with alumina, and thus may not be involved in deacetylation catalysis. As for the previous simulations, the correlation between experimental and computed data according to the chosen model is excellent with a coefficient of 0.99983 *(Fig. 103)*.

Table 44: Degradation functions modelling the thermo-oxidative degradation steps of vulcanized EVM and the flame retarded matrix

	Vulcanized EVM	ATH-filled vulcanized EVM
1	n^{th} order	n^{th} order
2	Prout-Tompkins, autocatalysis	n^{th} order
3	n^{th} order	n^{th} order
4	n^{th} dimension Avrami-Erofeev	n^{th} dimension Avrami-Erofeev
5	n^{th} order	n^{th} order

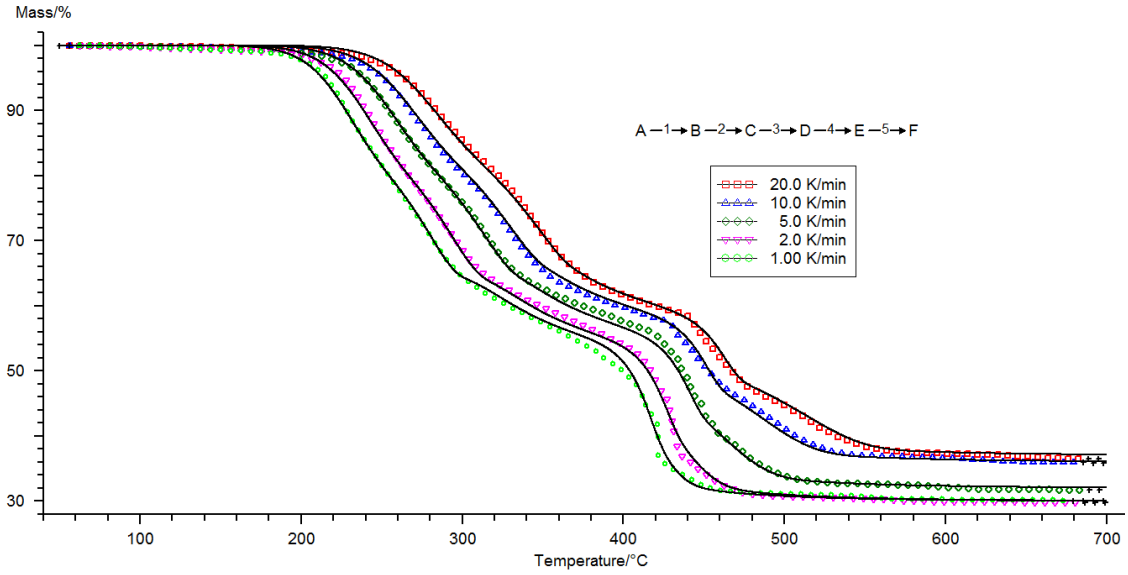


Fig. 103: Simulation of the degradation of vulcanized EVM flame retarded with ATH 120E under air

The resulting kinetic parameters are gathered in *Table 45*. The first step exhibits a pre-exponential factor of 10.0 and an activation energy of 125 kJ/mol, corresponding to the ATH dehydration (110 kJ/mol reported in the literature [160]) coupled with the cross-linking scission reactions occurring in the polymeric matrix (106 kJ/mol in cured EVM). Then, the deacetylation leads to the formation of polyene with roughly the same kinetic parameters. It is noticeable that compared to the deacetylation of the pure cured polymer the reaction is non-catalytic. As explained previously, this can be linked to the

formation of aluminium acetate, chemically "trapping" the acidic species, preventing them to catalyze the deacetylation reaction.

In the next step, the charring of the residue occurs: the activation energy and pre-exponential factor are very high compared to that observed in the pure polymer: 211 kJ/mol and 15.3 respectively compared to 56 kJ/mol and 3.7. The reason we suggest is that the in-situ degradation of ATH leads to the formation of a protective structure of alumina, delaying the charring of the polymer.

The two final steps correspond to the degradation of the remaining polyenes (logA = 11.5 and Ea = 185 kJ/mol) and to the oxidation of the aromatic compounds (logA = 4.2 and Ea = 100 kJ/mol), which exhibit lower activation energies compared to the unfilled polymeric matrix. The decrease of the activation energies of the char degradation reactions is attributed to the presence of alumina. Indeed, alumina is known to be an oxidation catalyst [161-163], it thus facilitates the degradation of the residue in oxidative conditions. This is consistent with the ^{13}C NMR characterization of the heat treatment residues of the EVM/ATH formulation that shows that at 550°C no carbon is maintained in the residue whereas it was not the case for pure EVM.

Table 45: Kinetic parameters of thermo-oxidative degradation of ATH-filled vulcanized EVM

	Log A (A: s^{-1})	**Ea (kJ/mol)**	**n**
Step 1	10.0 ± 0.2	125 ± 1	1.45 ± 0.1
Step 2	8.1 ± 0.1	117 ± 1	0.72 ± 0.2
Step 3	15.3 ± 0.7	211 ± 7	0.61 ± 0.1
Step 4	11.5 ± 0.2	185 ± 7	1.88 ± 0.1
Step 5	4.2 ± 0.1	100 ± 5	1.37 ± 0.2

The following simulation models the inert degradation of the ATH-containing EVM *(Fig. 104 and Table 46)*. The corresponding model is a four-successive-step model, characterized by Avrami-Erofeev and n-th order functions. The simulated and experimental TG curves are well superimposed. Indeed, the correlation between experimentation and computed data is good, with a coefficient of 0.999923.

The first degradation step corresponds to the dehydration of the ATH in the polymeric matrix and to the cleavage of some cross-linking bonds (acetate groups). It is noticeable that the activation energy values are the same in nitrogen or in air. Then deacetylation occurs, leading to the formation of polyenes. This reaction exhibits an activation energy of 147 kJ/mol. Aliphatic and ethylenic volatile products are further produced (Ea = 243.2 kJ/mol). The next step consists in the degradation of the remaining polyenes and to the formation of aromatic compounds, with kinetic parameters of 7.3 for the pre-exponential factor and 165 kJ/mol for the activation energy. The kinetic of these three last degradation steps are very close to that of non-vulcanized EVM and are also close to those reported in the literature [26].

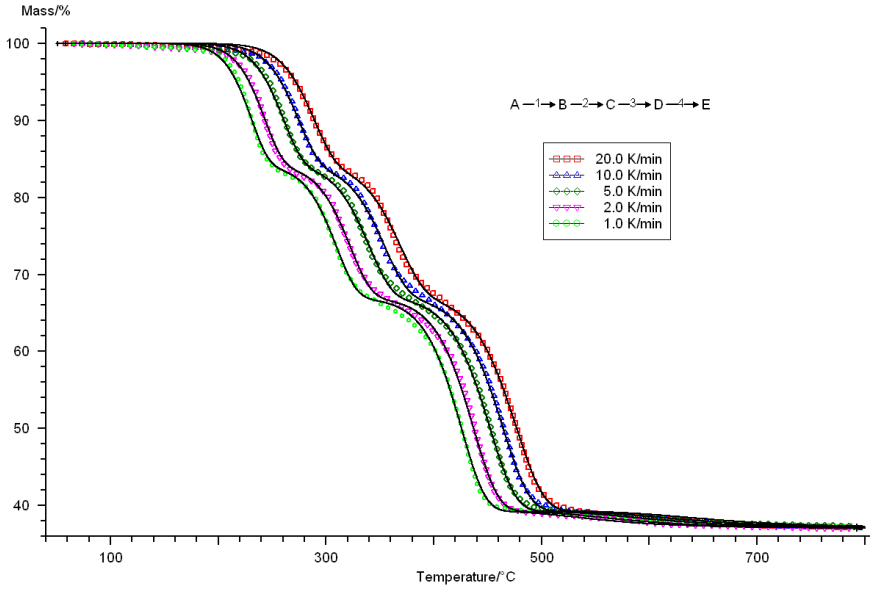


Fig. 104: Simulation of the degradation of vulcanized EVM flame retarded with ATH 120E under nitrogen

Table 46: Kinetic parameters of inert degradation of ATH-filled vulcanized EVM

	Log A (A : s^{-1})	Ea (kJ/mol)	n
Step 1	8.73 ± 0.05	113.6 ± 0.5	1.13 ± 0.01
Step 2	10.06 ± 0.06	146.8 ± 0.7	1.07 ± 0.02
Step 3	15.11 ± 0.04	243.2 ± 0.6	0.69 ± 0.01
Step 4	7.33 ± 0.04	165 ± 0.8	2.9 ± 0.1

2.5 Conclusion

The kinetic modeling of the thermal degradation of vulcanized EVM and of the ATH-containing matrix allowed the determination of the kinetic parameters of each degradation step. Moreover, the degradation mechanisms of the materials previously established can be correlated to the kinetic parameters.

The kinetic parameters related to the thermo-oxidative degradation reactions are compared for vulcanized EVM and for the flame retarded matrix in *Table 47*.

If the presence of ATH (or alumina produced by ATH dehydration) does not modify the chemical reaction occurring during the thermal degradation, it influences the kinetic parameters of these reactions. Compared to vulcanized EVM, the filled matrix exhibits similar log A and Ea values for the two first degradation steps. It is however noticeable that the autocatalysis occurring for the deacetylation of the cross-linked polymer disappears when ATH is added in the material. This could be reasonably attributed to Lewis acid-base reactions occurring between alumina and the released acetic acid [164] *(Fig. 105)*, which is thus deactivated, preventing these acid acetic molecules to catalyze the deacetylation.

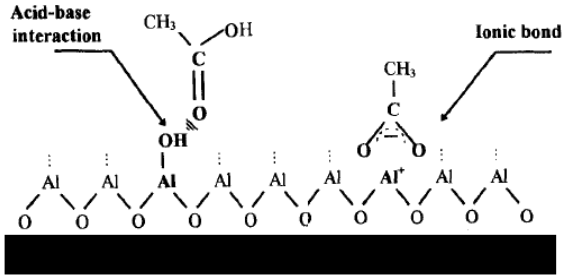


Fig. 105: Schematic representation of the acid-base interaction and the ionic bonding between acetic acid and alumina

On the other hand, higher values of the kinetic data are noticeable for the charring reaction in presence of ATH. This is consistent with the study of the degradation mechanism of the materials that shows that the condensation of the aromatic products is thus supposed to be less important in the presence of alumina. Concerning the last two steps (char degradation and oxidation), the flame retarded material exhibits lower log A and Ea, indicating that these reactions are favored in presence of ATH. This effect is attributed to the catalytic role of alumina in terms of degradation and oxidation of organic compounds [161-163].

Table 47: Comparison of the kinetic parameters for the thermo-oxidative degradation of vulcanized EVM and of the matrix flame retarded with ATH

Vulcanized EVM				**Vulcanized EVM with ATH**			
Degradation step	**Kinetic function**	**LogA ($A:s^{-1}$)**	**Ea (kJ/mol)**	**Degradation step**	**Kinetic function**	**LogA ($A:s^{-1}$)**	**Ea (kJ/mol**
Chain scissions + deacetylation	n^{th} order	8.4 ± 0.4	106 ± 2	Chain scissions + ATH dehydration+ deacetylation	n^{th} order	10.0 ± 0.2	125 ± 1
Deacetylation	autocatalysis	7.5 ± 0.3	102 ± 2	Deacetylation	n^{th} order	8.1 ± 0.1	117± 1
Charring	n^{th} order	3.71 ± 0.07	56.2 ± 0.8	Charring	n^{th} order	15.3 ± 0.7	211± 7
Char degradation	Avrami	18.1 ± 0.1	274 ± 2	Char degradation	Avrami	11.5 ± 0.2	185 ± 7
Char oxidation	n^{th} order	9.53 ± 0.06	179.4 ± 0.9	Char oxidation	n^{th} order	4.2 ± 0.1	100 ± 5

In the case of the pyrolysis, the presence of ATH does not modify the kinetic parameters when compare with the ones of unfilled vulcanized EVM. Indeed, as presented in *Table 48*, the pre-exponential factors (logA) and the activation energies of the deacetylation process and of polyene degradation are similar for the filled and unfilled matrices.

Table 48: Comparison of the kinetic parameters for the pyrolysis of vulcanized EVM and of the matrix flame retarded with ATH)

Vulcanized EVM				**Vulcanized EVM with ATH**			
Degradation step	**Kinetic function**	**logA ($A:s^{-1}$)**	**Ea (kJ/mol)**	**Degradation step**	**Kinetic function**	**logA ($A:s^{-1}$)**	**Ea (kJ/mol)**
-	-	-	-	ATH dehydration	Avrami	8.73 ± 0.05	113.6 ± 0.5
Deacetylation	Avrami	12.12 ± 0.05	165.7 ± 0.5	Deacetylation	Avrami	10.06 ± 0.06	146.8 ± 0.7
Polyenes degradation (aliphatics)	Avrami	15. 6 ± 0.2	246 ± 2	Polyenes degradation (aliphatics)	Avrami	15.11 ± 0.04	243.2 ± 0.6
Polyenes degradation (aromatics)	Avrami	6.6 ± 0.1	163.5 ± 0.6	Polyenes degradation (aromatics)	n^{th} order	7.33 ± 0.04	165.0 ± 0.8

It is thus possible to conclude that ATH has an impact on the kinetic parameters of the thermal degradation of vulcanized EVM in oxidative conditions. The influence of this filler on the degradation and thus on the flame retardant properties of the material has to be discussed. This is the objective of the next part of the chapter.

3. General discussion

Some questions have arisen all along of this chapter. First, during the investigations about the thermal degradation mechanism of vulcanized EVM, the influence of the cross-linking of the matrix on the mechanism of degradation of the matrix appeared to be an important issue that is not reported in the literature. Thus, it will be the first point of this discussion.

Then, another question concerns the role of ATH on the thermal degradation and thus on the flame retardant properties of the cross-linked polymer. Its effect on the thermal degradation of the material has been highlighted, but the point is now to understand in what extent the influence of the filler on the degradation reactions of the polymer has an effect on the flame retardant behaviour. This question and the answers thereof will be discussed in a second part of this general discussion.

In these two parts, the influence of the atmosphere (oxidative or inert) on the degradation will also be commented.

Finally, an applicative part will consist in investigating the evolution of the structure of the residues obtained in fire conditions, simulated through mass loss calorimeter experiments. We will then be able to precise the hypotheses proposed about the influence of ATH on the thermal degradation of cured EVM and the flame retardant mechanism of the metal hydroxide.

3.1 Effect of vulcanization on the thermal degradation of EVA

The literature data relating the thermal degradation of EVA has been described in *Chapter 1*. The main issue of this section is to discuss the effect of the cross-linking on the thermal degradation of the polymer.

The thermo-oxidative degradation steps and the corresponding kinetic data for EVA (according to the literature [26]) and for the vulcanized polymer are gathered in *Table 49*.

The cross-linking of the material mainly affects the degradation of EVA at the first stages of its degradation. Indeed, the first degradation step for vulcanized EVM consists in the cleavage of some cross-linking bonds together with the beginning of the deacetylation (the auto-catalytic deacetylation mainly occurs in a second step), while in pure EVA the deacetylation, which is non-catalytic, is completely achieved at the end of the first degradation step. The fact that acetic acid plays a catalytic role in cured EVM but not in the pure polymer can be explained by a physical effect. Indeed, in pure EVM (not cured) acetic acid is evolved as a gaseous compound which is eliminated and thus cannot react with the polymeric chains. In the cured polymer, the structure in three dimensions of the matrix traps the evolved acetic acid, which can thus participate to acidic catalysis.

Table 49: Comparison of the kinetic parameters for the thermo-oxidative degradation of vulcanized EVM and of pure EVA (EVA70, from Rimez et al.[26])

Vulcanized EVM			**EVA**		
Degradation step	**logA ($A:s^{-1}$)**	**Ea (kJ/mol)**	**Degradation step**	**logA ($A:s^{-1}$)**	**Ea (kJ/mol)**
Chain scissions + deacetylation	8.4 ± 0.4	106 ± 2	-		
Deacetylation	7.5 ± 0.3	102 ± 2	Deacetylation	12.6	177.5
Charring	3.71 ± 0.07	56.2 ± 0.8	Charring	10.5	173.2
Char degradation	18.1 ± 0.1	274 ± 2	Char degradation	20.3	302.6
Char oxidation	9.53 ± 0.06	179.4 ± 0.9	Char oxidation	11.9	211.6

The charring is also promoted by the vulcanization. This is in correlation with the degradation mechanism of the cured polymer: some cross-linking bonds (in particular the acetate bridges) are broken during the first degradation step, but a large part of cross-linking bridges are preserved. The presence of such nodes in the polymeric chains favors the aromatization of the polyenes, as confirmed by the ^{13}C NMR spectra exhibiting a broadening of the aromatic signal.

The kinetic parameters and the corresponding chemical degradation reactions are compared for the pyrolysis of EVA (data from the literature) and of the cross-linked polymer in *Table 50*.

Table 50: Comparison of the kinetic parameters for the inert degradation of vulcanized EVM and of pure EVA (EVA70, from Rimez et al.[26])

Vulcanized EVM			**EVA**		
Degradation step	**logA ($A:s^{-1}$)**	**Ea (kJ/mol)**	**Degradation step**	**logA ($A:s^{-1}$)**	**Ea (kJ/mol)**
Deacetylation	12.12 ± 0.05	165.7 ± 0.5	Deacetylation	12.7	177.5
Polyenes degradation	15. 6 ± 0.2	246 ± 2	Polyenes degradation	16.3	260.7
Polyenes degradation	6.6 ± 0.1	163.5 ± 0.6	Polyenes degradation	10.4	176.9

Concerning the influence of the cross-linking, it surprisingly apparently does not influence the thermal degradation of EVA. The mechanism is unchanged and the pre-exponential factors and activation energies are similar.

Nevertheless, a residue is obtained for the cured polymer, whereas raw EVM degrades entirely. Vulcanization (and the resulting cross-link nodes) promotes the condensation of the aromatic compounds formed during the polyenes degradation, thus producing some carbonaceous stable residue. This supports the analysis of the NMR spectra of the heat-treated residues. It is noteworthy that the same mechanism is implied in the thermo-oxidation of vulcanized EVM, but the presence of oxygen during the degradation greatly influences its degradation pathway. As proposed in the first part of the chapter, oxygen plays a role on the deacetylation, which is favored (activation energy of 105 kJ/mol in air versus 166 kJ/mol in nitrogen) and on the charring of the material. During the charring in oxidative conditions there is only a very slight mass loss, and a very low release of gaseous compounds: the degradation of the carbonaceous residue occurs in an additional step at higher temperature. In nitrogen, the formation of the carbonaceous residue and its degradation into volatiles run in the meantime. It can be proposed that the acidic functions trapped in the matrix, in presence of oxygen, form radical species promoting the charring.

To conclude on the influence of curing on the thermal degradation of EVM, it can be said that, whatever the degradation atmosphere, the cross-linked structure enhances the thermal stability of the material favoring the charring.

3.2 Influence of ATH on the thermal degradation of vulcanized EVA

Kinetic analysis associated to the degradation mechanisms of neat EVM and EVM/ATH provides information about the influence of ATH on the vulcanized polymer and thus about the flame retardant role of ATH. To determine its mode of action the thermal degradation of the filled material was investigated in oxidative and in inert conditions.

If the presence of ATH (or alumina produced by ATH dehydration) does not modify the chemical reactions occurring during the thermal degradation, it influences the kinetic parameters of these reactions under oxidative conditions.

One of the main effects of alumina is the Lewis acid-base interactions leading to the deactivation of acetic acid, and thus to the disappearance of the autocatalysis phenomenon. Indeed, compared to vulcanized EVM, the filled matrix exhibits a better thermal stability as shown by the mass loss difference curve (+5 %) due to the formation of aluminium acetate *(Fig. 106)*. In inert conditions, the deacetylation is not affected by the presence of alumina. Aluminium acetate can be formed such as in oxidative conditions, but since the inert degradation process is not catalytic it does not modify the reaction kinetics.

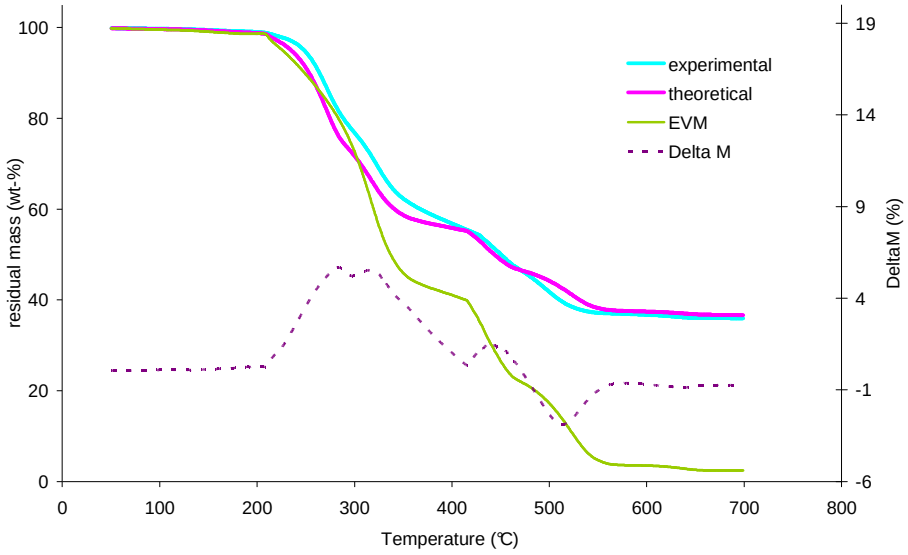


Fig. 106: Difference weight loss curve for ATH-filled vulcanized EVM, and TG curve of EVM (in air, 10 °C/min)

It is also noteworthy that the ATH endothermal dehydration does not influence the degradation kinetics of the polymer. This is in contradiction with the literature, assuming that the main effect of ATH during the degradation, and especially its main flame retardant effect, is a cooling phenomenon due to its dehydration [165-168]. It has been demonstrated in this chapter, by the kinetic modeling of the vulcanized EVM degradation, that this endothermal effect is overestimated. Moreover, the ATH dehydration occurs in a very short time and at the very beginning of the polymer degradation. It can thus reasonably be concluded that the “cooling effect” of ATH is not its major way of action in terms of flame retardancy.

Compared to pure vulcanized EVM, it is noticeable that under oxidative conditions, ATH modifies the charring of the material since the activation energy is greatly increased. This can be explained by the formation of a protective alumina structure trapping the aliphatic compounds and polyenes, thus preventing their aromatization.

In oxidative conditions, it also appears that the char degradation is facilitated by the presence of alumina, especially the oxidation process. Indeed, when the char is formed, the protective alumina structure beyond 400 °C promotes the char degradation. This phenomenon is due to the fact that alumina is a well-known oxidation catalyst [161-163]. Indeed, the activation energies of the char degradation and oxidation reactions are greatly lowered in presence of the filler, and the difference weight loss curve exhibits a small thermal destabilization at these temperatures confirming this effect.

It has been determined that ATH does not play a significant cooling effect during the thermal degradation of vulcanized EVM/ATH formulation. Its endothermal effect is thus overestimated in the flame retardant mechanism of ATH reported in the literature. It has been proposed that the ATH mode of action consists in the creation of a protective alumina structure during combustion. To confirm this suspected effect, the structure of the material is studied during combustion in addition to the analyses done on materials prepared by heat treatment.

3.3 Investigation of the structure of the residues in fire conditions

To reproduce fire scenario conditions, the formulation flame retarded with ATH was submitted to mass loss calorimeter experiments at an external heat flux of 35 kW/m² (corresponding to a mild fire). The combustion residues are collected at characteristic times, as reported in *Fig. 107*: just before the ignition of the material at 250 s, at the peak of RHR (PRHR) (350 s) and at the end of the combustion at 1100 s.

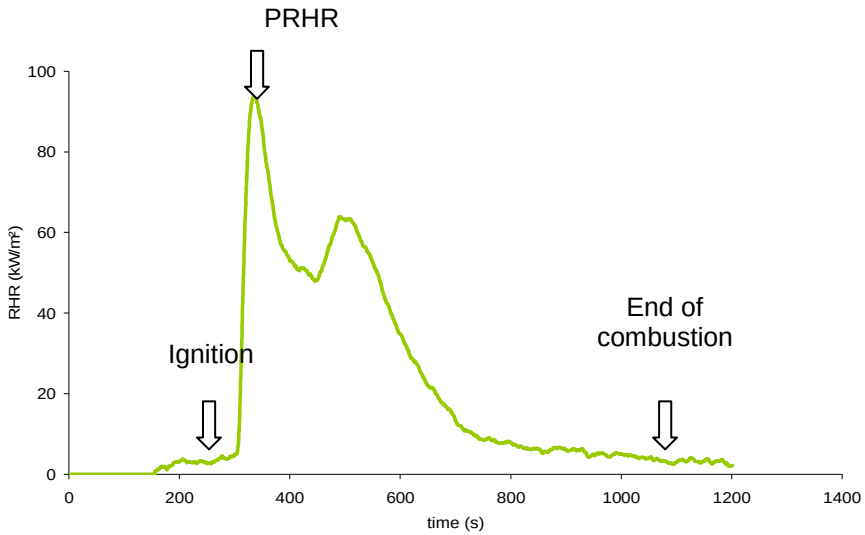


Fig. 107: RHR curve of the vulcanized EVM/ATH formulation

The obtained residues are pictured in *Fig. 108*. Just before ignition the material exhibits a “bubbled” dark skin covering the yellow/brown polymeric sample. At the PRHR, the formulation presents a layered structure: at the top a dark thin cracked layer is observed, and under this structure some polymer remains unburnt. At the end of the combustion, the material still exhibits a layered aspect, but the residue seems highly mineral, as suggested by its white colour.

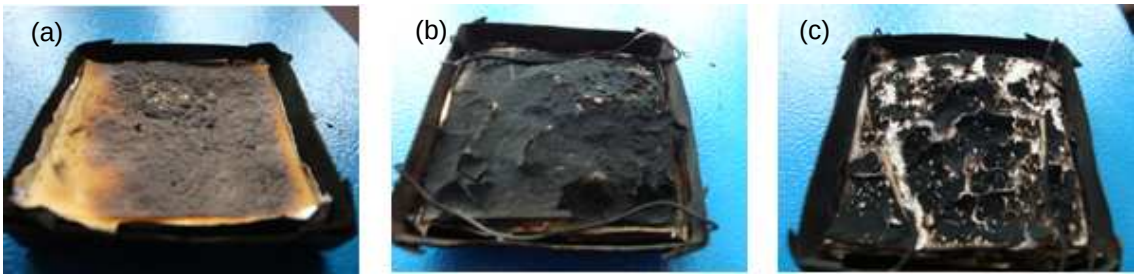


Fig. 108: Mass loss calorimeter residues of vulcanized EVM/ATH collected before ignition (a), at PRHR (b) and at the end of combustion(c)

^{27}Al solid state NMR (which was preferred for the study of the thermal degradation of the materials) does not allow distinguishing the different degradation products of gibbsite (in particular the formation of boehmite). So, to characterize the combustion residues its use was avoided. XRD presents the advantage to investigate the structure of a material, to allow more precise identifications of the crystalline phases (when the material is not amorphous) and to be a rapid technique. The residues were thus analyzed through XRD. The results are presented in *Fig. 109*. The identification of the crystalline phases was performed with the Powder Diffraction File (PDF) 2008 database (International Centre for Diffraction Data (ICDD), Philadelphia)**.**

The diffractogram corresponding to the material collected before ignition exhibits some characteristic peaks at 13, 14, 18, 20 37, 38 and 47°. They reveal the presence of ATH in a gibbsite form. Boehmite (peaks at 14, 28, 29, 38, 49 and 64°) is also detec table.

At the PRHR, the crystalline phases of the sample are modified. Three types of compounds are detected: alumina Al_2O_3 (hexagonal) with the peaks at 18, 32, 37, 46, 46 and 67°, boehmite and aluminium oxide hydrate with the signals at 14, 28, 38, 46, 49, 52, 55, 60°. This hydrated compound is supposed to be due not to the ATH dehydration but to the partial rehydration during the cooling of the residue. The last residue, at the end of combustion, contains tetragonal aluminium oxide.

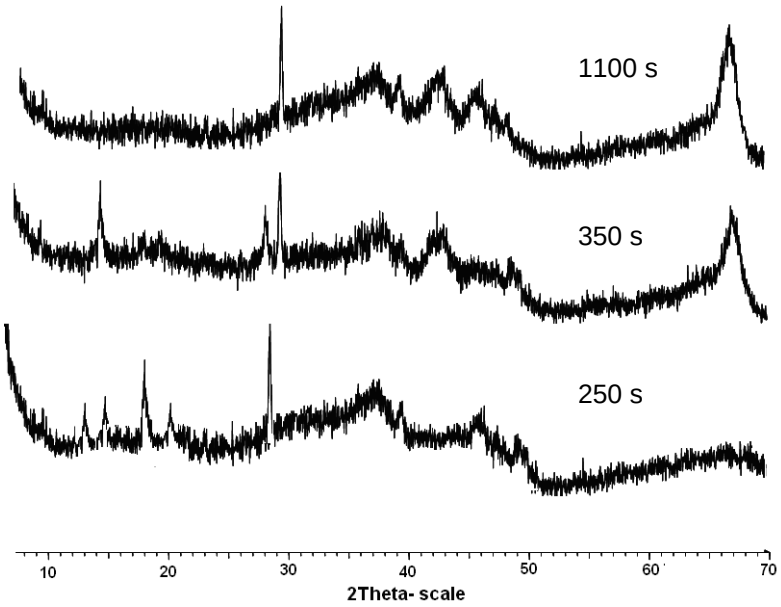


Fig. 109: XRD diffractograms of vulcanized EVM-ATH combustion residues (from bottom to top: before ignition, at PRHR, end of combustion)

The kinetic analysis showed that the ATH "cooling effect" resulting from its endothermal dehydration does not influence the degradation of the polymer. Thus, the fact that we obtain hydrated alumina forms (boehmite) at the PRHR is greatly surprising. This suggests that the cooling effect may be implied in the flame retardant mechanism of ATH. Nevertheless, the temperatures reached during combustion (before the PRHR) are significantly above that of ATH dehydration (the surface temperature before ignition, measured by infra-red camera, reaches 300℃), so that the probability of the presence of hydrated alumina is low. The explanation we propose to explain this phenomenon (and the difference between the TGA results and the fire conditions) is based on the difficulty for the water steam to evolve from the sample plate during combustion. Indeed, at the surface of the sample the ATH particles can evolve rapidly the dehydration water (some little bubbles are formed at the surface and beak, releasing the gas), but in the three-dimension network of the cured polymer, the gaseous evolution is more difficult, and some water can be trapped in the polymer. Then during the cooling of the collected sample some rehydration of alumina (with an activation energy of 130-190 kJ/mol [169], in the same range as that of dehydration) can occur. This phenomenon does not occur in TGA measurements, since with this technique mass transfers are neglected.

Concerning the hypothesis of the formation of a protective alumina structure, it was investigated by SEM. The residue at the PRHR cannot be analyzed because of the overload of the electron beam, but we can reasonably assume that the structure formed at PRHR is identical to that remaining at the end of combustion.

Fig. 110 and *Fig. 111* show the structure of the combustion residues of the formulation at different magnifications. It appears that the ATH particles lead to the formation of a macroscopic layered residue. The traces of some "bubbles" are also noticeable (highlighted by the red circles), confirming our hypothesis about the trapped dehydration water. The images at higher magnification show the inner structure of the macroscopic layers *(a)*. It appears that the alumina structure is cohesive since

the platelets are stacked to each other and unidirectionally oriented, as confirmed by the SEM image at higher magnification *(b)*.

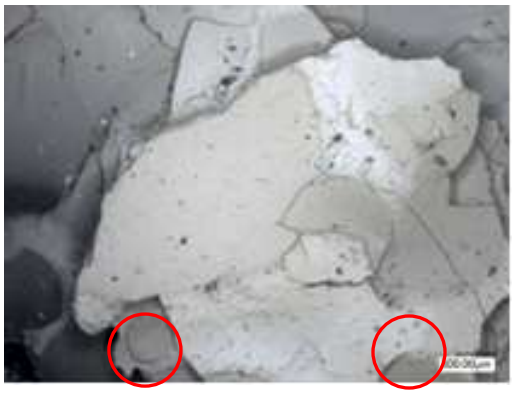


Fig. 110 : SEM image of the combustion residue of vulcanized EVM containing Apyral 120E (at low magnification)

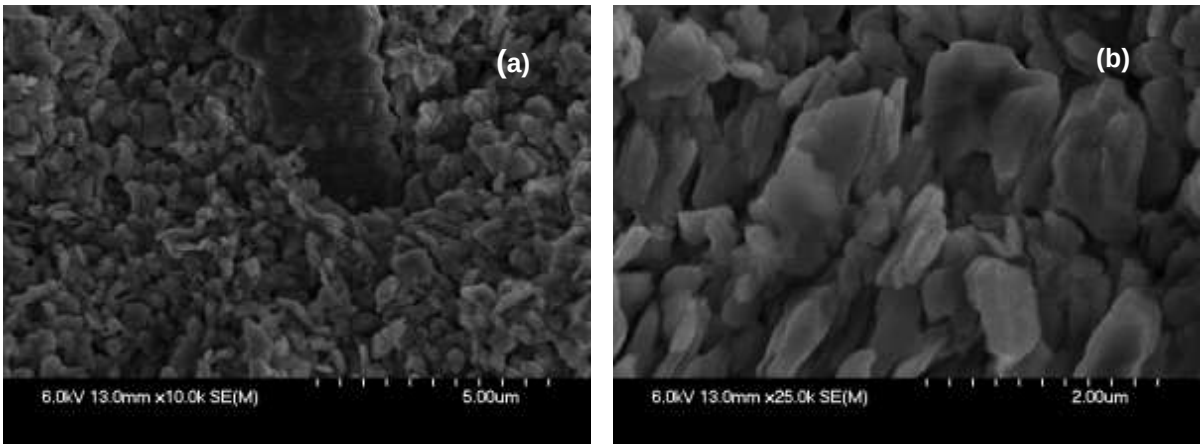


Fig. 111 : SEM image of the combustion residue of vulcanized EVM containing Apyral 120E (a) and at higher magnification (b)

During combustion, the gibbsite forms successively in the sample boehmite and aluminium oxide (hexagonal), for a final residue of tetragonal aluminium oxide. It appears that the dehydration “cooling effect”, which was not predominant in the TG measurements, plays a role in terms of time to ignition (the water release dilutes the flame and thus prevents ignition). The fact that some hydrated species remain at the PRHR is attributed to water trapped into the cured polymer (and into the alumina structure) rehydrating alumina during the cooling of the sample. In terms of flame retardancy, this continuous release of water is not sufficient to stop the flame feeding, but can slightly diminish the heat transfers.

The observation of the combustion residue also leads to think that a cohesive alumina structure is formed, protecting the polymer and slowing down its degradation. This hypothesis proposed through the investigation of the thermal decomposition of the material is confirmed in a fire scenario.

4. Conclusion

The aim of this chapter was to elucidate the flame retardant mechanisms of ATH in vulcanized EVM, since it has never been investigated in cured EVM matrix. To achieve this goal, this work proposed a novel approach based on the kinetic study of the thermal degradation of the materials to determine the flame retardant role of ATH.

To understand the mode of action of the mineral filler, the thermal degradation of the pure and flame retarded polymer was investigated in oxidative and in inert conditions. The degradation mechanism of vulcanized EVM was fully characterized, and the influence of the curing and of the degradation atmosphere was discussed.
It was determined that the influence of ATH on the polymer degradation is mainly due to condensed phase action: acid-base Lewis reactions with the released acetic acid, preventing the autocatalysis of deacetylation, the formation of a protective structure and an oxidation catalytic effect on the char. The supposed “endothermal effect” of ATH in the polymer is only slightly observed.

The investigations on the structure of vulcanized EVM flame retarded with ATH in fire conditions moderates the previous results. The cooling effect of ATH, neglected in TGA, is suspected in fire conditions since hydrated alumina species are detected in the PRHR residue. Concerning the protective alumina structure, its formation has been confirmed. The supposed flame retardant “barrier effect” of ATH is demonstrated.

The optimal formulation developed in the previous chapter is flame retarded with an ATH-phosphinate combination. The flame retardant mechanism of action of ATH was fully determined. To have a complete understanding of the mode of action of the ATH-phosphinate combination, it is now necessary to investigate the potential interactions between the flame retardant additives and between the combination and the polymeric matrix. This is the objective of the next chapter.

CHAPTER 5 –FLAME RETARDANCY MECHANISM OF OP1230 AND ATH-OP1230 IN EVM

The industrial challenge has been achieved: developing a flame retarded formulation with lower hardness than the commercial RPW formulation and presenting high mechanical properties (see chapter 3). The FR combination involving aluminium trihydroxide (ATH) and an aluminium diethyl phosphinate (OP1230), provides outstanding flame retardancy performances to the polymeric formulation.

The previous chapter, Chapter 4, was dedicated to the comprehensive aspect of the flame retardant effect of ATH in vulcanized EVM through the investigation of the thermal degradation of the pure and flame retarded materials. The present chapter aims to elucidate the synergism observed between ATH and OP1230 in vulcanized EVM. We will attempt to answer three main questions:

- Are there chemical interactions between the flame retardant additives?
- If there are some, are they responsible for the improvement of the observed synergistic effect?
- If there is no chemical interaction between ATH and OP1230, do the additives have a “physical“ effect on the fire retardancy mechanism, such as for example a modification of the protective effect of the barrier created when the material burns as previously described?

The first part of this chapter will try to give some clues about these questions. It consists in investigating the interactions between the flame retardant additives ATH and OP1230. The thermal degradation of the combination will be studied to determine the potential interactions in terms of chemical degradation pathway.

As a second step, the influence of the phosphinate alone and in combination with aluminium trihydroxide on the thermal degradation of vulcanized EVM will be determined. The modifications in the condensed phase as well as in the gas phase will be investigated.

The last part of the chapter comments the flame retardant synergism mechanisms between aluminium trihydrate and phosphinate ATH-OP1230 combination. The characterization of thermal degradation of the flame retarded materials and the chemical interactions occurring will allow discussing the flame retardant mechanism of OP1230 and the ATH-OP1230 combination. The morphology of the residue obtained by the simulation of a fire scenario will be discussed in order to elucidate the flame retardant properties of the materials.

1. Aluminium trihydroxide - phosphinate interactions

The flame retardant synergisms provided by additives combinations are generally explained in the literature by chemical [42, 60, 124] or physical interactions [123, 125] between the additives. The efficiency of the ATH-OP1230 combination in vulcanized EVM can thus be suspected to be due to a chemical interaction between the two compounds. This part of the chapter aims to study these potential interactions. For that, the thermal degradation of the combined compounds will be compared to that of the pure additives.

In this section, the thermal degradation of the materials will only be investigated in pyrolysis conditions. Indeed, the diethyl aluminium phosphinate OP1230 exhibits an unstable thermal degradation in air (see Braun *et al.*[170]) leading to unrepeatable measurements and which is not understood yet.

The characterization of the thermal degradation of ATH was presented in *Chapter 4* (see section 1.2.1). The degradation of ATH can be schemed by:

$$Al(OH)_3 \text{ (gibbsite)} \xrightarrow{20\text{-}200℃} AlOOH \text{ (boehmite, suspected)} + \text{gibbsite} \xrightarrow{200\text{-}225\ ℃} \text{amorphous } Al_2O_3 \xrightarrow{225\text{-}800\ ℃}$$

The next step now consists in investigating the thermal decomposition of the second additive of the combination, that is to say OP1230.

1.1 Thermal decomposition of OP1230

1.1.1 Thermogravimetric analysis of OP1230

Fig. 112 presents the thermogravimetric analysis of the aluminium diethyl phosphinate. The degradation of OP1230 occurs in a single step from 390 to 520 ℃ with a maximum degradation rate at 475 ℃, leading to a stable residue of 6.2 wt-%. The final residue appears to be a carbonaceous expanded material (visual observation in the pan after the experiment).

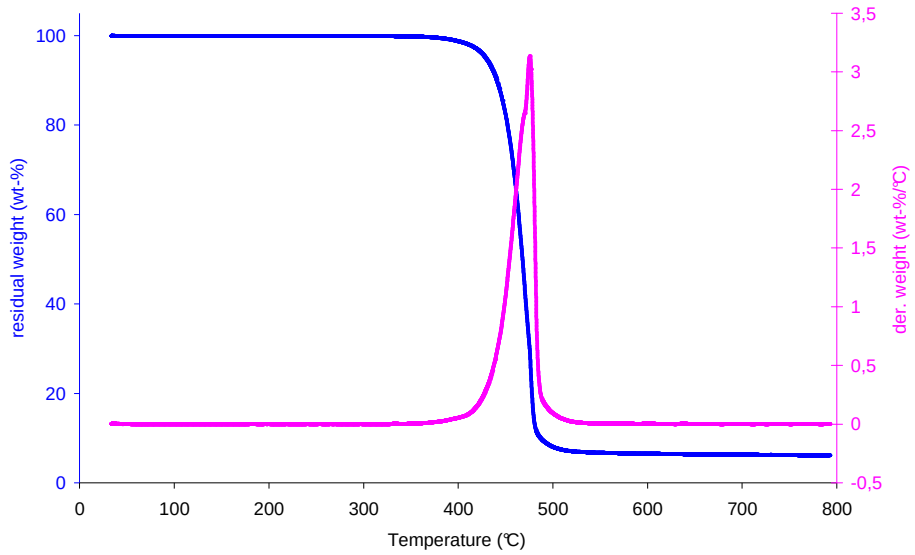


Fig. 112: TG and DTG curves of OP1230 (10°C/min in nitrogen)

The condensed phase resulting from the thermal decomposition of OP1230 was studied by Samyn et *al.* [123]. It was found that the aluminium phosphinate first degrades leading to the formation of some carbonaceous char and aluminophosphonate $Al_2(CH_3\text{-}CH_2\text{-}P(O)(O^-)_2)_3$ composed of octahedral aluminium and phosphonate groups ($CH_3\text{-}CH_2\text{-}P(O)(O^-)_2$). This aluminophosphonate decomposes in a transitory aluminium phosphonate with a penta-coordinated aluminium and then in an amorphous aluminophosphate $AlPO_4$. At 800°C, it only remains some char, and aluminop hosphates crystallize.

1.1.2 Crystallographic structure

The evolution of the crystallographic structure of OP1230 for different heat treatment temperatures was followed by XRD *(Fig. 113)*. The analyses were carried out on the residues after thermal treatments, not during the in-situ degradation.

The material at ambient temperature exhibits a crystalline structure characterized by peaks at 9, 19, 20, 21.5, 24, 25.5, 26.5, 27, 31.5 and 38°. The dif fractogram of the material heated at 350 °C shows the appearance of additional peaks at 17 and 34.5°, suggesting that the crystalline OP1230 form is slightly modified, or that additional species are created. Since, at this temperature, no mass loss on TGA was observed, the preferred hypothesis is the morphological modification.

Up to 425 °C, there is not any evidence about cryst allographic changes; the observed bands are not modified. After a thermal treatment at 500 °C, the residue becomes amorphous, and its diffractogram exhibits a broad band between 20 and 30° suggesting the formation of pre-graphitic carbon [171]. This is consistent with the previously described char formation. At 800 °C a crystalline phase appears, attributed to the formation of aluminophosphates (source: Powder Diffraction File 2008).

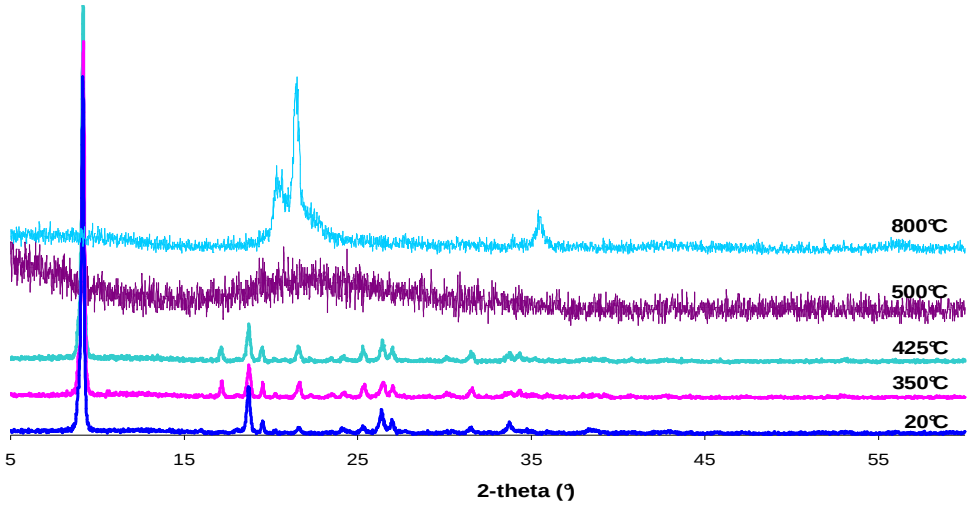


Fig. 113:XRD diffractograms of the degradation residues of OP1230 vs. temperature [123]

1.1.3 Evolved gases

To complete the characterization of the reported degradation of OP1230, it is necessary to get more information about the gas phase. That is why we investigated by TGA-GCMS the nature of the gases evolved during the thermal decomposition of OP1230 at 10 ℃/min in inert atmosphere (in Argon).
The analyses *(Fig. 114)* revealed that aluminium diethyl phosphinate emits ethene, but-2-ene, some carbon dioxide, phosphine PH_3, ethyl phosphonate ($OOP(C_2H_5)O$-) and phosphinate.

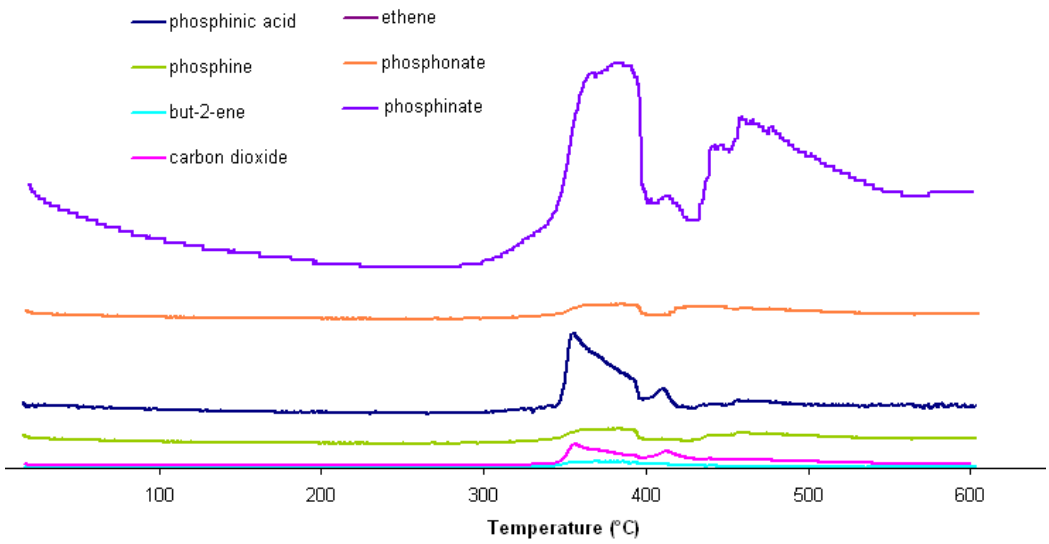


Fig. 114: Evolution of released gaseous compounds

1.1.4 Degradation mechanism

According to the collected information about the gas phase and the condensed phase and to previous work of our laboratory, it is possible to draw a global scheme of the phosphinate degradation *(Fig. 115)*.

The aluminium phosphinate first degrades leading to the formation of aluminophosphonate $Al_2(CH_3\text{-}CH_2\text{-}P(O)(O^-)_2)_3$ and releasing in the gas phase ethene and but-2-ene resulting from the degradation of the organic part of the phosphinate, and also carbon dioxide and diethylphosphinic acid. The aluminophosphonate thus degrades into transitory aluminium phosphonate with a penta-coordinated aluminium, amorphous aluminophosphate and some char, while in addition to the previously cited products ethyl phosphonate and phosphine are released as gaseous products. At the end of the degradation it only remains crystallized aluminophosphate and some char.

It is noteworthy that the increase of the oxidation state of the phosphorous compounds in the condensed phase and the oxidation into carbon dioxide of carbonaceous parts (phenomena which are quite surprising in inert atmosphere) is compensated by the reduction of some species into phosphine.

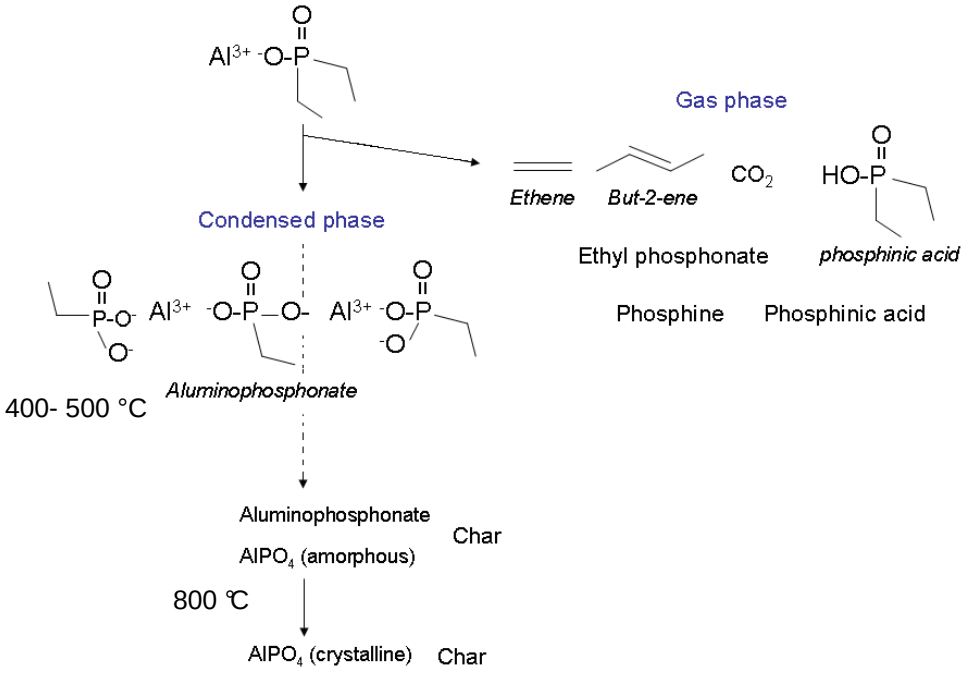


Fig. 115:OP1230 degradation scheme

The thermal decomposition of the pure additives is clearly defined. It appears that ATH entirely degrades 150 °C before OP1230. Chemical interactions can be suspected between the formed amorphous alumina and the phosphorous-based compounds evolved when OP1230 degrades because of previous work reporting the adsorption binding of phosphonic acids on alumina and its hydrated forms (boehmite) [172-174]. This phenomenon can be extended for phosphinate and some of its degradation products [175], and it can thus be assumed that the adsorption could lead to a modification of the degradation of the phosphorous compounds. The next step of this study is, as a consequence, dedicated to the investigation of the thermal decomposition of the flame retardant combination, in order to detect some modifications in the degradation pathway or in the decomposition temperatures.

1.2 Thermal degradation of the ATH-OP1230 combination

The first step we have followed in order to identify potential interactions between aluminium trihydroxide and the diethyl aluminium phosphinate consists in the determination of the characteristic degradation temperatures of the mixture ATH/OP1230 by using TGA. In a second step, the intermediate degradation residues, obtained after heat treatment at those defined temperatures, will be analyzed.

It was previously demonstrated that the 2:1 ratio was the best compromise between a preserved mechanical behaviour and increased flame retardant properties. However, in order to highlight the potential chemical interactions between the two additives, the chosen study was carried out with a ratio for the combination of 1:1.

1.2.1 Thermogravimetric analysis of ATH/OP1230 mixture

TG curves (experimental and calculated) as well as the difference weight loss curve of the ATH-OP1230 combination at a 1:1 ratio are presented in *Fig. 116*. It appears that the flame retardant combination degrades into two steps. The first step from 200 to 300 ℃ exhibits a mass loss of 16 wt-% corresponding to the ATH dehydration. Indeed, ATH degrades into alumina leading with a mass loss of 34.6 wt-% (see *Chapter 4* section 1.2) since the combination contains 50 wt-% ATH the mass loss is of 0.5 x 0.346 = 17.3 wt-%. The observed difference (1.3 wt-%) is comprised in the experimental margin of error. The second degradation step from 400 to 500 ℃, where OP1230 decomposes, leads to a 47 wt-% mass loss. This is consistent with the expected value of 46.9 wt-% (OP1230 losses 93.8 wt-% during its degradation, since the combination contains 50 wt-% of phosphinate the mass loss reaches theoretically 0.5 x 93.8 = 46.9 wt-%).

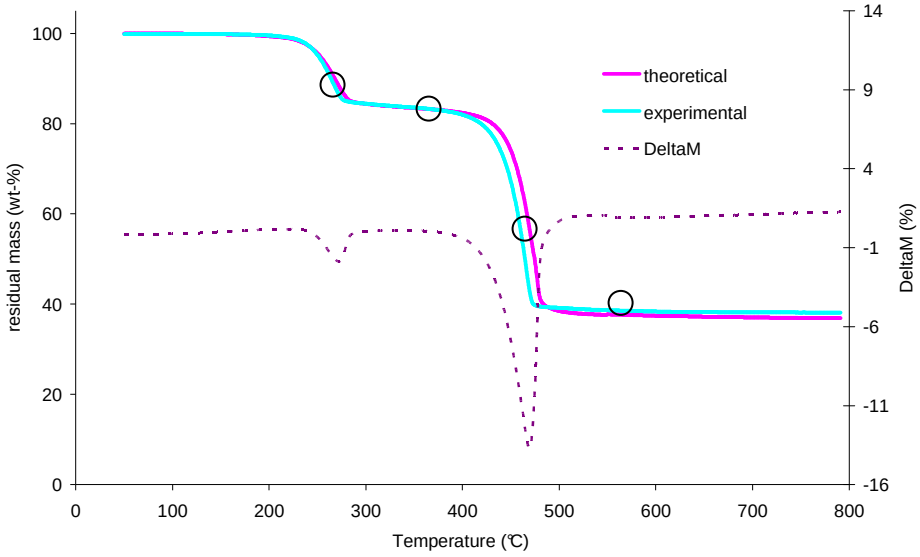


Fig. 116: Experimental and calculated TG curves as well as difference weight loss curves of the ATH-OP1230 combination (10℃/min, in nitrogen)

It is noteworthy that the experimental degradation curve and the calculated one are very close to each other. Nevertheless the difference weight loss curve shows a significant thermal destabilization (13 %) around 475 ℃. It suggests that it would be an inte raction between the additives. It was thus decided to characterize the residues of the thermal degradation of the combination of additives in order to characterize this interaction. The characteristic temperatures chosen for the thermal treatments are 250℃ corresponding to the first degradation step, 350 ℃ (between step one and two), 450 ℃ for the second step and 550 ℃ to obtain a fully degraded m aterial. The treatment temperatures are symbolized by the black circles in *Fig. 116*.

The pictures of the residues obtained after the thermal treatments under nitrogen are presented in *Fig. 117*. There is no significant modification in the aspect of the material. At room temperature, the mixture is a white fine powder, which remains white up to 450 ℃ where it becomes greyish, probably because of the degradation of the organic part of OP1230. It was expected a black residue, since OP1230 at these temperatures starts producing a char. On the contrary to OP1230, we do not observe any charring of the OP1230-ATH combination.

It is noticeable that there are some differences between the expected mass loss and that observed after thermal treatments (differences due to heat and mass transfer effects). It is considered that if the experimental mass loss is in the range of the selected degradation step (for example the second step leads to a mass loss between 18 and 61 wt-%, the experimental data has to be comprised within these values) the heat treatment is appropriate for our approach .

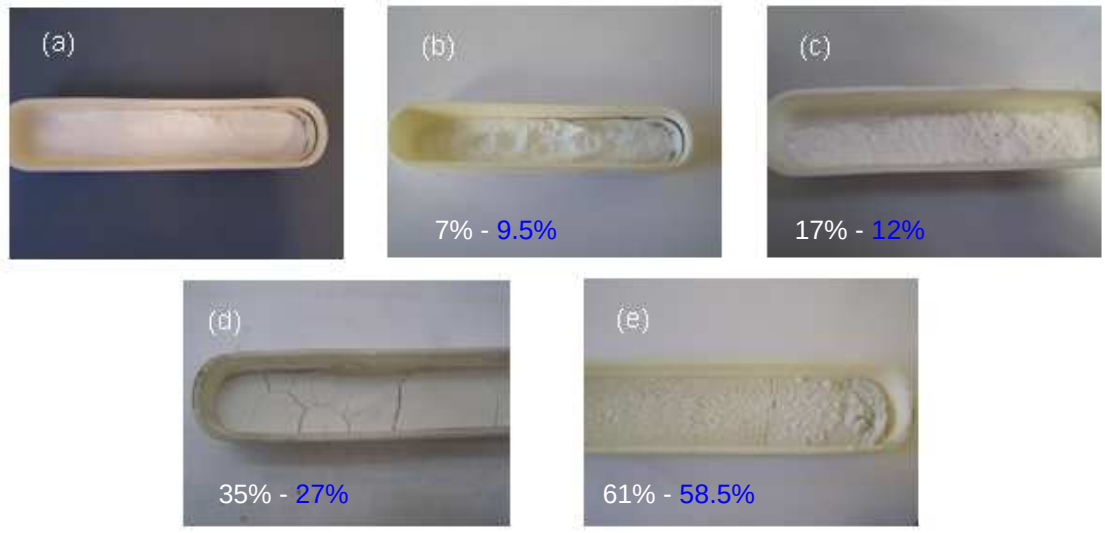


Fig. 117: : Pictures of the thermal treatment residues of the ATH-OP1230 combination (1:1) at 20 ℃ (a), 250 ℃ (b), 350 ℃ (c), 450 ℃ (d) and 550 ℃ (e) - in whi te: expected mass loss (according to the TGA), in blue: experimental mass loss

The obtained residues are then characterized using different adapted tools to point out the presence (or the absence) of interactions between the two compounds.

1.2.2 Evolution of the crystallographic structure

The first investigations are dedicated to the crystallographic structure of the additives combination during its degradation. The evolution of the crystallographic structure could provide some additional information about the chemical evolution of the ATH/OP1230 mixture. If there is no interaction, according to the evolution of the pure additives during their thermal decomposition, it is expected to obtain an amorphous phase of alumina *(Fig.15* in *Chapter 4)* and a crystalline phase of aluminium phosphate *(Fig. 113)* at high temperature.

The XRD diffractograms of the flame retardant mixture versus temperatures are pictured in *Fig. 118*. It appears that the non-heated material exhibits a crystalline structure, composed of gibbsite (depicted as red arrows) and crystallized OP1230 (blue arrows). The bands at 38, 44 and 65 °correspond to the sample holder (of gold), symbolized with green arrows.
There are not any changes up to 175 °C where the peaks corresponding to gibbsite structure (18°, 20.5°, between 26.5 and 28.5°, 36.5°, between 39 and 41.5°, between 44 and 47.5°, 50.5°, 52°, 54° and between 63.5 and 68°) decrease while the intensity of some bands linked to the OP1230 crystals increases. It is noteworthy that several bands related to the phosphinate disappear beyond this temperature, suggesting another crystallographic modification which was not detected during the degradation of the pure additive. It is thus suspected that during the dehydration of ATH some interaction occurs between the metal hydroxide and the phosphinate, leading to a crystallographic modification. The ATH gibbsite form completely disappears at 250 °C.

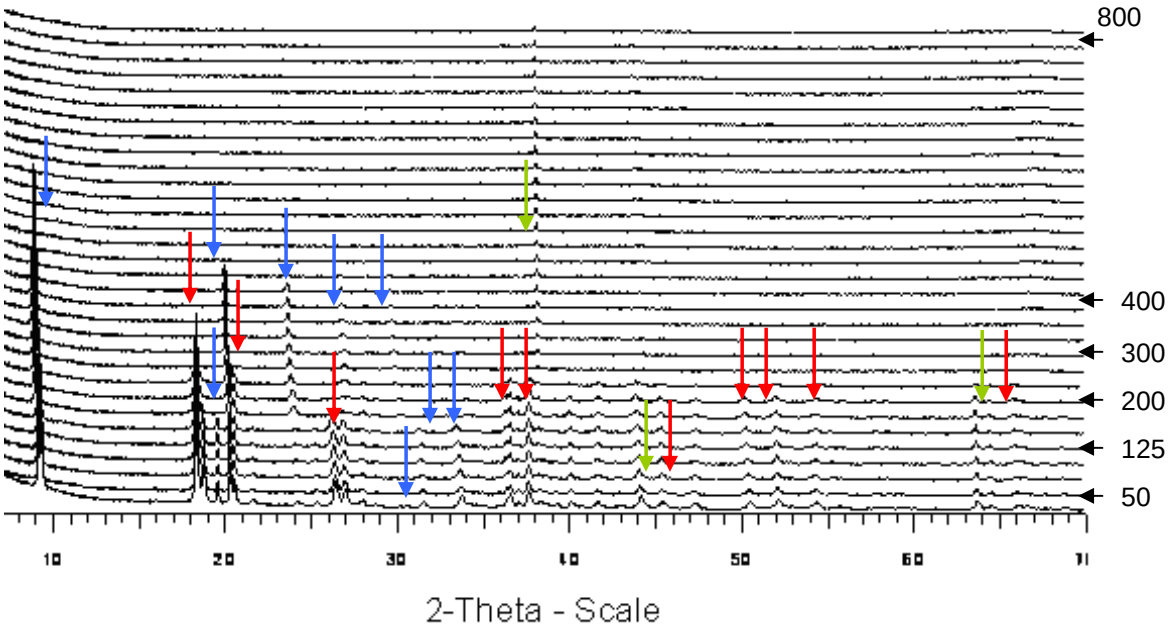


Fig. 118: High-temperature XRD of the ATH-OP1230 combination (from 50 to 800 °C, a diffractogram is collected every 25 °C)

From 250 to 400 °C, the diffractograms remain identical, exhibiting the remaining small peaks related to crystalline OP1230. Beyond this temperature, no signal can be detected, except one from the gold

holder (38°). This indicates that the heated material becomes totally amorphous, and the glass formed thereof covers the sample holder, thus diminishing or eliminating its signals.

The evolution of the crystallographic morphology of the combination during the pyrolitic degradation suggests that some interactions occur, since the crystalline structure of OP1230 is modified after the ATH dehydration, in a different way from that observed for pure OP1230 (XRD signals are not the same). Moreover, the crystalline aluminophosphate expected from the thermal degradation of OP1230 is not formed during the combination thermal decomposition. Since the heated material is amorphous after 400 °C, the XRD analyses did not provide enough information to characterize the intermediate compounds formed during the degradation of the mixture (such as amorphous aluminophosphates). It was then decided to further investigate the chemistry of the heat treatment residues using adapted spectroscopic tools to identify the potential interactions.

1.2.2 Analysis of the residues

The residues of thermal treatment of the combination, as they contain aluminium and phosphorus, were analyzed through MAS ^{27}Al and dipolar-decoupling MAS ^{31}P solid state NMR. The investigations on the carbon element were not performed because of the too low quantity of carbonaceous residue formed during the thermal degradation of the ATH-OP1230.

The spectra obtained through ^{27}Al NMR are gathered in *Fig. 119*. The untreated sample generates three signals at -12, -3.2 and 7.9 ppm. The peaks at 7.9 and -3.2 ppm were previously attributed in *Chapter 4* to the presence of aluminium trihydroxide. The first one corresponds to the single octahedral resonance of aluminium in a gibbsite structure [176]; the second one is related to the resonance of extra-framework aluminium in octahedral coordination [146]. Concerning the signal at -12 ppm, it characterizes cationic Al^{3+} in octahedral coordination with phosphorus atoms in their second coordination sphere [177], and is thus assigned to the aluminium phosphinate.

The sample heated at 250 °C exhibits a similar spectrum to that of the untreated material, but 100 °C higher (350 °C), the signal of the octahedral aluminium site of gibbsite at 7.9 ppm decreases while an additional peak appears around 65 ppm. The appearance of this tetrahedral aluminium is a consequence of the elimination of structural water in alumina trihydroxide with the formation of a close-packed oxygen lattice in which some of the tetrahedral interstices are occupied by Al [178]. Concerning the peak at 7.9 ppm, it is not possible to distinguish if it corresponds to boehmite (γ-AlOOH) or to octahedral Al in alumina, or to aluminophosphate (expected around 10 ppm). It is noteworthy that the signals linked to dehydrated ATH are very broad. This is consistent with the amorphization of the material, as revealed by the XRD analyses.

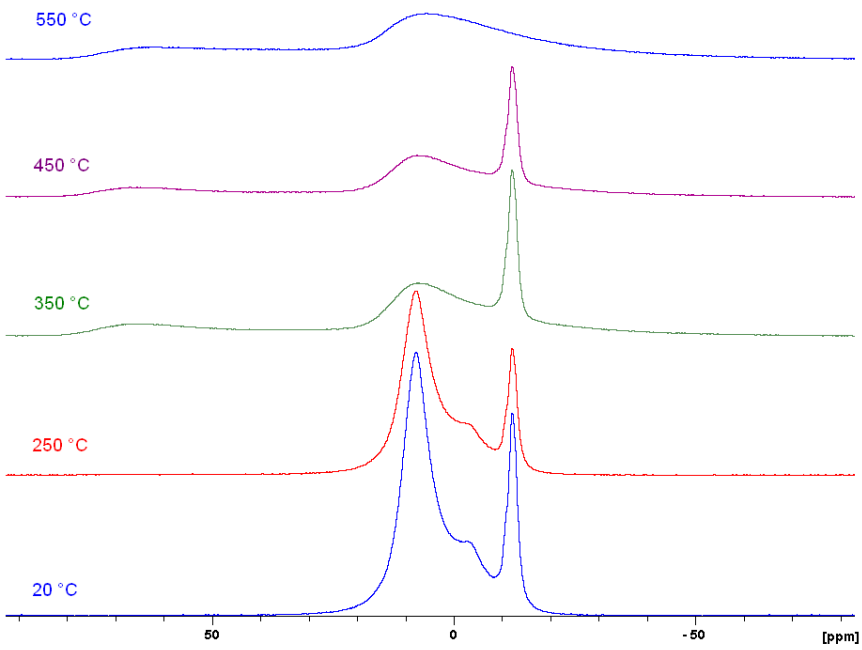


Fig. 119: ^{27}Al MAS NMR spectra of the thermal degradation residues of the ATH-OP1230 combination (degradation in nitrogen) at various heat treatment temperatures

The observed spectrum is the same for the material treated at 450 ℃, but some changes are noticeable for the last part of the degradation (550 ℃). The spectrum shows no peak at -12 ppm, indicating that the degradation of the phosphinate compound has occurred. The two broad bands at 7.9 and 67 ppm are still detectable. To ensure that the quadrupolar broadening of these signals (characterized by an asymmetric widening) does not hide any additional band the same NMR analysis was performed at higher magnetic field (18.8T vs. 9.4T) to reduce induced quadrupolar effects and to increase the peak resolution. The obtained spectrum is reported in *Fig. 120*. It appears that there is no signal hidden by the peak broadening at 10 ppm, but at 35 ppm an additional band is revealed. This signal is characteristic from penta-coordinated aluminium, in particular from AlO_4 entities in an aluminophosphate structure. These AlO_4 unities are generally observed at higher chemical shifts, but they are shielded because of the connectivity with phosphorous (shift toward the lower fields) [179].

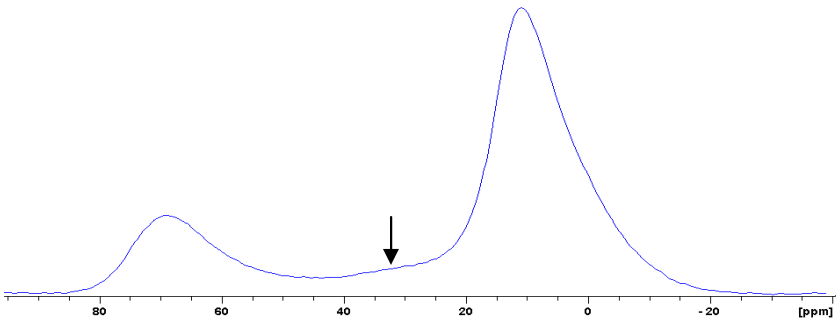


Fig. 120: ^{27}Al MAS NMR spectra (800MHz) of the thermal degradation residue of the ATH-OP1230 collected after a heat treatment carried out at 550℃

To confirm the presence of this third signal the simulation of the spectrum was done using Dmfit software [180]. The resulting calculations, depicted in *Fig. 121*, confirm that we have three aluminium sites at 71, 14.5 and 46 ppm.

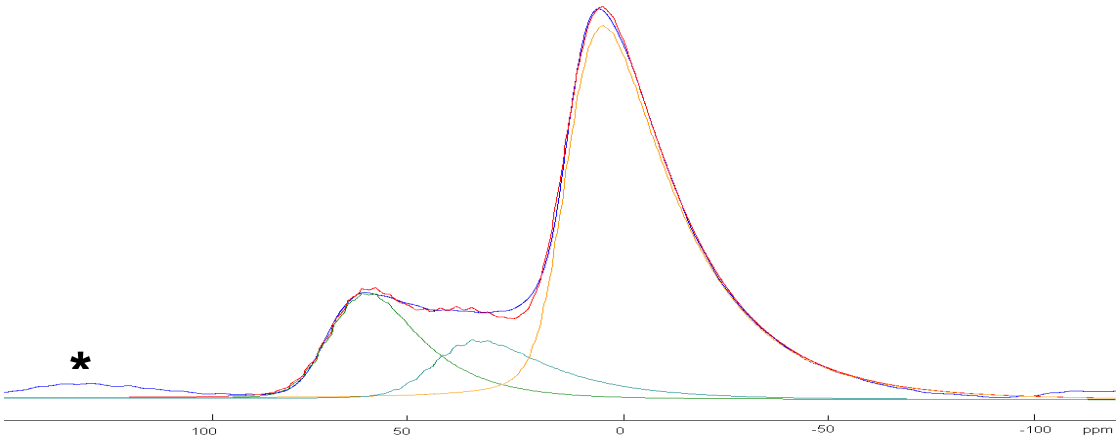


Fig. 121: Experimental ^{27}Al spectrum at 550°C (in blue) and simulated one (in red); * = spinning sideband

It is noteworthy that the expected signals at 6 and -20 ppm reported by Samyn [123] for the degraded pure phosphinate at 500 °C are not present on the spectrum. They respectively correspond to octahedral alumina (AlO_6) connected by Al-O-P bridges (aluminophosphonate) and the same AlO_6 entities with incomplete second coordination sphere. It is thus possible to conclude that the formed species are different for the degradation of pure OP1230 and for OP1230 mixed with ATH. This hypothesis will be then investigated by the analysis of the phosphorous species.

The evolution of the ^{31}P spectrum of the ATH-OP1230 combination versus heat treatment temperature is presented in *Fig. 122*.

The spectrum of the untreated mixture exhibits two narrow peaks at 41.3 and 43 ppm respectively. These signals correspond to phosphorus sites in phosphinate compounds (CH_3-CH_2-P(O)-O^-) [181]. They are detected at higher chemical shifts than expected because of the deshielding effect induced by the connectivity of the phosphinate with the Al^{3+} cation [182]. It is noticeable that the intensity of the two peaks varies between 250 and 350 °C (the respective intensities are inversed). These two bands are assumed to correspond to two crystalline forms of OP1230. Between 20 and 350 °C, the crystalline structure of OP1230 is modified, as noticed on the XRD diffractograms in *Fig. 113*. Thus it can be suspected that this modification implies the growth of a type of crystallite, at the detriment of the other form: the peaks intensities are then different.

The degradation of the phosphorous compound begins after 450 °C. Up to this temperature, the spectra of the degradation residues are identical. Beyond this temperature, the signals at 41.3 and 43 ppm disappear, replaced by two bands centred on 17 ppm (very low intensity) and -15.5 ppm. The broad signal at -15.5 ppm could be the overlap of several. This is confirmed by the Dmfit simulation *(Fig. 123)* where four sites at -10.9, -18.7, -25 and -30 ppm are necessary to obtain a good agreement between calculated and experimental signals. This broadening can result from the distribution of several phosphorous species in a glassy structure. This is in correlation with the XRD analyses

showing an amorphous structure of the residues. On the other hand, the signals between -10 and -30 ppm are characteristic of tetrahedral phosphates connected to aluminium centres [183]. However, it is not possible to go further in more specific assignments to the diverse P environments: complementary investigations are needed.

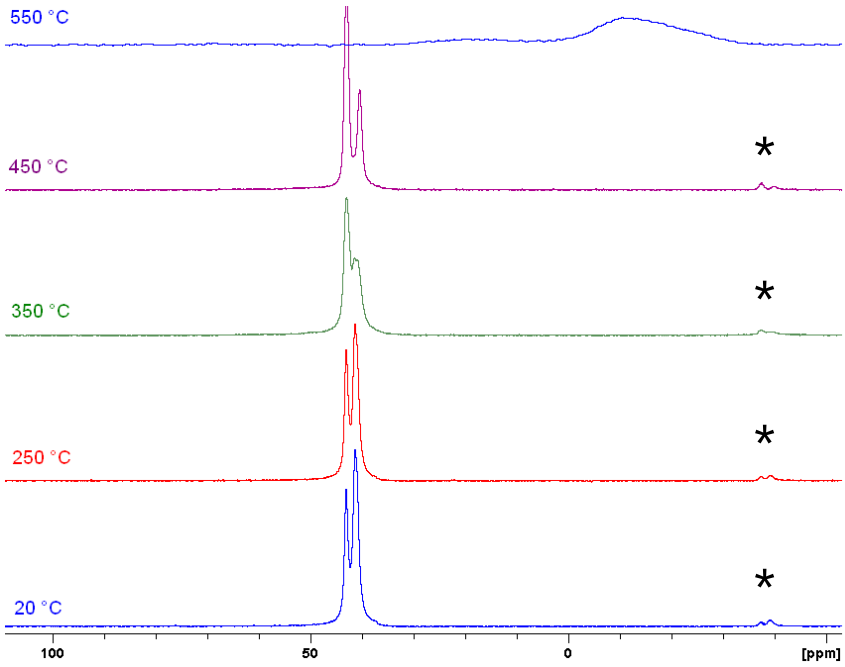


Fig. 122: ^{31}P DD- MAS NMR spectra of the thermal degradation residues of the ATH-OP1230 combination (degradation in nitrogen) for different heat treatment temperature; *= spinning sideband

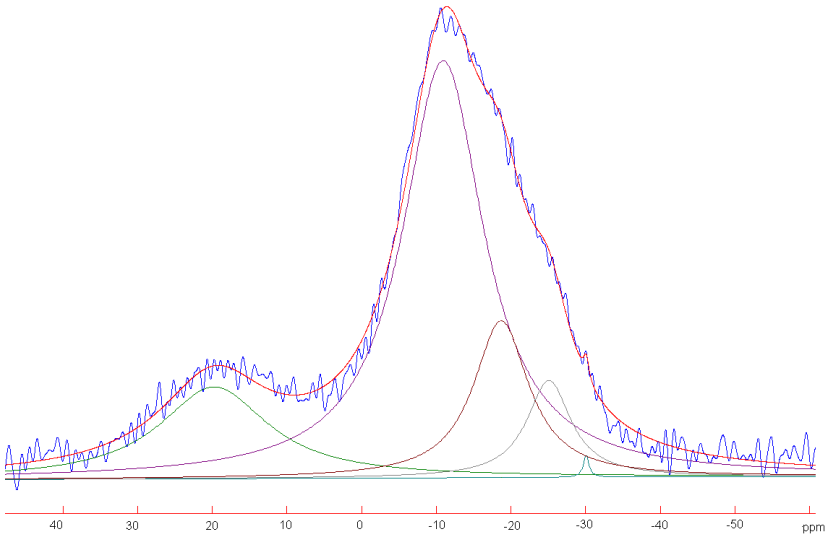


Fig. 123: Experimental ^{31}P spectrum at 550℃ (in blue) and simulated one (in red)

It appears that the degradation of the phosphinate results in the production of phosphonates since the peak at 17 ppm can be reasonably attributed to this specie [184]. However, since the aluminium signals do not exhibit the peaks of aluminophosphonate (-6 and -20 ppm), the hypothesis of the formation of diethyl phosphonic acid seems more reasonable. Pyrophosphates can be also assumed

since they produce a signal around -10 ppm [139]. Two peaks in the zone of 17 and -25 ppm, respectively attributed to aluminium phosphonate and aluminophosphate, were also observed by Samyn when studying the thermal degradation of pure OP1230 under nitrogen.

The degradation of the phosphinate-ATH mixture is assumed to provide alumina and aluminium phosphates and phosphonic acid, but the composition of the final degradation residue is not fully established, since the attributions of the signals between -10 and -30 ppm on the ^{31}P spectrum are not clearly defined.

In order to go further into those investigations, 2D MAS-NMR D-HMQC (Dipolar Heteronuclear Multiple Quantum Coherence) sequence was performed on the collected residue of the ATH/OP1230 after a heat treatment at 550℃. Those data reveal the correlation signals between spatially close atoms *(Fig. 124)*.

The spatial correlation between phosphorus and aluminium nuclei reveals that the aluminium signals (tetra, penta and octahedral sites) are corellated to the phosphorous signals located at -10 and -30 ppm. The correlation between octahedral aluminium sites (10 ppm) and these phosphorous sites are particularly intense, suggesting that this signal is linked to aluminophosphates. In that structure the phosphates are constituted of tetrahedral phosphorus surronded by four aluminium second nearest neighbour ($P(OAl)_4$ sites) [179]. It is interesting to note that the ^{31}P signals betweens -10 and -30 ppm also exhibits correlation with tetrahedral ^{27}Al peaks (peak at around 65 ppm). This indicates the co-presence of AlO_4 and AlO_6 species. There must be at least two Al atomes in the phosphorus second coordination sphere, one tetrahedral and one octahedral aluminium [185]. These coordinations of the phosphorus sites (with AlO_6 and AlO_4 entities) are consistent with the chemical shifts of the resoning nuclei [179].

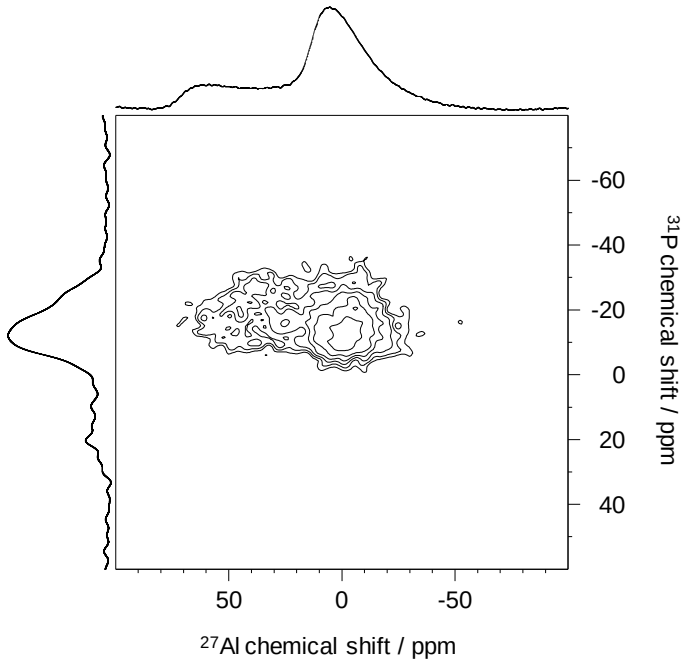


Fig. 124: 2D MAS-NMR $^{27}Al(^{31}P)$D-HMQC spectrum of the ATH-OP1230 mixture after heat treatment carried out at 550 ℃ under nitrogen

All aluminium sites are connected to phosphorous nuclei, but the phosphorous sites generating the signal at 17 ppm on the ^{31}P spectrum (previously attributed to aluminium phosphonates) have no aluminium in their neighborhood: this indicates that this signal does not correspond to aluminium phosphonates. It can thus be proposed that the band at 17ppm because of its specific chemical shift could be attributed to ethyl phosphonic acid [186].

In order to confirm this hypothesis, ^{1}H MAS experiments were performed on the sample heat treated at 550 °C (3.2 mm probe, MAS = 24 kHz). Note it was done at high MAS in order to remove (at least partially) 1H-1H homonuclear interactions leading to the broadening of the bands. The obtained spectrum is depicted in *Fig. 125*. The spectrum reveals that the material still contains protons but the signal is quite complex. The bands between 1 and 3 ppm can be related to proton belonging to alkyl compounds while the broad signal at 5.5 ppm can be attributed to P-OH groups [185]. The signals on the spectrum thus tend to validate our hypothesis since they are compatible with the presence of organic phosphonic acid.

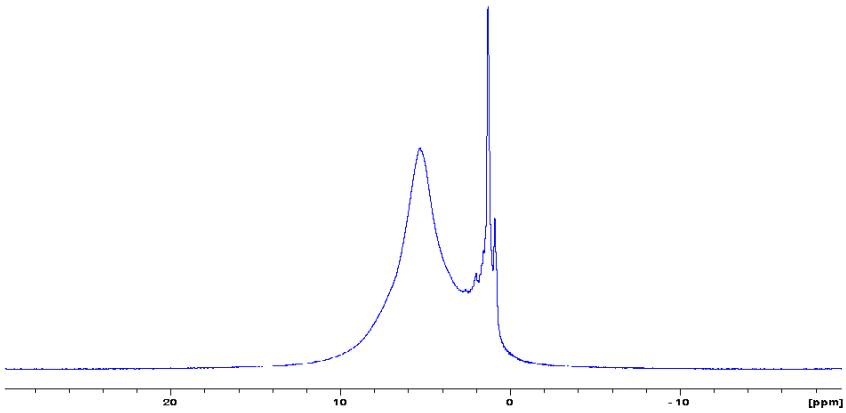


Fig. 125:^{1}H MAS-NMR spectrum of the ATH-OP1230 mixture heat treated at 550 °C (800MHz)

So, it is assumed that the ATH-OP1230 mixture degrades into aluminophosphates (tetrahedral phosphorus sites with AlO_6 entities and Q_0 sites with AlO_6 and AlO_4 entities in their second coordination sphere) and some organic phosphonic acid (most probably ethyl phosphonic acid).

1.2.4 Gas phase analysis

In addition to the characterization of the condensed phase, the gas phase analysis was performed using TGA-FTIR.

The FTIR spectra versus time of the gases evolved during the TGA of the mixture ATH/OP1230 in nitrogen are presented in *Fig. 126*. The degradation begins at 25 min (corresponding to a temperature of 250 °C) and ends at 75 min (corresponding to a temperature of 750 °C). At the beginning of the pyrolysis, some broad peaks appear between 3400 and 3600 cm^{-1} and between 1300 and 1600 cm^{-1}. No additional peak appears up to 40 minutes where the previously cited signals disappear, replaced

by signals of low intensity at 2940 cm^{-1} and 1100-1200 cm^{-1}. At the end of the degradation very intense peaks are noticeable around 2900 cm^{-1} and between 950 and 1150 cm^{-1}.

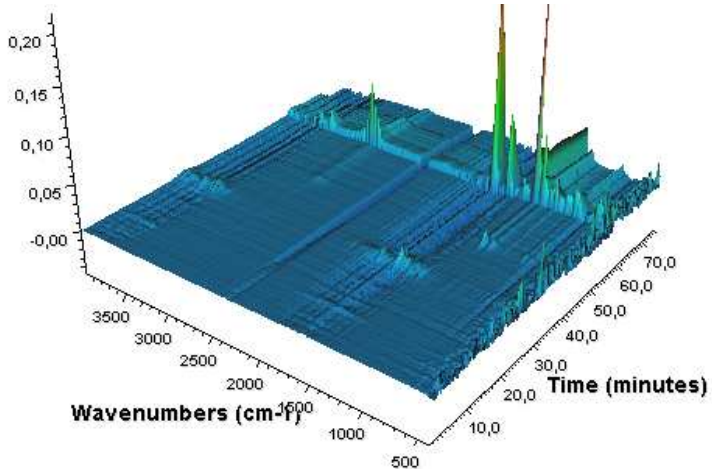


Fig. 126: FTIR spectra of the gases evolved during the pyrolysis of ATH-OP1230 combination versus time

In order to discuss more easily those results, the spectra collected at several characteristic temperatures are pictured in *Fig. 127*. The attributions of the observed bands are gathered in *Table 37*.

At 250 °C, corresponding to the beginning of the de composition, several peaks are noticeable. The bands between 3400- 3600 cm^{-1} and 1300- 1600 cm^{-1} are linked to the presence of water. It can be reasonably assumed that it results from the ATH dehydration.

At 400 °C, some bands are observed at 2938, 2850, 1 154, 1085 and 774 cm^{-1} and can be attributed to the presence of phosphonate, phosphonic and/or phosphinic acid. However, the FTIR spectra enable to demonstrate the presence of characteristic functional groups (phosphinate for example) but the exact nature of the compound can only be determined if its spectrum has been collected in a database. It was not the case in our study.

At 550 °C, the spectrum shows an increase of the in tensity of the bands linked to the phosphorous compounds evolved during the second degradation step. An additional signal attributed to P-ethyl groups appears at 1274 cm^{-1}. This suggests a sublimation of OP1230 during its decomposition, or the production of diethyl phosphinic acid, as confirmed by the comparison of the FTIR spectra of the gases evolved during the decomposition and that of OP1230 *(Fig. 128)*. Moreover, the presence of some bands at 1600, 1440 and 950 cm^{-1} attributed to the release of ethene and but-2-ene demonstrate that the P-C bonds of the OP1230 break, leading to the evolution of carbonaceous volatiles. This is consistent with the decomposition process of OP1230, since the degradation of aluminium diethyl phosphinate into aluminophosphates necessarily provokes the degradation of the ethyl groups.

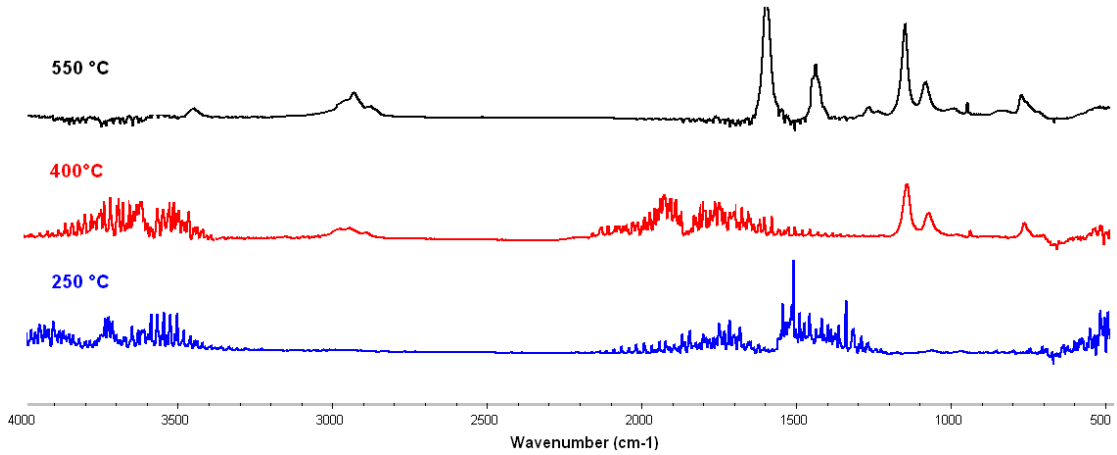


Fig. 127: FTIR spectra of the gases evolved during the pyrolysis of ATH-OP1230 combination at characteristic temperatures

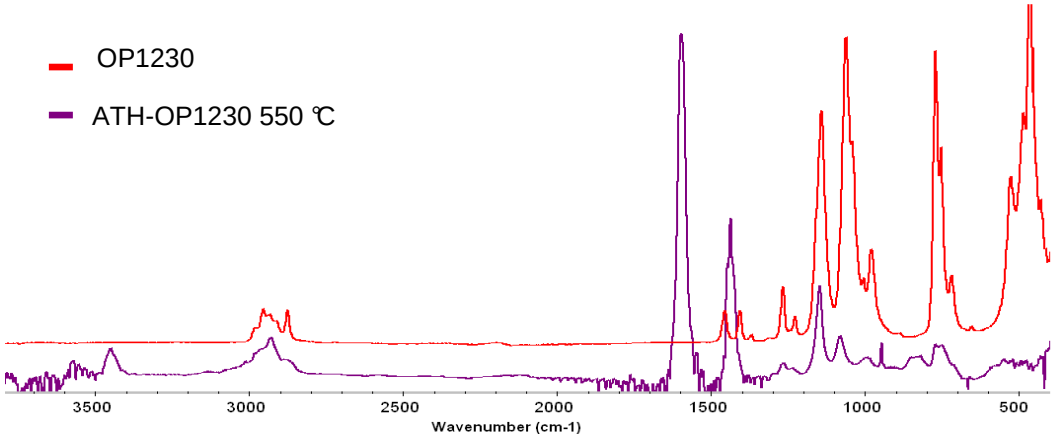


Fig. 128: FTIR spectra of OP1230 and of the gases evolved at 550 ℃ during the pyrolysis of ATH-OP1230 combination

Table 51: Attribution of the IR bands of the gases evolved during pyrolysis of the ATH-OP1230 combination [170]

Wave number (cm^{-1})	Attribution	Wave number (cm^{-1})	Attribution
3400-3600	O-H stretch (H_2O)	1274	P-ethyl asym. deformation
3452	O-H stretch	1144	P=O stretch
2939	Asym. Stretch $CH_3R_1R_2$	1063	P-O stretch
2879	Sym. stretch $CH_3R_1R_2$	1030	P-OH stretch
1600	C=C stretch	982	=C-H stretch (ethene)
1440	Asym. CH_3 deformation	775	Phosphinate

1.3 Conclusion on the ATH-OP1230 interactions

The investigations about the thermal decomposition of the ATH-OP1230 mixture in inert conditions allowed drawing a global degradation scheme, depicted in *Fig. 129*. Aluminium trihydrate first

degrades into alumina evolving water. Then, the mixture of amorphous alumina and aluminium diethyl phosphinate decomposes to form amorphous aluminophosphates in the condensed phase. It is supposed that some ethyl phosphonic acid is also formed. In the gas phase, carbonaceous organic compounds are released resulting from the degradation of OP1230 (ethene and but-2-ene) and some phosphorous compounds. The species which can be potentially released are phosphonate, phosphonic and/or diphosphinic acid, sublimated OP1230 and diethylphosphinic acid.

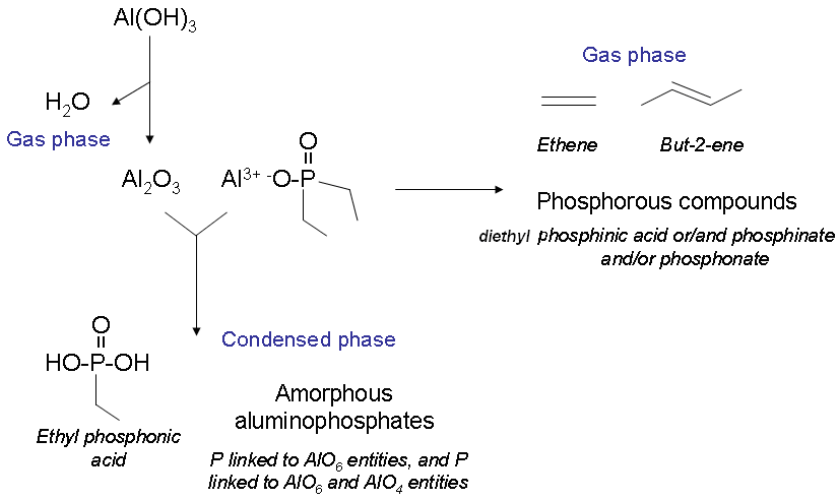


Fig. 129: Thermal degradation scheme of the ATH-OP1230 combination in inert conditions

According to TG analysis of the aluminium trihydroxide and aluminium diethyl phosphinate mixture, it was expected that their combination degrades in a similar way. However, it appears that the formation of aluminophosphonate, observed in thermal degradation of pure OP1230 [123] does not occur. Moreover, a phosphorous based entity (assigned to ethyl phosphonic acid) which is not linked to aluminium centres is formed. Moreover the charring of OP1230 was not observed. This differs from the degradation of the pure phosphinate.

The mechanism we propose is the chemisorption of the phosphinate, activated by the temperature increase, on alumina *(Fig. 130)*. The phosphinate is linked to gibbsite at first by hydrogen bonds. Then the dehydration of gibbsite leads to the chemisorption of the phosphorous compound by oxygen bonding, favouring the decomposition of the organic part of the additive (the ethyl groups). This chemisorption, modifying the crystallinity of the phosphinate, is consistent with the XRD analyses revealing a modification of the OP1230 structure. At the final stage aluminophosphates and ethyl phosphonic acid are formed. According to the literature, the proposed mechanism is compatible with the temperatures of the degradation [187], so that we can assume that this hypothesis is physically reasonable.

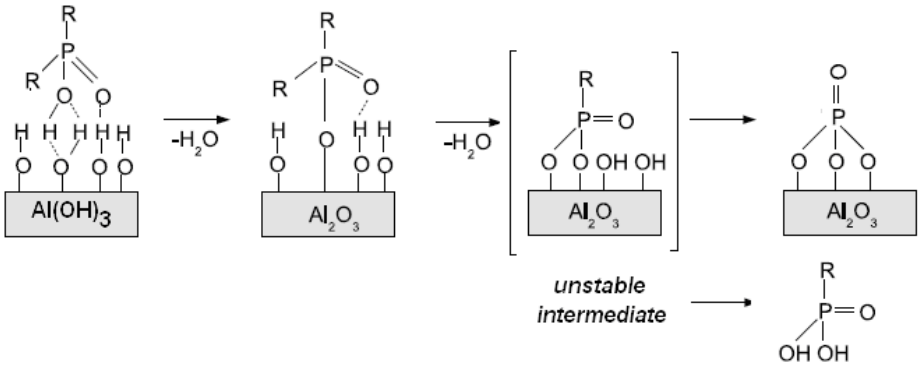


Fig. 130: Chemical binding of phosphinate during the thermal degradation

It can be concluded that there is a chemical interaction between ATH and OP1230, since some additional species (supposed to be ethyl phosphonic acid) are formed during the thermal decomposition of the flame retardant mixture. The point is now to determine if this interaction has an effect on the mechanism of degradation of vulcanized EVM.

2. Chemical interactions between the polymeric matrix, ATH and OP1230

It has been found that a chemical interaction occurs during the thermal degradation of the ATH-OP1230 combination. The objective of the following part is to determine if interactions occur when the additives are used in the polymeric matrix. For that, the thermal degradation of the polymer filled first with OP1230 alone and then with the combination of the two additives will be investigated and compared (the thermal degradation of vulcanized EVM containing ATH has been already detailed in *Chapter 4*).

2.1 Thermal degradation of vulcanized EVM flame retarded with OP1230

In this section, the thermal degradation of OP1230 in the vulcanized polymeric matrix is investigated. *Table 52* presents the composition of the studied formulation.

Table 52 : Composition of the tested material

Additive	phr	wt-%
EVM	100	61.7
Peroxide	1	0.7
Coagent (TAC)	6	0.6
OP1230	55	34
Total	***162***	***100***

The thermal degradation of the formulation, in inert conditions, is then investigated (condensed and gas phases).

2.1.1 Thermogravimetric analysis of EVM/OP1230

The thermogravimetric analysis of vulcanized EVM flame retarded with OP1230 is presented in *Fig. 131*. The degradation occurs into two steps. The first one occurs between 275 °C and 385°C with a mass loss of 43 wt-% *(1)*. The theoretical mass loss of acetic acid is of 61.7 x 0.418 = 25.8 wt-%, so that this first step may be due to deacetylation and some additional reaction (OP1230 sublimation for example). The second step from 385 to 515 °C leads to a mass loss of 55 wt-% *(2)*. It only remains a tiny amount of black residue of 2 wt-% in the pan.

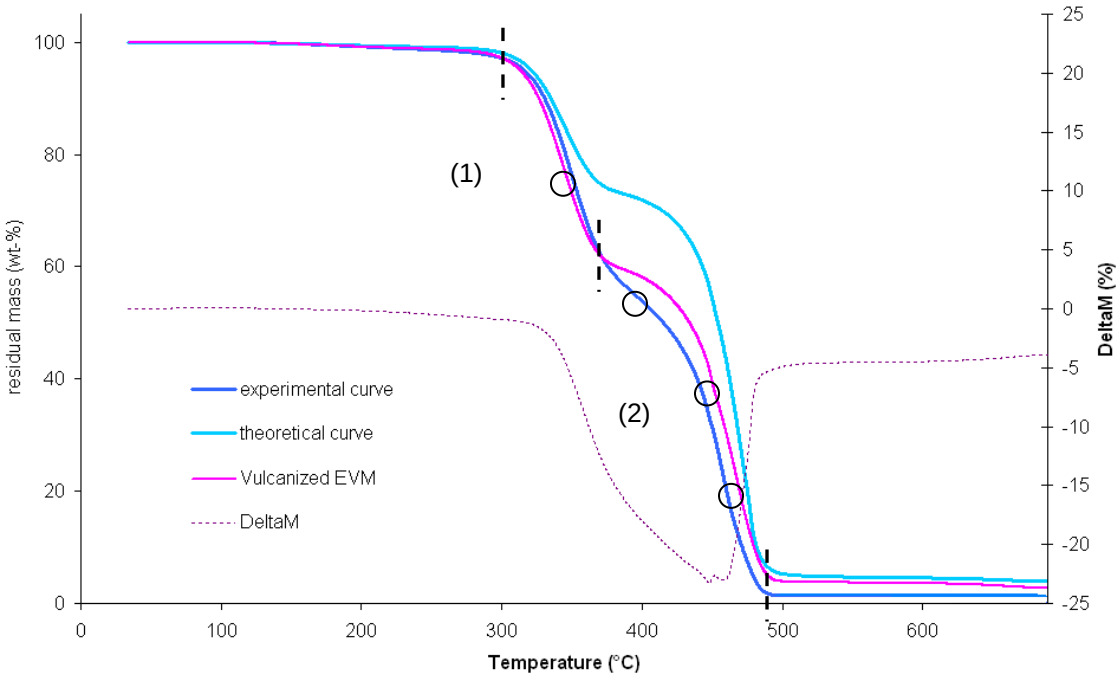


Fig. 131: Difference weight loss and experimental and calculated TG curves of vulcanized EVM flame retarded with OP1230 and TG curve of vulcanized EVM (10°C/mi n, in nitrogen)

The experimental TG curve is also compared with the calculated one and the difference weight loss curve (ΔM) points out the differences between those two curves. A thermal destabilization is observed

from 320℃ up to 700℃. Some interactions between t he polymer and OP1230 can thus be suspected in this range of temperature.

The material was heated at different treatment temperatures (symbolized as black circles in *Fig. 131*): 350 ℃ corresponding to the first degradation step, 400 ℃ at the beginning of the second step, 450 ℃ at the maximum destabilization and 480 ℃ at the en d of the thermal degradation.
The residues are pictured in *Fig. 132*. The untreated barrel is a white and flexible material, which becomes a grey crunchy residue, exhibiting some nodules at its surface when heat treated at 350℃. At 400 ℃, the decomposition produces a black carbo naceous residue, which turns into a foamy fragile structure at 450 ℃. The material obtained at 580 ° C is a black carbonaceous powder.

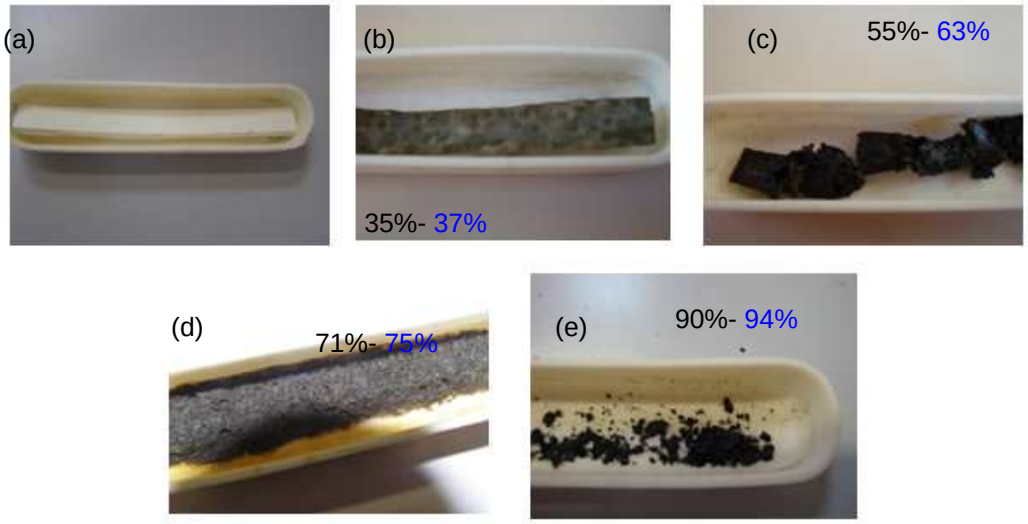


Fig. 132: Pictures of the thermal treatment residues of vulcanized EVM flame retarded with OP1230 at 20 ℃ (a), 350 ℃ (b), 400 ℃ (c), 450 ℃ (d) and 480 ℃ (e) - in black: expected mass loss (according to the TGA), in blue: experimental mass loss

As explained for the thermal degradation of the flame retardant combination, it is considered that if the experimental mass loss is in the range of the selected degradation step the heat treatment is considered as appropriate for our approach. This is the case for all treated samples.

2.1.2 Analysis of the residues

The first investigation was dedicated to the identification of the “nodules” observed on the sample treated at 350 ℃. The transverse sections of the u ntreated and heated at 350 ℃ samples were observed through Scanning Electron Microscopy (SEM). The obtain images are depicted in *Fig. 133*. The untreated material exhibits homogeneously dispersed OP1230 micro-sized aggregates. The heat-treated sample, in which some macroscopic nodules were noticed, shows that the “nodules” are in fact holes in the polymer containing crystallized compounds (red circles). Around the holes the matrix is relatively dense (blue circles), whereas the rest of the matrix is quite porous (green circles).

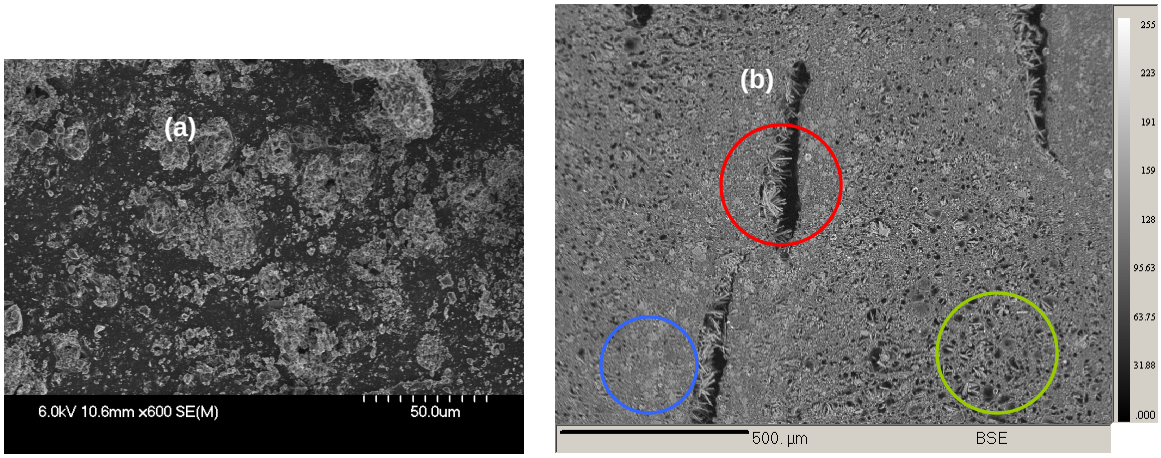


Fig. 133: SEM image of the untreated (a) and heat-treated (b) sample at 350℃ (transverse section)

The mapping of specific elements (carbon, aluminium and phosphorus) was realized through Electron Probe Micro-Analysis (EPMA). The results are presented in *Fig. 134*.

The mapping shows that the nodules are constituted of crystalline compounds containing aluminium and phosphorous, and some low quantity of carbon. They can be assigned to crystallized OP1230, which has sublimated, migrated through the polymer porosity and, trapped in a polymer hole, then has re-crystallized during the cooling of the sample (the density of phosphorous compounds is higher in the neighbourhood of these holes). Moreover some aggregates noticeable on the aluminium and phosphorous cartographies, confirming that OP1230 is not homogeneously dispersed in the material.

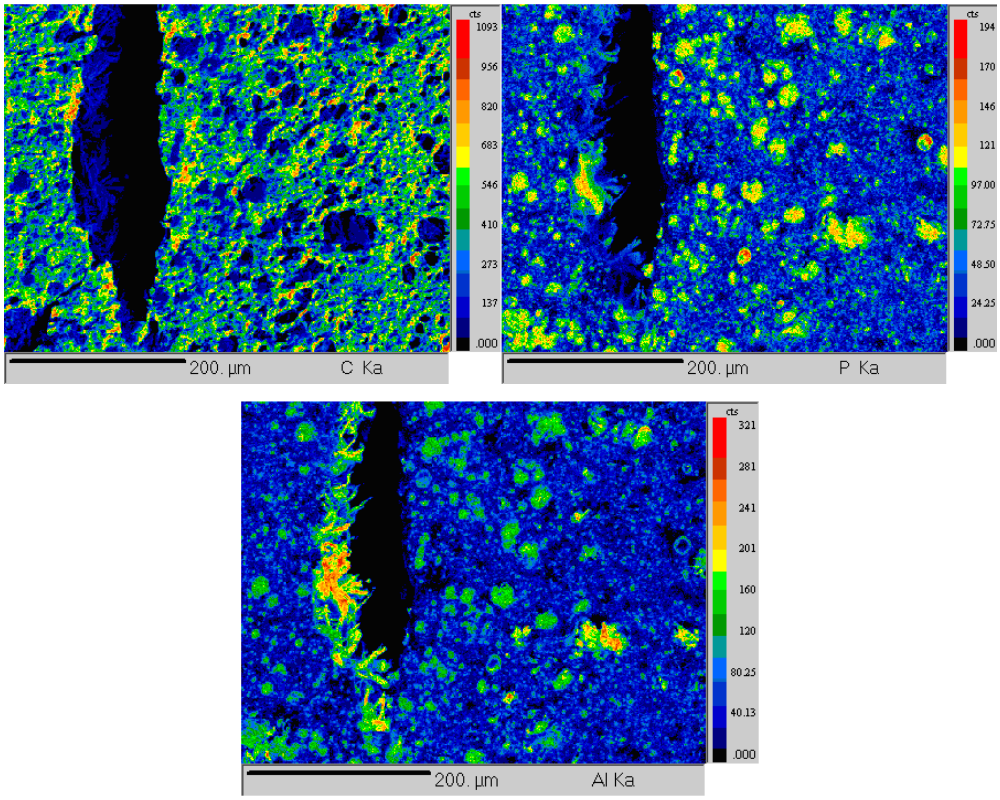


Fig. 134: Elemental mapping of the sample heat-treated at 350℃ (transverse section)

It is noteworthy that some areas on the map apparently contain aluminium, phosphorous but no carbon (in the bottom of the hole for example). This phenomenon cannot be clearly assigned to a degradation of the phosphinate. Indeed, in the case of very low quantities of carbon the energy of the electron beam can be too low to allow their detection. Moreover, the porosity of the material can complicate the detection of the species, since the crystal orientation for the analysis is not able to detect carbon atoms located deeper in the holes. As a consequence, it is considered that the detected compound is undegraded OP1230.
The nodules formed during the degradation of the material can thus be attributed to the sublimation, migration and crystallization of OP1230 through the degraded polymer.

The rest of the samples have also been characterized by NMR spectroscopy. The evolution of the ^{27}Al and ^{31}P spectra during the thermal degradation of vulcanized EVM/OP1230 formulation is respectively presented in *Fig. 135* and *Fig. 136*.

From ambient temperature up to 450°C, the spectra a re similar to those obtained for the degradation of pure OP1230 [123]. The 27-aluminium NMR spectra shows only one site located at -12 ppm which is attributed to Al^{3+} cations with an octahedral geometry and possessing phosphorus atoms in their second coordination sphere. The phosphinate site (connected to aluminium and thus deshielded) is observed on the ^{31}P spectra. Apparently the phosphinate is not degraded before this temperature, but this is in contradiction with the mass lost by the formulation in TGA at the same temperature (71 wt-%), which implies at least the partial degradation of the additive. Since the structure of OP1230 remaining in the condensed phase is not modified, it is reasonable to assume the sublimation of OP1230 during degradation. In this case the flame retarded formulation effectively loses some mass but the additive is not degraded. This point will be investigated by gas phase analysis (OP1230 is expected as a gaseous product).

At 480° C, three distinct sites at -16, 6.4 and 37. 3 ppm are detected on the 27-aluminium NMR spectrum. The width of the bands suggests that an amorphous network is obtained. The signal at -16 ppm corresponds to the presence of octahedral aluminum (AlO_6 unit) connected by Al-O-P bonds [188]. Octahedral aluminum atoms are detected at around 6 ppm, they are assigned to isolated units with an incomplete second coordination sphere of phosphorus partially connected via Al-O-Al bonds [188]. The last signal appearing around 37 ppm is characteristic of the formation of tetrahedral AlO_4 entities in an aluminophosphate structure.

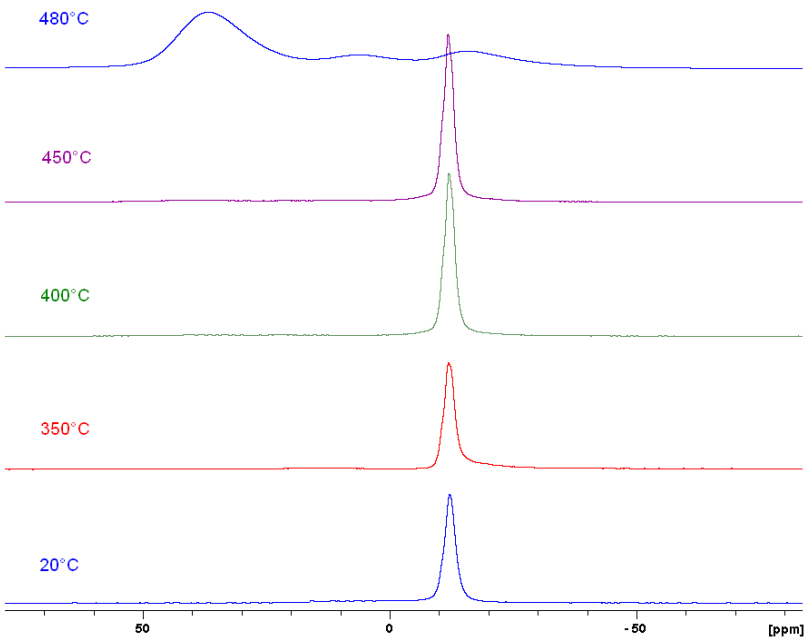


Fig. 135: ^{27}Al MAS NMR spectra of the thermal degradation residues of vulcanized EVM flame retarded with OP1230 (degradation in nitrogen)

On the phosphorus spectrum, as for OP1230 or the ATH-OP1230 combination, an inversion of the peaks intensities is noticed.

At 480 ℃ two broad bands centered at 12 and -27 pp m are observed. The first one is probably due to the formation of aluminum phosphonate (between 4 and 30 ppm) since the signal on the 27-Aluminium NMR spectrum at -16 ppm corresponds to these types of structure. The second one can be attributed to aluminophosphate structures. In aluminium phosphonate, aluminum atoms have an octahedral environment. The signal on the aluminum spectrum around -16 ppm corresponds to these types of structure.

According to the previous observations, the aluminium phosphinate follows the same degradation pathway in the polymer when heated alone. It degrades into aluminophosphonate (composed of octahedral aluminium) and into aluminium phosphonate. This aluminophosphonate decomposes in an aluminophosphate $AlPO_4$. Those results suggest that the presence of EVM does not affect the degradation mechanism of OP1230, but according to the observed thermal destabilization, the thermal degradation of EVM is suspected to be influenced by the phosphinate compound.

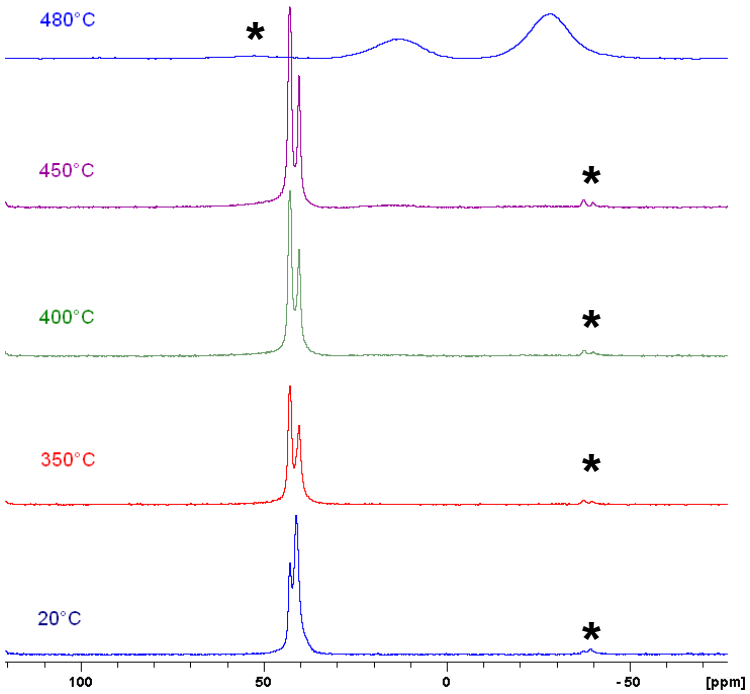


Fig. 136: ^{31}P DD- MAS NMR spectra of the thermal degradation residues of vulcanized EVM flame retarded with OP1230 (degradation in nitrogen) * = spinning sideband

The analysis of the ^{13}C NMR spectra versus temperature of the EVM/OP1230 formulation *(Fig. 137)* complements the previous results. It is noticeable that the intensity of the peaks of the last spectrum (480 ℃) was increased for a better visibility.

The characteristic peaks observed for vulcanized EVA and for OP1230 are similar to those obtained for the untreated material. The signal at 170 ppm is attributed to the ester function of the acetate. The peaks from 25 to 36 ppm (25.6, 30.7 and 36.5 ppm) were assigned to CH_2 in ethylene sequences and linked to vinyl acetate. The multiplicity of those peaks is attributed to the monomer sequence distribution in the copolymer chain as discussed in the previous chapter. The methine group of the polymer backbone is also observed (around 70 ppm). The two peaks at 21 ppm are assigned to the methyl group of the acetate function and to the CH_2 of the ethyl group of OP1230 (which is shielded by the presence of phosphorus). The single peak at 8 ppm corresponds to the methyl group of OP1230.

The deacetylation of the polymer starts around 300 ℃, as observed on the TG curve, leading to the disappearance on the signals attributed to the acetate function for a heat treatment of 350℃. Moreover, for such a temperature, a band at 130 ppm corresponding to carbon double bonds is noticeable. The ethylenic region of the spectrum exhibits a broadening of the signals that could be explained by chain scission reactions, producing carbons with various chemical environments (and thus with a large range of chemical shift). Moreover the black surface of the residue suggests that the sample charred.

At 400 ℃, the characteristic peak of the OP1230 methyl (8 ppm) is still noticeable. The intensity of the other signals decreases and, on the contrary to that occurs for pure vulcanized EVM (see Chapter 4, section 1.1.3, *Fig. 11*), the band linked to carbon double bonds does not increase in intensity or

broaden. This indicates that the presence of OP1230 prevents the formation of aromatic and ethylenic compounds in the condensed phase. This phenomenon is confirmed by the spectrum at 480 °C where the only two or three peaks remains in the aliphatic region, especially peaks at 8 and 20 ppm resulting from the resonance of aliphatic part of phosphorous compounds (aluminium phosphate, aluminium ethyl phosphonate). A large signal at 130 ppm is also noticeable corresponding to the charring of the sample.

If we compare the obtained spectra for pure vulcanized EVM in pyrolysis conditions (*Fig. 78* in *Chapter 4*) and for the same matrix flame retarded with OP1230, it clearly appears that the degradation of the material is the same up to 350 °C. Deacetylation occurs, leading to the formation of carbon-carbon double bonds. However, on the contrary to the unfilled polymer there is no evidence of acetic acid remaining in the condensed phase. In addition, the deacetylation (which was fully achieved in the pure cured EVM) is not complete at this temperature. Beyond 350 °C the characteristic band for aromatic or ethylenic compounds is narrowed compared to the pure polymer. This suggests that the formation of the carbonaceous residue formed during the degradation is slowed down, or that it is continuously degraded. This possibility will be investigated by the examination of the gases evolved during degradation.

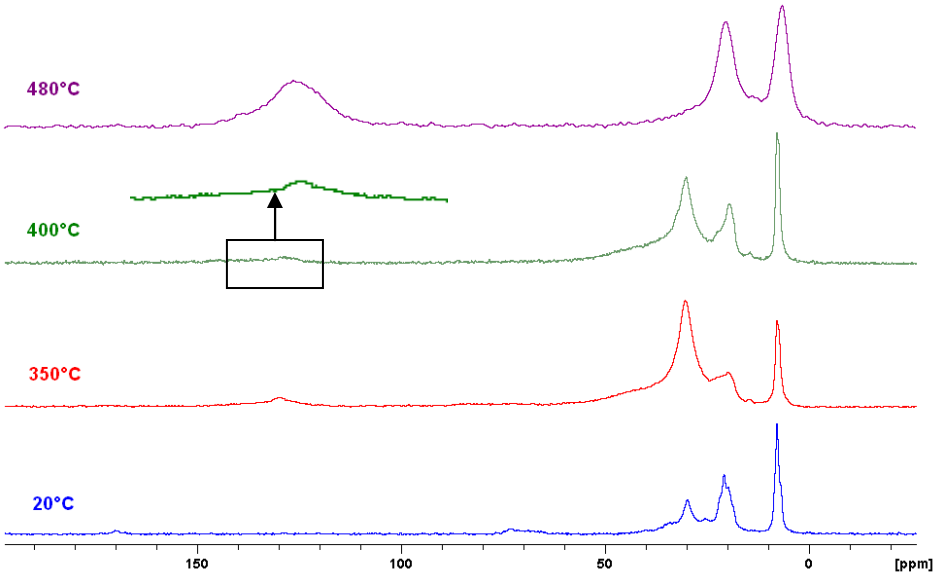


Fig. 137: ^{13}C CP-DD-MAS NMR spectra of the thermal degradation residues of vulcanized EVM flame retarded with OP1230 (degradation in nitrogen)

2.1.3 Analysis of the gas phase

The analysis of the gases evolved during the pyrolysis of the material provides some additional information about the degradation mechanism and the interactions between the phosphinate additive and the polymeric matrix.

Fig. 138 presents the evolution of the FTIR signal versus time. The beginning of the degradation is marked at 30 min (corresponding to a temperature of 300 °C) with the appearance of intense signals around 3500, 1800, and 1000- 1400 cm^{-1}. The signals then disappear at 400 °C (40 min) and are replaced by peaks at 3000, 800-1200 cm^{-1}.

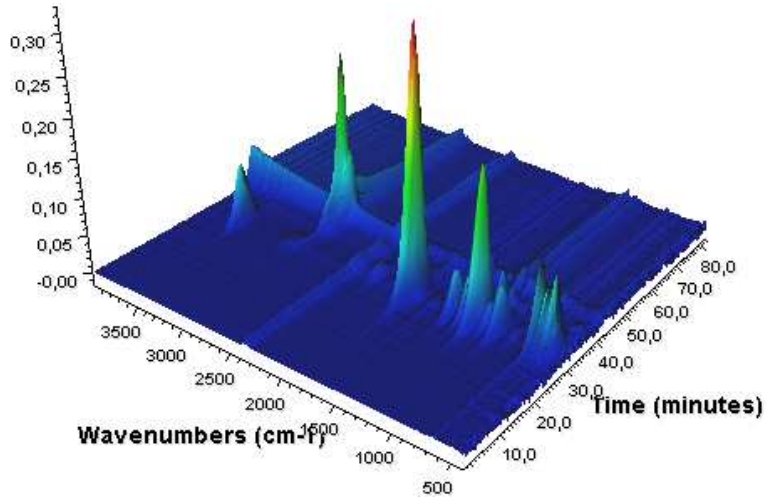


Fig. 138: FTIR spectra of the gases evolved during the inert degradation of vulcanized EVM flame retarded with OP1230 (in inert conditions) versus time

The same spectra obtained at characteristic temperatures are pictured in *Fig. 139*. The attributions of the observed bands are gathered in *Table 53*.

The degradation starts at around 250°C with the evolution of volatile products. Several peaks are noticeable on the IR spectrum collected at 300 °C at 3580, 1796, 1774, 998 and between 1397 and 1084 cm^{-1}. They are attributed to the release of acetic acid. Their intensity increases up to 330 °C according to *Fig. 138* before their disappearance. Indeed, the spectrum at 360 °C does not show any peak related to acetic acid: this is consistent with the solid state NMR analysis demonstrating that the deacetylation is complete at 350 °C. Some additional peaks appear from 3100 to 2850 cm^{-1} thus revealing the evolution of carbonaceous compounds. Moreover the previous bands and those at 1085 and 1200 cm^{-1} can be attributed to sublimated OP1230, confirming our previous hypothesis.
On the spectrum collected at 450 °C, some phosphorous compounds are still noticeable, and the intensity of the peaks in the region 2850- 3100 cm^{-1} increases, indicating that the polymeric chains decompose into aliphatic volatile compounds. Moreover, a peak characteristic of aromatic species is noticeable at 3050 cm^{-1}; the aromatic compounds formed during the degradation of the polymer are also volatilized.
The same degradation products are observed up to 550 °C.

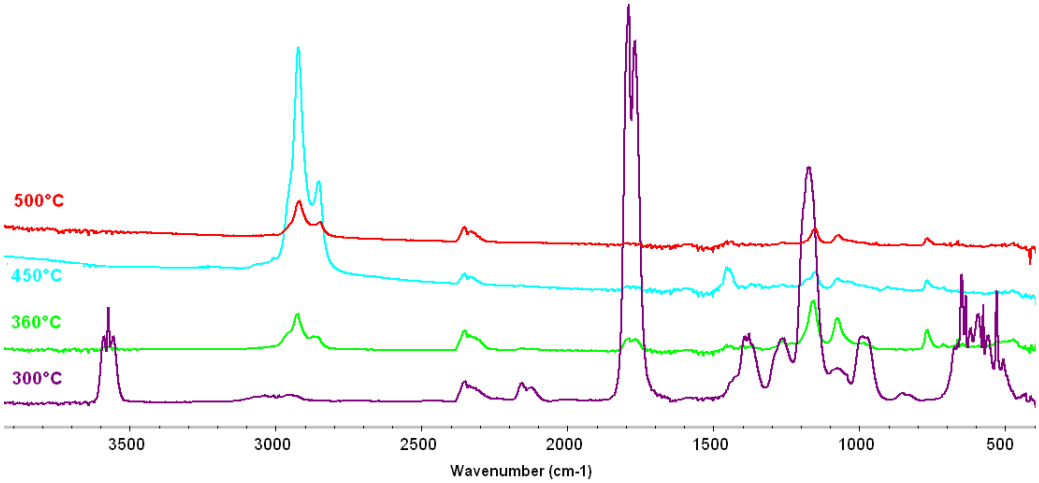


Fig. 139: FTIR spectra of the gases evolved during the inert degradation of vulcanized EVM flame retarded with OP1230 (in inert conditions) at characteristic temperatures

Table 53: Attribution of the IR bands of the gases evolved during the thermal degradation of vulcanized EVM flame retarded OP1230 (in inert conditions) [189]

Wave number (cm^{-1})	Attribution	Wave number (cm^{-1})	Attribution
2939	Asym. Stretch $CH_3R_1R_2$	1396	-O-H bend (acetic acid)
2879	Sym. stretch $CH_3R_1R_2$	1270	C-O asym stretch (acetic acid)
2358-2310	O=C=O asym. stretch (CO_2)	1182	P=O stretch
2100-2200	CO stretch (carbon monoxide)	1085	-C-OH stretch (acetic acid) P-O stretch
1796	C=O asym.stretch (acetic acid)	998	-O-H bend (acetic acid)
1772	C=O sym. stretch (acetic acid)	982	=C-H stretch (ethene)
1600	C=C stretch	775	Phosphinate
1456	Asym. CH_3 deformation		

2.1.4 Conclusion on vulcanized EVM-OP1230 interactions

According to the analysis of the condensed and gas phase, the thermal decomposition mechanism of vulcanized EVM flame retarded with OP1230 has been determined *(Fig. 140)*.

It was found that the evolution of the phosphorus-based species is identical for the decomposition of OP1230 alone or incorporated into the polymeric matrix, that is to say the formation of aluminophosphonate (composed of octahedral aluminium and phosphonate groups) and of aluminophosphate $AlPO_4$. The gas phase analyses showed that OP1230 not only degrades but also sublimates in the first degradation stage around 350 °C. The remaining residue of carbonaceous compounds, aluminophosphonates and aluminophosphates then decomposes into aromatic, ethylenic and aliphatic volatiles and some phosphonic or phosphonate volatiles. At the end of the degradation it only remains some carbonaceous residues (polyenes or char) and aluminophosphates.

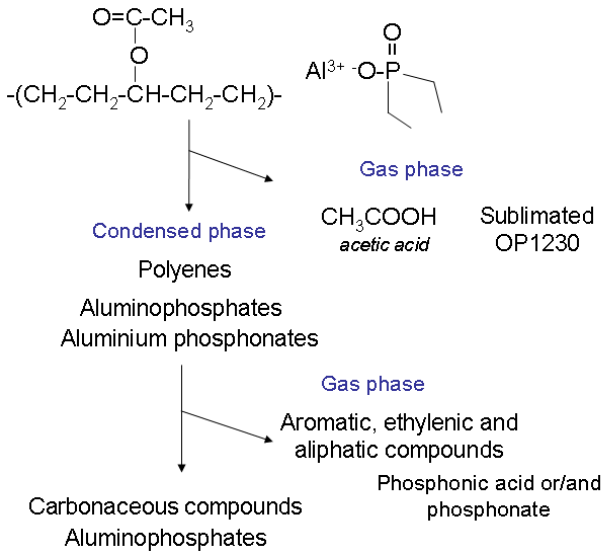


Fig. 140: Degradation scheme of vulcanized EVM flame retarded with OP1230

The chemical interactions do not influence the decomposition of the additive. Nevertheless, some changes in the polymer decomposition were pointed out. The polymer deacetylation is accelerated by the presence of the phosphorous compounds in the condensed phase, such as the polyene volatilization, leading to a thermal destabilization. The species evolved in the gas phase (sublimated OP1230, carbonaceous volatiles and phosphonic acid) are those expected from the thermal degradation of the separate polymer and OP1230.

The thermal degradation of the polymer containing the aluminium diethyl phosphinate has been investigated, revealing the accelerating effect of the additive on the decomposition of the matrix. The next section focuses on the thermal degradation of the formulation flame retarded with the ATH-OP1230 combination. The comparison of the determined mechanisms is expected to provide information about the suspected interactions between the additives and the matrix.

2.2 Thermal degradation of vulcanized EVM flame retarded with ATH and OP1230

In this section the thermal degradation of the flame retardant additives combination in the vulcanized polymeric matrix is investigated. *Table 54* presents the composition of the studied formulation. The chosen ATH and OP1230 contents and ratio are the same as in the optimized flame retarded complete formulation defined in *Chapter 3*.

Table 54 : Composition of the studied material

Additive	phr	wt-%
EVM	100	55.2
Peroxide	1	0.7
Coagent (TAC)	6	3.3
ATH 120E	50	27.6
OP1230	24	13.2
Total	***181***	***100***

The thermal degradation of the formulation, in inert conditions, is then investigated.

2.2.1 Thermal degradation

The thermogravimetric analysis of the flame retarded vulcanized EVM in inert atmosphere is pictured in *Fig. 141*. The degradation occurs into three steps. It starts at 200 ℃ with a mass loss of 19 wt-% up to 300 ℃ *(1)* while the expected mass of released water is of 9.5 wt-%. The second step from 300 to 375 ℃ leads to a mass loss of 18 wt-% *(2)* (while acetic acid release with a mass loss of 24.7 wt-% was expected), immediately followed by the last step ending at 500 ℃ *(3)* with a residue of 23 wt-%. The mass of the thermally stable residue obtained at the end of the TGA correspond to the theoretical calculated value.

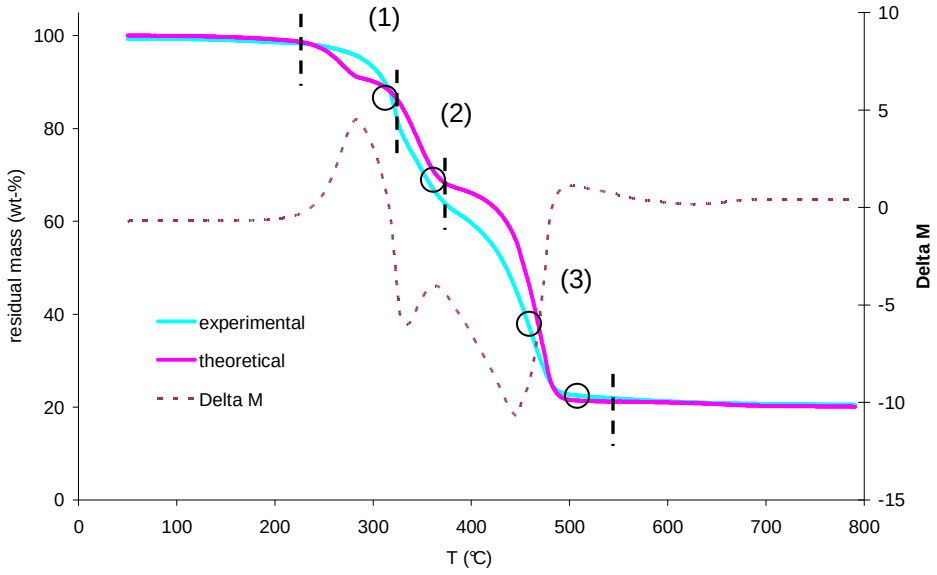


Fig. 141: Experimental and calculated TG curves and difference weight loss curves of vulcanized EVM flame retarded with the ATH-OP1230 combination (10℃/min, in nitrogen)

The experimental TG curve is also compared to the calculated one, and the difference weight loss curve ΔM points out the differences. A thermal stabilization is noticeable at the very beginning of the degradation (250- 300 ℃), whereas for the rest of the degradation, a thermal destabilisation is

obviously observed (with at 450 °C a maximum difference of 10 wt-%). Interaction between the polymer and the additives can thus be suspected.

To investigate the potential chemical interactions between the additives and the polymeric matrix, characteristic heat treatment temperatures were determined according to the TG curve. It was decided to carry out the thermal treatments at 310 °C to obtain an intermediate residue of the first degradation step, 340 °C for the second step, 450 °C as an intermediate temperature of the last step and 500 °C to achieve a complete degradation. The temperatures are symbolized by black circles in *Fig. 141*.

The residues obtained after thermal treatments under nitrogen are pictured in *Fig. 142*. The untreated material is a white flexible barrel which becomes slightly yellowish when heated at 310 °C. For a heat treatment of 340 °C, the material becomes foamy and expands a little. The barrel heated at 450 °C remains foamy but exhibits a brownish colour due to the degradation of the carbonaceous parts of the sample. The last residue, for which a thermally stable residue is obtained, consists in a greyish powder.

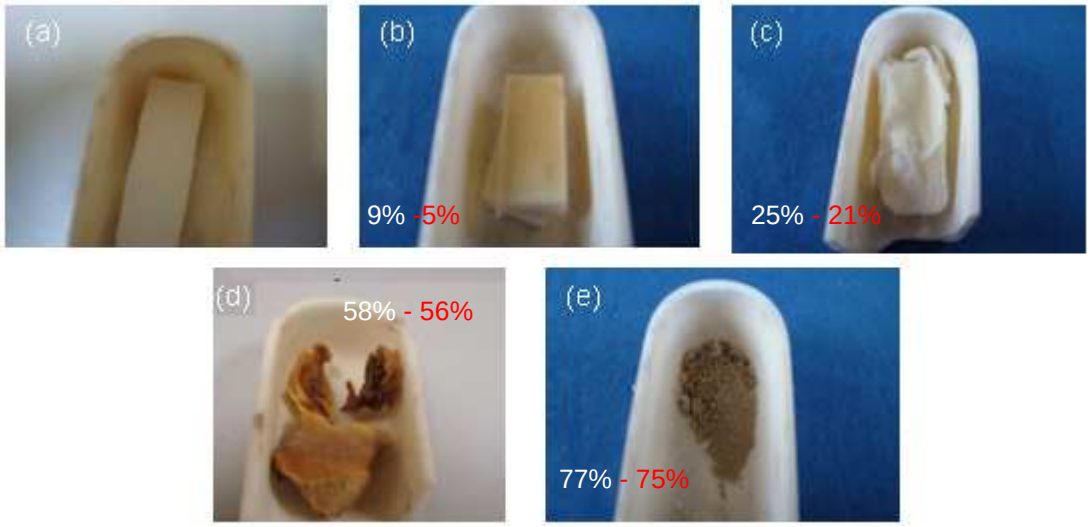


Fig. 142: Pictures of the thermal treatment residues of the ATH-OP1230 combination(2:1) in vulcanized EVM (in N_2 at 20 °C (a), 310 °C (b), 340 °C (c), 450 °C (d) and 500 °C (e) - in white: expected mass loss according to TGA, in red: experimental mass loss)

The next step of the investigations consists in the characterization of the obtained residues.

2.2.2 Analysis of the residues

The solid state NMR techniques are used to characterize the intermediate degradation residues and to determine if some chemical interaction occurs between the additives and the polymeric matrix.

The evolution of the ^{31}P NMR spectra of the degraded material in inert conditions is reported in *Fig. 143*. The spectrum of the untreated exhibits a double peak at 41.3 and 43 ppm, corresponding to phosphinate sites deshielded by Al^{3+}.

At 310 ℃, an additional peak appears at 46.5 ppm. It is characteristic of the formation of phosphinic acid [190]. This result is quite surprising since for the other studied systems, the degradation did not occur before 400 ℃.

At 340 ℃, the chemical shifts of the peaks are not modified, but a broadening of the signal is observed which can be attributed to an amorphization of the material.

When the flame retarded formulation is heated at 450 ℃, its spectrum exhibits an additional large band around 60 ppm, suggesting the presence of organic diphosphinic acid. Moreover, the characteristic double peak at 41 and 43 ppm is transformed into a single band centred at 42 ppm, indicating that the structure of the remaining phosphinate is modified.

The spectrum at 500 ℃ shows an increase of the intensity of the signals linked to the acidic compounds (organic phosphonic and diphosphonic acids), a decrease of the signal of the phosphinate and the appearance of a band around 20 ppm, attributed to the formation of organic phosphonic acid.

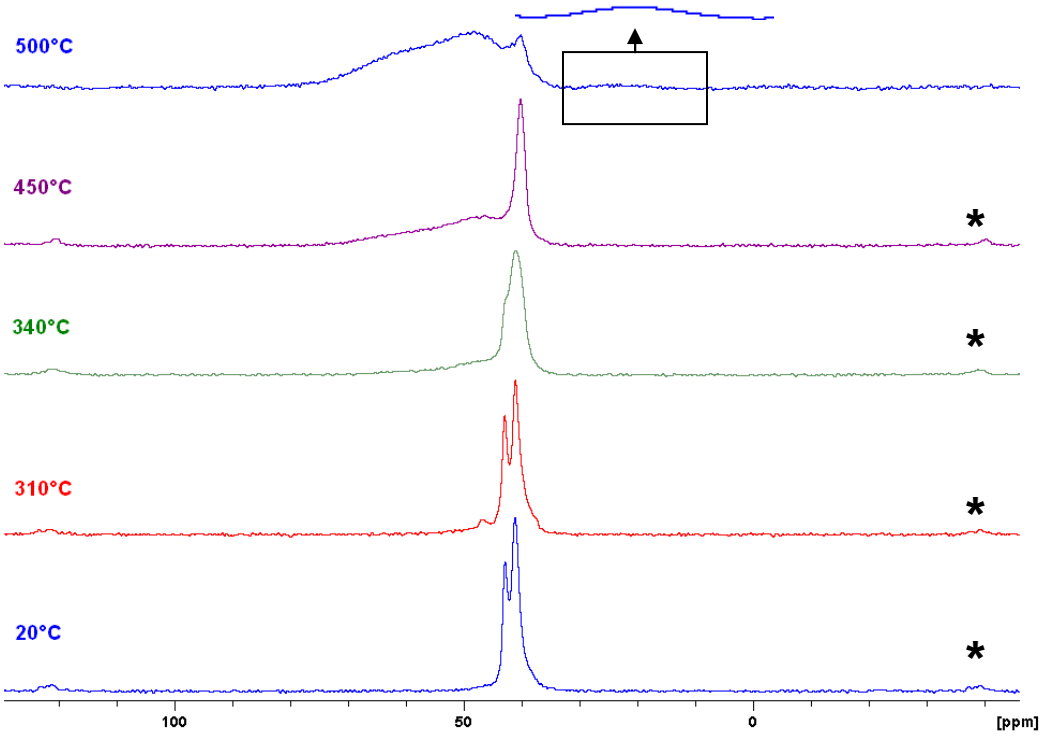


Fig. 143: ^{31}P DD- MAS NMR spectra of the thermal degradation residues of vulcanized EVM flame retarded with the ATH-OP1230 combination (degradation in nitrogen), * = spinning sideband

Those results demonstrate that whereas the degradation of OP1230 was observed at high temperature when mixed with ATH or EVM (^{31}P NMR spectra were similar up to a HTT of 450℃), this is not the case when the ATH-OP1230 mixture is incorporated into the polymer. Moreover, the degradation pathway of the OP1230 is different since diphosphinic acid is detected for the tri-component material, this was not the case for the bi-component mixtures or the pure additive.

The ^{27}Al MAS spectra of the heated material *(Fig. 144)* are identical to those obtained for the ATH-OP1230 combination *(Fig. 119)*, except from the peaks intensity ratio (this is explained by the fact that the ratio of pure ATH-OP1230 combination was of 1:1, versus 2:1 in the polymer). They are thus not fully commented. It is just recalled that the resonance at 7.7 ppm is expected for octahedral aluminium in a gibbsite structure [145]. The site at –4.7 ppm is attributed to extra-framework aluminium in octahedral coordination impurities [146]. The dehydration of ATH produces an additional signal located at 68 ppm attributed to tetrahedral coordination aluminium in alumina or boehmite. Nevertheless, the signal attributed to the phosphinate is still observed at 500℃ demonstrating that octahedral aluminium sites linked to phosphorus, in a structure close to that of phosphinates, remain in the formulation.

Those results demonstrate that the species resulting from the decomposition of OP1230 when incorporated in EVM (aluminophosphates and aluminophosphonates) are not detected when ATH is added in the formulation. Moreover, the compounds which are formed do not correspond to that expected from the thermal decomposition of the flame retardant combination (aluminophosphates and ethyl phosphonic acid). It implies that the chemical interactions between the flame retardant additives determined in the first part of the chapter are modified when the additives are incorporated in the polymer. This suggests chemical interactions between the combination of FR additives and the polymer.

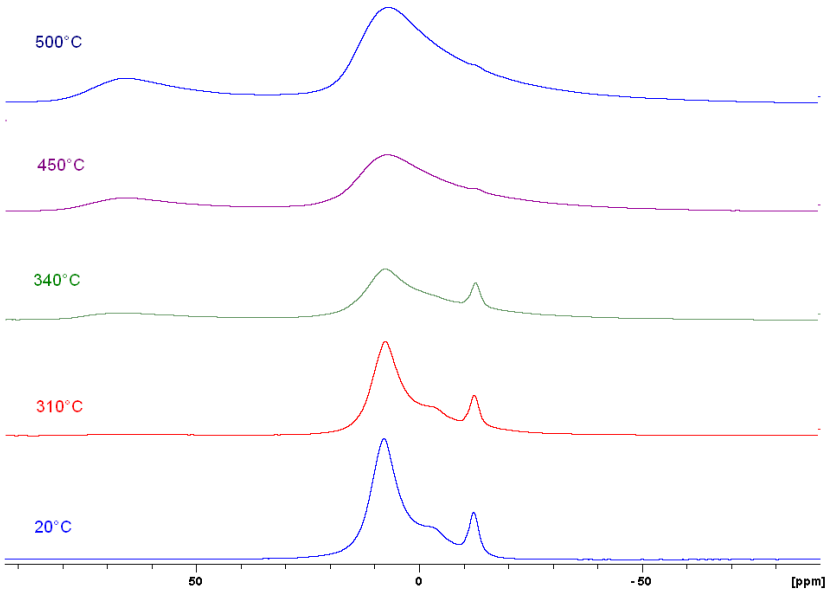


Fig. 144: ^{27}Al MAS NMR spectra of the thermal degradation residues of vulcanized EVM flame retarded with the ATH-OP1230 combination (degradation in nitrogen)

The characterization of the residues was completed by ^{13}C NMR analyses *(Fig. 87)*.
It is noticeable that the aliphatic carbons of the phosphinate (8 and 20 ppm) are visible on the spectra whatever the heat treatment temperatures. This confirms the presence of remaining phosphinate or

phosphinic / diphosphinic acid in the condensed phase. In addition, the signal at 8 ppm is doubled at 340 ℃, supporting the hypothesis of the formation of both species.

The evolution of the carbon species shows that the deacetylation of the polymeric matrix begins at 310 ℃ and the decrease of the peak intensity at 21 and 170 ppm. The presence of the peak at 70 ppm (carbon in the polymeric chain linked to the acetate group) shows that the deacetylation is not complete. At 340 ℃, the spectrum is quite the same , the only difference concerns the additional resonance at 185 ppm attributed to the presence of acetic acid trapped in the polymeric matrix. As above, the signal at 70 ppm shows that some acetate groups are still linked to the polymer chains.

The spectrum of the residue collected after a heat treatment carried out at 450℃ exhibit several peaks. The signal linked to carbon-carbon double bonds is widen, suggesting that the chain scission reactions have provided a wider range of ethylenic (and/or aromatic) compounds. The aliphatic region also presents intense peaks, linked to the remaining aliphatic compounds. It is noteworthy that the signals assigned to carboxylic acid carbons (185 ppm) and acetate (70 ppm) disappear. This indicates that there is no more acetate or acetic acid in the material.

At 500 ℃ two broad but not intense bands are noticeable at 130 and 140 ppm. As previously described for the unfilled polymer, the signal is attributed to the presence of highly unsaturated polyenes (around 135- 140 ppm) and to some polycyclic aromatic compounds (130- 135 ppm). Some oxidation is suspected since the peak at 185 ppm reappears: this phenomenon is attributed to the conditions of the cooling of the sample, where some oxidation (at relatively high temperature, when the tube is disconnected from the gas line to be removed from the furnace, before being reconnected) can occur.

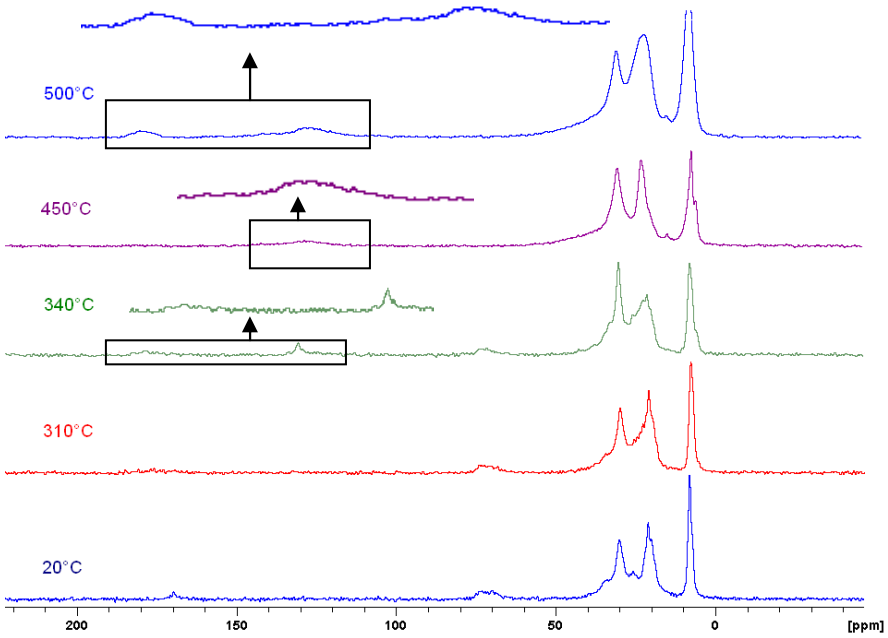


Fig. 145: ^{13}C CP-DD-MAS NMR spectra of the thermal degradation residues of vulcanized EVM flame retarded with the ATH-OP1230 combination (degradation in nitrogen)

It appears that the thermal degradation of the flame retarded vulcanized EVM with the additives mixture in inert atmosphere leads to the formation of quite similar carbonaceous compounds than

those formed when ATH-filled polymer degrades *(detailed in Chapter 4)*. There is also no significant difference in the degradation temperatures. However, it is noteworthy that the peak at 30 ppm, assigned to CH_2 groups in EVM is conserved for the ATH or ATH-OP1230 filled polymer but not in the case of the OP1230-filled material. This confirms the catalytic effect of the phosphinate on the thermal decomposition of the polymer.

The analyses of the condensed phase show that the modification of the degradation pathway mainly concerns OP1230 in the formulation EVM/ATH/OP1230. However the ATH dehydration and the deacetylation occur at slightly higher temperatures than expected.

2.2.3 Analysis of the gas phase

In addition to the characterization of the condensed phase, the gas phase analysis was performed using TGA-FTIR analyses.

The FTIR spectra versus time of the gases evolved during the TG measurement under nitrogen are presented in *Fig. 146*. The degradation starts at 25 min (corresponding to a temperature of 250 °C) and ends at 50 min (that is to say 500 °C). On the map, the beginning of the inert degradation is marked by broad bands at 4000- 3600 and 1600- 1800 cm^{-1}, and then some peaks around 1800 and 1000- 1400 cm^{-1}. Then some bands in the region of 2900 cm^{-1} appear, accompanied by several signals around 1200 cm^{-1}.

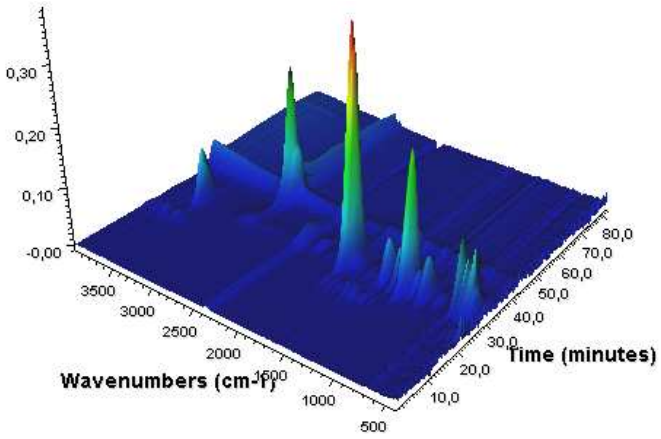


Fig. 146: FTIR spectra of the gases evolved during pyrolysis of vulcanized EVM flame retarded with the ATH-OP1230 combination versus time

The spectra collected at characteristic temperatures *(Fig. 147)* reveal what sorts of gases are evolved during the pyrolysis of the flame retarded EVM. The attributions of the observed bands are gathered in *Table 55*.

At 250 °C the evolution of water from the ATH dehyd ration is noticeable (broad bands at 4000- 3600 and 1600- 1800 cm^{-1}). At 300 °C, the degradation begins with the relea sed of acetic acid, as shown by the peaks at 3580, 1790, 1397, 1270, 1176, 1122, 1105, 1084 and 998 cm^{-1}. As for the unfilled polymer, the first degradation step consists in the deacetylation of the material. In our case we also

observe the ATH dehydration. On the spectrum collected at 350 ℃, some very weak bands corresponding to acetic acid are noticeable, and some at 2938, 2850, 1154, 1085 and 774 cm^{-1} and can be attributed to the release of phosphonate compounds and/or phosphinic acid. It is noteworthy that the signals at 2938 and 2850 cm^{-1} can also be linked to the production of aliphatic volatiles from the decomposition of vulcanized EVM. The quasi-disappearance of the signals of acetic acid corresponds to the observations made about the condensed phase, where the complete deacetylation is observed after 340 ℃.

At 420 ℃ the intensity of bands previously discussed (linked to aliphatic and phosphorous compounds) increases, confirming the release of phosphorous compounds in the gas phase. This is coherent with the formation in the condensed phase of diethyl phosphinic and diphosphinic acid: part of them can evaporate into the gas phase. Two additional signals appear at 1600 and 1440 cm^{-1}, indicating that the organic part of OP1230 degrades in ethene and but-2-ene. These two last peaks disappear at 500 ℃, suggesting that the organic part of the flame retardant combination is fully degraded.

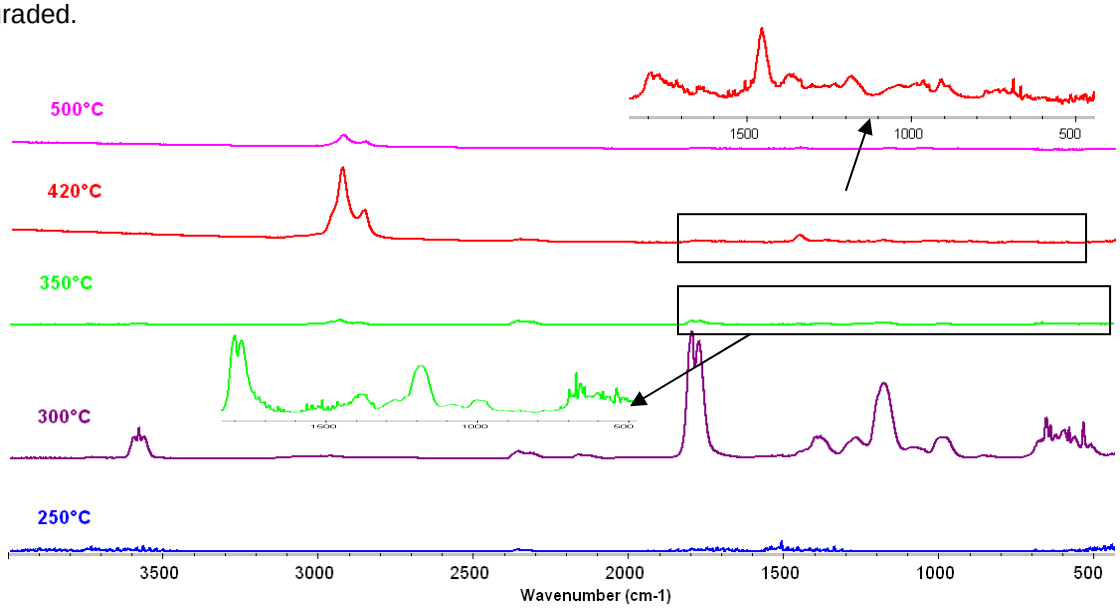


Fig. 147: FTIR spectra of the gases evolved during pyrolysis of vulcanized EVM flame retarded with the ATH-OP1230 combination at characteristic temperatures

Table 55: Attribution of the IR bands of the gases evolved during the thermal degradation of vulcanized EVM flame retarded with the ATH-OP1230 combination (in inert conditions) [170, 189]

Wave number (cm^{-1})	Attribution	Wave number (cm^{-1})	Attribution
2939	Asym. Stretch $CH_3R_1R_2$	1456	Asym. CH_3 deformation
2879	Sym. stretch $CH_3R_1R_2$	1396	-O-H bend (acetic acid)
2358	O=C=O asym. stretch (CO_2)	1270	C-O asym stretch (acetic acid)
2310	O=C=O sym. stretch (CO_2)	1182	P=O stretch
1796	C=O asym.stretch (acetic acid)	1085	-C-OH stretch (acetic acid) P-O stretch
1772	C=O sym. stretch (acetic acid)	998	-O-H bend (acetic acid)
1600	C=C stretch	775	Phosphinate

At the end of the thermal decomposition, it only remains the characteristic bands of the phosphorous compounds (1085 and 1082 cm^{-1}) and/or aliphatic species (2938, 2850 cm^{-1}).

The gaseous products evolved during the thermal degradation of the flame retarded polymer in inert conditions are the same than those evolved by the pure polymer and the pure ATH-OP1230 combination. There is no evidence of chemical interaction between the flame retardant combination and the polymer according to the gas phase analysis.

2.2.4 Vulcanized EVM-ATH-OP1230 interactions

The interpretations about the condensed and gas phase analyses allow the drawing of a global degradation scheme of vulcanized EVM flame retarded with the aluminium trihydroxide- phosphinate combination *(Fig. 148)*.

It is assumed that the polymer and ATH degrade at the same time: ATH dehydrates into alumina while the vulcanized EVM releases acetic acid by deacetylation process, thus forming polyenes. At this degradation stage are present in the matrix polyenes, aluminium diethyl phosphinate and alumina. These compounds thus decompose, evolving phosphorous-based compounds in the gas phase (phosphinic acid, sublimated phosphinate and phosphonate are suspected) and the degradation products of the ethyl groups of the phosphinate, that is to say ethene and but-2-ene. The degradation of the polymer results in the release of ethylenic compounds. In the condensed phase were detected phosphonic, phosphinic, diphosphinic acid, alumina and some carbonaceous residue.

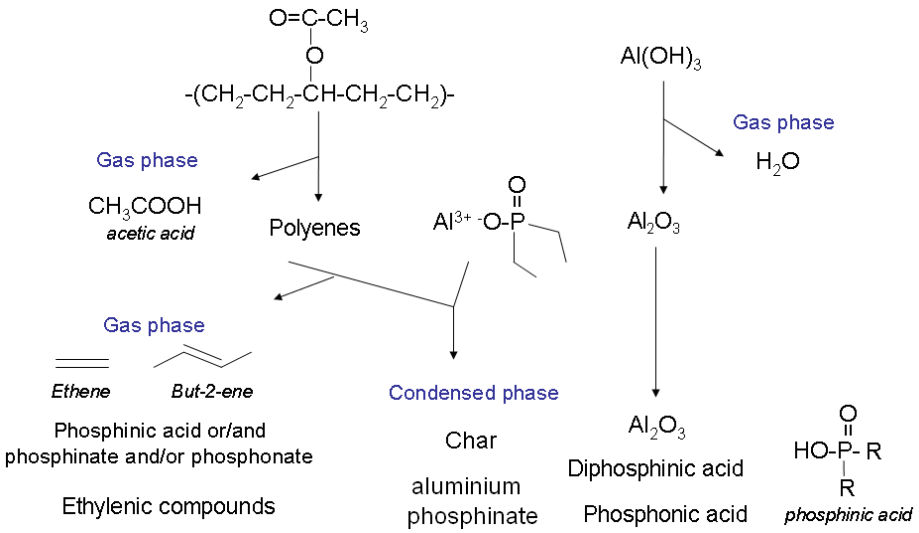


Fig. 148: Degradation scheme of vulcanized EVM flame retarded with the ATH-OP1230 combination

The degradation of the flame retardant combination in the polymer does not provide the same products than heated alone. Indeed, a wider range of phosphorous-based compounds are obtained for the polymeric formulation, whereas the pure additive mixture (ATH+OP1230) only provides phosphonic acid and aluminophosphates. However, the compounds produced by the degradation of

the polymeric matrix are the same as those produced by the pure polymer. The main difference concerns the temperatures of degradation, which are shifted to lower values.

2.3 Conclusion on the matrix-additives interactions

The thermal decomposition mechanism of vulcanized EVM flame retarded with OP1230 has been determined. It was found that the evolution of the OP1230 in vulcanized EVM is identical to the decomposition of OP1230 alone, that is to say it leads to the formation of aluminophosphonate (composed of octahedral aluminium and phosphonate groups) and aluminophosphate. It is noticeable that the additive sublimates in the material during thermal degradation, and goes through the porosities of the material to form OP1230 aggregates which are trapped in the matrix. Some OP1230 is also detected in the gas phase. The main interaction occurs between the cited compounds and the polymer, leading to the catalysis of the polyenes degradation. The incorporation of OP1230 is thus detrimental to the thermal stability of the polymer.

The thermal degradation of the polymer containing ATH and OP1230 has been also investigated, revealing the effect of the additives on the decomposition of the matrix. The presence of ATH induces the production of several phosphorus-based products (diethyl phosphinic, diphosphinic and ethyl phosphonic acid) which provoke a thermal destabilization of the formulation. But on the contrary to the EVM/OP1230 formulation the char degradation is not promoted. On the other hand, it is noteworthy that the dehydration of ATH occurs simultaneously with the polymer deacetylation, and at a temperature higher than expected.

The interactions between the polymer and the additives have been pointed out, but revealed no positive effect of the additives on the char formation or on the thermal stability of the material. The aim of the next section is now to correlate these results (that is to say the beneficial role of the interactions) with the flame retardant behaviour of vulcanized EVM flame retarded with the ATH-OP1230 combination, and to investigate the potential physical role of the combination, for example a modification of the protective effect of the barrier created when the material burns.

3. Relationship between ATH-OP1230-EVM interactions and flame retardant properties

The structure of the materials during combustion was studied in addition to the analyses done on materials prepared by heat treatment.

To reproduce fire scenario conditions, the flame retarded formulations were submitted to mass loss calorimeter experiments at an external heat flux of 35 kW/m² (corresponding to a mild fire). The combustion residues are collected at characteristic times, as reported in *Fig. 149*. The materials flame retarded with OP1230 and ATH/OP1230 were collected respectively at 45 and 95 s (just before the ignition), at 115 and 220 s (at the peak of RHR) and at the end of the combustion (at 600 s).

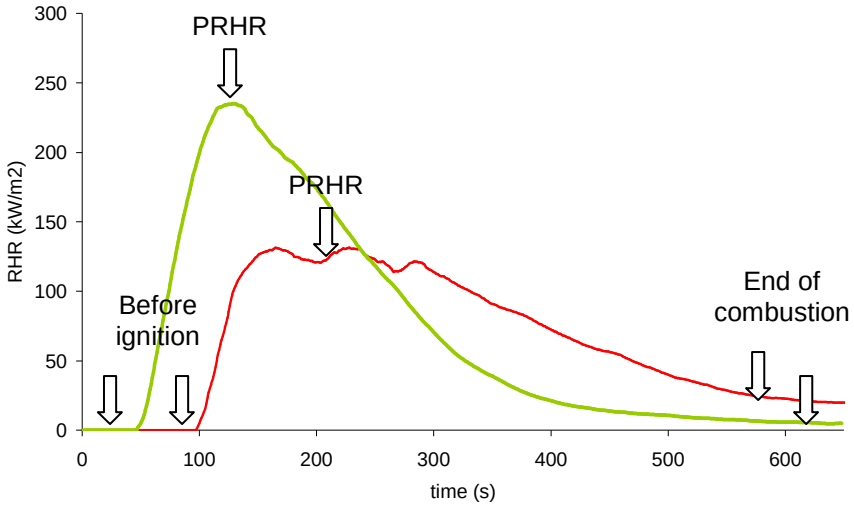


Fig. 149: RHR curves of the vulcanized EVM/OP1230 (in green) and EVM/ATH/OP1230 (in red) formulations

The residues are presented in *Fig. 150* and *Fig. 151*. When exposed to heat the surface of the samples become black brownish, and some bubbles are noticeable for the formulation containing ATH and OP1230. At the PRHR the difference between the two samples is huge since it only remains a thin fragile greyish layer for the material with OP1230 whereas the polymer is quite preserved, covered by a grey thick layer when the two additives, ATH and OP1230, are used. At the end of combustion it only remains for EVM flame retarded with OP1230 a low amount of black/grey residue, constituted of thin fragile layers which are completely destroyed. On the contrary the material containing the flame retardant combination exhibits a thick black greyish residue exhibiting a better cohesion.



Fig. 150: Mass loss calorimeter residues of vulcanized EVM/OP1230 collected before ignition (a), at PRHR (b) and at the end of combustion(c)



Fig. 151: Mass loss calorimeter residues of vulcanized EVM/ATH/OP1230 collected before ignition (a), at PRHR (b) and at the end of combustion(c)

The upper parts of the residues (the black surface for the samples collected before ignition) were first analyzed by XRD. It was not possible to obtain the diffractograms for the vulcanized EVM/ATH/OP1230 formulation before ignition and at PRHR, because of the elastomeric behaviour of the residues which did not permit to obtain a powder-like sample (the experiment is only possible with a perfectly flat sample, made of homogeneous powder). However, the XRD diffractograms obtained for the other samples are gathered in *Fig. 152*.

The signal of high intensity at 18° corresponds to the diffraction ray of Teflon, used as sample holder. It is thus not to be considered. The diffractograms of the vulcanized EVM/OP1230 formulation shows an evolution of the structure of the material during combustion. The signals of the sample collected at 45 s at 9, 19, 20, 21.5, 24, 26, 27, 31.5 and 38° are attributed to OP1230. The other peaks (42 and 67°) cannot be attributed with the database at our disposal. The diffractograms of the sample at PRHR shows the appearance of pre-graphitic carbon (broad band around 20- 25° [171]). The formation of aluminophosphate $AlPO_4$ (bands at 20, 21.5, 30, 35.5, 38°) and the presence of OP1230 might be also suspected, but the poor quality of the background signal does not allow precise characterization. At the end of the combustion, there is no great evolution of the crystallographic structure: the same species are present in the material.

Concerning the EVM/ATH/OP1230 mixture, it appears that the residue obtained at the end of combustion exhibits the same crystallographic structure as the EVM/OP1230 sample collected before ignition. The presence of OP1230 in the material can thus reasonably be assumed. Alumina is not detected on the diffractogram, because of its amorphous structure.

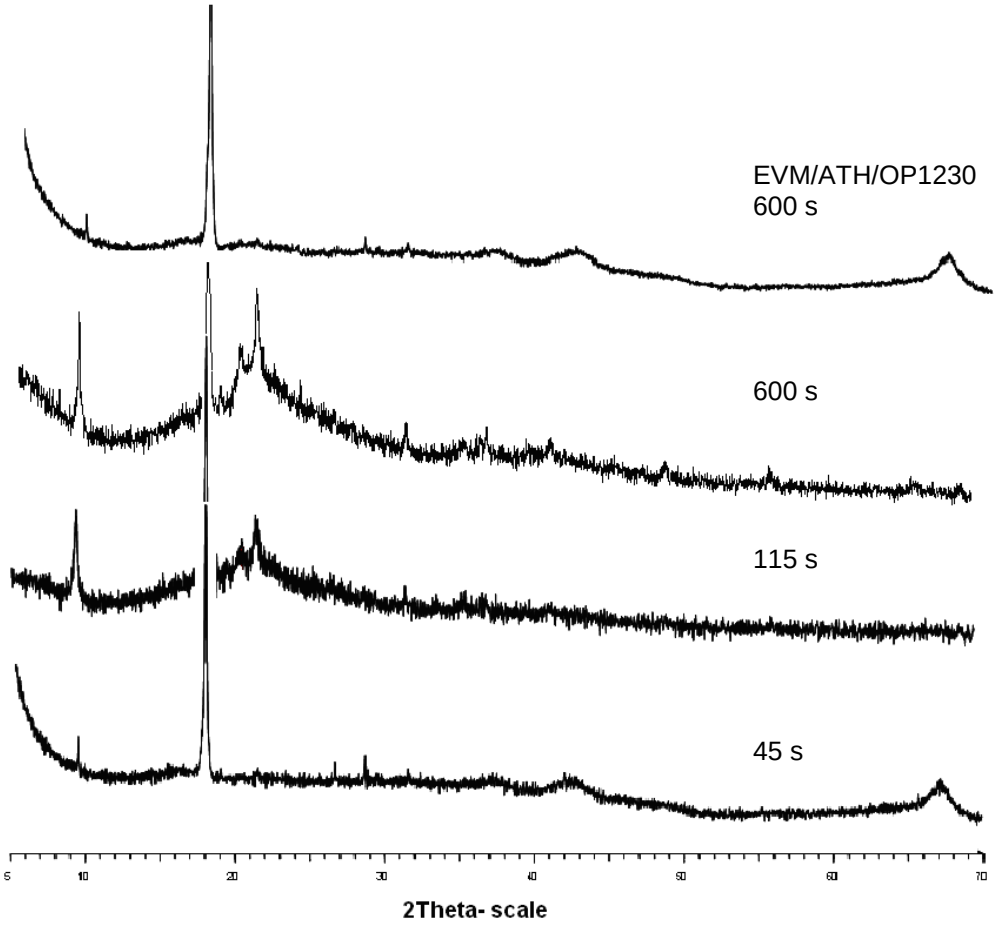


Fig. 152: XRD diffractograms of vulcanized EVM-OP1230 combustion residues (from bottom to top: before ignition, at PRHR, end of combustion) and EVM/ATH/OP1230 end of combustion residue

The species identified in the combustion residues of the EVM/OP1230 formulation are consistent with the established degradation mechanism, that is to say the formation of aluminophosphate and the sublimation of OP1230. On the contrary to the materials heat treated in an oven, some char (resulting from the OP1230 and/or from the polymer degradation) is noticeable in the final burnt residue. According to the visual observations on the collected samples, it can be proposed that the EVM/OP1230 formulation, when exposed to heat, degrades on its upper surface to form a black thin layer (supposed to be charred carbonaceous compounds). According to the thermal degradation of this formulation, OP1230 is supposed to migrate (by sublimation through the porous degraded polymer) to form aggregates in the sample. The evolution is the same for the material flame retarded with ATH and OP1230, but additionally some ”bubbles” are noticeable at the surface *(Fig. 153)*. These bubbles are attributed to the simultaneous deacetylation of the polymer and endothermic dehydration of aluminium trihydroxide. The surface of the sample is then cooled by this endothermic dehydration (explaining the higher time to ignition observed for this formulation), and the gas trapped in the bubbles can play a role in terms of flame retardancy. Indeed, the thermal conductivity of gases is lower than those of liquids and solids and the resulting material exhibit a foamed structure with low heat conductivity playing the role of heat barrier. Moreover when the bubbles break, water is evolved and further dilutes the flame-feeding gases.

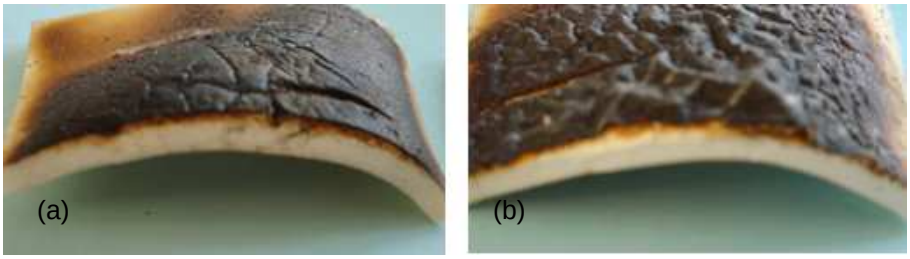


Fig. 153: Transversal view of the vulcanized EVM/OP1230 (a) and EVM/ATH/OP1230 (b) residues collected before ignition

After ignition, the material containing OP1230 then degrades with releasing the phosphinate at its surface (explaining the frost-like grey powder on the residue) and forms a layer composed of crystallized aluminophosphate and some char. Since no residue remains at the end of combustion, and since the structure of the residue is unmodified, it can be supposed that the cohesion of this layer is too poor to plays a protective role, so that it is rapidly degraded: its effect is limited to the very beginning of the combustion. The layer is then degraded continuously when burning; a novel layer is formed and degraded, up to a quite complete degradation of the sample. The sublimation of OP1230, which "migrates" to the surface, also provides a flame retardant effect in the gas phase, as a phosphorus tank. The degradation of the material in fire conditions can thus be schemed as presented in *Fig. 154*.

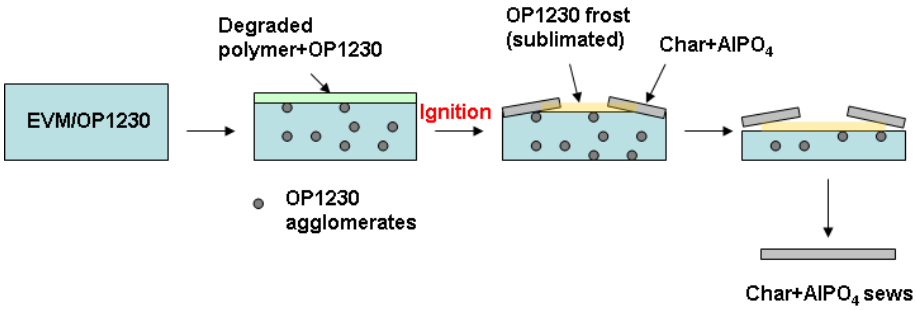


Fig. 154: Schematic evolution of the structure of the vulcanized EVM/OP1230 formulation in fire conditions

Concerning the formulation flame retarded with the synergistic combination of ATH and OP1230, it exhibits a similar type of protection since of protective layer is formed during combustion. On the contrary to the burnt EVM/OP1230 sample, the created layer is thick and resistant, and the integrity of the underlying material is mainly conserved. The composition of this layer is supposed to be aluminium phosphinate and amorphous alumina, plus some phosphorous-based acidic species (phosphinic, diphosphinic and/or phosphonic acid). When compared to the PRHR residue obtained for the vulcanized EVM/ATH sample *(Fig. 155)* which is constituted of ATH "platelets" stacked to each other, the residue of the EVM/ATH/OP1230 sample appears more cohesive since it is not made of assembled single elements but of a homogenous ceramic structure. The phosphorous compounds and ATH are thus combined in a ceramization process leading to the formation of the glassy (transparent in XRD) but porous structure. This layer insulates the underlying material from the heat source.

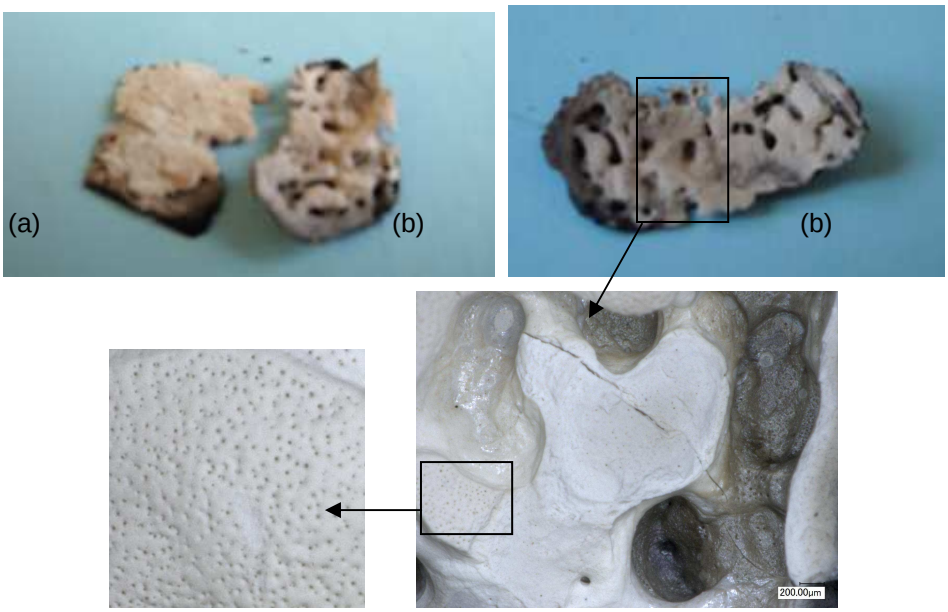


Fig. 155: Upper layer of the residues collected at PRHR of vulcanized EVM/ATH (a) and EVM/ATH/OP1230 (b)

Concerning the expected phosphonic, phosphinic and diphosphinic acids, it can be reasonably supposed that at the high temperatures reached during combustion they are released in the gas phase, thus providing a flame inhibition effect as suggested by Braun *et al.* [124].

The protective layer formed during combustion has high mechanical resistance, but exhibits some holes through all its surface, due to the "bubbles" cited previously. The isolative role is maintained, but the "gas filtration" role, reducing the amount of flammable gases evolved during combustion (and thus feeding the flame) is limited. Nevertheless, tortuosity resulting from this structure makes the gas evolution more difficult and longer. The gaseous compounds are evolved less rapidly, the flame feeding is limited and the combustion is slowed down. This can be correlated to the "plateau shaped" RHR curve obtained for the formulation.

At the end of combustion, it only remains the glassy structure and some carbonaceous residue (plus maybe some frost-like OP1230 according to the XRD analyses). The degradation can be resumed as follows *(Fig. 156)*.

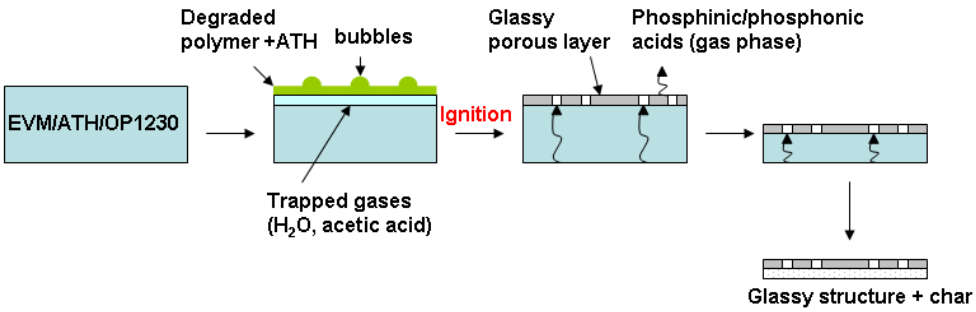


Fig. 156: Schematic evolution of the structure of the vulcanized EVM/ATH/OP1230 formulation in fire conditions

4. Conclusion

This chapter investigated the flame retardant mechanism of the aluminium trihydroxide- aluminium diethyl phosphinate combination.

The suspected chemical interactions occurring between the two additives during their thermal degradation (in pyrolysis conditions), have been identified. It was found that the chemisorption of the phosphinate on ATH and alumina modifies its degradation pathway.
The interactions between the additives and the polymeric matrix were also investigated by the characterization of the thermal degradation residues of the flame retarded samples. If the phosphinate has a negative interaction with the cured polymer (its degradation is favored in presence of OP1230), the ATH/OP1230 combination increases the thermal stability of the material at the very beginning of its degradation. Then a thermal destabilization occurs. A gas phase action is also suspected with the release of phosphinic and/or phosphonic acid, inhibiting the flame

Finally, the study of the combustion residues of the materials submitted to fire conditions through mass loss calorimeter tests, combined to the determined degradation pathway of the formulations, allowed to propose a mechanism of action for the flame retardant additives in vulcanized EVM. In both cases (OP1230 used alone and the ATH/OP1230 combination) a protective barrier is formed, but the mechanical resistance of the aluminophosphate $AlPO_4$ layer in the case of EVM/OP1230 is not sufficient to insulate the underlying material, which degrades further. For the OP1230/ATH combination, a porous resistant glassy structure is formed, limiting the release of flame feeding gases and providing a heat barrier to the underlying polymer. Moreover a gas phase action, such as for the formulation filled with OP1230, can occur with the release of phosphinic, diphosphinic and/or phosphonic acid.

GENERAL CONCLUSION - OUTLOOK

GENERAL CONCLUSION

This work was devoted to the development of a flame retarded EVM-based formulation for cables or for transportation applications, and to the understanding of the flame retardancy mechanisms.
Flame retarded EVM vulcanizates are currently available on the market, but the conventional FR additive, aluminium trihydroxide, is used in relatively high quantity to be efficient. It is detrimental to the mechanical properties of the resulting material, especially to the hardness. The challenge of this work was to develop a fire resistant material, maintaining the flame retardant and mechanical performances of the formulations containing ATH but presenting a lower hardness.

To find satisfying substitutes to ATH, a screening of the flame retardant additives was first performed. Different flame retardant additives families were evaluated through LOI, UL-94 and mass loss calorimeter. Firstly, flame retardant additives were used separately in the complete commercial formulation, to determine what type of compound would be valuable. The testing of metal hydroxides, phosphorous-based compounds, melamine derivatives and graphite-type flame retardants allowed the selection of some interesting additives: ATH thanks to its low price and high efficiency, and phosphinate-based compound (OP1230) which in particular showed promising fire properties. Secondly, the use of nano-additives was envisaged, but did not provide significant improvement. Finally, the last approach consisting in combining additives allowed designing a novel flame retardant combination (ATH and OP1230), exhibiting superior flame retardancy compared to the formulation containing only ATH, and a low hardness, with regard to the mechanical properties.

The industrial challenge was achieved: developing an efficient flame retardant formulation with lower hardness but high mechanical properties. The next step consisted in having a better understanding of the flame retardant mechanisms. Before investigating the synergism between ATH and the phosphinate OP1230, the flame retardant role of ATH was investigated. The mechanism was revisited by a kinetic approach of the thermal degradation of the EVM/ATH formulation in oxidative and pyrolytic conditions, associated with the investigation of the evolution of the material in simulated fire conditions. The methodology which was followed allowed the complete description of the mode of action of ATH. It was found that the generally assumed one, widely described in the literature, as a “cooling effect” due to the endothermal dehydration of ATH, is not as simple as expected. Indeed, it was shown that the formation during combustion of a protective alumina structure also takes part in the flame retardant efficiency of the additive.

The understanding of the flame retardant mechanism of the novel combination (ATH + phosphinate) is a major concern of this work. Chemical interactions, between additives and/or between an additive and the polymer are generally responsible for the high level of flame retardancy of polymeric formulations. The protocols we implemented were thus dedicated to the detection and characterization of such interactions. The systematic characterization of the thermal degradation of the ATH-OP1230

combination (in pyrolysis conditions) and that of EVM/OP1230 and EVM/ATH/OP1230 formulations allowed pointing them out.

It was found that the chemisorption of the phosphinate on ATH and alumina modifies its degradation pathway. Concerning the polymer-additives interactions, they are suspected to lead to a flame retardant gas phase action with the release of phosphinic and/or phosphonic acid, inhibiting the flame. Nevertheless, some physical interactions are involved in the flame retardant process, as confirmed by the examination of the combustion residues of the materials submitted to fire conditions through mass loss calorimeter tests. In both cases (OP1230 used alone and the ATH/OP1230 combination) a protective barrier is formed, but the mechanical resistance of the aluminophosphate $AlPO_4$ layer in the case of EVM/OP1230 is not sufficient to insulate the underlying material, which degrades further. For the OP1230/ATH combination, a porous resistant glassy structure is formed, limiting the release of flame feeding gases and providing a heat barrier to the underlying polymer.

OUTLOOK

Many questions have arisen all along this dissertation. The ATH mode of action was fully described, but some interrogations remains about the influence of the particle size. Indeed the flame retardancy of vulcanized EVM is improved when the particle size of ATH decreases, down to a limit of 0.9 µm (for which no supplementary improvement is observed). It is noteworthy that the “nano” aspects were not investigated, because of the high additive loadings which do not allow nano-dispersion. An interesting outlook would be to elucidate the reasons of these modifications based on the determined mechanism of action of ATH.

The phosphinate OP1230 was found efficient in combination with ATH. Nevertheless this additive generates high amounts of smoke during combustion, as reported in *Chapter 3*. During the screening of the additives, it has been demonstrated that the combination of OP1230 with melamine borate MB significantly reduces the smoke release during combustion. It will be thus interesting to determine what is the smoke suppression mechanism. This aspect could be a novel development axis.

The following part will propose, with the aim to try to understand the relationship between ATH particle size and flame retardant efficiency, some research axes. Then, as a second outlook, a protocol to investigate the smoke suppression mechanism of melamine borate on phosphinate will be proposed.

1. Influence of ATH particle size and dispersion on the thermal degradation and on flame retardant properties of vulcanized EVM

It has been shown that decreasing ATH particle size down to a limit of 0.9 µm leads to an improvement of the flame retardant properties of cured EVM/ATH formulations. Two hypotheses are proposed. The first one supposes that the decreasing ATH particle size induces an effect on the degradation of the vulcanized polymer. To investigate this hypothesis it is suggested to:

- perform TG analyses on the EVM/ATH systems
- model the kinetics of the degradation

The second one proposes an influence of the ATH particle size on the dispersion of the filler, and thus on the protective structure formed during combustion since it is known that the quality of dispersion is a governing parameter for mechanical and flame retardant properties of materials [73, 191]. For that it is necessary to:

- evaluate the efficiency of a dispersing aid (stearic acid for example) in terms of flame retardancy (LOI, UL-94, mass loss calorimeter)

- characterize the dispersion state of the additive, with and without the dispersant, through SEM,
- compare the protective structures formed in a fire scenario. As described in the dissertation, the combustion residues during mass loss calorimeter tests have to be collected at characteristic burning times, and can thus be observed by SEM
- investigate the dispersion aspects on the influence of the formation of a protective structure, and determine its formation kinetics

Some primary results about these investigations are presented in the following part.

The supposed effect on the degradation (i.e. the possibility that the high specific surface of ATH leads to an increase of the kinetics of degradation) was investigated through thermogravimetric analyses. The derivative TG curves of vulcanized EVM containing the different ATH grades at 130 phr are presented in *Fig. 157*. The first step corresponds to the dehydration of ATH, the second one to the degradation of EVM (loss of acetic acid) and the last one to the degradation and oxidation of the remaining ethylenic chains. It appears that the first degradation peak is not really influenced by the ATH particle size. The second and third peaks attributed to the degradation of EVM are influenced by the ATH specific surface area. It is noticeable that the oxidation rate is greatly increased (+100 %) by the decrease of the ATH particle size.

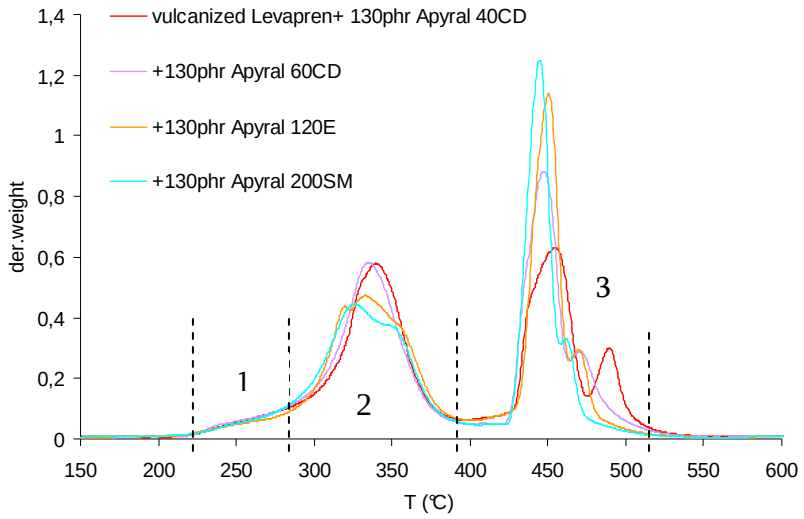


Fig. 157 : Derivative TG curves of vulcanized EVM containing ATH of different particle size, in air (40CD =1.3µm, 60CD= 1.0µm, 120E=0.9µm, 200SM=0.3µm)

Decreasing the ATH particle size allowed an improvement of the UL-94 rating, an increased LOI value and a higher time to ignition *(Table 56)*. These better flame retardant properties can be due to a better quality of dispersion in the polymeric matrix and/or to a catalytic effect on the degradation induced by the higher specific surface area. Derivative TG curves of the formulations showed that the peak attributed to the degradation rate of EVM is greatly increased by the decrease of the ATH particle size. To verify the hypothesis of a catalytic effect a kinetic study was implemented.

Table 56: Cone calorimeter data of vulcanized EVM containing different Apyral grades

	Apyral 40CD	Apyral 60CD	Apyral 120E	Apyral 200SM
Particle size (D_{50}, µm)	1.3	1.0	0.9	0.3
LOI	32	32	35	34
UL-94	V1	V0	V0	V0
Ti (s)	78	72	94	109

The details of the kinetic modeling of the thermal degradation are presented in *Appendix 6*. The obtained kinetic parameters are gathered in *Table 57*.

The five steps of the thermal degradation of ATH-containing vulcanized EVM exhibit similar activation energy Ea or pre-exponential factor logA, whatever the particle size of the filler. The first and the second steps present pre-exponential factor around 10 and activation energies around 130 kJ/mol. The third and the fourth steps of the thermal degradation are characterized by a logA about 15 and activation energies of respectively 200 and 250 kJ/mol. The only exception concern the formulation with the 60CD grade which exhibit lower values, around 11 for the pre-exponential factor and 180 kJ/mol for Ea.

The last step presents the lowest logA values (around 5) and an activation energy of 100 kJ/mol.

Table 57: Kinetic parameters of the thermo-oxidative degradation of vulcanized EVM flame retarded with various ATH grades

		Log A (s^{-1})	Ea (kJ/mol)		Log A (s^{-1})	Ea (kJ/mol)
40CD	Step 1	9.84 ± 0.05	126 ± 1	60CD	9.4 ± 0.05	119 ± 1
	Step 2	12.1 ± 0.1	156 ± 2		8.1 ± 0.05	117 ± 1
	Step 3	16.7 ± 0.8	232 ± 8		10.8 ± 0.2	174 ± 5
	Step 4	15.50 ± 0.02	245 ± 4		11.6 ± 0.2	184 ± 3
	Step 5	4.7 ± 0.2	106 ± 3		4.5 ± 0.3	102 ± 2
120E	Step 1	10.05 ± 0.05	125 ± 1	200SM	10.0 ± 0.1	124 ± 1
	Step 2	9.18 ± 0.05	129 ± 1		9.1 ± 0.2	129 ± 1
	Step 3	15.3 ± 0.2	211± 2		13.2 ± 0.3	205 ± 2
	Step 4	16.5 ± 0.2	255 ± 2		14.9 ± 0.3	231 ± 4
	Step 5	2.4 ± 0.2	71 ± 6		4.8 ± 0.3	98 ± 4

According to these results, the modification of the ATH particle size does not significantly influence the thermal degradation kinetics of the flame retarded vulcanized EVM. The first hypothesis to explain the increased flame retardant efficiency of low particle size ATH is not valid.

The second hypothesis, dealing with the modification of the morphology of the material versus the ATH dispersion quality, is then evaluated. The dispersion of ATH was investigated through scanning electron microscopy (SEM). To obtain the cross-section of the samples, they were immerged in liquid

nitrogen and frozen to avoid deformation during the fracture. The obtained pictures are presented in *Fig. 158*.

Apyral 40CD *(a)* presents some agglomerates in the polymer. Moreover it seems to induce some porosity in the material. Indeed the observation of the sample at higher magnification *(b)* reveals the presence of some micro-holes, larger than the ATH particle size, and thus not due to the imprint of the fillers particles. Apyral 60CD *(c),* 120E *(d)* and 200SM *(e)* in vulcanized EVM appear to be fine and well dispersed in the polymeric matrix, since the particles homogeneously cover the surface of the sample. The sample containing the 120E grade at 130phr *(d)* presents some little ATH agglomerates, but this phenomenon is endemic.

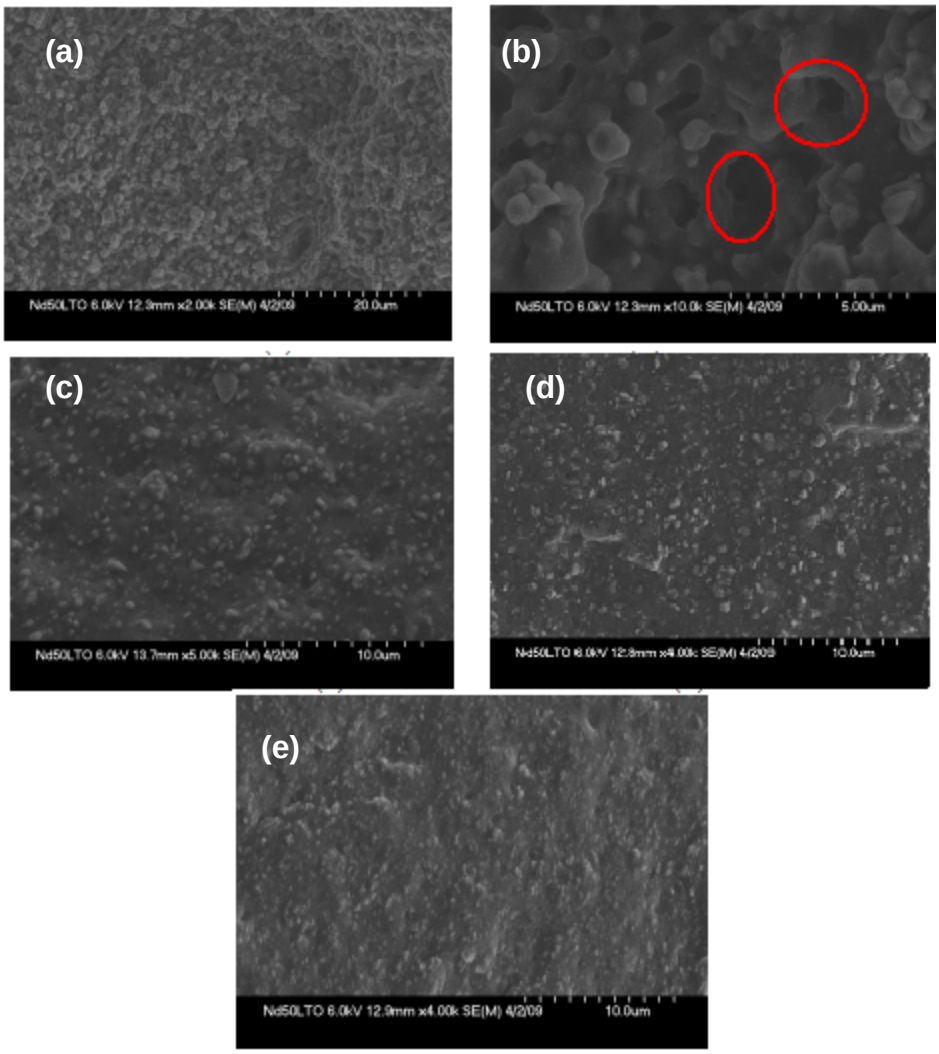


Fig. 158 : SEM images of vulcanized Levapren containing 130phr ATH, (a) Apyral 40CD, (b) same view at a smaller scale, (c) Apyral 60CD, (d) Apyral 120E, (e) Apyral 200SM

The supposed porosity induced by 40CD could be linked to the poorer flame retardant properties in comparison with the other grades. The other ATH types seem well-dispersed in the polymeric matrix but the observed morphology is not the same for all grades.

To conclude on the influence of the dispersion on the creation of a protective alumina structure (as demonstrated in *Chapter 4*), it would be interesting to use a dispersing aid and to characterize the dispersion state not only at t=0 but also its evolution from t=0 up to the ignition. Moreover, the structure of the residue of mass loss calorimeter tests should be studied.

2. Smoke suppressant mechanism of the OP1230-melamine borate combination in vulcanized EVM

The phosphinate OP1230 generates high amounts of smoke during combustion. During the screening of the additives, it has been demonstrated that the combination of OP1230 with melamine borate MB significantly reduces the smoke release during combustion. It is thus interesting to determine what is the smoke suppression mechanism.

To characterize this mechanism, two aspects should be taken into account. Indeed, the reactions occurring in the condensed phase between the additives can affect their thermal degradation and then the gaseous compounds emitted thereof. In the gas phase, some reactions between the cited gaseous compounds can lead to a reduction of soots production. It is thus necessary to study the reactions in the condensed as well as the gas phase.
The preliminary investigations we propose consist in the determination of the thermal degradation mechanism of the OP1230-MB combinations in EVM, to determine how borates reduce soot formation by:

- TGA to determine the heat treatment characteristic temperatures, in inert conditions
- TGA-FTIR analyses to determine the evolved species (can be completed by TGA-GCMS)
- Thermal treatments, XRD, solid state NMR and RAMAN spectroscopy to follow the evolution of the structure of the residues
- Determination of a thermal degradation mechanism and of chemical interactions

The goal is to understand how soots are formed during the polymer degradation, and how the incorporation of the melamine borate interferes with this formation.

The thermo-oxidative degradation of OP1230 is known to be not reproducible [170]. Nevertheless, the oxidation may play a role in the smoke suppressant mechanism. To determine the influence of oxygen on the thermal degradation of the combination, we propose to carry out TG experiments (coupled with FTIR) in controlled atmosphere with various oxygen contents. The reproducibility of the analyses will be verified to determine the “limit oxygen quantity” modifying the thermal decomposition mechanism of the combination. The planned investigations are:

- carrying out TGA in controlled atmospheres
- following the gas phase evolution by TGA-FTIR
- following the evolution of the condensed phase by thermal treatments analyzing the heat treated residue using adapted spectroscopic tools (FTIR, solid state NMR…)

- determining the thermo-oxidative behaviour of the combination OP1230+MB

Then, the degradation in fire conditions of the flame retarded formulation EVM/OP1230/MB has to be investigated in fire conditions, through mass loss calorimeter by:

- collecting residues at characteristic burning times
- characterizing them with XRD and solid state NMR (evolution in the condensed phase)
- characterizing the gas phase by smoke chamber test (coupled with FTIR)

These characterizations will then allow the drawing of a smoke suppressant mechanism.

These proposed outlooks could be a step further to the comprehension of the flame retardancy of cured EVM. The determination of the relationship between ATH particle size and flame retardancy efficiency can be an open door to further developments of efficient ATH-based formulations. Moreover, the understanding of the soot formation mechanisms and of the way to reduce their release during combustion could allow to the design of novel smoke suppressant additives and combinations.

REFERENCES

1. Trombetta M., Armaroli T., Alejandre A.G., Solis J.R., and Busca G. (2000) *An FT-IR study of the internal and external surfaces of HZSM5 zeolite*, Applied Catalysis A: General. 192:125-136.
2. Perrin M.W. (1938) *Production of a copolymer of ethylene and vinyl acetate*, ICI
3. Perrin M.W. (1938) *The influence of hydrostatic pressure on reaction velocity*, Transactions of the Faraday Society. 34:144-153.
4. Burkhart R.D.,Zutty N.L. (1963) *Copolymerization studies. III. Reactivity ratios of model ethylene copolymerizations and their use in Q-e calculations*, Journal of Polymer Science Part A: General papers. 1:1137-1163.
5. Erussalimsky B., Tumarkin N., Dunthoff F., Lyobetzky S., and Goldenberg A. (1967) Makromol. Chem. 104:288.
6. Rätzsch M., Schneider W.,Musche D. (1971) *Reactivity of ethylene in the radically initiated copolymerization of ethylene with vinylacetate*, Journal of Polymer Science Part A-1: Polymer Chemistry. 9:785-790.
7. Leder F.,Wisotsky M.J. (1972) *Effect of fluid-phase equilibria on ethylene-vinyl acetate copolymer composition*, Journal of Polymer Science Part A-1: Polymer Chemistry. 10:447-454.
8. Wu T.K., Ovenall D.W.,Reddy G.S. (1974) Journal of polymer Science, Polymer Physics Edition. 12:901.
9. Zutty N.L., Faucher J.A.,Bonotto S., in Encyclopedia of Polymer Science and Technology, H.F. Mark, Editor. 1967, John-Wiley and Sons: New York
10. Wisotsky M.J., Kober A.E.,Zlochower I.A. (1971) *Copolymerization of ethylene with vinyl acetate. I. Effect of polymerization temperature on degree of branching*, Journal of Applied Polymer Science. 15:1737-1742.
11. EP0453205, Saga K.,Naito Y. (1990) *Process for producing polyolefin*, Tosoh Corp.
12. Gilby G.W., *Thermoplastic rubbers*, in Development in rubber technology. 1982, Applied Science Publishers: London
13. US 3325460, Schellenberg W.D.,Bartl H. (1967) *Process for the continuous preparation of ethylene/vinyl acetate copolymers using serially arranged reaction zones*, Bayer AG
14. EP0307755, Bartl H. (1989) *Process for the preparation of ethene/vinyl acetate copolymers, ethene/vinyl acetate copolymers and their use*, Bayer AG
15. EP 0341499, Wolf B.,B.Will (1989) *Solution polymerization for the preparation of gel-free copolymers of ethylene and vinyl acetate.* , Bayer AG
16. EP 0374664, Sutter H.,Kolwert A. (1990) *Process for the manufacture of copolymers of ethylene and vinyl acetate, copolymers of ethylene and vinyl acetate, and use thereof*, Bayer AG
17. US 4485225, Satoh K.,Yonezu K. (1983) *Method for continuous copolymerization of ethylene and vinyl acetate*, Kuraray Co.
18. EP 0136559, Tanaka J.,Matsumoto K. (1985) *Process for continuous production of ethylene-vinyl acetate copolymer*, Kuraray Co
19. EP 0495495, Hisamichi Y.,Takanori K. (1992) *Process for producing ethylenevinyl ester copolymers, process for producing ethylene-vinyl alcohol copolymers and process for producing shaped articles*, Kuraray Co
20. Scott P.J., Penlidis A.,Rempel G.L. (1992) *Ethylene-vinyl acetate semi-batch emulsion copolymerization: Experimental design and preliminary screening experiments*, Journal of Polymer Science Part A: Polymer Chemistry. 31:403-426.
21. Zhang Y., Yu H.,Ren W. (2009) *Ethylene-vinyl acetate copolymers toughen nylon 1010*, Plastics Research online.
22. Meisenmeier H.,Zens A., *Ethylene Vinyl Acetate Elastomers (EVM)*, in Handbook of Specialty Elastomers, R.C. Klingender, Editor. 2008, CRC Press
23. Azom. http://www.azom.com.
24. Leszczynska A., Njuguna J., Pielichowski K., and Banerjee J.R. (2007) *Polymer/montmorillonite nanocomposites with improved thermal properties. Part II. Thermal stability of montmorillonite nanocomposites based on different polymeric matrixes*, Thermochimica Acta. 454:1-22.
25. Meisenheimer H.(2001) *Ethylene-Vinyl Elastomers (EVM) for Improved Safety in Mass Transit*. in Rapra Conference Proceedings, conference Location

26. Rimez B., Rahier H., Van Assche G., Artoos T., and Van Mele B. (2008) *The thermal degradation of poly(vinyl acetate) and poly(ethylene-co-vinyl acetate), Part II: Modelling the degradation kinetics*, Polymer Degradation and Stability. 93:1222-1230.
27. Rimez B., Rahier H., Van Assche G., Artoos T., Biesemans M., and Van Mele B. (2008) *The thermal degradation of poly(vinyl acetate) and poly(ethylene-co-vinyl acetate), Part I: Experimental study of the degradation mechanism*, Polymer Degradation and Stability. 93:800-810.
28. Simon P.,Ryba¡r M. (1992) *Kinetics of polymer degradation involving the splitting off of small molecules: Part 8. Thermal degradation of polyvinyl esters*, Polymer Degradation and Stability. 38:255-259.
29. Henning S.K. (2008) *Use of coagents in the radical cure of elastomers*, Wire & Cable Technology International. 36:
30. Boye W.M. (2009) *Utilizing coagents in the electron beam cure of elastomers*, Rubber World. 241:38-43.
31. Henning S.K.(2007) *The use of coagents in the radical cure of elastomers*. in 56th IWCS Conference - Proceedings of the International Wire and Cable Symposium, Inc., IWCS 2007, conference Location
32. Datta R.N.,Huntink N.M., *Degradation and Protection*, in Current Topics in Elastomers Research, A.K. Bhowmick, Editor. 2008, CRC Press
33. Harmsworth N., Abts G.,Moakes C.A. (1996) *Improvement in the ozone resistance of elastomers with non-staining antioxidants*, KGK-Kautschuk und Gummi Kunststoffe. 49:597-606.
34. Fukahori Y., *Mechanism of the Carbon Black Reinforcement of Rubbers*, in Current Topics in Elastomers Research, A.K. Bhowmick, Editor. 2008, CRC Press
35. Kohls D.J., Schaeffer D.W., Kosso R., and Feinblum E., *Silica Fillers for Elastomer Reinforcement*, in Current Topics in Elastomers Research, A.K. Bhowmick, Editor. 2008, CRC Press
36. Meisenheimer H.,Zens A., *Ethylene Vinylacetate Elastomers (EVM)*, in Handbook of Specialty Elastomers, R.C. Klingender, Editor. 2008, CRC Press
37. Meisenheimer H. (1993) *Low smoke, non-corrosive fire retardant cable jacket based on HNBR and EVM*, Kautschuk und Gummi Kunststoffe. 463:230-232.
38. Lanxess (2007) *Levapren- the cost effective specialty rubber*
39. Pazur R.J., Richard J.,Meisenheimer H. (2005) *EVM copolymers: the forgotten rubber*, Rubber World.
40. Park Y.J., Joo H.S., Kim H.J., and Lee Y.K. (2006) *Adhesion and rheological properties of EVA-based hot-melt adhesives*, International Journal of Adhesion and Adhesives. 26:571-576.
41. Rothon R.N.,Hornsby P.R. (1996) *Flame retardant effects of magnesium hydroxide*, Polym. Degrad. Stab. 54:383-385.
42. Bourbigot S., Le Bras M., Leeuwendal R., Shen K.K., and Schubert D. (1999) *Recent advances in the use of zinc borates in flame retardancy of EVA*, Polymer Degradation and Stability. 64:419-425.
43. Horn W.E., in Inorganic hydroxides and hydroxycarbonates: their function and use as flame retardant additives, A.F. Grand and C.A. Wilkie, Editors. 2000, Marcel Dekker Inc: New York
44. Bourbigot S., Le Bras M., Duquesne S., and Rochery M. (2004) *Recent advances for intumescent polymers*, Macromol. Mater. Eng. 289:499-511.
45. Cullis C.F., Hirschler M.M.,Tao Q.M. (1991) *Studies of the effects of phosphorus-nitrogen-bromine systems on the combustion of some thermoplastic polymers*, Eur. Polym. J. 27:281-289.
46. Spence D.,McHale E.T. (1975) *The role of negative halogen ions in hydrocarbon flame inhibition*, Combustion and Flame. 24:211-215.
47. Atwell R. F.W., Stallings A., Termine JP., Enrico J. (1991) *Flame retardant graft copolymers of ethylene vinyl acetate*
48. Troitzch J. (2004) *Plastics flammability handbook*, Hanser,Berlin
49. Clarke F.B. (1999) *Effects of brominated flame retardants on the elements of fire hazard: A re-examination of earlier results*, Fire and Materials. 23:109-116.
50. Rahman F., Langford K.H., Scrimshaw M.D., and Lester J.N. (2001) *Polybrominated diphenyl ether (PBDE) flame retardants*, Science of the Total Environment. 275:1-17.
51. Simon P.L., Scott S.K., Kalliadasis S., and Merkin J.H. (2005) *The effect of a radical scavenger on the propagation of flames in an exothermic-endothermic system*, Journal of Mathematical Chemistry. 38:203-231.

52. Artoos T.(2005) *Degradation mechanism and kinetic of poly(vinylacetate) and poly (ethylene co-vinylacetate): flame retardancy,* Vreij Universiteit Brussels
53. Engineers N.B.o.C. (2009) *Handbook on Textile Auxiliaries, Dyes and Dye Intermediates Technology*, Asia Pacific Business Press Inc.,
54. Yang C.-P.,Chen W.-T. (1988) *EFFECTS OF BROMINATED FLAME RETARDANTS AND CROSSLINKING AGENTS ON THE FLAME RETARDANCY OF RUBBERS*, Journal of Applied Polymer Science. 36:963-978.
55. Smith R., Georlette P., Finberg I., and Reznick G. (1996) *Development of environmentally friendly multifunctional flame retardants for commodity and engineering plastics*, Polymer Degradation and Stability. 54:167-173.
56. Santillo D.,Johnston P. (2003) *Playing with fire: The global threat presented by brominated flame retardants justifies urgent substitution*, Environment International. 29:725-734.
57. Camino G., Maffezzoli A., Braglia M., De Lazzaro M., and Zammarano M. (2001) *Effect of hydroxides and hydroxycarbonate structure on fire retardant effectiveness and mechanical properties in ethylene-vinyl acetate copolymer*, Polymer Degradation and Stability. 74:457-464.
58. Ok J.,Matyjaszewski K. (2006) *Synthesis of magnesium dihydroxide hybrid nanocomposites via ATRP*, Journal of Inorganic and Organometallic Polymers and Materials. 16:129-137.
59. Zhang X., Guo F., Chen J., Wang G., and Liu H. (2005) *Investigation of interfacial modification for flame retardant ethylene vinyl acetate copolymer/alumina trihydrate nanocomposites*, Polymer Degradation and Stability. 87:411-418.
60. Carpentier F., Bourbigot S., Le Bras M., Delobel R., and Foulon M. (2000) *Charring of fire retarded ethylene vinyl acetate copolymer - magnesium hydroxide/zinc borate formulations*, Polymer Degradation and Stability. 69:83-92.
61. Camino G., Riva A., Vizzini D., Amigouët P., Pereira P.B., and Castrovinci A. (2005) *Effect of magnesium hydroxide on fire retardance mechanism of intumescent EVA composition*, The Royal Society of Chemistry,Oxford
62. Grand A.F.,Wilkie C.A., eds. *Fire Retardancy of Polymeric Materials*. 2000, Marcel Dekker Ltd: New York
63. Jiao C.M., Wang Z.Z., Ye Z., Hu Y., and Fan W.C. (2006) *Flame retardation of ethylene-vinyl acetate copolymer using nano magnesium hydroxide and nano hydrotalcite*, J. Fire Sci. 24:47-64.
64. Atkinson P.A., Haines P.J.,Skinner G.A. (2000) *Inorganic tin compounds as flame retardants and smoke suppressants for polyester thermosets*, Thermochimica Acta. 360:29-40.
65. Atkinson P.A., Haines P.J.,Skinner G.A. (2001) *Mechanism of action of tin compounds as flame retardants and smoke suppressants for polyester thermosets*, Polymer Degradation and Stability. 71:351-360.
66. Huang H., Tian M., Liu L., He Z., Chen Z., and Zhang L. (2006) *Effects of silicon additive as synergists of Mg(OH)2 on the flammability of ethylene vinyl acetate copolymer*, Journal of Applied Polymer Science. 99:3203-3209.
67. Fu M.,Qu B. (2004) *Synergistic flame retardant mechanism of fumed silica in ethylene-vinyl acetate/magnesium hydroxide blends*, Polymer Degradation and Stability. 85:633-639.
68. Hull T.R., Quinn R.E., Areri I.G., and Purser D.A. (2002) *Combustion toxicity of fire retarded EVA*, Polymer Degradation and Stability. 77:235-242.
69. Kim S. (2003) *Flame retardancy and smoke suppression of magnesium hydroxide filled polyethylene*, Journal of Polymer Science, Part B: Polymer Physics. 41:936-944.
70. Braun U.,Schartel B. (2004) *Flame retardant mechanisms of red phosphorus and magnesium hydroxide in high impact polystyrene*, Macromolecular Chemistry and Physics. 205:2185-2196.
71. Babushok V.,Tsang W. (2000) *Inhibitor rankings for alkane combustion*, Combustion and Flame. 123:488-506.
72. Le Bras M., Bourbigot S., Delporte C., Siat C., and Le Tallec Y. (1996) *New intumescent formulations of fire-retardant polypropylene - Discussion of the free radical mechanism of the formation of carbonaceous protective material during the thermo-oxidative treatment of the additives*, Fire and Materials. 20:191-203.
73. Bourbigot S.,Duquesne S. (2007) *Fire retardant polymers: Recent developments and opportunities*, Journal of Materials Chemistry. 17:2283-2300.
74. Ducrocq P., Duquesne S., Magnet S., Bourbigot S., and Delobel R. (2006) *Interactions between chlorinated paraffins and melamine in intumescent paint-investing a way to suppress chlorinated paraffins from the formulations*, Progress in Organic Coatings. 57:430-438.

75. Levchik S.V., Levchik G.F., Balabanovich A.I., Weil E.D., and Klatt M. (1999) *Phosphorus oxynitride: A thermally stable fire retardant additive for polyamide 6 and poly(butylene terephthalate)*, Angewandte Makromolekulare Chemie. 264:48-55.
76. Zilberman J., Hull T.R., Price D., Milnes G.J., and Keen F. (2000) *Flame retardancy of some ethylene-vinyl acetate copolymer-based formulations*, Fire and Materials. 24:159-164.
77. Siat C., Bourbigot S.,Bras M.L. (1997) *Thermal behaviour of polyamide-6-based intumescent formulations - A kinetic study*, Polymer Degradation and Stability. 58:303-313.
78. Le Bras M., Bourbigot S.,Revel B. (1999) *Comprehensive study of the degradation of an intumescent EVA-based material during combustion*, Journal of Materials Science. 34:5777-5782.
79. Bugajny M., Bourbigot S., Le Bras M., and Delobel R. (1999) *The origin and nature of flame retardance in ethylene-vinyl acetate copolymers containing hostaflam AP 750*, Polymer International. 48:264-270.
80. 6365071, Jenewein E., Kleiner H., Wanzke W., and Budzinsky W. (2002) *Synergistic Flame Protection Agent Combination for Thermoplastic Polymers*, Clariant GmbH
81. Riva A., Camino G., Fomperie L., and AmigouÃ«t P. (2003) *Fire retardant mechanism in intumescent ethylene vinyl acetate compositions*, Polymer Degradation and Stability. 82:341-346.
82. Gilman J.W., Jackson C.L., Morgan A.B., Harris Jr R., Manias E., Giannelis E.P., Wuthenow M., Hilton D., and Phillips S.H. (2000) *Flammability properties of polymer - Layered-silicate nanocomposites. Polypropylene and polystyrene nanocomposites*, Chem. Mater. 12:1866-1873.
83. Lewin M. (2003) *Some comments on the modes of action of nanocomposites in the flame retardancy of polymers*, Fire Mater. 27:1-7.
84. Gilman J.W., Kashiwagi T., Morgan A.B., Harris R.H, Jr., Brassell L., Awad W.H., Davis R.D., Chyall L., Sutto T., Trulove P.C., and DeLong H.(2001) *Recent advances in flame retardant polymer nanocomposites*. in International SAMPE Symposium and Exhibition (Proceedings), conference Location
85. Leszczynska A., Njuguna J., Pielichowski K., and Banerjee J.R. (2007) *Polymer/montmorillonite nanocomposites with improved thermal properties. Part I. Factors influencing thermal stability and mechanisms of thermal stability improvement*, Thermochim. Acta. 453:75-96.
86. Duquesne S., Jama C., Le Bras M., Delobel R., Recourt P., and Gloaguen J.M. (2003) *Elaboration of EVA-nanoclay systems - Characterization, thermal behaviour and fire performance*, Composites Science and Technology. 63:1141-1148.
87. Beyer G. (2002) *Short communication: Carbon nanotubes as flame retardants for polymers*, Fire Mater. 26:291-293.
88. George J.J.,Bhowmick A.K. (2009) *Influence of matrix polarity on the properties of ethylene vinyl acetate-carbon nanofiller nanocomposites*, Nanoscale Research Letters. 4:655-664.
89. Zhang Z., Lan B., Mei X., and Xu C. (2007) *Study on fire retardant mechanism of nano-LDHs in intumescent system*, Science in China, Series B: Chemistry. 50:392-396.
90. Huang H., Tian M., Liu L., Liang W., and Zhang L. (2006) *Effect of particle size on flame retardancy of Mg(OH)2-filled ethylene vinyl acetate copolymer composites*, J. Appl. Polym. Sci. 100:4461-4469.
91. Lv J.P.,Liu W.H. (2007) *Flame retardancy and mechanical properties of EVA nanocomposites based on magnesium hydroxide nanoparticles/microcapsulated red phosphorus*, J. Appl. Polym. Sci. 105:333-340.
92. Joseph H Koo S.D., Khiet C Ngujen, Jason C Lee, Wai K Ho, Morgan C Bruns, and Ofodike A Ezekoye (2010) *Flammability studies of a novel class of thermoplastic elastomer nanocomposites* J. Fire Sci. 28:
93. Gao F., Beyer G.,Yuan Q. (2005) *A mechanistic study of fire retardancy of carbon nanotube/ethylene vinyl acetate copolymers and their clay composites*, Polym. Degrad. Stab. 89:559-564.
94. Szep A., Szabe A., Teth N., Anna P., and Marosi G. (2006) *Role of montmorillonite in flame retardancy of ethylene-vinyl acetate copolymer*, Polym. Degrad. Stab. 91:593-599.
95. Beyer G. (2006) *Flame retardancy of nanocomposites based on organoclays and carbon nanotubes with aluminum trihydrate*, Polym. Adv. Technol. 17:218-225.
96. Laoutid F., Gaudon P., Taulemesse J.M., Lopez Cuesta J.M., Velasco J.I., and Piechaczyk A. (2006) *Study of hydromagnesite and magnesium hydroxide based fire retardant systems for*

ethylene-vinyl acetate containing organo-modified montmorillonite, Polym. Degrad. Stab. 91:3074-3082.

97. Lanxess (2007) *Portfolio of effective flame retardance Phosphorous compounds for plastics and polyurethanes* in UTECH North America
98. Samyn F., Bourbigot S., Duquesne S., and Delobel R. (2007) *Effect of zinc borate on the thermal degradation of ammonium polyphosphate*, Thermochimica Acta. 456:134-144.
99. Bayer (1971) *Handbuch für die Gummiindustrie*, Verlag W. Kohlhammer GmbH,Stuttgart-Berlin-Köln-Main
100. ASTM (2010) *Durometer Hardness* in D2240 - Standard Test Method for Rubber Property
101. ASTM (2006) *D412 Standard Test Methods for Vulcanized Rubber and Thermoplastic Elastomers*
102. ISO (1996) *4589 Plastiques - Détermination du comportement au feu au moyen de l'indice d'oxygène*
103. UnderwritersLaboratory (2006) *UL-94 Tests for Flammability of Plastic Materials for Parts in Devices and Appliances*
104. ASTM (2009) *E2102- Standard Test Method for Measurement of Mass Loss and Ignitability for Screening Purposes Using a Conical Radiant Heater*
105. Mullens J., Werde K.V., Vanhoyland G., Nouwen R., Bael M.K.V., and Poucke L.C.V. (2002) *The use of TGA-MS, TGA-FTIR, HT-XRD and HT-DRIFT for the preparation and characterization of PbTiO3 and BaTiO3*, Thermochimica Acta. 392:29-35.
106. Chace M.,Prada-Silva G. (1994) *Analysis of polymeric systems by TGA-MS*, American Laboratory. 26:18.
107. Marcilla A., Gomez A.,Menargues S. (2005) *TGA/FTIR study of the evolution of the gases evolved in the catalytic pyrolysis of ethylene-vinyl acetate copolymers. Comparison among different catalysts* Polymer Degradation and Stability. 89:454-460.
108. Wieboldt R.C., Lowry S.R.,Rosenthal R.J. *TGA/FT-IR: Thermogravimetric analysis with fourier transform infrared detection of evolved gases*, Microchimica Acta. 94:179-182.
109. ASTM (2009) *E662 Standard Test Method for Specific Optical Density of Smoke Generated by Solid Materials*
110. Ernst R.R., Bodenhausen G.,Wokaun A. (1987) *Principles of Nuclear Magnetic Resonance in One and Two Dimensions*, Oxford Science Publications,Oxford
111. Gopalakrishnan K.,Bodenhausen G. (2006) *Cross polarization from spins I = 1/2 to spins S = 1 in nuclear magnetic resonance with magic angle sample spinning*, Journal of Chemical Physics. 124:
112. Macomber R.S. (1998) *A complete introduction to modern NMR spectroscopy*, Wiley Interscience,New York
113. Hu B., TrÃ©bosc J.,Amoureux J.P. (2008) *Comparison of several hetero-nuclear dipolar recoupling NMR methods to be used in MAS HMQC/HSQC*, Journal of Magnetic Resonance. 192:112-122.
114. Fu R., Smith S.A.,Bodenhausen G. (1997) *Recoupling of heteronuclear dipolar interactions in solid state magic-angle spinning NMR by simultaneous frequency and amplitude modulation*, Chemical Physics Letters. 272:361-369.
115. Warren B.E. (1990) *X-ray difraction*, Dover Publications,New York
116. Bish D.L.,Post J.E., eds. *Modern Powder Diffraction*, Reviews in Mineralogy, ed. M.S.o. America. Vol. 20. 1989
117. Castaing R., *Electron probe microanalyzer*, in Advances in electronics and electron physics, L. Marton, Editor. 1955, Elsevier
118. Reuter W. (1971) *Electron probe microanalysis*, Surface Science. 25:80-119.
119. Horold S.(1999) *Phosphorus flame retardants for composites*. in International SAMPE Technical Conference, conference Location
120. George J.J.,Bhowmick A.K. (2008) *Ethylene vinyl acetate/expanded graphite nanocomposites by solution intercalation: Preparation, characterization and properties*, Journal of Materials Science. 43:702-708.
121. Cross M.S., Cusack P.A.,Hornsby P.R. (2003) *Effects of tin additives on the flammability and smoke emission characteristics of halogen-free ethylene-vinyl acetate copolymer*, Polymer Degradation and Stability. 79:309-318.
122. Hornsby P.R., Cusack P.A., Cross M., TÃ³th A., Zelei B., and Marosi G. (2003) *Zinc hydroxystannate-coated metal hydroxide fire retardants: Fire performance and substrate-coating interactions*, Journal of Materials Science. 38:2893-2899.

123. Samyn F.(2007) *Compréhension des procédés d'ignifugation du polyamide 6- Apport des nanocomposites aux systèmes retardateurs de flamme phosphorés,* Université de Lille1
124. Braun U.,Schartel B. (2008) *Flame retardancy mechanisms of aluminium phosphinate in combination with melamine cyanurate in glass-fibre-reinforced poly(1,4-butylene terephthalate)*, Macromolecular Materials and Engineering. 293:206-217.
125. Vannier A., Duquesne S., Bourbigot S., Castrovinci A., Camino G., and Delobel R. (2008) *The use of POSS as synergist in intumescent recycled poly(ethylene terephthalate)*, Polymer Degradation and Stability. 93:818-826.
126. Tsai J.L.,Lin Y.A. (2010) *Investigating Particle Effect on Tensile Strength of Particulate Nanocomposites*, Advanced Materials Research 123-125:559-562.
127. 6365071B1, Jenewein E., Kleiner H.-J., Wanzke W., and Budzinsky W. (2002) *Synergistic Flame Protection Agent Combination for Thermoplastic Polymers*, Clariant
128. Samyn P.,Schoukens G. (2008) *On the efficiency of internal lubricants for polymers under different sliding conditions* 126-135.
129. Szep A., Szabo A., Toth N., Anna P., and Marosi G. (2006) *Role of montmorillonite in flame retardancy of ethylene-vinyl acetate copolymer*, Polymer Degradation and Stability. 91:593-599.
130. Beyer G. (2002) *Nanocomposites: a new class of flame retardants for polymers*, Plastics, Additives and Compounding. 4:22-28.
131. Cárdenas M.A., García-López D., Gobernado-Mitre I., Merino J.C., Pastor J.M., Martínez J.d.D., Barbeta J., and Calveras D. (2008) *Mechanical and fire retardant properties of EVA/clay/ATH nanocomposites - Effect of particle size and surface treatment of ATH filler*, Polymer Degradation and Stability. 93:2032-2037.
132. Fina A., Tabuani D., Carniato F., Frache A., Boccaleri E., and Camino G. (2006) *Polyhedral oligomeric silsesquioxanes (POSS) thermal degradation*, Thermochimica Acta. 440:36-42.
133. Marin M.L., Jimenez A., Lopez J., and Vilaplana J. (1996) *Thermal degradation of ethylene (vinyl acetate). Kinetic analysis of thermogravimetric data*, Journal of Thermal Analysis. 47:247-258.
134. Maurin M.B., Dittert L.W.,Hussain A.A. (1991) *Thermogravimetric analysis of ethylene-vinyl acetate copolymers with Fourier transform infrared analysis of the pyrolysis products*, Thermochimica Acta. 186:97-102.
135. Stael G.C.,Tavares M.I.B. (1997) *NMR carbon-13 high resolution study of poly(ethylene-co-vinyl acetate)*, Polymer Testing. 16:193-198.
136. Delfini M., Segre A.L.,Conti F. (1973) *Sequence Distributions in Ethylene-Vinyl Acetate Copolymers. I. 13C Nuclear Magnetic Resonance Studies*, Macromolecules. 6:456-459.
137. Tang J., Mohan T.,Verkade J.G. (1994) *Selective and Efficient Syntheses of Perhydro-1,3,5-triazine-2,4,6-triones and Carbodiimides from Isocyanates Using ZP(MeNCH2CH2)3N Catalysts*, The Journal of Organic Chemistry. 59:4931-4938.
138. Grant D.M.,Paul E.G. (1964) *Carbon-13 magnetic resonance. II. Chemical shift data for the alkanes*, Journal of the American Chemical Society. 86:2984-2990.
139. Duncan T.M. (1990) *A Compilation of Chemical Shift Anisotropies*, Farragut Press,Madison
140. Lu J., Ma S., Gao J., Freitas J.C.C., and Bonagamba T.J. (2003) *Study on characterization of pyrolysis and hydrolysis products of poly(vinyl chloride) waste* 3252-3259.
141. Hansen P.E. (1979) *13C NMR of polycyclic aromatic compounds. A review* 109-142.
142. Peterson J.D., Vyazovkin S.,Wight C.A. (2001) *Kinetics of the Thermal and Thermo-Oxidative Degradation of Polystyrene, Polyethylene and Poly(propylene)*, Macromolecular Chemistry and Physics. 202:775-784.
143. Flynn J.H.,Stephen Z.D.C., *Chapter 14 Polymer degradation*, in Handbook of Thermal Analysis and Calorimetry. 2002, Elsevier Science B.V.
144. Tuttle R.W., Chowdury A., Bender E.T., Ramsier R.D., Rapp J.L., and Espe M.P. (2008) *Electrospun ceramic fibers: Composition, structure and the fate of precursors*, Applied Surface Science. 254:4925-4929.
145. Slade C.T.R., Southern J.C.,Thompson I.M. (1991) *27Al nuclear magnetic resonance spectroscopy investigation of thermal transformation sequences of alumina hydrates. Part 1.-Gibbsite, -Al(OH)3*, Journal of Materials Chemistry. 1:563 - 568.
146. Lezcano M., Ribotta A., Miró E., Lombardo E., Petunchi J., Moreaux C., and Dereppe J.M. (1997) *Spectroscopic Characterization of Dealuminated H-Mordenites: The Role of Different Aluminum Species on the SCR of NO with Methane*, Journal of Catalysis. 168:511-521.

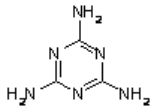
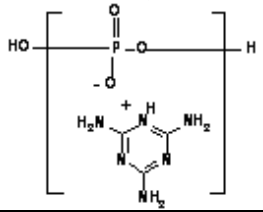
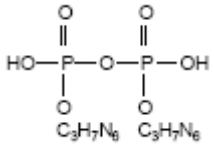
147. Jang S.W., Lee H.-Y., Lee S.-M., Lee S.W., and Shim K.-B. (2000) *Mechanical activation effect on the transition of gibbsite to α-alumina*, Journal of Materials Science Letters 19:507-510.
148. Tanashev Y., Moroz E., Isupova L., Ivanova A., Litvak G., Amosov Y., Rudina N., Shmakov A., Stepanov A., Kharina I., Kul'ko E., Danilevich V., Balashov V., Kruglyakov V., Zolotarskii I., and Parmon V. (2007) *Synthesis of aluminum oxides from the products of the rapid thermal decomposition of hydrargillite in a centrifugal flash reactor: II. Physicochemical properties of the products obtained by the centrifugal thermal activation of hydrargillite*, Kinetics and Catalysis. 48:153-161.
149. Opfermann J. (2000) *Kinetic Analysis Using Multivariate Non-linear Regression. I. Basic concepts*, Journal of Thermal Analysis and Calorimetry. 60:641-658.
150. Friedman H.L. (1965) *Kinetics of thermal degradation of char-forming plastics from thermogravimetry*, Journal of Polymer Sciences. 6:183-187.
151. Kissinger H.E. (1957) *Reaction kinetics in differential thermal analysis*, Analytical Chemistry. 29:1702-1706.
152. Ozawa T. (1965) Bulletin Chemical Society of Japan. 188-192.
153. Opfermann J.R., Kaisersberger E.,Flammersheim H.J. (2002) *Model-free analysis of thermoanalytical data-advantages and limitations*, Thermochimica Acta. 391:119-127.
154. Zsakó J. (1996) *Kinetic analysis of thermogravimetric data*, Journal of Thermal Analysis and Calorimetry. 46:1845-1864.
155. Kaisersberger E.,Opfermann J. (1991) *Kinetic evaluation of exothermal reactions measured by DSC*, Thermochimica Acta. 187:151-158.
156. Sewry J.D.,Brown M.E. (2002) *"Model-free" kinetic analysis?*, Thermochimica Acta. 390:217-225.
157. Edelmann M.,Heinrich G. *Thermokinetic analysis of two-step curing reactions in melt: Part II. Investigation of polymeric model systems*, Thermochimica Acta. 499:160-165.
158. Tang W., Chen D., Yang Z., Zhang A., and Peng Y. (2005) *Thermal characterization and thermal degradation of copolyimides containing fluorine and phosphine oxide* 2139-2143.
159. Sánchez-Jiménez P.E., Pérez-Maqueda L.A., Perejón A., and Criado J.M. *A new model for the kinetic analysis of thermal degradation of polymers driven by random scission*, Polymer Degradation and Stability. 95:733-739.
160. McGarry K., Zilberman J., Hull T.R., and Woolley W.D. (2000) *Decomposition and combustion of EVA and LDPE alone and when fire retarded with ATH*, Polymer International. 49:1193-1198.
161. Glinrun T., Mekasuwandumrong O., Panpranot J., Chaisuk C., and Praserthdam P. *Improvement of propane oxidation activity over Pt/Al2O3 by the use of MIXED gamma- and theta Al2O3 supports*, Reaction Kinetics, Mechanisms and Catalysis. 100:441-448.
162. Rakottyay K., Kaszonyi A.,VajÃ-Ä□ek S. *Oxidation of amines over alumina based catalysts*, Applied Catalysis A: General. 378:33-41.
163. Brouwer D.M. (1962) *Oxidation of aromatic hydrocarbons by silica-alumina*, Journal of Catalysis. 1:372-378.
164. Bertazzo S.,Rezwan K. (2009) *Control of gamma-Alumina Surface Charge with Carboxylic Acids*, Langmuir. 26:3364-3371.
165. Anon (1977) *Aluminium hydroxide - Flame protective agent and filler for plastics*, Kunstst Ger Plast. 67:14-16.
166. Herbiet R. (2000) *New metal hydroxides with improved performance for flame retardancy in plastics*, Polymers and Polymer Composites. 8:551-555.
167. Hornsby P.R.,Watson C.L. (1990) *A study of the mechanism of flame retardance and smoke suppression in polymers filled with magnesium hydroxide*, Polymer Degradation and Stability. 30:73-87.
168. Qu H., Wu W., Jiao Y., and Xu J. (2006) *ZnO and metal hydroxides as flame-retardants and smoke suppressants for flexible poly (vinyl chloride)*, Huagong Xuebao/Journal of Chemical Industry and Engineering (China). 57:1259-1263.
169. Ma W.,Brown P.W. (1999) *Mechanisms of Reaction of Hydratable Aluminas*, Journal of the American Ceramic Society. 82:453-456.
170. Braun U., Bahr H., Sturm H., and Schartel B. (2008) *Flame retardancy mechanisms of metal phosphinates and metal phosphinates in combination with melamine cyanurate in glass-fiber reinforced poly(1,4-butylene terephthalate): The influence of metal cation*, Polymers for Advanced Technologies. 19:680-692.

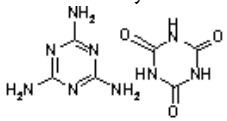
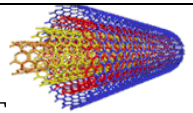
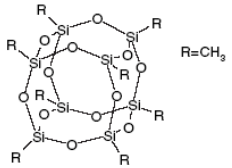
171. Burket C.L., Rajagopalan R.,Foley H.C. (2007) *Synthesis of nanoporous carbon with pre-graphitic domains*, Carbon. 45:2307-2320.
172. Cooper R.J., Camp P.J., Henderson D.K., Lovatt P.A., Nation D.A., Richards S., and Tasker P.A. (2007) *The binding of phosphonic acids at aluminium oxide surfaces and correlation with passivation of aluminium flake*, Dalton Transactions. 1300-1308.
173. Thissen P., Valtiner M.,Grundmeier G. (2009) *Stability of Phosphonic Acid Self-Assembled Monolayers on Amorphous and Single-Crystalline Aluminum Oxide Surfaces in Aqueous Solution*, Langmuir. 26:156-164.
174. Luschtinetz R., Oliveira A.F., Frenzel J., Joswig J.-O., Seifert G., and Duarte H.A. (2008) *Adsorption of phosphonic and ethylphosphonic acid on aluminum oxide surfaces*, Surface Science. 602:1347-1359.
175. Majoral J.-P., Vioux A., Le Bideau J., Mutin P.H., and Leclercq D., *Hybrid Organic-Inorganic Materials Based on Organophosphorus Derivatives*, in New Aspects in Phosphorus Chemistry IV. 2004, Springer Berlin / Heidelberg
176. Slade R.C.T., Southern J.C.,Thompson I.M. (1991) *27Al nuclear magnetic resonance spectroscopy investigation of thermal transformation sequences of alumina hydrates. Part 1.- Gibbsite, [gamma]-Al(OH)3*, Journal of Materials Chemistry. 1:563-568.
177. Müller D., Hallas E., Ladwig G., Grünze I., G.Berger, and Haubenreisser U. (1983) *Solid-state high-resolution 27Al nuclear magnetic resonance studies of the structure of CaO-Al2O3-P2O5 glasses*, Physics and Chemistry of Glasses. 24:37-42.
178. Jang S.W., Lee H.Y., Lee S.M., Lee S.W., and Shim K.B. (2000) *Mechanical activation effect on the transition of gibbsite to α-alumina*, Journal of Materials Science Letters. 19:507-510.
179. Tricot G., Delevoye L., Palavit G., and Montagne L. (2005) *Phase identification and quantification in a devitrified glass using homo-and heteronuclear solid-state NMR*, Chemical Communications. 5289-5291.
180. D.Massiot, F.Fayon, M.Capron, I.King, Calvé S.L., B.Alonso, J.O.Durand, B.Bujoli, Z.Gan, and G.Hoatson (2002) *Modelling one and two-dimensional solid-state NMR spectra*, Magn. Reson. Chem. 40:70-76.
181. Sampson N.S.,Bartlett P.A. (1988) *Synthesis of phosphonic acid derivatives by oxidative activation of phosphinate esters*, The Journal of Organic Chemistry. 53:4500-4503.
182. Kuivalainen T., El-Bahraoui J., Uggla R., Kostiainen R., and Sundberg M.R. (2000) *Correlation of the 31P NMR Chemical Shift with the Position of Bond Critical Points in Some Phosphorothionates*, Journal of the American Chemical Society. 122:8073-8074.
183. Tiemann M., Schulz M., Jäger C., and Fröba M. (2001) *Mesoporous aluminophosphate molecular sieves synthesized under nonaqueous conditions*, Chemistry of Materials. 13:2885-2891.
184. Guerrero G., Mutin P.H.,Vioux A. (2001) *Organically modified aluminas by grafting and sol-gel processes involving posphonate derivatives*, Journal of Materials Chemistry. 11:3161-3165.
185. Shen W., Yang J., Li S., Hu W., Xu J., Zhang H., Zou Q., Chen L., and Deng F. *Multinuclear solid-state NMR studies on phase transition of mesostructured aluminophosphate*, Microporous and Mesoporous Materials. 127:73-81.
186. Dutasta J.P., Robert J.B.,Wiesenfeld L. (1981) *31P Solid state NMR geometrical effects on the chemical shift tensor*, Chemical Physics Letters. 77:336-338.
187. Mingalyov P.G.,Lisichkin G.V. (2006) *Chemical modifications of oxide surfaces with organophosphorus (V) acids and their esters*, Russian Chemical Reviews. 75:541-557.
188. Bobonich F.M., Turutina N.V., Brei V.V., Voloshina Y.G., and Il'in V.G. (1995) *Peculiarities of the coordination state of the aluminum atoms in aluminophosphate AlPO4-5*, Theoretical and Experimental Chemistry. 30:180-183.
189. Kiss-Eross K. (1976) *Analytical Infrared Spectroscopy, Comprehensive Analytical Chemistry* Elsevier,Amsterdam
190. Maier L. (1972) *Organic Phosphorus Compounds. 55. The direct synthesis of hydroxymethylphosphonic acid, bis(hydroxymethyl)phosphinic acid, and methyl(hydroxymethyl)phosphinic acid* 117-124.
191. Mills S.L., Leesa G.C., Liauwa C.M., Rothona R.N., and S.Lynch (2005) *Prediction of Mechanical Properties Following the Dispersion Assessment of Flame Retardant Filler/Polymer Composites Based on the Multifractal Analysis of SEM Images* Journal of Macromolecular Science, Part B. 44:1137-1151.

APPENDICES

APPENDIX 1:
COMPOSITION AND PROPERTIES OF FIRE RETARDANTS AND SYNERGISTS

Commercial reference	Supplier	Composition	Particle size (µm)	Specific surface (m^2/g)	Shape	Applications
Magnifin H5	Albemarle	$Mg(OH)_2$, 99.8%	d_{90}= 2.1-4.1	4-6	Platelets, pseudo-hexagonal	Wire and cable (EVA, PP-EPDM)
Apyral 40CD	Nabaltec	$Al(OH)_3$, 99.5%	d_{90}= 3.2	3.5	platelets	Wire and cable (EVA,PP-EPDM)
Charmax FS-ZHSA-10	Polymer Additives Group	$Al(OH)_3$ coated zinc hydroxystannate	Average size:2-3			PVC based wire and cable, sheet and film, and coatings
AP 423	Clariant	$(NH_4PO_3)_n$	d_{50}= 8		spherical	FR for PET, PP, PU, epoxy resins, textiles
AP 765	Clariant		d_{50}=20		spherical	FR for PP
AP 766	Clariant		d_{50}= 20		spherical	FR for PP
Budit 3167	Budenheim	Coated intumescent combination based on ammonium polyphosphate			spherical	FR for PP and PE

Commercial reference	Supplier	Composition	Particle size (µm)	Specific surface (m^2/g)	Shape	Applications
Budit 3178	Budenheim					FR for PP and PE
OP 950	Clariant	Zn phosphinate	d_{50}= 350		More or less spherical	FR for polyester
OP1230	Clariant	Al phosphinate	d_{50}= 25		More or less spherical	FR for polyamide
OP 1311	Clariant	OP1230+MP200 (2-1 ratio)	d_{50}= 20		More or less spherical	FR for polyamide
melamine	DSM	Melamine 99% 	Average size: 360			Laminates, wood-based panels, coatings, FR, paper and textile
MP 200	Ciba	Melamine polyphosphate 	d_{99}= 25			FR for Bisphenol-A and PA66
Budit 311	Budenheim	Melamine pyrophosphate 				FR for PP,PA, PU foam
Melagard MB	Italmatch	Melamine borate				after glow and smoke suppressant for cellulose materials and organic polymers

Commercial reference	Supplier	Composition	Particle size (µm)	Specific surface (m^2/g)	Shape	Applications
Melagard MC	Italmatch	Melamine cyanurate 				FR for PA6 and PA 66
Melagard MP	Italmatch	Melamine orthophosphate				Smoke suppressant for thermoplastics, elastomers, intumescent FR coatings
Phoslite	Italmatch	Mg/Al/Ca-salts of phosphinates				
Graphite	INCA	acid (sulphuric acid, nitric acid, or acetic acid are commonly used) intercalated into the crystal layer of the graphite			platelets	Flame retardant, smoke suppressant, lubricant
Nanocyl 7000	Nanocyl	MWNT 	1.5µm length, Ø9nm	250-300	tubes	physical reinforcement for fibers and plastics, improves thermal conductivity
OMPOSS	Hybrid Plastics	Octamethyl polyedral oligomeric silsesquioxane 	0.7-30 Å		Nano-cages	Improves hydrophobicity, printability, processing (for PA, PU, PP, PE)
Cloisite 30B	Southern Clay	Organically modified bentonite clay: bis(hydroxyethyl)methyl tallow alkyl ammonium salts with bentonite	d_{90}=13	750	Platelets (interlayer distance 18 Å)	Physical reinforcement for plastics and coatings

APPENDIX 2:

MECHANICAL AND FIRE TESTING RESULTS OF THE SCREENING IN THE COMPLETE FORMULATION

Flame Retardant	Content (phr)	Hardness (Sh A)	Elongation at break (%)	Tensile strength (MPa)	LOI (vol-%)	UL-94 rating
Magnifin H5	200	68	570	6,1	49	V0
Apyral 40CD	200	60	582	5,3	44	V0
Charmax	200	74	482	6,8	35	V0
AP 423	60	59	582	9,6	27	NC
	80	66	582	7,8	28	V0
AP 765	60	53	589	7,4	25	NC
	80	60	579	6,7	26	NC
AP 766	60	42	638	7,4	28	V0
	80	47	626	6,3	28	V0
Budit 3167	60	55	593	7,7	26	NC
	80	59	570	6,7	26	V0
Budit 3178	60	52	578	7,2	26	NC
	80	60	561	6,5	26	NC
OP 1230	60	44	614	7,6	37	NC
	80	48	600	6,8	40	NC
OP 950	60	44	523	4,1	25	NC
	80	51	531	4,4	25	NC
OP 1311	60	46	612	8,1	36	V1
	80	50	595	7,7	35	V0
Melamine	60	39	592	6,3	25	NC
	80	42	553	4,8	27	NC

Flame Retardant	Content (phr)	Hardness (Sh A)	Elongation at break (%)	Tensile strength (MPa)	LOI (vol-%)	UL-94 rating
MP200	60	56	582	8,3	27	NC
	80	60	589	7,5	27	NC
Budit 311	60	57	596	8,1	27	NC
	80	65	565	6,9	27	NC
Melagard MB	60	53	572	8,7	27	NC
	80	57	579	8,1	28	NC
Melagard MC	60	54	610	10,4	26	NC
	80	59	596	9,7	27	NC
Melagard MP	60	47	592	7,8	27	NC
	80	50	584	7,1	27	NC
Phoslite B55 CM	60	52	622	9,5	27	NC
	80	57	611	8,6	30	V0
Expandable Graphite	20	44	567	11,1	24	NC
	30	47	547	10,5	25	NC
Expanded Graphite	20	48	578	11,3	25	NC
	30	53	563	11	25	NC

APPENDIX 3:
MECHANICAL AND FIRE TESTING RESULTS OF APP-MELAMINE DERIVATIVES COMBINATIONS IN VULCANIZED EVM

This study completes the investigations about the phosphorus compounds-melamine derivatives combinations. AP766 was selected to be combined with melamine derivatives since it is the most efficient phosphate-based additives. As for the phosphinate-based combinations the loading is chosen 55 phr, and two ratios were tested: 2:1 and 3:1. The compounding loadings are presented in *Table 1*.

Table 1: Flame retardant loadings in vulcanized EVM

AP766	MP200	Melagard MP	Melagard MB
55	-	-	-
37	18	-	-
37	-	18	-
41	-	14	-
37	-	-	18
41	-	-	14

The LOI and UL-94 rating were evaluated *(Fig.1)*. It appears that theuse of melamine derivatives is detrimental to the LOI as it decreases for all combinations compared to AP766 used alone. Moreover melamine borate MB induces a degradation of the UL-94 ranking as the samples with this additive are non classified. It is noticeable that there is no influence of the combination ratio on the flame retardant properties.

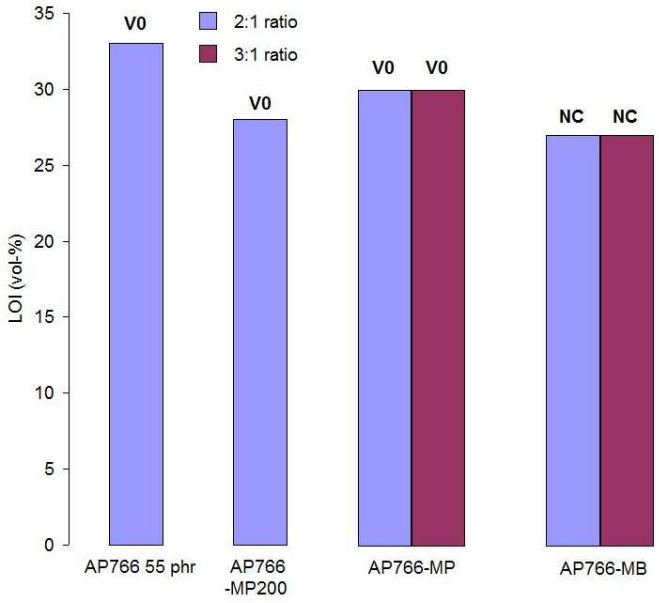


Fig.1: LOI and UL-94 rating of vulcanized EVM flame retarded with AP766 and combinations

To conclude with, phosphate-melamine derivatives combinations are not valuable.

APPENDIX 4:

MECHANICAL AND FIRE TESTING RESULTS OF THE ATH-OP1230-MELAMINE DERIVATIVES TERNARY COMBINATIONS IN THE COMPLETE FORMULATION

The ATH/OP1230 and ATH/OP1230-melamine derivatives ratios are chosen to be a compromise between mechanical, fire properties and the cost of such combinations. The OP1230-MP and OP1230-MB ratios, respectively 2:1 and 3:1, correspond to the optimum ratios in terms of flame retardant properties.

The flame retardant loadings are presented in *Table 1*. The recipe of the complete commercial formulation is detailed in *Chapter 1 (RPW recipe)*.

Table 1: ATH/OP1230/Melagard loadings (phr) of the formulations of Study 11

ATH (Apyral 120E)	OP1230	Melagard MB	Melagard MP	Loading (wt-%)
120	-	-	-	41
84	36	-	-	41
84	27	9	-	41
84	24	-	12	41

The mechanical properties are slightly influenced by the substitution of ATH by OP1230 or OP1230-MP or MB, as shown in *Fig.1*.

Substituting ATH by OP1230 or OP1230-melamine derivatives combinations seems beneficial to the elongation at break as it increases from 490% for the formulation with ATH to 530% for the samples flame-retarded with the combinations of additives.

The tensile strength is slightly decreased when ATH is substituted by OP1230 or OP1230/MP-MB (from 7.3 to 6.4 MPa) but the observed change is comprised within the margin of error.

The major interest of decreasing the ATH content is to reach lower hardness vales. This aim was fulfilled since the hardness decreases for the samples containing the combinations for example from 68 ShA (for ATH based formulation) to 58 ShA (for the ATH-OP1230 flame retarded formulation).

The combinations of ATH, OP1230 and melamine derivatives in a complete formulation proved to be interesting in terms of mechanical properties as they cover a larger range of hardness values without modifying TS and EAB.

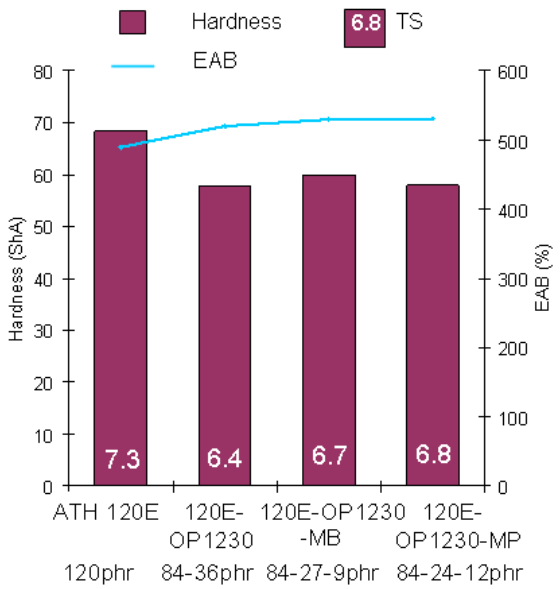


Fig.1: Evolution of hardness, elongation at break and tensile strength of the formulations of Study 11

The interest of using such combinations was not only the modification of the hardness but also the improvement of the resistance to fire of the material. As shown in Fig.2 the LOI is significantly increased by the use of OP1230 in combination with ATH in the complete formulation: it goes up from 35 to 40 vol-%.

The UL-94 rating is also modified. The sample containing ATH without phosphinate does not pass the UL-94 test while the formulation flame retarded with the combination of the two additives obtains a V0 ranking. Moreover the incorporation of melamine derivatives has no influence on the flame retardant properties of ATH/OP1230 based formulations. All formulations remain V0 with a LOI value around 40 vol-%.

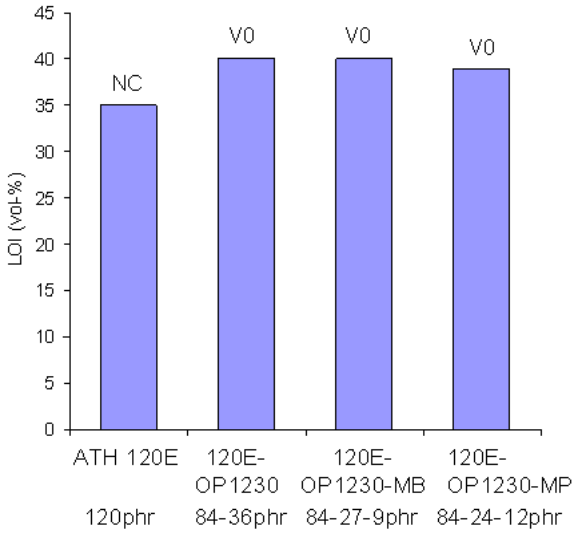


Fig.2: Evolution of LOI and UL-94 rating of the formulations

The ATH-OP1230 combination exhibits a synergistic effect in terms of flame retardancy (LOI, UL-94), but the addition of melamine derivatives does not show any beneficial effect.

The reaction to fire of the materials is also evaluated using mass loss calorimeter, under an irradiance of 35 kW/m². It appears in *Fig.3* and *Table 2* that the time to ignition of the complete formulations is slightly modified by the substitution of ATH by the phosphinate and the phosphinate-melamine derivatives combinations. It is comprised between 49 and 75 s, which is in the margin of error of the experiment.

The shape of the RHR curves remains unchanged by the use of the flame retardant combinations. The PRHR are also comparable (around 130 kW/m²) for all samples except from the formulation flame retarded with the ATH-OP1230-MP mixture which presents a slightly lower value (115 kW/m²).

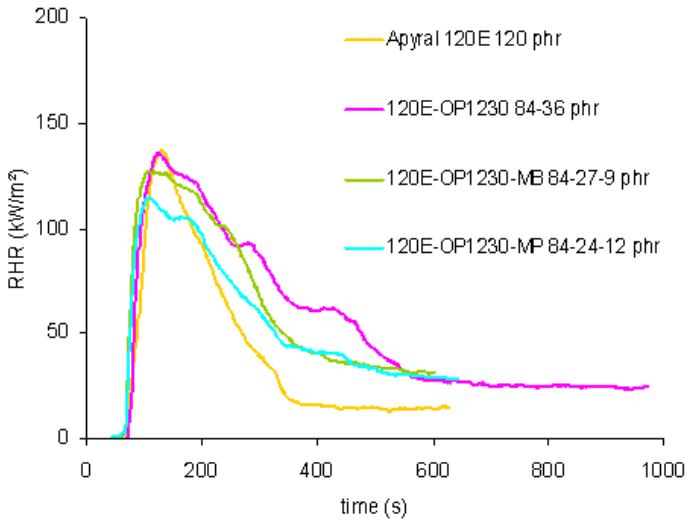


Fig.3: RHR curves of the formulations (35kW/m²)

Table 2: Mass loss calorimeter data

Formulations containing	Time to ignition (s)	PRHR (kW/m²)
120E 120 phr	49	136
120E-OP1230 84-36 phr	75	135
120E-OP1230-MB 84-27-9 phr	59	127
120E-OP1230-MP 84-24-12 phr	56	115

The combinations of ATH, OP1230 and melamine derivatives in a complete formulation proved to be interesting in terms of mechanical properties as they cover a larger range of hardness values without modifying the elastomeric behaviour of the material.

In terms of flame retardancy the ATH-OP1230 combination exhibits a synergistic effect as the LOI and the UL-94increase, but the addition of melamine derivatives does not show any beneficial effect. Moreover the mass loss calorimeter tests show no detrimental effect of OP1230 (same PRHR and time to ignition) and melamine derivatives, but the use of these latter is not significantly beneficial.

As a conclusion the use of melamine derivatives in ATH-OP1230-melamine derivatives ternary combinations is not valuable in the complete commercial formulation.

APPENDIX 5:

FRIEDMAN ANALYSIS OF THE THERMAL DEGRADATION OF VULCANIZED EVM AND OF THE FLAME RETARDED MATRIX

The apparent activation energy Ea (red curve) and logA (blue curve) obtained through the Friedman analysis are plotted versus the fractional mass loss.

The Friedman analysis for the vulcanized EVM thermo-oxidative degradation is presented in *Fig.1*.
It appears that the energy is not constant during the whole degradation: five areas can be defined. Between 0.2 and 0.4 fractional mass loss the energy is stable around 130 kJ/mol, from 0.4 to 0.6 around 150 kJ/mol. Then it increases up to 300 and 350 kJ/mol. The last part (from 0.85 to 1) presents an energy of 130 kJ/mol.
This indicates that the thermal decomposition occurs in a complex way including several degradation reactions.

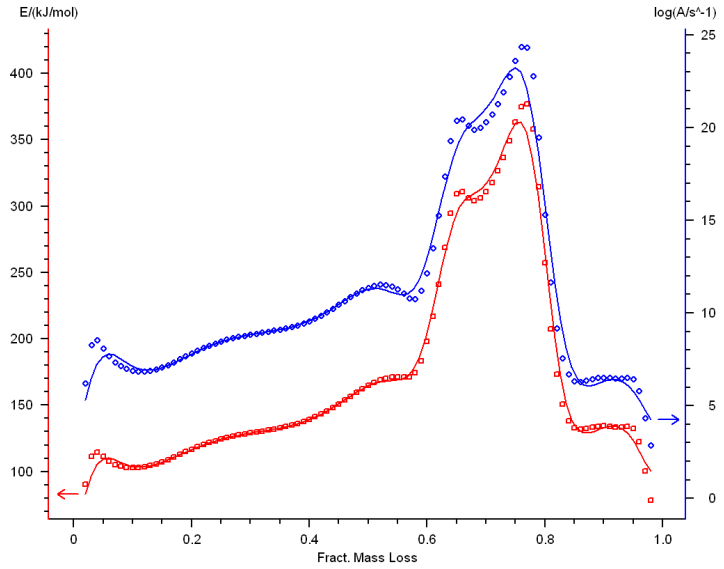


Fig.1 : Friedman energy plot of vulcanized EVM (in air)

The Friedman analysis for the inert degradation of vulcanized EVM *(Fig.2)* indicates that the thermal decomposition occurs into more than one degradation step. Indeed, the analysis reveals that between the fractional mass loss of 0.02 and 0.4 the energy remains stable at 160 kJ/mol and also between 0.45 and 0.95 at 250 kJ/mol before it decreases.

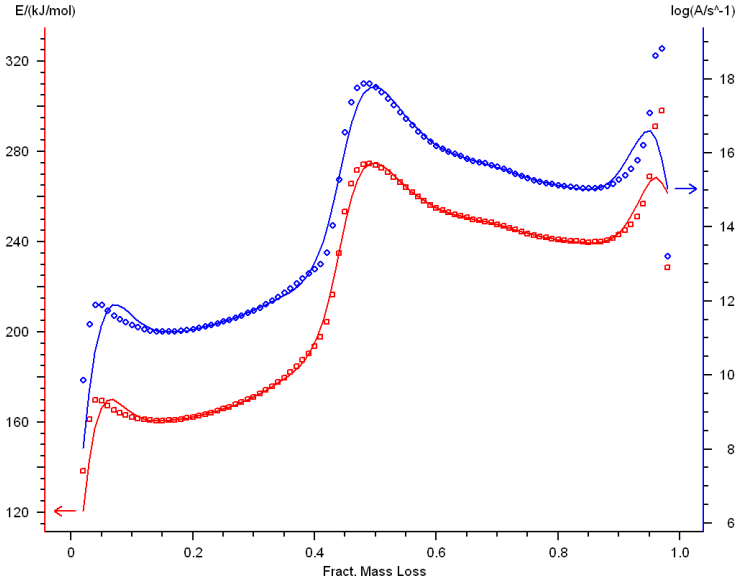


Fig.2 : Friedman energy plot of vulcanized EVM (in nitrogen)

The same analysis will be performed on the TG data of the flame retarded matrix.

2.3.3 Flame retarded matrix

The Friedman analysis for the flame retarded vulcanized EVM thermo-oxidative degradation is presented in *Fig.3*.

It appears that the energy varies during the degradation. Between 0.1 and 0.3 fractional mas loss the energy is stable around 130 kJ/mol, from 0.3 to 0.5 around 140 kJ/mol. Then it increases up to 200 kJ/mol. Between 0.6 and 0.85 the energy reaches 250 kJ/mol. The last part (from 0.85 to 1) presents an energy of 140 kJ/mol.

These five “zones” indicates a multi-steps degradation.

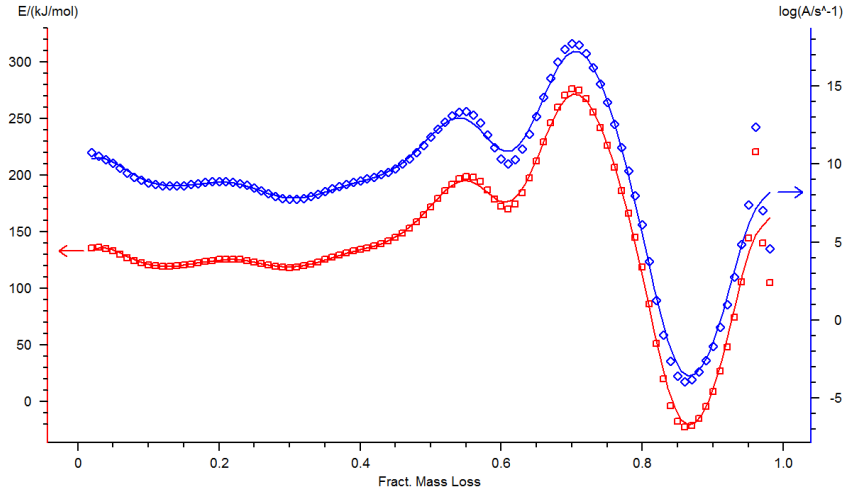


Fig.3: Friedman energy plot of vulcanized EVM flame retarded with ATH 120E (in air)

In inert atmosphere the Friedman energy plot of the thermal degradation of the ATH-filled polymer exhibits three different areas *(Fig.4)*. Between 0 and 0.2 fractional mass loss the activation energy remains stable around 120 kJ/mol, then a second threshold at 160 kJ/mol is noticeable. The last part between 0.5 and 0.95 fractional mass loss presents a constant activation energy of 200 kJ/mol. Unbranched multi-steps degradation are thus suspected.

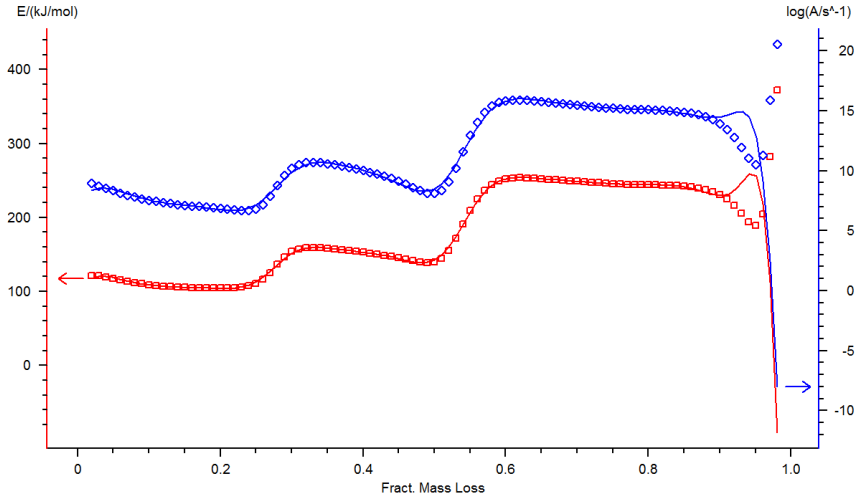


Fig.4: Friedman energy plot of vulcanized EVM flame retarded with ATH 120E (in nitrogen)

APPENDIX 6:
KINETIC MODELING OF THE THERMAL DEGRADATION OF VULCANIZED EVM CONTAINING DIFFERENT ATH GRADES

To determine the influence of the ATH particle size on the thermal degradation of vulcanized EVM the kinetic modeling of the thermal degradation of the matrix flame retarded with various ATH grades was investigated.

The experimental TG curves at 1, 2, 5, 10 and 20 ℃/min are presented in *Fig.1*. It appears that the shape of the curves is identical for all ATH particle sizes: five degradation steps and a final residue around 35 wt-%.

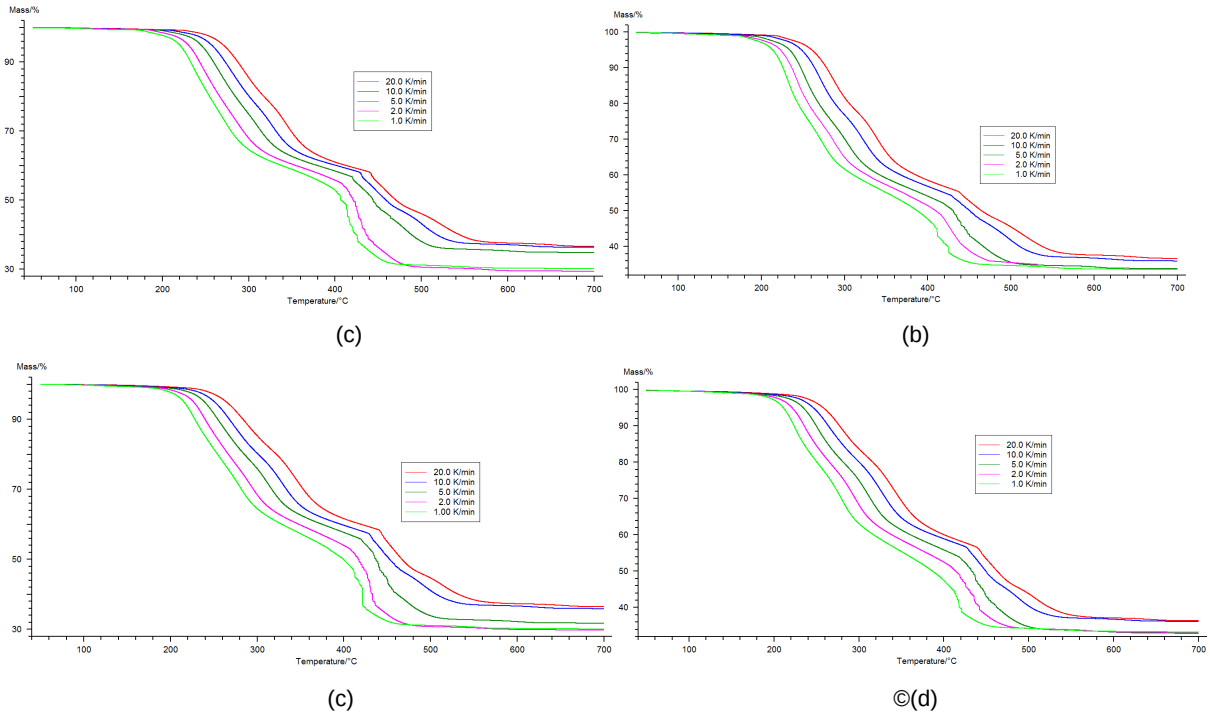


Fig.1: Experimental TG curves of vulcanized EVM flame retarded with 40CD (a), 60CD (b), 120E (c), 200SM (d)

The Friedman analysis of the experimental data provided the apparent activation energy and the pre-exponential factor values *(Fig.2)*.

Five kinetic steps are noticeable for all formulations. The activation energies are similar whatever the ATH particle size. The chosen degradation model is thus the same for all samples: five non-competitive steps.

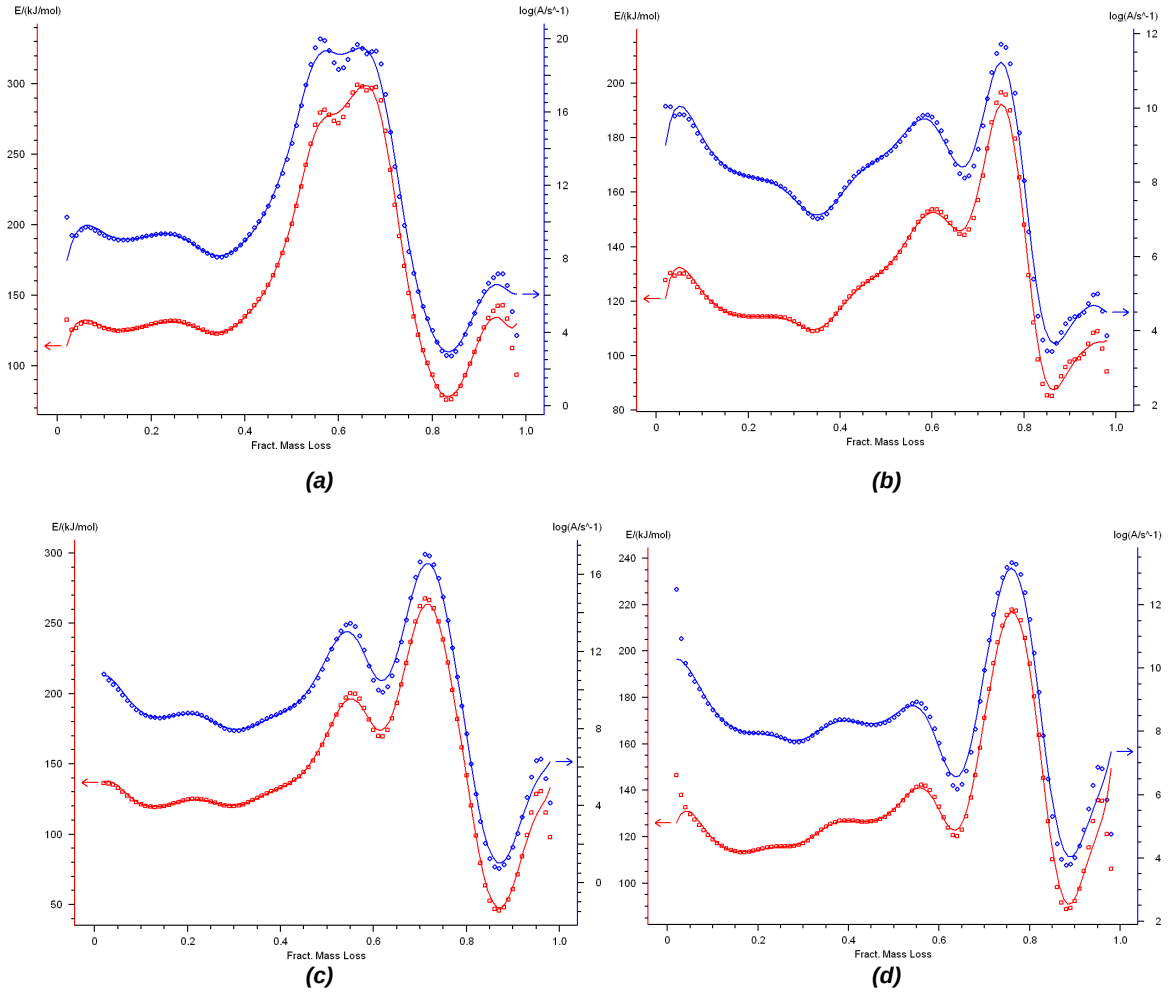


Fig.2: Results of the Friedman analysis of the TG curves of vulcanized EVM flame retarded with ATH 40CD (a), 60CD (b), 120E (c), 200SM (d)

The degradation functions selected for the degradation modeling are presented in *Table 1*. The two functions are the n-th order and the Avrami-Erofeev equation simulating random nucleation.

Table 1: Degradation functions of the kinetic degradation model of flame retarded vulcanized EVM depending on the ATH particle size

	40CD (1.3µm)	**60CD (1.0µm)**	**120E (0.9µm)**	**200SM (0.3µm)**
Step 1	n-th order	n-th order	n-th order	n-th order
Step 2	n-th order	n-th order	n-th order	n-th order
Step 3	n-th order	n-th order	n-th order	n-th order
Step 4	Avrami-Erofeev	Avrami-Erofeev	Avrami-Erofeev	n-th order
Step 5	Avrami-Erofeev	Avrami-Erofeev	n-th order	Avrami-Erofeev

The simulation of the thermo-oxidative degradation of vulcanized EVM containing ATH of various particle sizes are presented in the following figures (from *Fig.3* to *Fig.6*). The so-determined kinetic parameters are gathered in *Table 2* to *Table 5*.

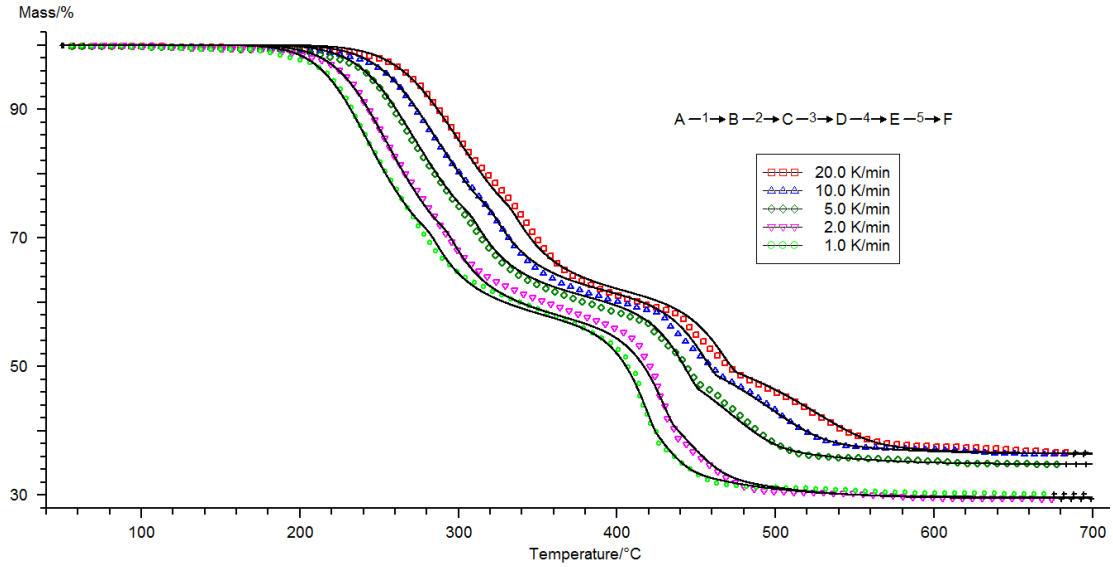


Fig.3: Simulation of the degradation of vulcanized EVM flame retarded with ATH 40CD under air

Table 2: Kinetic parameters of the degradation of vulcanized EVM flame retarded with ATH 40CD under air

	Log A (s^{-1})	Ea (kJ/mol)	n
Step 1	9.8	126	1.48
Step 2	12.1	156	1.93
Step 3	16.7	232	0.13
Step 4	15.5	245	0.36
Step 5	4.7	106	1.61

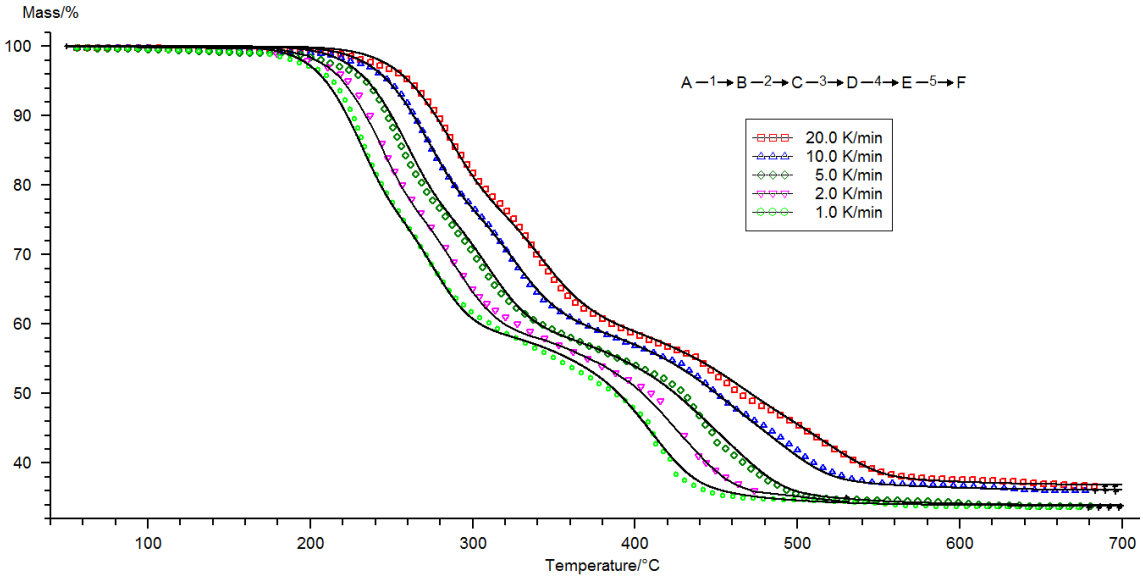


Fig.4: Simulation of the degradation of vulcanized EVM flame retarded with ATH 60CD under air

Table 3: Kinetic parameters of the degradation of vulcanized EVM flame retarded with ATH 60CD under air

	Log A (s^{-1})	Ea (kJ/mol)	n
Step 1	9.4	119	1.02
Step 2	8.1	117	1.11
Step 3	10.8	174	0.58
Step 4	11.6	184	3.00
Step 5	4.5	102	1.81

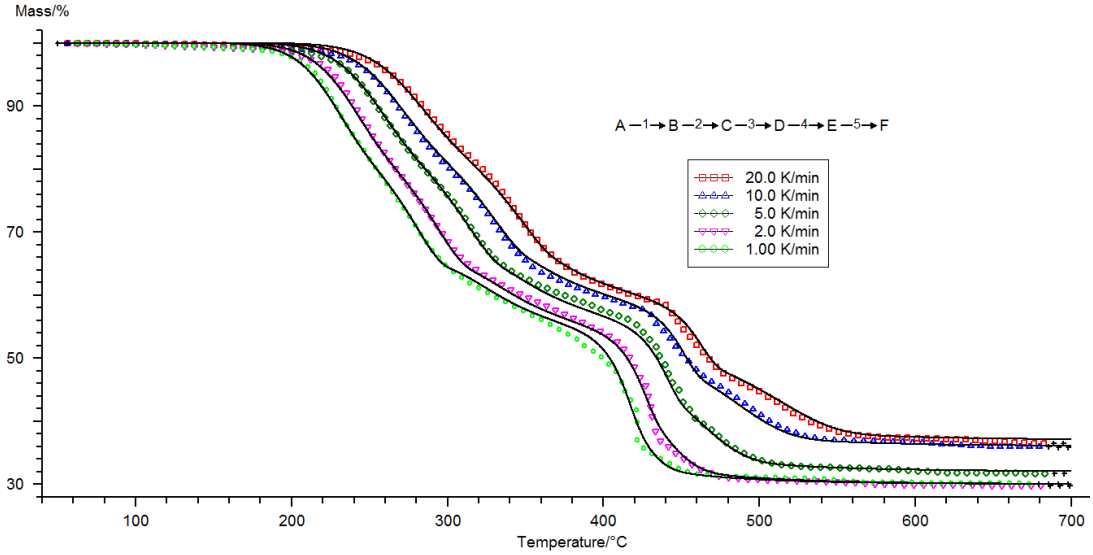


Fig.5: Simulation of the degradation of vulcanized EVM flame retarded with ATH 120E under air

Table 4: Kinetic parameters of the degradation of vulcanized EVM flame retarded with ATH 120E under air

	Log A (s^{-1})	Ea (kJ/mol)	n
Step 1	10.0	125	1.45
Step 2	9.1	129	0.72
Step 3	15.3	211	0.61
Step 4	16.5	255	1.88
Step 5	2.4	71	1.37

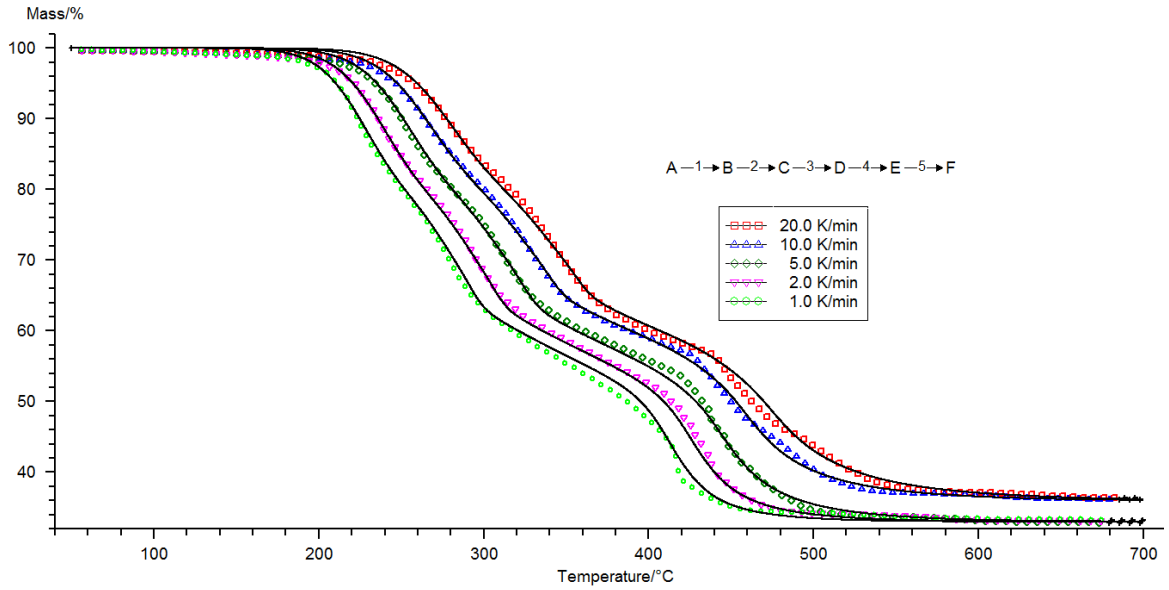


Fig.6: Simulation of the degradation of vulcanized EVM flame retarded with ATH 200SM under air

Table 5: Kinetic parameters of the degradation of vulcanized EVM flame retarded with ATH 200SM under air

	Log A (s^{-1})	**Ea (kJ/mol)**	**n**
Step 1	10.0	124	1.46
Step 2	9.1	129	0.80
Step 3	13.2	205	0.9
Step 4	14.9	231	1.35
Step 5	4.8	98	0.32

The correlation between experimental and computed data is excellent for all formulations.

Résumé - Cette étude s'intéresse aux procédés d'ignifugation d'un élastomère, le copolymère d'éthylène acétate de vinyle (EVM) vulcanisé, et plus particulièrement à l'ajout en masse de retardateurs de flamme commerciaux. L'objectif de ce travail consiste à mettre au point une formulation à base EVM destinée aux domaines de la câblerie et des transports, ignifugée et à haute tenue mécanique, ainsi qu'à comprendre les phénomènes d'ignifugation mis en jeu. L'évaluation de différents types d'additifs, sur le plan mécanique et retard au feu, a permis de dégager une combinaison innovante associant le trihydroxyde d'aluminium (ATH) et le diéthylphosphinate d'aluminium (OP1230). Le mode d'action de l'ATH dans l'EVM, généralement attribué à sa déshydratation endothermique, a été revisité à l'aide d'une approche cinétique de la dégradation du système EVM/ATH. Ces résultats ont été corrélés à l'étude de l'évolution du matériau soumis à des conditions incendie. Il a été montré que l'endothermicité de la réaction n'a un rôle que secondaire, l'additif agissant principalement en formant au sein du matériau une structure protectrice d'alumine jouant le rôle de barrière thermique et ralentissant ainsi le transfert de masse lors de la combustion. Pour la formulation complète (EVM/ATH/OP1230), les interactions chimiques entre additifs et polymère et les mécanismes d'action de l'OP1230 et de la combinaison ATH/OP1230 ont été étudiés. L'effet de synergie observé entre les deux additifs est attribué à la formation d'une couche protectrice vitreuse résistante à la surface du matériau pendant la combustion, couplée à la libération d'espèces phosphorées agissant en phase gaz comme inhibiteurs de flamme.

Abstract - This study is dedicated to the formulation of an innovative flame retardant material based on elastomeric vulcanized ethylene-vinyl acetate copolymer (EVM) used in the fields of cable and transportation, and to the comprehension of the flame retardant phenomena. The screening of various additives, evaluated in EVM in terms of mechanical and fire retardant properties, allowed the determination of an innovative combination, made of aluminium trihydroxide (ATH) and aluminium diethyl phosphinate (OP1230). The ATH mode of action, generally assumed to be a cooling effect, was revisited by a kinetic approach of the thermal degradation of the EVM/ATH formulation in oxidative and pyrolytic conditions, associated with the investigation of the evolution of the material in simulated fire conditions. It was found that the cooling effect occurs, but the main protective effect of ATH consists in the formation during combustion of an alumina layer, diminishing the mass and heat transfer and thus the flame feeding. In the complete formulation (EVM/ATH/OP1230), the chemical interactions between ATH, OP1230 and the polymer were investigated, revealing that the synergistic effect provided by the two additives results from the creation during combustion of a resistant glassy layer. Moreover phosphorous species are evolved in the gas phase during combustion, acting as flame inhibitors.